Durham E-Theses

Interactions of lactam containing compounds based on kinetic hydrate inhibition polymers

GOODWIN, MELISSA,JANE

How to cite:

Use policy

Interactions of lactam containing compounds based on kinetic hydrate inhibition polymers

A thesis submitted for the degree of

Doctor of Philosophy

In the Department of Chemistry at Durham University

By

Melissa Goodwin

2016

Abstract

As the supply of natural gas becomes more scarce, it is becoming increasingly more attractive and financially viable to start using reserves that were previously determined to be to impure to use. H_2S and CO_2 are a couple of the major impurities found in natural gas. Natural gas high in these chemicals is referred to as sour gas. Presence of these impurities increases the chances of clathrate hydrate formation in pipelines, which can lead to pipe blockages or ruptures. To prevent clathrate hydrate formation, low dosage, polymeric, kinetic hydrate inhibitors (KHIs) are used. KHIs are water soluble polymers, most commonly polyvinylcaprolactam (PVCap) and polyvinylpyrrolidone (PVP). There is to date no definitive answer to the method of hydrate inhibition by KHIs and knowing how they work could lead to the design and manufacture of more effective inhibitors.

This thesis begins with the synthesis of model compounds. Low molecular weight compounds containing pyrrolidone and/or caprolactam rings were created to mimic PVP and PVCap. To look at the crystallisation behaviour of the model compounds, a wide range of different multicomponent crystallisations were attempted with pharmaceutical coformers, hydrogen bond donors, halogen bond donors and metal salts. Successfully formed cocrystals were analysed by single crystal x-ray crystallography. Cocrystals formed with boronic acids were tested for their ability to gel guar and compared with the commercially used boric acid.

The effect of sour gas on the interactions of the KHIs and model compounds with water was investigated using IR and NMR techniques. Small angle neutron diffraction was used to explore the synergistic effect between butoxyethanol and PVCap which leads to a significant improvement in hydrate inhibition.

Finally the ability of the model compounds to prevent crystallisation was applied to pharmaceuticals. Attempts to stabilise the amorphous forms of a range of drugs by creating coamorphous mixtures with the model compounds were investigated by hot-stage microscopy, DSC and PXRD.

Declaration

The work described in this thesis was carried out in the Department of Chemistry at Durham University (UK) between October 2013 and December 2016, under the supervision of Professor Jonathan W. Steed. PXRD, DSC and DVS experiments were carried out at Durham University School of Medicine, Pharmacy and Health. Neutron experiments were carried out at the Rutherford Appleton Laboratory in Oxfordshire. The material contained in this thesis has not been previously submitted for a degree at this or any other university.

Statement of copyright

Financial Support

Acknowledgements

Publication list

M. J. Goodwin, O. M. Musa and J. W. Steed, *Energy Fuels*, 2015, 29, 4667–4682.

Abbreviations

BisHEP	Bishydroxyethylpyrrolidone
BisVP	Bisvinylpyrrolidone
BisVCap	Bisvinylcaprolactam
CSD	Cambridge crystal structure database
CMC	Critical micelle concentration
DSC	Differential scanning calorimetry
DVS	Dynamic vapour sorption
Et(OVCap)$_2$	1,1'-[ethane-1,2-diylbis(oxyethane-1,1-diyl)]di(azepan-2-one)
Et(OVP)$_2$	1,1'-[ethane-1,2-diylbis(oxyethane-1,1-diyl)]dipyrrolidin-2-one
GRAS	Generally regarded as safe
H$_2$bisVCap	Hydrogenated bisvinylcaprolactam
H$_2$bisVP	Hydrogenated bisvinylpyrrolidone
HEP	Hydroxyethylpyrrolidonw
IR	Infrared
LCST	Lower critical solution temperature
NIMROD	Near and intermediate range order diffractometer
NMR	Nuclear magnetic resonance
MEP	Methylethoxypyrrolidone
Pr(OVCap)$_2$	1,1'-[propane-1,3-diylbis(oxyethane-1,1-diyl)]di(azepan-2-one)
Pr(OVP)$_2$	1,1'-[propane-1,3-diylbis(oxyethane-1,1-diyl)]dipyrrolidin-2-one
PVA	Polyvinylalcohol
PVCap	Poly(N-vinylcaprolactam)
PVP	Poly(N-vinylpyrrolidone)

PVPip	Poly(N-vinylpipiridone)
RH	Relative humidity
SANS	Small angle neutron scattering
TFA	Trifluoroacetic acid
VP	N-vinylpyrollidone
VCap	N-vinylcaprolactam

Contents

1   Introduction

1.1   Clathrate hydrates

Natural gas reserves can be generalised into two categories: sweet and sour. Sour gases contain a significant amount of acid gas components. The acid gases are most commonly CO_2 and H_2S, although other sulfur-containing compounds (mercaptans) can also be present. Due to an increase in gas consumption and the depletion of many sweet gas reserves, sour gas is becoming more frequently exploited.[1] There are a plethora of danger associated with sour gas, including its toxicity, its ability to corrode pipes and that it is more likely to form clathrate hydrates than sweet gas.[2] Clathrate hydrates are cages of hydrogen-bonded water molecules which form around small molecules, for example methane found in natural gas, in favourable conditions of low temperatures and high pressures, such as those in undersea pipelines. When grown to a large enough size, these clathrates can form plugs that block pipes causing large delays that are costly and hazardous. Pipe rupturing and the flammable nature of the clathrates are a significant concern.[3]

The size of the guest molecule determines the structure of clathrate that is formed.[4,5] The structures shown below in Figure 1.1 are the most commonly formed clathrates, the cubic structure I and structure II and the hexagonal structure H.[6] It is possible to form more exotic structures with certain guests, for example dimethyl ether promotes the formation of a trigonal structure T. In pipelines it is usually structure I and structure II that occur. The smaller components such as methane, CO_2 and H_2S form structure I clathrates whilst larger components like ethane form structure II clathrates.[7]
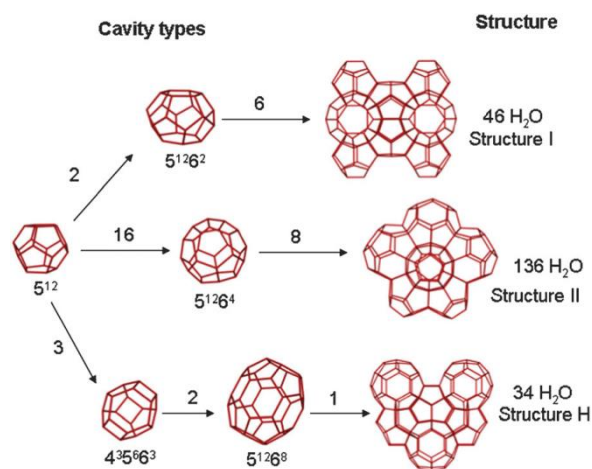
Figure 1.1 - The structures of the most common types of clathrate hydrate.

It was originally thought that clathrate hydrates are metastable crystal structures and that favourable interactions with a guest increased the stability. Rodger[8] simulated the formation of clathrates to test the validity of the assumptions made in the cell theory by van der Waals and Platteeuw.[9] Van der Waals and Platteeuw created a statistical thermodynamic model based on the assumptions that the free energy of the clathrate lattice is unaffected by the guest molecule, cavities only have one guest, guest-guest interactions do not occur and quantum effects can be ignored. Rodger used these assumptions to run a molecular dynamics simulation of clathrate formation and found that the free energy of the water crystal is significantly affected by the guest, thus the assumption that the free energy is not affected is not appropriate. He further concluded that clathrate hydrates are not in fact metastable, but will collapse to an ice phase, Ih, or liquid water upon removal of the guest, depending which is the more thermodynamically stable state under the conditions used. His calculations suggest that it is not the favourable interaction between cage and guest that give the hydrates their stability, but the hydrophobic interaction between an aliphatic guest and the water, that keeps the cage open, agreeing with the observation of Jeffrey in 1984[10] that molecules with either many or strong hydrogen bonding groups do not readily form clathrates. Looking at the temperature of decomposition for hydrates of propane, ethane thiol and ethanol, ethanol shows by far the least stable structure. The ethanol hydrate decomposes at -73 °C compared to ethane thiol at 3 °C and propane at 6 °C.[11] The OH of the ethanol hydrogen bonds with the water, introducing defects into crystal structure, decreasing the stability. This further evidences the theory that repulsive interactions stabilise the clathrates. Adding polar species, such as ethanol and methanol, destabilise the clathrate enough to act as inhibitors.

Hydrogen sulfide forms hydrates at the lowest partial pressure of all the components in sour gas. This seemingly contradicts the theory that more polar molecules make less stable clathrate hydrates as H_2S is more polar than methane.[11] One theory of the unexpected low clathrate formation pressure of H_2S is that the presence of H_2S changes the polarity of the system and increases the level of moisture in the gas.[12] The more water there is in the system, the higher the likelihood of it crystallising and hydrates forming. It has also been proposed that favourable size could more readily form clathrates.[13] Addition of H_2S to a mixture of cyclohexane and water actually promotes formation of a cyclohexane clathrate hydrate.[14] Normally cyclohexane is too big to be a suitable guest in a structure II type cage, but H_2S fills the smaller cavities in the structure stabilising the clathrate, smaller molecules stabilising clathrates that wouldn't normally form are referred to as help gases.[15] In

methane/H$_2$S clathrates H$_2$S fills the smaller cavities of the structure I clathrate whilst methane fills the larger cavities.[16]

The favourability of H$_2$S clathrate formation brings added danger to the system as hydrates formed in a sour system are rich in H$_2$S.[13,17] In a mixture of methane and H$_2$S with 1 % H$_2$S, the resulting clathrate will on average contain 12 % H$_2$S as a guest.[16] As well as the health hazard associated with the formation of clathrate hydrates, such as flammability and pipe blockage, these H$_2$S rich clathrates also bring all the troubles associated with H$_2$S toxicity.

1.1.1   Hydrate inhibition

Thermodynamic inhibitors, like methanol, are commonly used to prevent pipe blockages by clathrate hydrates. The requirement for very high loading, between 20 and 50 %,[18] makes them a very costly method of inhibition, though less costly than cleaning up after and repairing a ruptured pipe. A desire for a less high loading, and thus, less expensive, inhibitors started research into low dosage hydrate inhibitors (LDHIs). Water soluble synthetic polymers were tested as a method of inhibiting hydrate formation, as many such polymers were already in use for other applications so are readily and cheaply available for testing. It was found by Colorado School of Mines that polyvinylpyrrolidone (PVP) (**1**), a polymer already used for a wide range of applications from blood plasma expanders[19] to hair curling,[20] showed potential as a hydrate inhibitor.[18] Though PVP is not as effective as anti-freeze proteins at hydrate inhibition,[21] it is effective enough to prevent blockages during the timeframe and conditions required and the relative cost of production makes it much more desirable in an industrial setting. The low toxicity of PVP is an added bonus, as this would minimise the environmental impact of a pipe rupture, if one should occur. Replacement of methanol with PVP has been successfully implemented at many sites, including a Texaco site in southwest Wyoming for example.[22] These inhibitors are referred to as kinetic hydrate inhibitors (KHIs) as they do not make it thermodynamically unfavourable to form clathrates, just delay their formation until it is no longer a concern.

PVP (1)   PVPip (2)   PVCap (3)
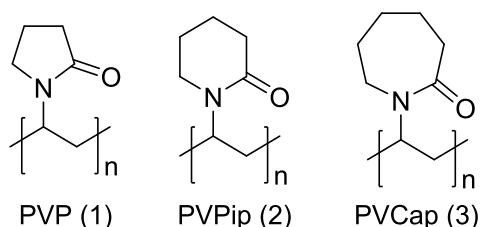
To further improve the efficiency of the inhibitor other similar compounds were tested Such as polyvinylpipiridone (PVPip) (**2**) and polyvonylcaprolactam (PVCap) (**3**). PVCap shows a greater ability than PVP to inhibit hydrate formation, though the reason for this is not fully

understood.[23] A range[24] of copolymers have also proven effective, an example of which being a vinylcaprolactam (VCap)/vinylpyrollidone (VP)/dimethylaminoethyl methacrylate terpolmer.[18] Copolymers show greater hydrate inhibition than PVP alone, whilst bringing down the costs of using solely the more expensive PVCap. Addition of a third type of monomer can impart other desirable properties, such as increasing the cloud point, corrosion resistance or helping improve compatibility with existing pipeline corrosion inhibitors. A VCap/phosphoric acid copolymer (**4**) is an example of adjusting the properties of PVCap by copolymerisations.[25] The phosphoric acid groups make the polymer an effective corrosion inhibitor and anti-agglomerant as well as a KHI, forgoing the need of multiple additives to control the corrosion and hydrate formation that occur in sour pipelines. Another example of copolymer modification is VCap/vinyl alcohol copolymer (**5**) which is been produced to supply the hydrate inhibition associated with pure PVCap with a superior biodegradability.[26]

VCap/phosphoric acid
copolymer (4)

VCap/vinyl alcohol
copolymer (5)
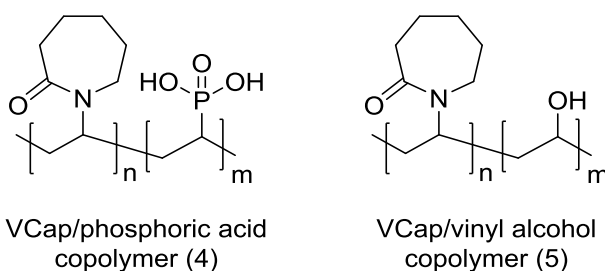
With PVP and PVCap being effective hydrate inhibitors, it would be expected that the 6-membered lactam analogue, PVPip, also referred to as polyvinylvalerolactam (**2**), would be so as well. Chua *et al*.[23] tested the hydrate inhibiting ability of PVPip compared to PVP and PVCap. They did find PVPip to be an effective inhibitor, better in fact than PVP. Though still less effective than PVCap, PVPip is not as effective as the current inhibitors, and the monomer is not commercially available, raising the cost. Though there are no examples of PVPip based polymers being used in an operating system, they have been patented for use as hydrate inhibitors,[27,28] so may come into use if economic considerations allow.

Inspiration for designing LDHIs can also be taken from nature, as a number of biological systems have developed natural antifreezes.[21,29] Cold water fish, such as winter flounder, live in polar regions, yet their blood does not freeze in the sub-zero temperatures they encounter. Antifreeze proteins, high in hydrophilic amino acids, prevent ice from forming in the blood.[29] Synthesis of these proteins has been successful and their ability of hydrate inhibition is as good as expected.[18] Unfortunately, it is not an economically viable option, with protein synthesis being costly and time consuming.

Most inhibitors are not sold as pure polymer. The polymer powder is messy to handle and does not easily disperse in the pipeline, so is often sold in a solution. The solvent chosen can have a big effect on the efficiency of the inhibitor. Whilst some solvents may retard the inhibitor, others actually improve it. One such solvent is butoxyethanol.

1.1.2 Butoxyethanol

PVCap is commercially available in a 50 wt% mix with 2-butoxyethanol. The 2-butoxyethanol acts as a solvent, creating a syrup that aids in the dispersion of the inhibitor throughout the pipeline. Butoxyethanol also works as a synergist, improving the inhibition of the product. Butoxyethanol functions as a hydrate inhibitor in its own right, though unlike PVCap that is a kinetic hydrate inhibitor (KHI), butoxyethanol is an anti-agglomerant (AA).

KHIs prevent the formation of hydrate crystals, AAs on the other hand, do not prevent the formation of hydrate crystals, but prevent the formation of pipeline blockages. AAs are surfactant like molecules that surround a forming hydrate, hydrophilic head groups interact with the water of the hydrate, and hydrophobic tails interact with the surrounding hydrocarbon environment in the pipeline. This stabilises small hydrate crystals, preventing agglomeration. This stops plugs forming and keeps the pipeline flowing as a slurry of small hydrate particles.

Butoxyethanol's properties as a surfactant are well documented, with studies using small angle x-ray scattering,[30] small angle neutron scattering[31–34] and dynamic and Rayleigh light scattering[35] techniques. Butoxyethanol is only a weak anti-agglomerant, with most commercial AAs consisting of long chain, quaternary ammonium salts.[36] Addition of butoxyethanol to a KHI, greatly increases the amount of time before a macroscopic hydrate is formed. For the example of a VP/VCap/(dimethylamino)ethylmethacylate terpolymer, the onset time is increased from 40 min to 1200 min.[28] This is a very large improvement, much larger than would be expected just from the addition of weak anti-agglomeration effect of butoxyethanol. This suggests that there is a truly synergistic effect, that the butoxyethanol is interacting with the KHI to enhance its inhibiting ability. Though to date, there has been no research into how the synergistic effect works.

1.1.3 Mechanism of hydrate inhibition

To further the understanding of the mechanisms in systems using polymers, it is often advantageous to use model compounds. Polymers are large and have a range of chain lengths making them difficult to study by common techniques such as NMR. Suitable models can be as small as a monomer up to moderate sized oligomers, with the longer chain lengths

being more true to polymer, but harder to analyse. Davenport *et al.*[37] synthesised two vinylcaprolactam dimers (**6** and **7**), which infrared spectroscopic analysis shows to interact with water in a very similar fashion to the polymer, making it a suitable model for the inhibitor.

bisVCap (6)   H₂bisVCap (7)
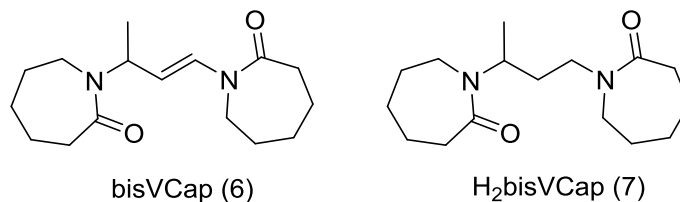
Simulating polymers can also be very computationally expensive so similar model compounds are used in simulations. Kuznetsova *et al.*[38] used up to a PVP octamer in their simulations with methane and water. Oligomers around this length have also been shown to be more effective as inhibitors than the larger polymers,[39] making an octamer a good model to choose when wishing to observe how hydrate inhibition occurs. They established that PVP does not interact with the surface of a forming hydrate, but may create a barrier between the aqueous and hydrocarbon phase. The barrier slows down diffusion of the natural gas into the water, slowing the onset of clathrate formation. Contrastingly, a small angle neutron study of PVP in water by Hutter *et al.*[40] concluded that PVP does adsorb onto the surface of the forming ice. Anderson *et al.*[41] proposed a two-step mechanism based on molecular dynamics simulations. The first step is that KHIs disrupt the local organization of the water molecules making nucleation much more difficult. The second step occurs after nucleation, the KHI adsorbs onto the hydrate blocking further growth. A number of different KHIs were modelled and they hypothesised that the more effective inhibitors would bind more strongly to the forming hydrate with the simulations agreeing. Molecular dynamic simulations by Moon *et al.*[42] however, do not come to the same conclusion. In their simulation the KHI, PVP in this case, does not bind to the forming hydrate. They state that the PVP resides in an environment independent of the hydrate and remains typically two solvation shells away from the hydrate. Instead it is concluded that PVP forms halos of ordered water around the lactam functionalities, which whilst being more ordered than bulk water, actually disrupt the ordering required for nucleation. These contrasting conclusions suggest that more research into the mechanism of hydrate inhibition is needed before the mode of action can be fully understood.

To study how KHIs prevent crystallisation it is of interest to see if it is possible to crystallise low molecular weight models of the polymers in a range of different conditions. Knowing under what conditions crystallisation occurs may help elucidate how KHIs prevent

crystallisation. If the goal is to create crystals or prevent them occurring, an understanding of what crystallisation is and how the crystallisation process proceeds is a useful tool to have.

1.2   Crystallisation

Crystallisation is a commonly used technique for purifying products in synthesis and is generally taken as standard lab practice. Whilst purification is a useful application of crystallisation, it is far from the full potential which can be achieved. Large enough single crystals can be analysed by single crystal x-ray diffraction to give crystal structures, showing, within an often small amount of error, the relative positions of the atoms in the crystal structure and revealing the molecular structure. Comparing and analysing crystal structures can give information of the stability of solids forms, interactions between molecules and favourable conformations of compounds. Single crystals can even be used as models to study the mechanism of solid state catalysts.[43,44]

Crystallisations can be performed by a range of different methods: evaporation of solvent, cooling of a heated, solvent containing system, antisolvent diffusion, melting and freezing and conversion of an amorphous solid. The best method to crystallise a particular compound cannot be predicted, so it is advisable to try a wide range of different solvents and methods.[45]

In solvent based crystallisations the compound of interest is required to completely dissolve in the chosen solvent. From an undersaturated solution, crystals will never form. For the formation of crystals the solution must become supersaturated.[46,47] A supersaturated solution is usually formed in one of three ways. The first is to dissolve as much of the desired solid as possible in a heated solvent then slowly cool the solution down. Solubility increases with temperature, so as a hot saturated solution cools down the saturation level increases until a supersaturated solution is formed. The second method is to dissolve the desired solid in a solvent then allow this solvent to evaporate, reducing the amount of solvent until supersaturation occurs. The final method is to add an antisolvent, either by vapour or liquid diffusion. This involves adding a second solvent, called an antisolvent, in which the solute is not soluble. As the antisovent:solvent ratio of the solution increases, the solute becomes less soluble, finally forming a supersaturated solution.[48] Supersaturated solutions are metastable and convert over time to a solid, the desired crystals or a precipitate, and a saturated solution. For crystals to form nucleation must occur.[47] To prevent too many nucleation points from forming, which would result in many small crystals which may agglomerate, the level of supersaturation must be increased slowly. This is achieved by slowing down the rate of cooling,[49] solvent evaporation or antisolvent addition.[50] There are two types of nucleation: heterogeneous and homogeneous.

Homogeneous nucleation is where the solution nucleates itself without external influence. Classical nucleation theory states that nucleation occurs due to fluctuations in concentration which occur when multiple molecules of the solute come together, this is a statistical event in a fluid system which must overcome a kinetic barrier.[51] The more concentrated the solution, the higher the probability of molecules of solute being near each other, so the more supersaturated a solution, the more likely nucleation is to occur. For a nucleus to form the surface energy of the forming nucleus must be less than that of the bulk solution, which requires a critical minimum size for the surface energy to reduced adequately,[52] as illustrated in Figure 1.2. This critical radius is system dependant and not predictable. As crystals form, the smaller crystals, which have higher surface energy so are less stable than larger particles. The smaller crystals dissolve and the dissolved material adds to the larger crystals, promoting their growth. This mechanism of crystal dissolution and growth, where the small crystals dissolve and the large particles grow, is called Ostwald ripening.[53,54] To calculate the rate of nucleation, classical nucleation theory assumes that the nuclei which form have the same structure and properties as the final crystal.[51] Ostwald's rule of stages states that in polymorphic systems the less stable polymorph will form first then convert to the more stable polymorph over time,[55] so in polymorphic systems calculation of rate using classical nucleation theory is not accurate.[56] An example of this if the crystallisation of calcium carbonate which is reported to first precipitate as an amorphous form and converting to a more stable crystal after.[57]
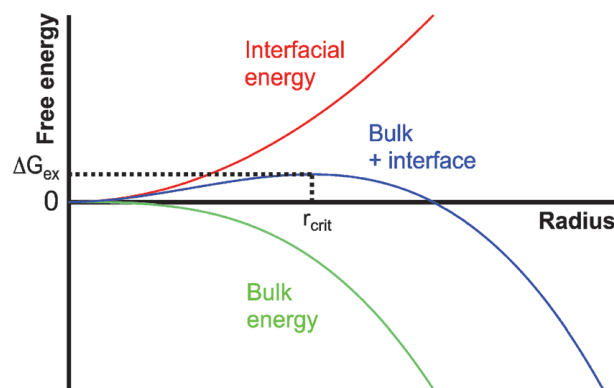
Figure 1.2 – Graph of free energy against radius showing how size dictates the energetics of nuclei in solution in classical nucleation theory.[56]

To further classical nucleation theory, pre-nucleation clusters have been proposed. Pre-nucleation clusters are defined be Gebauer *et al.*[56] as small, thermodynamically stable species with no official phase boundary between them and the bulk solution, which are highly dynamic and have structural similarities to the polymorph which will form first, which allows for more accurate analysis of polymorphic systems than is possible with classical

nucleation theory. Pre-nucleation clusters can involve more than one species, for example solvent molecules could have a role in pre-nuclei whilst not appearing in the final crystal structure. As pre-nucleation theory does not treat nuclei the same as the bulk material, much more accurate models of nucleation can be achieved than in classical nucleation theory.

Melt crystallisation often proceeds by homogeneous nucleation. Upon cooling a metastable state is reached, similar to supersaturation in solutions, where it begins to be more stable to have two phases: the molten product and crystals. Forming crystals from a melt is highly dependent on the rate of cooling.[45,51] Crystals are more thermodynamically stable than amorphous forms so slow cooling allows for the more stable, crystalline phase to form.

Heterogeneous nucleation is where an entity which is not the desired crystal, nucleates crystal formation. Heterogeneous nucleation can occur at interfaces between solutions, at defects or scratches in the crystallisation vessel, by pieces of dust or other contaminants. Heterogeneous nucleation lowers the energetic barrier for crystal formation as the interfacial energy between the heterogeneous nucleus and the forming crystal is less than the interfacial energy between the crystal and bulk solution.[52] As well as lowering the barrier to crystallisation, heterogeneous nucleation can lead to particular crystal shapes or polymorphs forming. In nature, heterogeneous nucleation is used to uniformly form crystals, one example of which is the growth of hydroxyapatite crystals,[52] which make bones hard and stiff. It is believed that the periodic fashion in which the collagen fibres in bones pack, results in the uniform size and orientation of the apatite crystals. Microemulsions[58,59] and gels[60] heterogeneously nucleate supersaturated solutions. This can aid polymorph selectivity by supplying nucleation points which lower the thermodynamic energy barrier to crystallisation as well as offering a unique enclosed environment which may favour certain polymorphs.

Secondary nucleation occurs when an already formed crystal nucleates crystal growth.[61] Seeding is a form of secondary nucleation which is used to promote and control crystallisation.[47] A small amount of crystalline material is added to a supersaturated solution, this solid material nucleates the solution, allowing crystal growth on its surface. One use of seeding is used to promote protein crystal growth.[62] There has been extensive work into looking for a 'universal nucleant' which would cause any protein to crystallise, making protein crystallisation a much more reproducible and simple endeavour.[63] Whilst no perfect solution has been found, limited success has been achieved with charged surfaces, epitaxy[64] and porous materials.[65] Another commonly employed use for seeding is selectively forming a particular polymorph. Polymorphs of the same chemical can have varying physical properties, such as solubility and melting point.[45] Controlling which polymorph forms is

important in a variety of applications. The exact polymorph can change the colour of a pigment,[66] decrease or increase the efficiency of explosives[67] and vary the bioavailability of drugs.[68,69] A small crystal of the desired polymorph is added to the supersaturated solution. This acts as a nucleation point and promotes formation of the same polymorph which was used to seed.

So far, the focus has been on crystallising single components. Sometimes in solvent crystallisations the solvent becomes part of the crystal structure, creating solvates. Not only solvent, but a whole host of other materials can be incorporated into crystal, creating multicomponent crystals.

1.3 Multicomponent crystals

1.3.1 Cocrystals

By the classification system by Grothe *et al*.[70] a cocrystal is a crystal containing two or more coformers which are defined as neutral components which are solid at room temperature which is defined as 293.15 K. The cocrystal classification can be broken down into four sub classifications: true cocrystals containing only coformers; solvate cocrystals containing two or more coformers and a one or more solvent molecules; salt cocrystals contain two or more ions and at least one coformer and finally cocrystal salt solvates which contain at least two ions, one or more solvent molecule and one or more coformer. A cocrystal can show different physical properties to the pure sample, such as variations in melting point and often a change in the solubility. Similar to polymorph selection, the variation in cocrystal solubility is of particular interest in pharmaceutics to aid the bioavailability of poorly water soluble drugs and possibly give an easy route to patenting a product without going through the full clinical trials required by analogues.[71]

There exists a list of potential cocrystallising compounds (coformers) which are generally recognised as safe (GRAS) which forms the foundation of cocrystal screening in the pharmaceutical industry. A few programs, such as COSMOfrag,[72] exist to calculate the expected interaction between a compound and this list of additives. The top 10% of additives which are shown to be eligible are usually chosen for further screening. This at the time of writing results in 37 potential additives, which is not an insignificant number to work with. After this selection is made, there are two main ways of screening for cocrystals.

The first is to dissolve the two components together and allow the solution to crystallise, often by slow evaporation, but cooling can be also used. This method can run afoul of the difference in solubility between the two components.[73,74] For example, in a 1:1 mixture of A

and B, where B is more soluble, when evaporating crystals of A will form, whilst B will stay in solution, line L in Figure 1.3. There are two options to avoid this. First, mix the components in the ratio of their solubility then evaporate, line P in Figure 1.3. Second, create a saturated (or almost saturated) solution of one component, in this case B, then add small amounts of A, following line R (or Q if almost saturated) on the diagram.
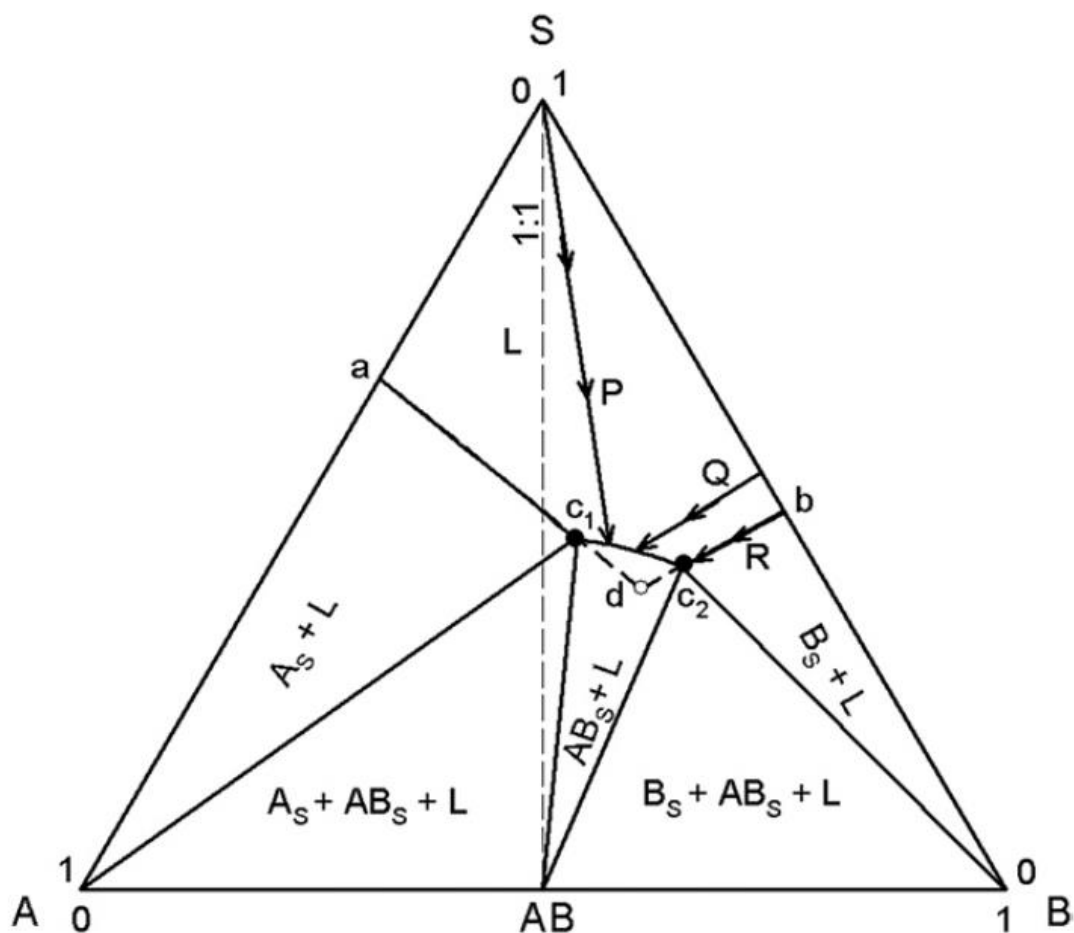
Figure 1.3 - Ternary diagram with coformers A and B, where B is more soluble than A and solvent S. Path L shows the evaporation of a 1:1 mixture of A and B. Path P shows the evaporation of the conformers mixed in the ratio of their solubility. R and Q are A being added to a saturated and nearly saturated solution of B respectively.[73]

The second method of screening is mechanochemistry, such as grinding.[75–78] A mix of components are ground together and then analysed by a technique not requiring single crystals, such as powder x-ray diffraction, IR and Raman spectroscopy. If the interactions are not sufficient for cocrystal formation, the powder pattern will just show a mixture of the two components. In a successful cocrystal formation, a new species, that of the ground cocrystal, should appear. Grinding can be done by hand, in a mortar and pestle, or mechanically in a mill. It can be advantageous to add a small amount of solvent. This increases the surface area by dissolving a small amount of material, so facilitates the interactions between the two components. This is referred to as solvent drop grinding.[79,80] Another method is sonic slurry.

The coformers are added to a solvent in which they are not soluble to make a slurry. This slurry is then sonicated. This mixes the coformers in a similar way to the grinding process, potentially creating a cocrystal powder.[73,78]

1.3.2 Hydrates

Solvates are classified by Grothe *et al.*[70] as crystals contain one or more solvent molecules, with a solvent being defined as a compound which is liquid at 293.15 K and another component. In true solvates this second component is a single coformer; in salt solvates it is two or more ions; in cocrystal solvates it is two or more coformers and in a cocrystal salt solvate it is at least two ions and at least two coformers. Hydrates are the most commonly formed type of solvate. Searching for 'hydrate' in the Cambridge Structure Database (CSD)[81] returns over 83,000 results. The large number of hydrate structures is at least partially due to the ubiquity of water. Water can get into a crystallisation from a damp solvent, absorption from the air, or left over from a previous reaction step.

There is not yet a completely reliable method for reliably predicting the formation of hydrates, or the stoichiometry. Predicting if a hydrate will form is more complicated than simply looking for potential interactions between the molecule and water. Inclusion of hydrogen bonding groups, such as OH, NH or SH, will not necessarily result in a hydrate crystal. For example, 2,4-dihydroxybenzoic acid forms two different hydrates, with different stoichiometry, whilst 2,5-hydroxybenzoic acid forms none, even though they are isomers.[82] Braun *et al.*[82] successfully predicted which hydroxybenzoic acid hydrates would form by comparing calculated lattice energy of the hydrate structures to the lattice energies of a selection of ice polymorphs. Those with a more negative lattice energy than ice, or that fall within the range of the ice polymorphs, are capable of forming hydrated crystals. The predictions held true for which hydrates of 2,4-dihydroxybenzoic acid will form and that 2,5-hydroxybenzoic acid forms none, though the relative stability of the structures was not successfully predicted. Whilst a promising start into hydrate prediction, there are improvements to be made before this method can be applied reliably to other systems.

Even though there are not steadfast rules, analyses of the CSD has given rise to a number of general trends.[83] The more hydrogen bonding groups that there are and the greater polarity a molecule has, the more likely for a hydrate to form. Also, a molecule which has more hydrogen bond accepting groups than donating groups, will mainly accept hydrogen bonds from water. Similarly if a molecule had more hydrogen bond donating groups than accepting groups, it will mostly donate hydrogen bonds to water. Water's ability to donate and accept multiple hydrogen bonds allows molecules with inequality in the number of donor and

acceptor groups to maximise the number of hydrogen bonds formed by hydrogen bonding with water molecules. This makes a more thermodynamically stable crystal structure and is suggested to be a possible driving force for hydrate formation.[83] This has not been proven though, as there is no correlation between the inequality in donor and acceptor groups and the formation of hydrates.[83]

In a system where there are multiple water molecules for every molecule of the crystal forming species, these water molecules hydrogen bond together. There is a range of commonly formed motifs, that almost all hydrate structures fall into.[84] There are five classifications of hydrogen bonded water motifs in hydrates and a sixth that is for the unclassified:

Discrete chains – a single water molecule or a small number of water molecules bonded acyclicly

Discrete rings – isolated rings of water atoms

Infinite chains – one dimensional lines of water with no rings

Infinite tapes – one dimensional, involves rings

Infinite layers – two dimensional layer, involves rings

Unclassified – complexes networks, possibly contains a mixture of the other classifications.

As most arrangements of water have been seen in a crystal structure before, there is debate on the novelty and use of trying to identify more hydrates. In a critical review on the matter, Mascal *et al.*[85] conclude that a new hydrate structure is probably in itself not novel, interesting or giving any specific information about the system studied. But as part of a whole, included with every other hydrate structure known, it adds to the collective information of the interaction of water with an immense range of different compounds, adding to the overall story of how water freezes in different environments.

1.4 Coamorphous materials

There are occasions where crystalline products are not desirable and instead an amorphous solid is required. One example of this is the prevention of ice crystals forming in ice cream. To help prevent ice formation and keep the texture smooth polymeric additives, such as guar gum, are added.[86,87] In the pharmaceutical industry coamorphous materials are of particular importance. As previously described in section 1.1, many drug molecules are highly polymorphic and making sure that only one polymorph is formed reliably on an industrial

scale can be challenging and variations in polymorph can result in variations in dosage and efficiency. Stabilising the amorphous form of a drug is a desirable alternative, as it is can be easier than harvesting a single polymorph, especially if the polymorph required readily converts to a different crystal form, or multiple forms crystallise from similar conditions. Amorphous materials are less thermodynamically stable than crystalline forms of the same chemical, this results in a higher solubility of the amorphous forms. With respect to drug formulation, this can lead to better bioavailability as more of the drug can dissolve. The exact degree of solubility improvement can be difficult to quantify as the metastable nature of amorphous forms may result in conversion to a crystal form before an accurate value has been recorded. Calculations based on the thermodynamic stability of the amorphous and crystalline forms of drugs predict increases in solubility between 10 and 1600 times greater for the amorphous form than the most stable crystal form.[88] In reality, values between 1.4 and 10 have been recorded,[89–93] though it has been suggested that only low levels of amorphous material, 10 % or less, can increase the solubility two fold or more.[88]

Amorphous drug formulations are often stabilised by dispersing the drug in a glassy polymer, such as PVP.[94–97] This stabilisation arises from decreasing the molecular mobility of the drug molecules.[98] Polymers can often have a relatively high glass transition temperature, $T_{g'}$ when compared to drug molecules and dispersion in the glassy polymer inhibits molecular mobility enough to prevent the rearrangement necessary for crystallisation. Chemical bonding, such as hydrogen bonding to the carbonyl groups in PVP, further lowers the molecular mobility of the drug molecules, increasing the amorphous stability. The down side of using polymers such as PVP, is that many which have enough interaction with the drug molecules to be effective stabilisers, also interact with water.[99] This leads to moisture uptake from the air. The water acts as a plasticiser, increasing molecular mobility and promoting crystallisation.[100] Another potential issue with hydrophilic polymers as amorphous stabilisers is the miscibility of the polymer and drug.[101] Poor miscibility requires a high loading of polymer which results in either large pills, or multiple pills, to achieve the necessary therapeutic dose.

To avoid complication due to moisture uptake and poor polymer miscibility, small molecule stabilisers have been investigated. In some cases, a second drug molecule can stabilise the amorphous form as well as administer two drugs at once.[102] Amino acids have also been tested, as many drugs interact with proteins in the body, it stands to reason that amino acids may interact with drug molecules outside of the body.[103,104] ROY (5-methyl-2-[(2-nitro-phenyl)amino]-3-thiophenecarbonitrile), standing for red, orange, yellow which are the colours of its many polymorphs, is a precursor to the antipsychotic drug olanzapine. ROY has

been extensively studied as it is highly polymorphic with 10 forms found so far.[105,106] Corner *et al.*[107] found it is possible to stabilise the amorphous form of ROY using pyrogallol which showed comparable efficiency to amorphous ROY stabilised with PVP.

1.5   Project aims and overview

The aim of this project is to get closer towards fully understanding how PVCap and PVP prevent clathrate hydrate formation by exploring the interactions of low molecular weight model compounds in a variety of different situations. In chapter 2, the synthesis of model compounds to mimic the KHIs is covered.

Chapter 3 covers attempts to cocrystallise the model compounds. The ideal conclusion would be to achieve a hydrated crystal which would allow observation of how the model compounds interact with water, though interactions with coformer without water would also give information on the behaviour of the model compounds.

Chapter 4 covers the crosslinking of guar using cocrystals of the model compounds. It is explored whether the interactions which hold the cocrystal together are persistent enough in solution to modify the reaction of boronic acids with guar.

The effects of the acid gases H_2S and CO_2 on the interactions of KHIs with water is explored in chapter 5. Clathrate hydrates are especially troublesome and dangerous in sour gas pipelines and it has been observed that more inhibitor must be added to control their formation.[13] Section 5 investigates if the acid gases interfere with the KHIs interactions with water.

Neutron scattering is used in chapter 6 to study butoxyethanol and PVCap in water. Butoxyethanol is a known synergist for PVCap.[24] Small angle neutron scattering (SANS) was used to try and visualise any interactions between PVCap and butoxyethanol.

Finally chapter 7 tests the model compounds' efficiency at stabilising amorphous forms of drugs. PVP is a used amorphous stabiliser,[94–97] so low molecular weight compounds designed to mimic PVP may also be capable at stabilising amorphous forms.

1.6   References

(1)   Natural Gas Infrastructure Implications of Increased Demand from the Electric Power Sector   http://energy.gov/sites/prod/files/2015/02/f19/DOE Report Natural Gas Infrastructure V_02-02.pdf.

(2)   Goodwin, M. J.; Musa, O. M.; Steed, J. W. *Energy Fuels* **2015**, *29* (8), 4667–4682.

(3)   Zarinabadi, S.; Samimi, A. *J. Am. Sci.* **2012**, *8* (8), 1007–1010.

(4)   Strobel, T. A.; Hester, K. C.; Koh, C. A.; Sum, A. K.; Sloan, E. D. *Chem. Phys. Lett.* **2009**, *478* (4–6), 97–109.

(5)   von Stackelberg, M. *Rec. Trav. Chim. Pays-Bas* **1956**, *75* (8), 902–905.

(6)   Steed, J. W.; Atwood, J. L. *Supramolecular Chemistry*, Second Edi.; Wiley, 2009.

(7)   Kuhs, W. F.; Klapproth, A.; Gotthardt, F.; Techmer, K.; Heinrichs, T. *Geophys. Res. Lett.* **2000**, *27* (18), 2929–2932.

(8)   Rodger, P. M. *J. Phys. Chem.* **1990**, No. 94, 6080–6089.

(9)   van der Waals, J. H.; Platteuw, J. C. *Adv. Phys. Chem.* **1959**, No. 2, 1–57.

(10)   Jeffrey, G. A. *J. Incl. Phenom.* **1984**, *1* (3), 211–222.

(11)   Alavi, S.; Udachin, K.; Ripmeester, J. A. *Chem. Eur. J.* **2010**, *16* (3), 1017–1025.

(12)   Carroll, J. J. In *Annual GPA Convention*; 2002.

(13)   Thieu, V.; Frostman, L. M. In *SPE International Symposium on Oilfield Chemistry*; 2005.

(14)   Ripmeester, J. A.; Tse, J. S.; Ratcliffe, C. I.; Powell, B. M. *Nature* **1987**, *325*, 135–136.

(15)   Sloan, E. D.; Koh, C. *Clathrate Hydrates of Natural Gases*, Third Edit.; CRC Press, 2007.

(16)   Schicks, J. M.; Lu, H.; Ripmeester, J. A.; Ziemann, M. In *International Conference on Gas Hydrates*; Vancouver, Canada, 2008.

(17)   Kastner, M.; Kvenvolden, K. A.; Lorenson, T. D. *Earth Planet. Sci. Lett.* **1998**, *156*, 173–183.

(18)   Kelland, M. A. *Energy Fuels* **2006**, *20* (3), 825–847.

(19)   McDonald, H. J.; Spitzer, R. H. *Circ. Res.* **1953**, *1* (5), 396–404.

(20)   Micchelli, A. L.; Koehler, F. T. *J. Soc. Cosmet. Chem.* **1968**, *19*, 863–880.

(21)   Ohno, H.; Susilo, R.; Gordienko, R.; Ripmeester, J.; Walker, V. K. *Chem. Eur. J.* **2010**, *16* (34), 10409–10417.

(22)   Notz, P. K.; Bumgardner, S. B.; Schaneman, B. D.; Todd, J. L. In *Offshore Technology Conference*; Houston, Texas, 1995.

(23)   Chua, P. C.; Kelland, M.; Reilly, R. O.; Ieong, N. S. In *7th International Conference on Gas Hydrates*; Edinburgh, Scotland, 2011.

(24)   Perrin, A.; Musa, O. M.; Steed, J. W. *Chem. Soc. Rev.* **2013**, *42* (5), 1996–2015.

(25)   Musa, O.; Lei, C. Polymers Having Acid and Amide Moieties and Uses Thereof. WO20130123147, 2011.

(26)   Musa, O. M.; Cuiyue, L. Musa, O M Cuiyue, L. WO2010117660, 2010.

(27)   Leinweber, D.; Roesch, A.; Schaefer, C. Additives for Inhibiting Gas Hydrate Formation. CA2766617A1, 2010.

(28)   Erfani, A.; Varaminian, F.; Muhammadi, M. In *2nd National Iranian Conference on Gas Hydrate*; 2013.

(29)   Yeh, Y.; Feeney, R. E. *Chem. Rev.* **1996**, *96* (2), 601–618.

(30)   Hayashi, H.; Udagawa, Y. *Bull. Chem. Soc. Jpn.* **1992**, *65*, 600–602.

(31)   Quirion, F.; Magid, L. J.; Drifford, M. *Langmuir* **1990**, *6*, 244–249.

(32)   D'Arrigo, G.; Teixeira, J.; Giordano, R.; Mallamace, F. *J. Chem. Phys.* **1991**, *95* (4), 2732.

(33)   D'Arrigo, G.; Giordano, R.; Teixeira, J. *Phys. Scr.* **1992**, *T45*, 248–250.

(34)   D'Arrigo, G.; Giordano, R.; Teixeira, J. *J. Mol. Struct.* **1997**, *404*, 319–334.

(35)   Ito, N.; Fujiyama, T.; Udagawa, Y. *Bull. Chem. Soc. Jpn.* **1983**, *56*, 379–385.

(36)   Sun, M.; Firoozabadi, A. *J. Colloid Interface Sci.* **2013**, *402*, 312–319.

(37)   Davenport, J. R.; Musa, O. M.; Paterson, M. J.; Piepenbrock, M.-O. M.; Fucke, K.; Steed, J. W. *Chem. Commun.* **2011**, *47* (35), 9891–9893.

(38)   Kuznetsova, T.; Sapronova, A.; Kvamme, B.; Johannsen, K.; Haug, J. *Macromol. Symp.* **2010**, *287*, 168–176.

(39)   Sloan, E. D.; Subramanian, S.; Matthews, P. N.; Lederhos, J. P.; Khokhar, A. A. *Ind. Eng. Chem. Res.* **1998**, *37* (8), 3124–3132.

(40)   Hutter, J. L.; King, H. E. J.; Lin, M. Y. *Macromol.* **2000**, *33* (7), 1–17.

(41)   Anderson, B. J.; Tester, J. W.; Borghi, G. P.; Trout, B. L. *J. Am. Chem. Soc.* **2005**, *127* (50), 17852–17862.

(42)   Moon, C.; Hawtin, R. W.; Rodger, P. M. *Faraday Discuss.* **2007**, *136*, 367-382.

(43)   Goodman, D. W. *Chem. Rev.* **1995**, *95* (3), 523–536.

(44)   Gates, B. C. *Top. Catal.* **2000**, *14* (1–4), 173–180.

(45)   Aaltonen, J.; Allesø, M.; Mirza, S.; Koradia, V.; Gordon, K. C.; Rantanen, J. *Eur. J. Pharm. Biopharm.* **2009**, *71* (1), 23–37.

(46)   Mersmann, A. *Crystallization Technology Handbook*, Second Edi.; CRC Press: New York, Basel, 2001.

(47)   Coquerel, G. *Chem. Soc. Rev.* **2014**, *43* (7), 2286–2300.

(48)   Mostafa Nowee, S.; Abbas, A.; Romagnoli, J. A. *Chem. Eng. Sci.* **2008**, *63* (22), 5457–5467.

(49)   Lang, Y.; Cervantes, A. M.; Biegler, L. T. *Ind. Eng. Chem. Res.* **1999**, *38* (4), 1469–1477.

(50)   Yu, Z. Q.; Tan, R. B. H.; Chow, P. S. *J. Cryst. Growth* **2005**, *279*, 477–488.

(51)   Oxtoby, D. W. *J. Phys. Condens. Matter* **1992**, *4* (38), 7627–7650.

(52)   De Yoreo, J. J.; Vekilov, P. G. *Rev. Miner. Geochem.* **2003**, *54* (1), 57–93.

(53)   Voorhees, P. W. *Annu. Rev. Mater. Sci.* **1992**, *22*, 197–215.

(54)   Niethammer, B. In *Analysis and Stochastics of Growth Processes and Interface Models*; Mörters, P., Moser, R., Penrose, M., Schwetlick, H., Zimmer, J., Eds.; Oxford University Press: Oxford, 2008.

(55)   Nyvlt, J. *Cryst. Res. Tech.* **1995**, *30* (4), 443–449.

(56)   Gebauer, D.; Kellermeier, M.; Gale, J. D.; Bergström, L.; Cölfen, H. *Chem. Soc. Rev.* **2014**, *43* (7), 2348–2371.

(57)   Hu, Q.; Nielsen, M. H.; Freeman, C. L.; Hamm, L. M.; Tao, J.; Lee, J. R. I.; Han, T. Y. J.; Becker, U.; Harding, J. H.; Dove, P. M.; De Yoreo, J. J. *Faraday Discuss.* **2012**, *159*, 509-523.

(58)   Chen, C.; Cook, O.; Nicholson, C. E.; Cooper, S. J. *Cryst. Growth Des.* **2011**, *11* (6), 2228–2237.

(59)   Nicholson, C. E.; Cooper, S. J. *Crystals* **2011**, *1* (4), 195–205.

(60)   Kumar, D. K.; Steed, J. W. *Chem. Soc. Rev.* **2014**, *43* (7), 2080–2088.

(61)   Botsaris, G. D. In *Industrial Crystallization*; Mullin, J. W., Plenum Press: New York, London, 1976.

(62)   Chayen, N. E. *Prog. Biophys. Mol. Biol.* **2005**, *88* (3), 329–337.

(63)   Chayen, N. E. *Curr. Opin. Struct. Biol.* **2004**, *14* (5), 577–583.

(64)   McPherson, A. *Crystallization of Biological Macromolecules. Cold Spring Harbor Laboratory Press, Cold Spring Harbor*; Cold Spring Harbor Laboratory Press: Cold Spring Harbor, 1999.

(65)   Chayen, N. E. *J. Mol. Biol.* **2001**, *312*, 591–595.

(66)   Zollinger, H. *Color Chemistry: Synthesis, Properties and Applications of Organic Dyes and Pigments*, Third Edit.; John Wiley & Sons: Zurich, Weinheim, 2003.

(67)   Larionov, L. V. *Combust. Explos. Shock Waves.* **1997**, *33* (5), 605–610.

(68)   Blandizzi, C.; Viscomi, G. C.; Scarpignato, C. *Drug Des. Dev. Ther.* **2014**, *9*, 1–11.

(69)   Bernstein, J. *Polymorphism in molecular crystals*; Oxford Science Publications: Oxford, 2007.

(70)   Grothe, E.; Meekes, H.; Vlieg, E.; Ter Horst, J. H.; De Gelder, R. *Cryst. Growth Des.* **2016**, *16* (6), 3237–3243.

(71)   Steed, J. W. *Trends Pharmacol. Sci.* **2013**, *34* (3), 185–193.

(72)   Hornig, M.; Klamt, A. *J. Chem. Inf. Model.* **2005**, *45* (5), 1169–1177.

(73)   Childs, S. L.; Rodríguez-Hornedo, N.; Reddy, L. S.; Jayasankar, A.; Maheshwari, C.; McCausland, L.; Shipplett, R.; Stahly, B. C. *Cryst. Eng. Comm.* **2008**, *10* (7), 856-864.

(74)   Chiarella, R. A.; Davey, R. J.; Peterson, M. L. *Cryst. Growth Des.* **2007**, *7*, 1223–1226.

(75)   Trask, A. V; Jones, W. *Top. Curr. Chem.* **2005**, *254*, 41–70.

(76)   Friščić, T.; Jones, W. *Cryst. Growth Des.* **2009**, *9* (3), 1621–1637.

(77)   Kaupp, G. *Cryst. Eng. Comm.* **2009**, *11* (3), 470-481.

(78)   Weyna, D. R.; Shattock, T.; Vishweshwar, P.; Zaworotko, M. J. *Cryst. Growth Des.* **2009**, *9* (2), 1106–1123.

(79)   Trask, A. V; Motherwell, W. D. S.; Jones, W. *Chem. Commun.* **2004**, No. 7, 890–891.

(80)   Shan, N.; Toda, F.; Jones, W. *Chem. Commun.* **2002**, No. 20, 2372–2373.

(81)   Allen, F. H. *Acta Crystallogr. Sect. B-Struct. Sci.* **2002**, *58* (3), 380–388.

(82)   Braun, D. E.; Karamertzanis, P. G.; Price, S. L. *Chem. Commun.* **2011**, *47* (19), 5443–5445.

(83)   Infantes, L.; Fábián, L.; Motherwell, W. D. S. *Cryst. Eng. Comm.* **2007**, *9* (1), 65.

(84)   Infantes, L.; Motherwell, S. *Cryst. Eng. Comm.* **2002**, *4* (75), 454.

(85)   Mascal, M.; Infantes, L.; Chisholm, J. *Angew. Chem. Int. Ed. Engl.* **2005**, *45* (1), 32–36.

(86)   Wang, S. T.; Barringer, S. A.; Hansen, P. M. T. *Food Hydrocoll.* **1998**, *12* (2), 211–215.

(87)   Adapa, S.; Schmidt, K. A.; Jeon, I. J.; Hereld, T. J.; FLores, R. A. *Food Revi. Int.* **2000**, *16* (3), 259–271.

(88)   Hancock, B. C.; Parks, M. *Pharm. Res.* **2000**, *17* (4), 397–404.

(89)   Sato, T.; Okada, A.; Sekiguchi, K.; Tsuda, Y. *Chem. Pharm. Bull.* **1981**, *29*, 2675–2682.

(90)   Mullins, J. D.; Macek, T. J. *J. Pharm. Sci.* **1960**, *49*, 245–248.

(91)   Imaizumi, H. *Chem. Pharm. Bull.* **1980**, *28*, 2565–2569.

(92)   Egawa, H.; S, M.; Yonemochi, E.; Oguchi, T.; Yamamoto, K.; Nakai, Y. *Chem. Pharm. Bull.* **1992**, *40*, 819–820.

(93)   Miyazaki, S.; Hori, R.; Arita, T. *Yakugaku Zasshi* **1975**, *95*, 629–633.

(94)   Lindfors, L.; Skantze, P.; Skantze, U.; Rasmusson, M.; Zackrisson, A.; Olsson, U. *Langmuir* **2006**, *22* (3), 906–910.

(95)   Nidhi, K.; Indrajeet, S.; Khushboo, M.; Gauri, K.; Sen, D. J. *Int. J. Drug Dev. Res.* **2011**, *3* (2), 26–33.

(96)   Pokharkar, V. B.; Mandpe, L. P.; Padamwar, M. N.; Ambike, A. A.; Mahadik, K. R.; Paradkar, A. *Powder Technol.* **2006**, *167* (1), 20–25.

(97)   Kaushal, A. M.; Gupta, P.; Bansal, A. K. *Crit. Rev. Ther. Drug Carr. Syst.* **2004**, *21*, 133–193.

(98)   Löbmann, K.; Laitinen, R.; Grohganz, H.; Gordon, K. C.; Strachan, C.; Rades, T. *Mol. Pharm.* **2011**, *8* (5), 1919–1928.

(99)   Rumondor, A. C.; Taylor, L. S. *Mol. Pharm.* **2010**, *7* (2), 477–490.

(100) Florence, A. T.; Attwood, D. *Physicochemical Principles of Pharmacy: In Manufacture, Formulation and Clinical Use*, Sixth Edit.; Pharmaceutical Press: London, 2015.

(101) Serajuddin, A. T. M. *J. Pharm. Sci.* **1999**, *88* (10), 1058–1066.

(102) Löbmann, K.; Strachan, C.; Grohganz, H.; Rades, T.; Korhonen, O.; Laitinen, R. *Eur. J. Pharm. Biopharm.* **2012**, *81* (1), 159–169.

(103) Löbmann, K.; Grohganz, H.; Laitinen, R.; Strachan, C.; Rades, T. *Eur. J. Pharm. Biopharm.* **2013**, *85*, 873–881.

(104) Löbmann, K.; Laitinen, R.; Strachan, C.; Rades, T.; Grohganz, H. *Eur. J. Pharm. Biopharm.* **2013**, *85*, 882–888.

(105) Chen, S.; Guzei, I. A.; Yu, L. *J. Am. Chem. Soc* **2005**, *127* (27), 9881–9885.

(106) Yu, L. *Acc. Chem. Res.* **2010**, *43* (9), 1257–1266.

(107) Corner, P. A.; Harburn, J. J.; Steed, J. W.; McCabe, J. F.; Berry, D. J. *Chem. Commun.* **2016**, *52*, 6537–6540.

2   Model compounds

2.1   Introduction

The KHIs used in the oilfield industry are all water soluble polymers.[1] Unfortunately polymers are notoriously difficult to study and characterise, as the large molecular weights and polydispersity of the samples makes commonly used analytical techniques, such as NMR spectroscopy, complicated. Well-defined, low molecular weight models of polymers are a useful tool to avoid the difficulties in analysis which arise from high molecular weights. Whilst low molecular weight models are easier to analyse, they may not exhibit the same characteristics or behaviour as the polymer. The nearer to the polymer a model is, the more relevant the data becomes. For example, a dimer is a better model than a monomer and an oligomer is a better model than a dimer, but increasing the chain length of the model soon leads to the same difficulties of analysis as the polymer. Davenport *et al.*[2] previously synthesised a vinylcaprolactam dimer, bisVCap and the hydrogenated version, H$_2$bisVCap to serve as models for PVCap. They went on to show by way of IR and NMR titrations, in which water was added to the model compounds and the polymer, PVCap, that the model compounds interact with water in a way comparable to PVCap, suggesting that the dimers are reasonable compounds to model the polymer.

The aim of this chapter is to synthesise low molecular weight model compounds of common KHIs. The most straightforward models are dimers of vinylpyrrolidone (VP) and vinylcaprolactam (VCap), the monomers used to produce PVP and PVCap respectively. Dimers of VP and VCap, bisVP and bisVCap, and their hydrogenated forms, H$_2$bisVP and H$_2$bisVCap are already known.[2,3] Model compounds containing a pyrrolidone and caprolactam ring are of interest as copolymers of VP and VCap are commercially used as hydrate inhibitors in pipelines.[1] Similarly alcohol and ether functionalities are common in KHI copolymers,[1] leading to new possibilities for low molecular weight model compounds of commercial KHIs.

2.2   Results and discussion

To mimic PVP and PVCap a range of low molecular weight compounds containing pyrrolidone and caprolactam rings have been synthesised as shown in Scheme 2.1. Compounds **6**-**9** have been previously synthesised in the group and **11** was supplied by Ashland Inc. all of which have previously been used by the group.[2,3] Perrin found **11** much more effective than **6**-**9** in

complexing metals,[3,4] so more model compounds containing ether links similar to **11**, compounds **11**-**16**, were designed and synthesised to attempt complexation with metals.

bisVCap (6)   H₂bisVCap (7)   bisVP (8)   H₂bisVP (9)

bisHEP (10)   HEPVCap (11)   MEP (12)   Et(OVCap)₂ (13)

Pr(OVCap)₂ (14)   Et(OVP)₂ (15)   Pr(OVP)₂ (16)
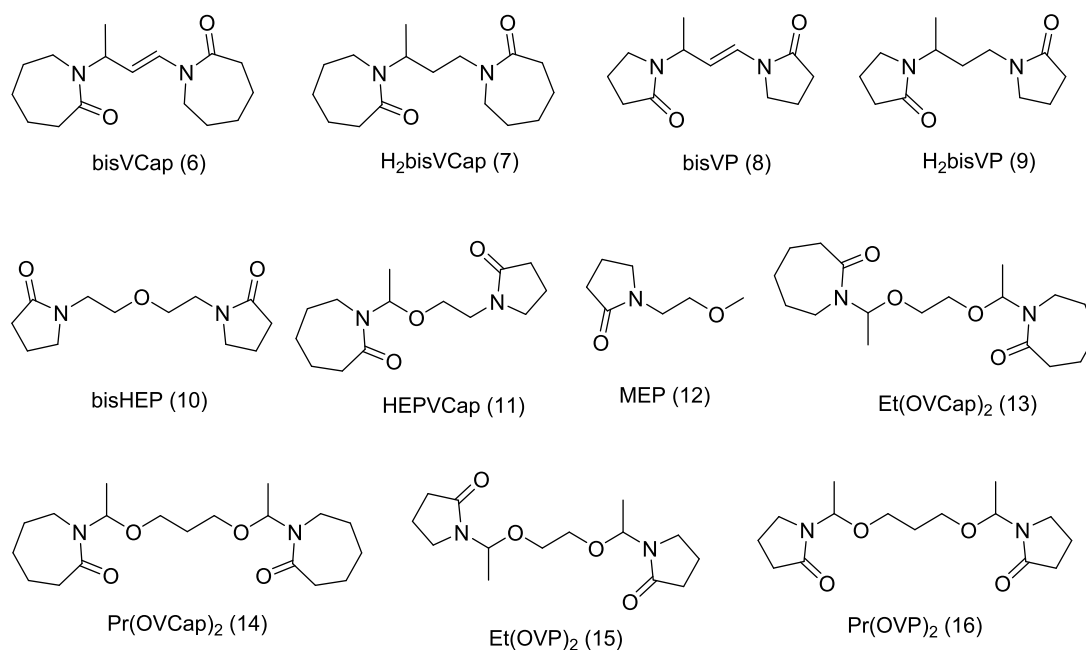
Scheme 2.1 – Structure of the models compounds based on industrially used KHI polymers.

2.2.1   BisVCap and H₂bisVCap

BisVCap was prepared by the method outlined by Davenport *et al.*[2] and resulted in a white powder. The hydrogenation to H₂bisVCap was performed using a balloon of hydrogen and a Pd/C catalyst, resulting in a viscous, pale yellow liquid.

Previously Davenport *et al.* synthesised bisVCap and bisVCap to model PVCap. To prove the validity of the model IR and NMR titrations, where water was added to acetonitrile solution of PVCap, bisVCap and H₂bisVCap and changes in the spectra monitored, were performed. The titrations showed the hydration behaviour of the model compounds, **6** and **7**, to be similar to that of PVCap and thus be appropriate models with which to study the hydrate inhibition effects of PVCap. To further assess the validity of the model compounds, the moisture absorption of PVCap, **5** and **6** was studied using dynamic vapour sorption (DVS).

DVS is used to study the uptake of water by a compounds against humidity. The sample is loaded onto an accurate microbalance and the relative humidity (RH) is increased and decreased. The changes in mass of the sample are measured and plot against RH. This gives information on hydroscopicity and hydrate formation. Samples begin at room humidity, often 40 %RH, the humidity is then increased to 90 %RH, decreased to 0 %RH, increased again to 90 %RH and finally decreased once more to 0 %RH. Percentage mass changes are

calculated using the smallest recorded mass, so if a sample began with some absorbed or adsorbed water which is lost on decreasing the RH, the lowest value, which is the mass closest to the mass of the completely dehydrated sample, is used as the mass of the sample.

In Figure 2.1 the DVS plots for PVP and PVCap can be found. Both show the hysteresis associated with hydroscopic materials which readily hydrate but require a significant decrease in humidity before it starts to lose water again because of the strong interactions between the water and the material. PVP shows a large increase in mass, 39.8 %, which is in agreement with the literature.[5] This mass increase corresponds to 2.5 water molecules per carbonyl group. PVCap on the other hand is less hydroscopic, showing a mass increase of 16.6 % which corresponds to 1.3 water molecules per carbonyl group.
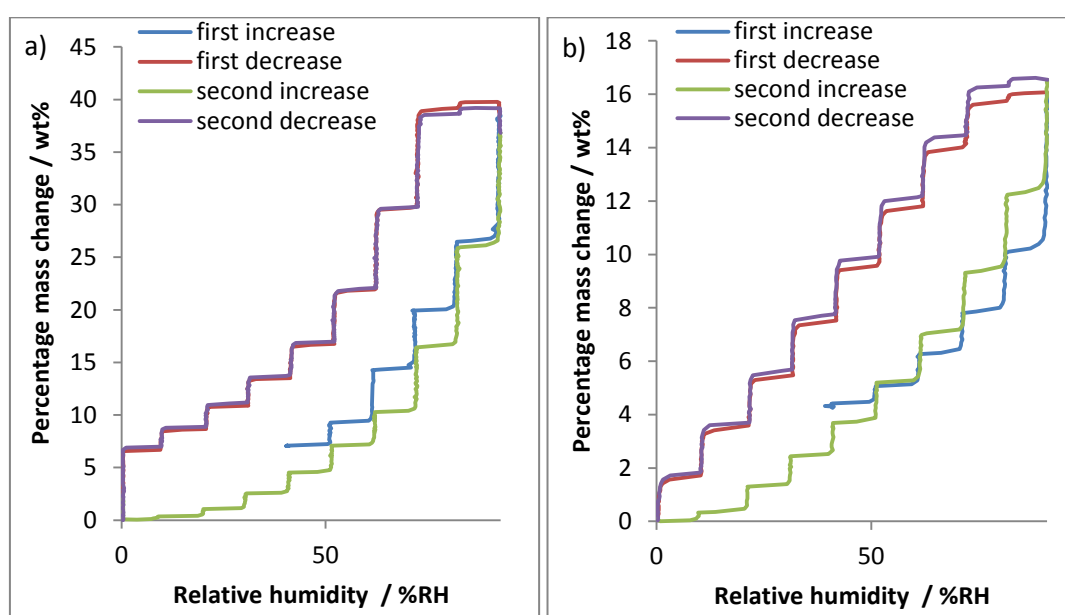
Figure 2.1 - DVS plot of a) PVP and b) PVCap.

The DVS plot for bisVCap, Figure 2.2, does not suggest the formation of any hydrates. The lack of hysteresis and small mass increase, 0.35 %, is indicative of moisture adsorption onto a surface with no strong interactions. As a mass increase of 0.35 % gives 0.05 water molecules per molecule of bisVCap, it is apparent that no hydrate structure is formed.
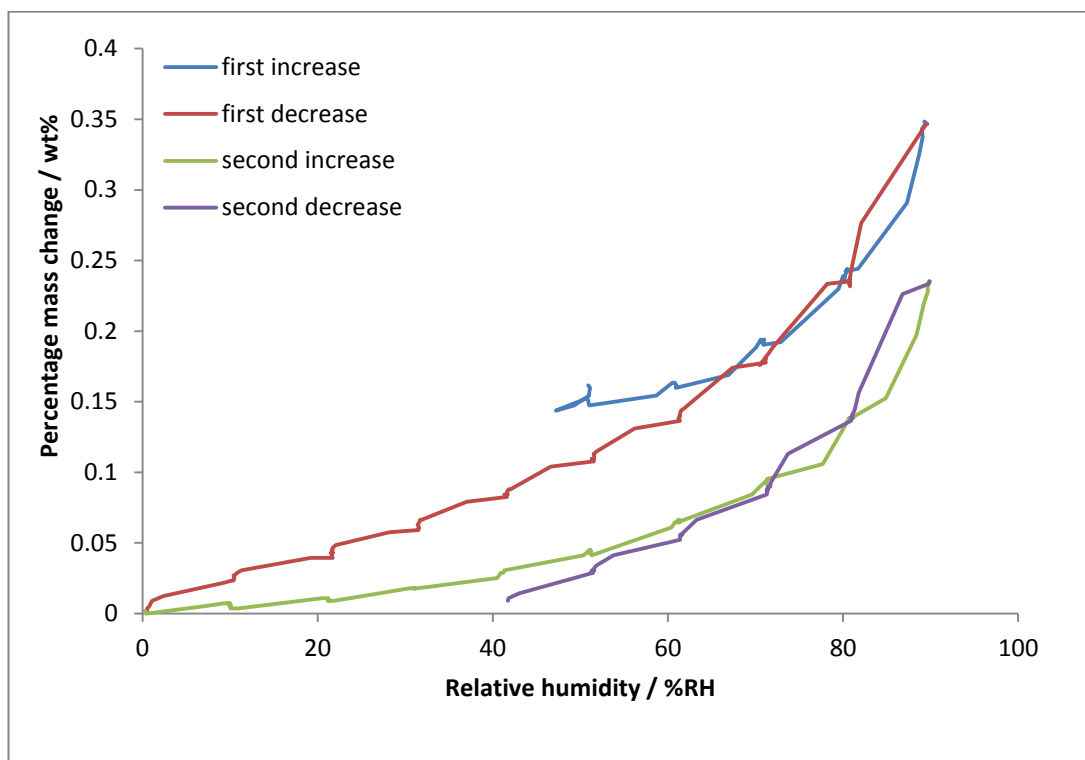
Figure 2.2 - DVS plot of bisVCap.

H_2bisVCap is normally a liquid at room temperature. As a crystal structure has been previously reported on a sample which had undergone very vigorous drying,[2] it is probable that H_2bisVCap is only liquid due to adsorbed water. During the DVS experiment the humidity was first set to 0 %RH and the sample was left until a mass change smaller than 0.001 % was detected to dehydrate the sample as much as is possible in the experimental setup. The humidity was then increased to 90 %RH, decreased to 0 %RH, increased again to 90 %RH. On the final decrease the humidity was only decreased to 40 %RH and a final increase to 96 %RH was performed as can be seen in Figure 2.3. The DVS plot for H_2bisVCap shows a significant hysteresis which is indicative of a hydroscopic material. From the smallest mass to the mass at 90 %RH there is a mass increase of 17.8 %, which corresponds to 2.8 water molecules per molecule of H_2bisVCap. As H_2bisVCap has two carbonyl moieties this results in 1.4 water molecules per carbonyl moiety. This is comparable to the 1.3 water molecules per moiety seen at 90 %RH with PVCap. DVS shows the hydrogenated dimer to be a much better model for H_2bisVCap, as it shows similar hydroscopic nature and the same degree of water adsorption by 90 %RH.
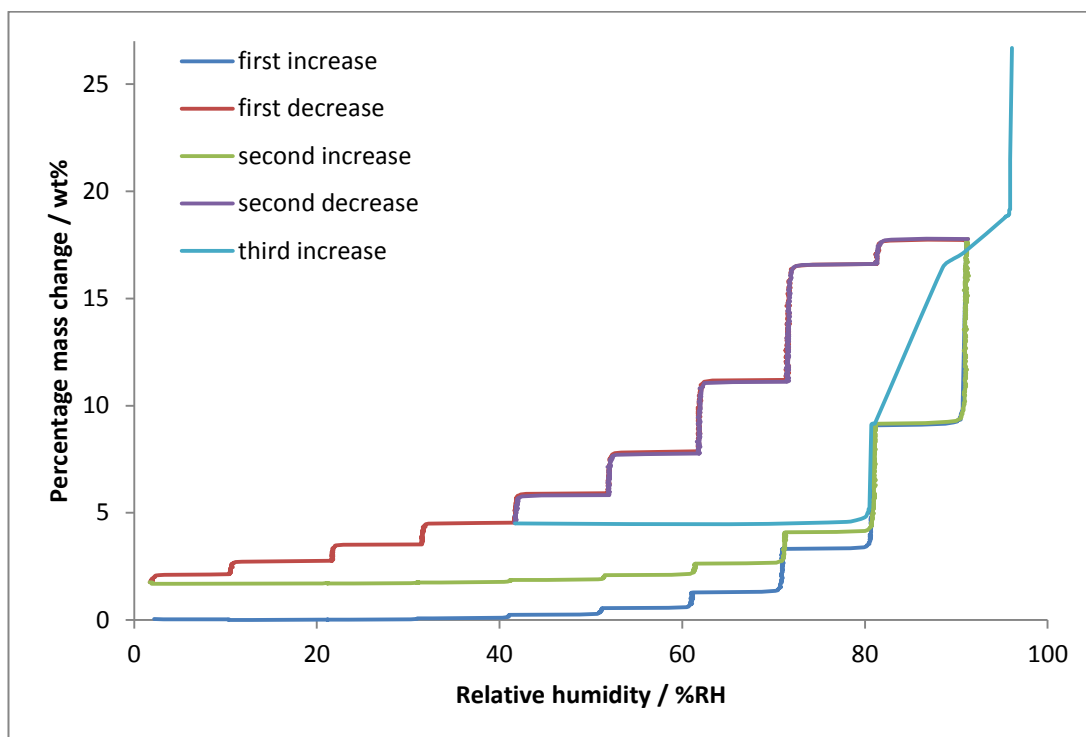
Figure 2.3 - DVS plot of H₂bisVCap.

Upon increasing the humidity to 96 %RH there is a further increase to 26.7 % mass increase. This corresponds to 4.2 water molecules per molecule of H$_2$bisVCap or 2.1 water molecules per carbonyl moiety. In a hydration study on PVP by Kobyakov *et al.*[6] it was proposed that at low water:PVP ratio, 1.7:1 or less, there was a single water molecule hydrogen bonding to the carbonyl groups, Scheme 2.2a, but at higher water:PVP ratio there was two water molecules, one hydrogen bonding to each lone pair of the oxygen, Scheme 2.2b. The absorption of two water molecules per carbonyl group in H$_2$bisVCap at 96 %RH probably follows a similar bonding scheme to that suggested for PVP, with both lone pairs of the carbonyl oxygen atoms hydrogen bonding with water.
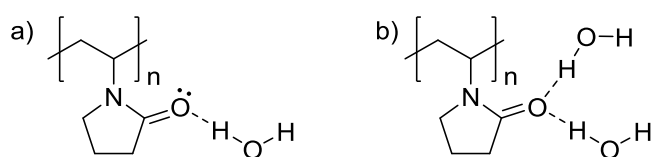
Scheme 2.2 – Schematic of PVP binding a) one water molecule and b) two water molecules as proposed by Kobyakow *et al.*[6]

For comparison a DVS plot of the monomer, VP, was also made. VP is usually not used as a model for PVCap as dimeric molecules are closer in structure to the polymer, so often better models to mimic the polymer. As can be seen in Figure 2.4, VP shows a small amount of hysteresis suggesting some hydroscopic behaviour. The mass increase is 5.4 % which corresponds to 0.4 water molecules per molecule of VP. Whilst the mass increase is greater

than that for bisVCap it is still lower than PVCap or H₂bisVCap, suggesting that whilst VP may show some hydroscopic characteristics, it does not interact as strongly with water as H₂bisVCap or PVCap so is a less suitable model to study PVCap than H₂bisVCap.
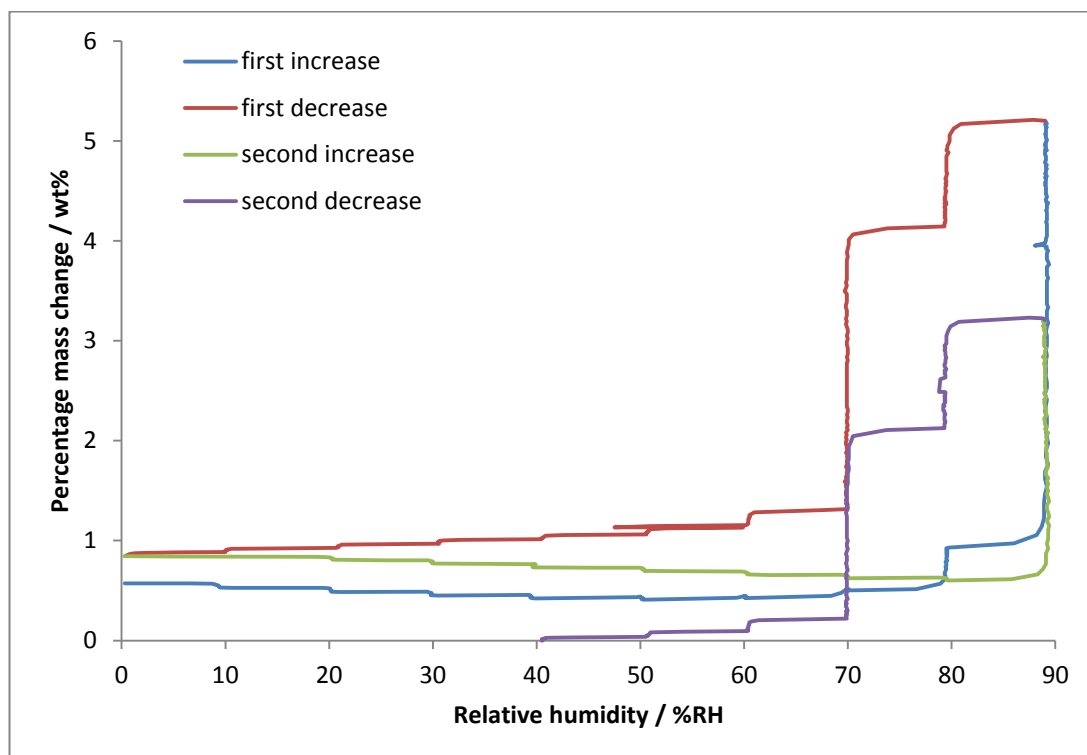
Figure 2.4 - DVS plot of VP.

In conclusion, the hydrogenated dimer, H₂bisVCap, is a good model for PVCap, better than either bisVCap or VCap, which is expected as it is the nearest in structure to PVCap. VCap is a monomer and both VCap and bisVCap have alkene functionalities which are not present in the polymer. The water uptake of H₂bisVCap is very similar to that of PVCap, including a hysteresis from being hydroscopic and adsorbing the same amount of water within error.

2.2.2 BisVP

BisVP was prepared using a modified version of the bisVCap preparation. The synthesis of bisVCap requires the use of trifluoroacetic acid (TFA).[2] In the case of bisVP, trifluoroacetic acid resulted in a very poor yield. Changing the acid catalyst to sulfuric acid proved to be a much more effective, resulting in a 96 % yield. BisVP was isolated from the reaction mixture as a viscous, orange oil and no crystal structure has previously been recorded for this compound. A small amount of impurity, less than 1 % as specified by Sigma Aldrich, present from the starting material, VP, may be part of the cause for this lack of crystallisation, as the weak NMR signals from the impurity visible in the starting material are still present in the product. Attempts to crystallise bisVP by solvent evaporation resulted in thick oils and

crystallisation attempts by freezing gave glassy, non-crystalline materials. As part of the experiments into the effects of sour gases on the interactions of KHIs with water, which are detailed in chapter 5, attempts to form clathrate structures of the model compounds with CO_2 and H_2S were performed. One such experiment involved preparing a solution of bisVP in acetone, bubbling CO_2 through this solution then leaving in the freezer at -20 °C under an atmosphere of CO_2. After 8 months at -20 °C, large yellow needles of diffraction quality were formed and analysed by single crystal x-ray analysis. Even though the crystal structure did not contain CO_2, this is the first crystal structure of bisVP to be recorded. The crystal packing of bisVP can be seen in Figure 2.5.
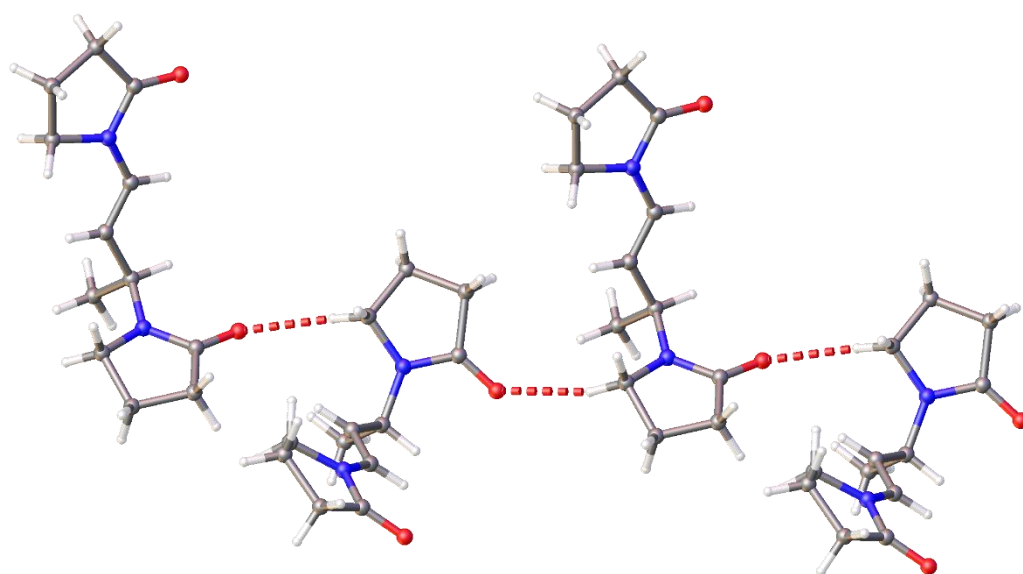
Figure 2.5 – Crystal packing in the structure of bisVP with the C-H···O hydrogen bonds shown by red dashed lines.

The Hirshfeld surface fingerprint plots of bisVP and bisVCap are shown in Figure 2.6. Both fingerprints plots are similarly shaped. The main feature of both fingerprint plots are the peaks symmetrically either side of the diagonal, indicated by arrows. The peak in the upper left of the plot arises hydrogen bond donation of a C-H···O bond, the bottom right from the acceptance of this bond. In both crystal structures this hydrogen bond is between the carbonyl of one lactam ring and a methylene C-H group of a lactam ring in a neighbouring molecule, as is illustrated by red dashed lines in Figure 2.5. The hydrogen bonds in bisVP have a C···O distance of 3.343(3) Å which is very similar to the length of the C-H···O hydrogen bond in the bisVCap crystal structure which has a C···O distance 3.346(2) Å. The fingerprint plot of bisVCap has more diffuse blue area than that seen in the fingerprint plot of bisVP. This diffuse blue area arises from more space in the crystal packing. This is reflected in the density of the two crystal structures, with bisVP being denser, 1.250 g cm^{-3}, than the crystal of bisVCap,

1.231 g cm^{-3}. The pyrrolidone rings of bisVP are smaller and less bulky than the caprolactam rings of bisVCap, allowing for closer packing and thus a denser crystal structure.
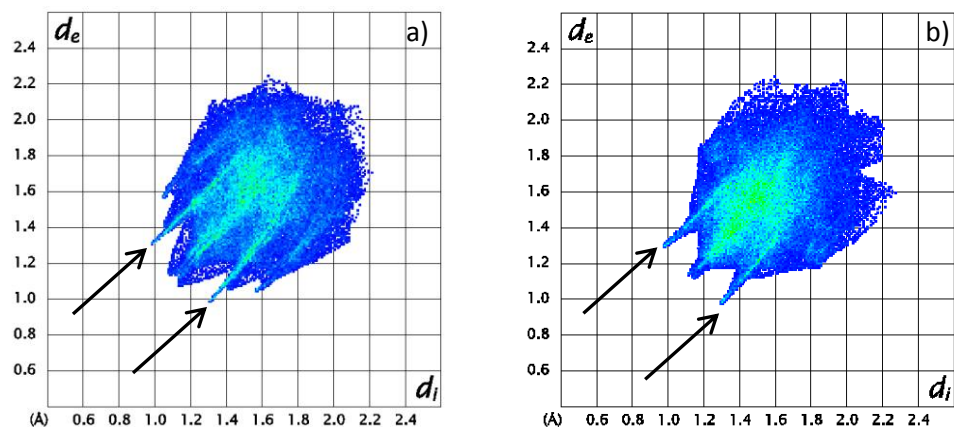
Figure 2.6 – Hirshfeld surface fingerprint plots of a) bisVP and b) bisVCap with the hydrogen bonding interactions shown by black arrows.

2.2.3   H$_2$bisVCap

Hydrogenation of bisVP was attempted using a hydrogen balloon and 5 % Pd/C in methanol heated to 55 °C for 6 hours. Whilst this method was adequate for hydrogenating bisVCap, it did not give satisfactory results with bisVP. Only around 85 % conversion, measured by ^{1}H NMR, was achieved and attempts to separate the hydrogenated dimer from the starting material using a column were challenging, resulting in broad peaks and many small unidentified peaks in the ^{1}H NMR spectrum suggesting the product decomposes and possibly polymerises on silica.

Compared to the hydrogen balloon reaction setup, a much higher pressure of hydrogen can be achieved using continuous flow hydrogenation equipment such the ThalesNano H-cube.[7] This often leads to greater selectivity and much higher yields. The ThalesNano H-cube can be used with a range of different catalysts, supplied in sealed cartridges.[2] The hydrogenation of bisVP was attempted with three different catalyst cartridges: 10 % Pd/C, 5 % Ru/C and Raney Nickel. All experiments were carried out at 60 °C in methanol.

None of the catalysts tested gave the desired 100 % conversion. In the experiment using the 10 % Pd/C catalyst 92 % conversion was achieved. The reaction mixture was reacted a second time using the 10 % Pd/C catalyst to see if a better yield could be achieved. After the second reaction a slight improvement in conversion was seen. Whilst 93 % conversion is greater than 92 % conversion, the improvement is small and the diminishing returns of continually reacting the same sample are not worth the long reaction times if a large enough sample for

crystal screening is to be achieved. Raney nickel gave 89 % conversion and 5 % Ru/C gave 93 %.

The NMR spectra of the crude H_2bisVCap products produced with the hydrogen balloon and 5 % Pd/C and those produced using the H-cube with either 10 % Pd/C, 5 % Ru/C or Raney Nickel all exhibited extra peaks in their NMR spectra which do not correspond to either bisVP of H_2bisVP. It is possible that these peaks arise from reduction of the lactam functionality instead of, or in addition to, the alkene. Usually amides are relatively unreactive due to the high degree of enol character,[8] but the ring strain in the pyrrolidone ring reduces the enol character,[2] making the carbonyl more reactive than would normally be expected and more susceptible to reduction.[9] Regardless of the nature of the side product, none of the hydrogenation methods attempted gave a pure product.

Attempts to purify the sample of H_2bisVP synthesised by the hydrogen balloon method were performed by HPLC-MS. A semi-prep scale HPLC was performed three times to recover enough of the fraction with a molecular mass of 225 to be able to obtain ^{1}H and ^{13}C NMR spectra. After evaporation of the solvent, a clear oil remained, ^{1}H and ^{13}C NMR spectra were consistent with the structure of pure H_2bisVP. Unfortunately even on the semi-prep scale only around 5-10 mg can be recovered from a 40 min experiment and the high volume of solvent required also increases the sample preparation time. As a minimum of 4 − 5 g of sample is required for cocrystal screening, HPLC is not a viable method for sample production.

Due to the difficulties in making H_2bisVP in reasonable purity, the crystallization experiments, detailed in section 3, proceeded with the crude product from the hydrogen balloon and 5 % Pd/C experiment. As crystallisation is itself a purification technique, it is possible that crystals or cocrystals of H_2bisVP can be achieved even from an impure starting material.

2.2.4   HEPVCap

The synthesis of HEPVCap (**10**) was a variation on the synthesises of bisVCap and bisVP. An acid catalyst, TFA, was added to VCap and HEP. No bisHEP or bisVCap were formed in the reaction. Some residual HEP and VCap remained in the reaction mixture and a small amount of ε-caprolactam was formed as a minor side product. Decreasing the reaction temperature and increasing the reaction time greatly reduced the amount of starting material and side product in the final product and the residual VCap can be removed using an alumina column with 75:25 volume ratio of ether:methanol. A six hour reaction at 40 °C results in a product

of acceptable purity and the analytical and characterisation data is given in the experimental section, section 2.3.5 .

2.2.5 Methoxyethylpyrrolidone (MEP)

PVP and PVCap are both hydrogen bond accepting but not strongly hydrogen bond donating. Model compounds to mimic them should also reflect this. To remove the hydrogen bond donating group from hydroxyethylpyrrolidone (HEP), the hydroxyl group was converted to a methyl ether using NaH followed by iodomethane. A white solid was collected in a 95 % yield.

2.2.6 Vinyl lactam diol reactions

The synthesis of new ether containing model compounds was attempted to bind metals in a fashion similar to bisHEP (**10**).[3,4] VP and VCap were reacted in acidic conditions with a range of diols: 1,2-ethandiol, 1,3-propanediol and 1,4-butanediol. The target products were two lactam rings, either two pyrrolidone or two caprolactam rings, attached by ether linkages to a carbon chain, compounds **13**-**16** in Scheme 2.1.

Reaction of VP and VCap with butanediol and a sulfuric acid or TFA catalyst respectively resulted in addition of only one vinyl lactam to the butanediol. Increasing the lactam:diol ratio and lengthening the reaction time did not result in the addition of a second vinyl lactam. As butanediol does not readily react with two equivalents of vinyl lactam, no further work on the butanediol with VP and VCap was undertaken.

Propanediol does not give a pure product with either VP or VCap. LCMS analysis suggests that bisVP and bisVCap are formed as major side products. As discussed in section 2.2.2, the lactam rings are not silica stable. For both the VP and VCap propanediol reaction mixtures, no solvent was found to give good separation on alumina. The crude products, 1,1'-[propane-1,3-diylbis(oxyethane-1,1-diyl)]di(azepan-2-one) (Pr(OVCap)$_2$) and 1,1'-[propane-1,3-diylbis(oxyethane-1,1-diyl)]dipyrrolidin-2-one (Pr(OVP)$_2$) were used in crystallisation attempts with metals (see section 3.2.3) as bisVCap and bisVP have shown only a very limited capacity for binding to metals[4] it is possible that complexed structure of these two new ether compounds will preferentially bind to metals over bisVCap and bisVP.

Reactions with VCap and VP with 1,2-ethanediol gave fewer side products than the reactions with propanediol. The VP derivative, 1,1'-[ethane-1,2-diylbis(oxyethane-1,1-diyl)]dipyrrolidin-2-one (Et(OVP)$_2$), contained a significant amount of bisVP, but the caprolactam/ethanediol product, 1,1'-[ethane-1,2-diylbis(oxyethane-1,1-diyl)]di(azepan-2-one) (Et(OVCap)$_2$), precipitated out as an off white solid with a 70 % yield. The full range of crystallisations attempted are detailed in section 3.2.3. Crystals of Et(OVCap)$_2$ were isolated

by slow evaporation from water as part of attempts to form cadmium(II) chloride and acetate complexes of the ligand. The compound was characterised by x-ray crystallography and the crystal packing can be seen in Figure 2.7
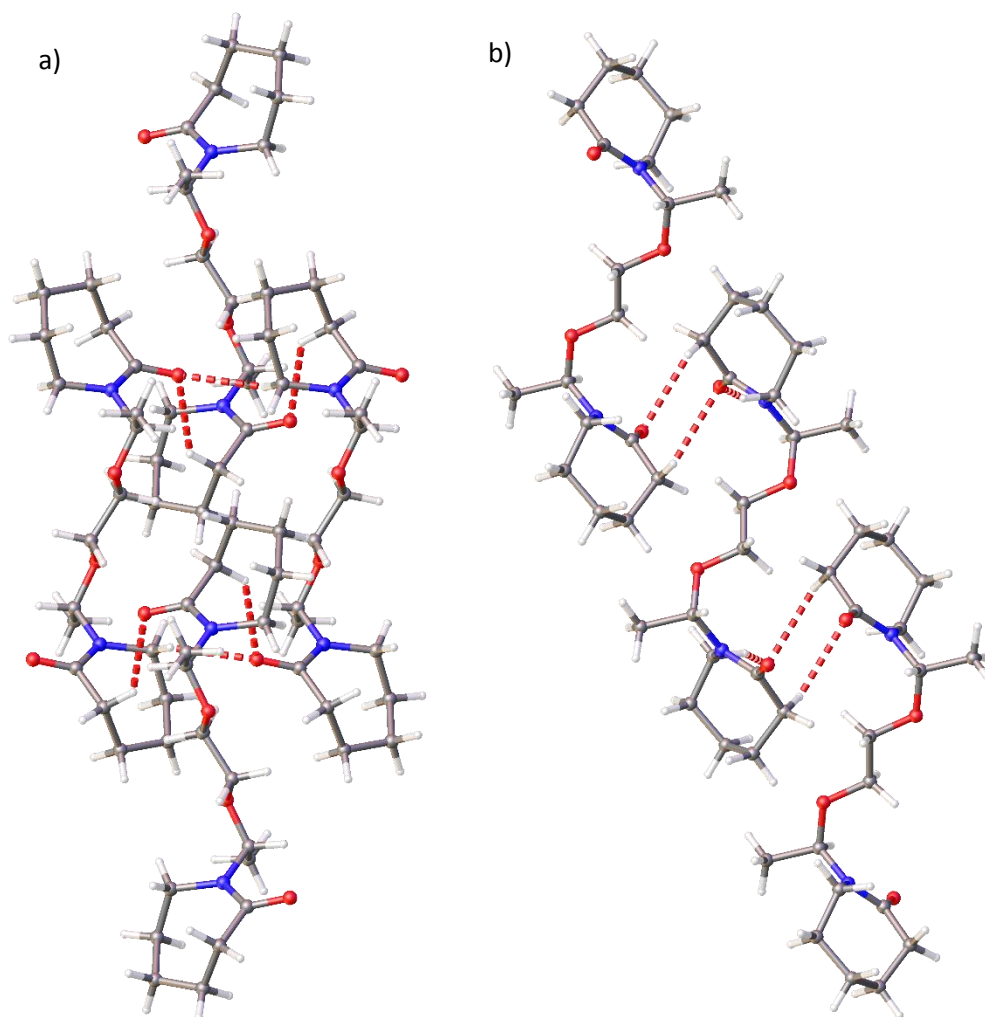
Figure 2.7 – Crystal packing of Et(OVCap)$_2$ with hydrogen bonds are shown by red dashed lines view down a) the crystallographic axis and b) the crystallographic b axis.

The asymmetric unit contains half of the molecule with a rotation relating the other half of the molecule. The crystal structure contains only a single diastereomer even though there are two chiral carbon atoms present so potentially three isomers possible. The crystals formed in the presence of CdCl$_2$ and the crystals formed in the presence of Cd(O$_2$C$_2$H$_3$)$_2$ both contain the same isomer. The NMR spectra of Et(OVCap)$_2$ also do not show two diasteroemers, suggesting that the reaction diastereomerically selective. The crystal structure is held together primarily by C-H⋯O hydrogen bonds. Each carbonyl group accepts two hydrogen bonds, one from the C-H next to the carbonyl group of one neighbouring molecule and the other from the C-H adjacent to the nitrogen of the lactam ring of a different molecule. These hydrogen bonds have C⋯O distances of 3.295(2) Å and 3.243(2) Å respectively. The hydrogen bonds can be seen in the Hirshfeld surface fingerprint plot in

Figure 2.8 as two peaks equidistant from the diagonal which are highlighted by black arrows. The symmetry of these peaks reflects that both the hydrogen bond accepting and donating character are identical, which is to be expected from the symmetry of the structure. The other feature of note in the Hirshfeld surface fingerprint plot is the green area of very high occurrence frequency in the centre of the plot, this arises from H-H proximity from the close packing of the crystal structure.
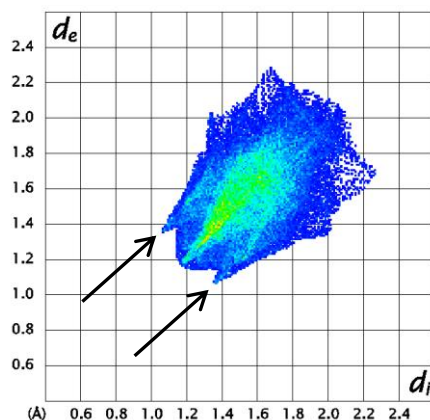
Figure 2.8 - Hirshfeld surface fingerprint plot of Et(OVCap)$_2$. Hydrogen bonding interactions are indicated by black arrows.

2.3   Experimental

2.3.1   Synthesis of BisVCap

Adapted from the procedure by Davenport *et al.*[2]
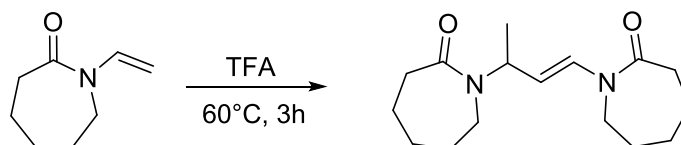
N-vinyl(caprolactam) (5.00 g, 6.0 mmol) was added to hexane (45 cm^3) in a 100 cm^3 two neck flask with a reflux condenser. Dissolution of the VCap occurred upon heating to 50 °C. TFA (0.2 cm^3) was added and the reaction mixture was then heated at 60 °C for 3 hours, during which a white precipitate formed. The solid was isolated by vacuum filtration using a Buchner funnel and subsequently washed with 3x20 mL of n-hexane to give the product as a while solid.

Yield 4.20 g, 15.0 mmol, 84 %

^{1}H NMR (400 MHz, CDCl$_3$) δ 7.27 (dd, J = 14.9, 1.8 Hz, 1H, vinyl NCH), 5.48-5.41 (m, 1H, NCH), 5.02 (dd, J = 14.9, 5.0 Hz, 1H, vinyl CH), 3.59-3.57 (m, 2H, CH$_2$), 3.21-3.18 (m, 2H, CH$_2$), 2.67-2.64 (m, 2H, CH$_2$), 2.58-2.55 (m, 2H, CH$_2$), 1.76-1.65 (m, 12H), 1.27 (d, J = 6.9 Hz, 3H, CH$_3$).

$^{13}C\{^{1}H\}$ NMR (101 MHz, CDCl$_3$) δ 200.61, 175.92, 76.69, 48.67, 44.74, 43.32, 43.04, 37.59, 36.49, 30.56, 29.93, 29.67, 29.33, 23.35, 23.16, 18.60.

IR v = 1667 (C=C), 1640 (C=O), 1621 cm^{-1} (C=O)

2.3.2   Hydrogenation of BisVCap
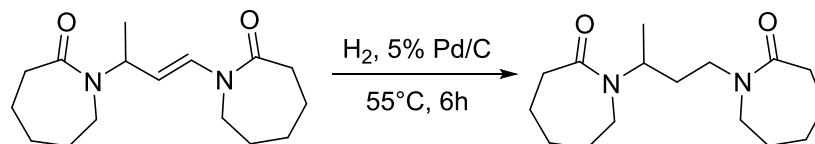
BisVCap (1.00 g, 3.60 mmol) was dissolved in 25 mL of methanol. 0.05 g of 5 % palladium on activated carbon was added. A hydrogen balloon and exit needle were used to purge the reaction for one minute before the exit needle was removed. The mixture was stirred at 55 °C for 6 hours. Every hour the exit needle was introduced to relieve pressure, once the exit needle was removed the reaction vessel was shaken to assure good accessibility of the hydrogen. After the 4 hours, the reaction was allowed to cool to room temperature. The solution was then filtered through Celite. The methanol was removed under vacuum leaving a yellow oil. This oil was then thoroughly mixed with 40 cm^3 of diethyl ether which was the evaporated under vacuum. The addition of ether and evaporation was repeated 3 times. The resulting yellow oil was left in a vacuum desiccator under vacuum overnight.

^{1}H NMR (400 MHz, CDCl$_3$) δ 4.77-4.68 (m, 1H), 3.59-3.52 (m, 1H), 3.36-3.33 (m, 2H), 3.29-3.24 (m, 2H), 3.09-3.01 (m, 1H), 2.61-2.45 (m, 4H), 1.82-1.53 (m, 14H), 1.12 (d, J = 6.9 Hz, 3H)

$^{13}C\ \{^{1}H\}$ NMR (101 MHz, CDCl$_3$) δ 176.06, 175.71, 50.12, 46.77, 46.46, 42.50, 37.65, 37.26, 32.46, 30.05, 29.99, 29.38, 28.68, 23.49, 23.37, 18.62

IR v = 1631 cm^{-1} (C=O)

2.3.3   Synthesis of BisVP

Adapted from the procedure by Zhuo.[10]
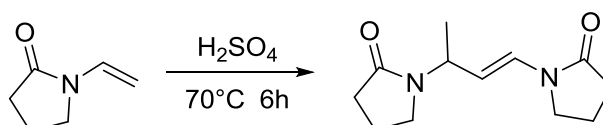
N-vinyl(pyrollidone) (29.0 cm^3, 272 mmol) was added to cyclohexane (13 cm^3) in a two neck round bottom flask with a reflux condenser. The mixture was heated to 50 °C and 3 drops of H$_2$SO$_4$ added. The mixture was then heated at 70 °C for 6 hours. A majority of the solvent was removed under vacuum to leave a thick yellow-orange oil. This oil was then thoroughly mixed with 40 cm^3 of ether which was the evaporated under vacuum. The addition of ether and evaporation was repeated 3 times. The resulting yellow-orange oil was left in a vacuum desiccator under vacuum overnight.

Yield 28.0 g, 126 mmol, 96 %

^{1}H NMR (400 MHz, CDCl$_3$) δ 6.95 (d, J = 13.9 Hz, 1H, vinyl NCH), 4.92-4.81 (m, 2H, vinyl CH and NCH), 3.45 (t, J = 7.2 Hz, 2H, CH$_2$), 3.33-3.20 (m, 2H, CH$_2$), 2.45 (m, 2H, CH$_2$), 2.35 (m, 2H, CH$_2$), 2.11-2.04 (m, 2H, CH$_2$), 1.99-1.92 (m, 2H, CH$_2$), 1.25 (d, J = 6.8 Hz, 3H, CH$_3$)

^{13}C {^{1}H} NMR (101 MHz, CDCl$_3$) δ 174.13, 173.22, 125.09, 110.66, 45.99, 45.16, 42.34, 31.46, 31.15, 26.85

IR ν = 1673 (C=O), 1659 cm^{-1} (C=O)

2.3.4   Hydrogenation of BisVP
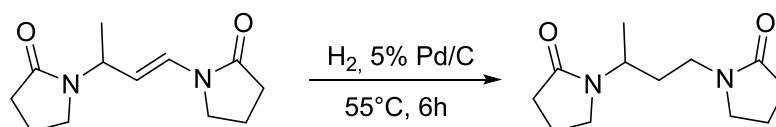
BisVP (7.00 g, 31.5 mmol) was dissolved in ca. 25 mL of methanol. 0.2 g of 5 % palladium on activated carbon was added. A hydrogen balloon and exit needle were used to purge the reaction for one minute before the exit needle was removed leaving the balloon attached to the apparatus. The mixture was stirred at 55 °C for 6 hours. Every hour the exit needle was introduced to relieve pressure, once the exit needle was removed the reaction vessel was shaken to assure dissolution of the hydrogen. The solution was filtered through Celite and the methanol evaporated under vacuum, leaving a yellow oil. This oil was then thoroughly mixed with 40 cm^3 of ether which was the evaporated under vacuum. The addition of ether and evaporation was repeated 3 times. The resulting yellow oil was left in a vacuum desiccator under vacuum overnight.

Conversion 85 % by NMR.

Four solutions of bisVP (0.5 g, 2.24 mmol) in methanol (20 mL) were hydrogenated using a ThalesNano H-Cube® Continuous-flow Hydrogenation Reactor at 60 °C, 5 bar of hydrogen and a flow rate of 1 mL min^{-1}. For three of the reactions different catalysts were used: 10 % Pd/C, 5 % Ru/C and Raney nickel. For fourth solution the 10 % Pd/C catalyst was used and the reaction mixture was run through the machine twice to try and convert and remaining unconverted material.

Conversion from 10 % Pd/C 92 % by NMR.

Conversion from 5 % Ru/C 93 % by NMR.

Conversion from Raney nickel 89 % by NMR.

Conversion from two runs of 10 % Pd/C 93 % by NMR.

Chromatography was performed with a semi-prep Varian LC with a UV-vis detector using a Sunfire C18 OBD 19x 100 mm i.d. 5 µm column. The solvent gradient used was 20 % methanol 80 % water changing to 40 % methanol 60 % water over the course of 10 minutes. Fractions were analysed by electrospray mass spectrometry.

The fraction relating to the peak at 5.91 minutes with a mass of 225 was collected. A majority of the solvent was removed under vacuum to leave a clear, colourless oil. This oil was then thoroughly mixed with 40 cm^3 of ether which was the evaporated under vacuum. The addition of ether and evaporation was repeated 3 times. The resulting clear oil was left in a vacuum desiccator under vacuum overnight.

^{1}H NMR (400 MHz, CDCl$_3$) δ 4.23-4.16 (m, 1H), 3.52-3.48 (m, 1H), 3.45 − 3.30 (m, 4H), 3.16-3.09 (m, 1H), 2.55 − 2.36 (m, 4H), 2.13-2.02 (m, 4H), 1.80 − 1.67 (m, 2H), 1.18 (d, *J* = 6.8 Hz, 3H)

^{13}C {^{1}H} NMR (101 MHz, CDCl$_3$) δ 175.40, 175.28, 47.65, 44.81, 42.31, 39.95, 31.45, 31.31, 30.92, 18.12, 17.99

2.3.5   Synthesis of HEPVCap
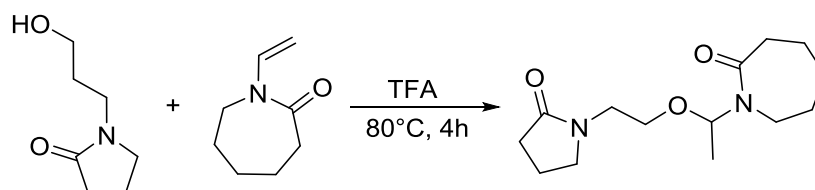
N-vinyl(caprolactam) (2.0 g, 14.4 mmol) and hydroxyethylpyrrolidone (1.9 g, 14.4 mmol) were added to cyclohexane (10 cm^3) in a two neck round bottom flask with a reflux condenser. 0.5 cm^3 of TFA was added and the mixture was heated at 40 °C for 6 hours. The solvent was removed under vacuum to leave an orange oil. Unreacted VCap was removed using an alumina column with 75:25 diethylether:methanol mobile phase. The solvent was removed under vacuum and the resulting yellow oil was left in a vacuum desiccator under vacuum overnight to remove any remaining solvent residues. The elemental composition was confirmed by accurate mass mass spectrometry.

^{1}H NMR (400 MHz, D$_2$O) δ 5.58 (q, *J* = 6.0 Hz, 1H), 3.54 − 3.37 (m, 6H), 3.37 − 3.28 (m, 1H), 3.23-3.15 (m, 1H) 2.63 − 2.42 (m, 2H), 2.35 (t, *J* = 8.1 Hz, 2H), 2.00 (q, *J* = 7.5 Hz, 2 H) 1.79 − 1.46 (m, 6H), 1.23 (d, *J* = 6.0 Hz, 3H).

^{13}C {^{1}H} NMR (101 MHz, CDCl$_3$) δ 176.70, 175.18, 79.33, 65.37, 48.34, 42.36, 40.96, 37.61, 30.82, 29.98, 29.26, 23.48, 19.19, 18.05.

m/z 559 (2M+H$^+$, 100%), 269 (M+H$^+$, 58), 140 (45), 130 (36), 65 (14)

2.3.6 Synthesis of methoxyethylpyrrolidone
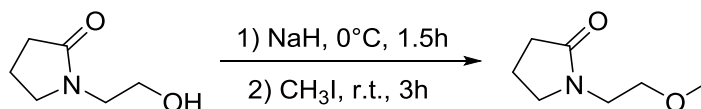
Hydroxyethylpyrollidone (5.00 g, 38.5 mmol) was dissolved in dry THF (50 cm^3). The mixture was cooled to 0 °C using an ice bath then NaH (1.38 g, 57.7 mmol) was added. The resulting suspension was stirred and allowed to slowly warm to room temperature for 1.5 hours. Iodomethane (2.24 cm^3, 38.5 mmol) was added and the reaction mixture was stirred at room temperature for 1.5 hours before a second addition of iodomethane (2.24 cm^3, 38.5 mmol) which was stirred at room temperature for a further 1.5 hours. The white precipitate was removed by filtration through a sintered glass funnel. This white solid was then dissolved in acetone, filtered through a sintered glass funnel and the solvent was removed under vacuum giving 2.5 g of a white solid. The filtrate from the reaction mixture had the solvent removed under vacuum, diethylether (20 cm^3) was added to the resulting yellow oil and the sample was sonicated for one minute. The sample was left for 2 minutes until two distinct layers had formed. The cloudy top layer was decanter away. The washing with diethylether (20 cm^3) was performed a total of 4 times, resulting in an off-white damp looking solid. The solid was left in a vacuum desiccator under vacuum overnight to remove any residual diethylether.

The resulting damp yellow solid was repeatedly pressed between two clean filter papers until a dry white powder, 3.2 g remained.

Yield 5.2 g, 36.4 mmol, 95 %

^{1}*H NMR* (400 MHz, D$_2$O) 3.56 (t, *J* = 5.3 Hz, 2H), 3.7 (t, 8.2 Hz, 2H), 3.39 (t, *J* = 5.3 Hz, 2H), 3.29 (s, 3H), 2.37 (t, *J* = 8.2 Hz, 2H), 1.98 (d, *J* = 8.2 Hz, 2H)

^{13}*C NMR* (101 MHz, D$_2$O) δ 178.65, 68.69, 57.87, 48.26, 41.91, 30.95, 17.26

m/z 144 (M+H$^+$, 58 %), 112 (100)

2.3.7   Synthesis of Et(OVCap)$_2$
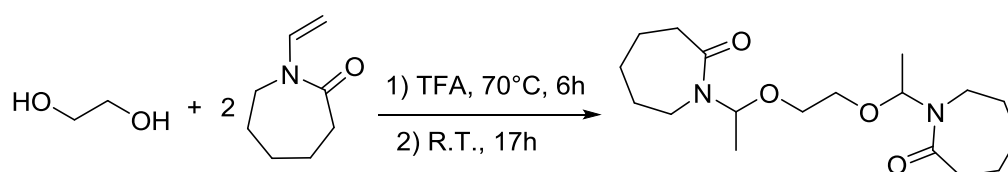
Ethylene glycol (1 cm^3, 17.9 mmol) and VCap (4.97 g, 35.8 mmol) were added to dry hexane (20 cm^3) in a 100 cm^3 two neck flask with a reflux condenser. TFA (0.2 cm^3) was added to the reaction was heated at 70 °C for 6 hours. The reaction was then allowed to cool to room temperature and left to stand overnight for 17 hours. Overnight an off white solid formed. This solid was filtered under vacuum and washed with hexane (2 x 10 cm^3).

Yield 4.2 g, 12.6 mmol, 70 %

^{1}*H NMR* (400 MHz, CDCl$_3$) δ 5.89 (q, *J* = 6.1 Hz, 2H), 3.57 − 3.42 (m, 4H), 3.42-3.32 (m, 7.1, 2H), 3.31-3.18 (m, 2H), 2.66-2.45 (m, 4H), 1.89 − 1.57 (m, 10H), 1.6-1.47 (m, 2H), 1.28 (d, *J* = 6.1 Hz, 6H)

^{13}*C NMR* (101 MHz, CDCl$_3$) δ 176.57, 79.62, 66.69, 41.02, 37.80, 30.14, 29.37, 23.63, 19.26

m/z 364 (M+Na+H$^+$, 100 %), 158 (72), 141 (85)

IR ν = 1636 cm^{-1} (C=O)

2.3.8   Synthesis of Et(OVP)$_2$
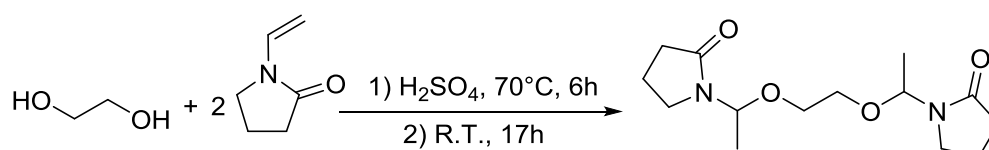
Ethylene glycol (1 cm^3, 17.9 mmol) and VP (3.97 g, 35.8 mmol) were added to dry hexane (20 cm^3) in a 100 cm^3 two neck flask with a reflux condenser. Sulfuric acid (0.2 cm^3) was added to the reaction was heated at 70 °C for 6 hours. The reaction was then allowed to cool to room temperature and left to stand overnight for 17 hours. A viscous orange oil formed and settled to the bottom of the reaction vessel. The solvent was decanter off and the product dried under vacuum in a desiccator overnight.

m/z 308 (M+Na+H$^+$, 100 %), 223 (90), 83 (50)

Due to impurity of the sample and long term HPLC issues, no clean NMR spectra were taken.

2.3.9   Synthesis of Pr(OVCap)$_2$
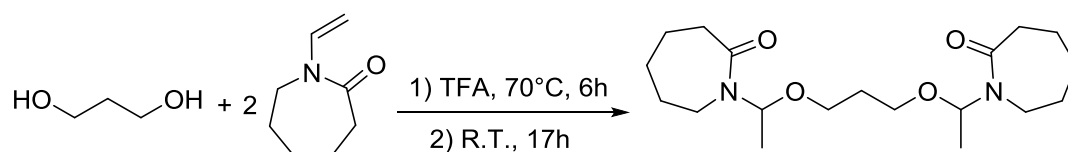
Propane-1,3-diol (1 cm^3, 14.1 mmol) and VP (3.94 g, 28.2 mmol) were added to dry hexane (20 cm^3) in a 100 cm^3 two neck flask with a reflux condenser. TFA (0.2 cm^3) was added to the reaction was heated at 70 °C for 6 hours. The reaction was then allowed to cool to room temperature and left to stand overnight for 17 hours. A viscous orange oil formed and settled to the bottom of the reaction vessel. The solvent was decanter off and the product dried under vacuum in a desiccator overnight.

m/z 378 (M+Na+H$^+$, 35 %), 140 (100), 83 (35)

Due to impurity of the sample and long term HPLC issues, no clean NMR spectra were taken.

2.3.10   Synthesis of Pr(OVP)$_2$
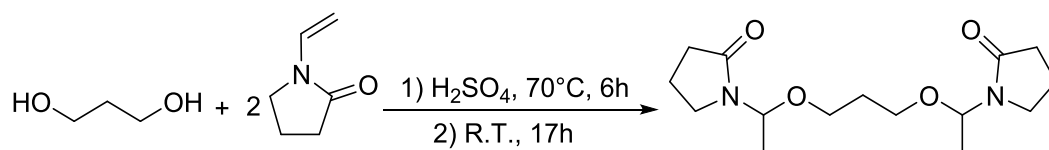
Propane-1,3-diol (1 cm^3, 14.1 mmol) and VP (3.12 g, 28.2 mmol) were added to dry hexane (20 cm^3) in a 100 cm^3 two neck flask with a reflux condenser. Sulfuric acid (0.2 cm^3) was added to the reaction was heated at 70 °C for 6 hours. The reaction was then allowed to cool to room temperature and left to stand overnight for 17 hours. A viscous orange oil formed and settled to the bottom of the reaction vessel. The solvent was decanter off and the product dried under vacuum in a desiccator overnight.

m/z 322 (M+Na+H$^+$, 10 %), 197 (57), 111 (100)

Due to impurity of the sample and long term HPLC issues, no clean NMR spectra were taken.

2.3.11 IR and NMR

NMR spectra were recorded on a Bruker-Advance spectrometer, operating at 400 MHz, chemical shifts reported in ppm (δ) relative to residual solvent.

IR experiments were performed on a Perkin Elmer FTIR spectrum 100 with an attenuated total reflectance (ATR) attachment. Data were recorded at a resolution of 1 cm^{-1} for 16 runs over the range 4000 – 600 cm^{-1}. Spectral analysis was performed using SpekWin32.[11]

2.3.12 Dynamic vapour sorption

DVS was performed using an SMS DVS-1 with a 10 %RH step between humidity values with equilibrium achieved at 0.01% weight change before moving to the next step. Methods began at the humidity of the room at ambient which was measured by a Rotronic A/H hygrometer. The humidity was then increased to 90%RH before cycling to 0%RH, to 90%RH, to 0%RH. Samples weighing between 5-20mg were used.

For the sample of H_2bisVCap the humidity was first set to 0 %RH and the sample was left until a mass change smaller than 0.001 %. The humidity was then increased to 90 %RH, decreased to 0 %RH, increased to 90 %RH decreased to 40 %RH and finally increased to 96 %RH

2.3.13 X-ray crystallography

Single crystal crystallographic analysis of bisVP was performed on a Bruker Photon D8 Venture diffractometer (ImuS microsource, λCuKα, λ = 1.54178 Å) equipped with a Cryostream (Oxford Cryosystems) open-flow nitrogen cryostat, at 120 K. The data collection and refinement was kindly carried out by Dr Dmitry S. Yufit.

BisVP crystal data: Empirical formula $C_{12}H_{18}N_2O_2$, space group *Pca*2_1, *a* = 12.4684(9) Å, *b* = 10.6073(8) Å, *c* = 8.9326(6) Å, α = 90.00°, β = 90.00°, γ = 90.00°, volume = 1181.39(15) Å^3, Z = 4, F(000) = 480.0, CuKα (λ = 1.54178) 2θ range for data collection = 8.34 – 139.88°, data = 2074, parameters = 146, goodness-of-fit on F^2 = 1.084, R$_1$ = 0.0583, wR$_2$ = 0.1860

Single crystal crystallographic analysis of bisVP was performed on a Bruker Photon D8 Venture diffractometer (ImuS microsource, λMoKα, λ = 0.71073 Å) equipped with a Cryostream (Oxford Cryosystems) open-flow nitrogen cryostat, at 120 K. The data collection and refinement was kindly carried out by Dr Dmitry S. Yufit.

Et(OVCap)$_2$ crystal data: Empirical formula $C_{18}H_{32}N_2O_4$, space group *P*2$_1$/n, *a* = 11.6915(3) Å, *b* = 6.1181(2) Å, *c* = 13.8658(4) Å, α = 90.00°, β = 109.617(3)°, γ = 90.00°, volume = 934.25(5)

$Å^3$, Z = 2, F(000) = 372.0, MoKα (λ = 0.71073) 2θ range for data collection = 5.582 – 59.996°, data = 2728, parameters = 110, goodness-of-fit on F^2 = 1.046, R_1 = 0.0799, wR_2 = 0.1210

2.4   References

(1)   Perrin, A.; Musa, O. M.; Steed, J. W. *Chem. Soc. Rev.* **2013**, *42* (5), 1996–2015.

(2)   Davenport, J. R.; Musa, O. M.; Paterson, M. J.; Piepenbrock, M.-O. M.; Fucke, K.; Steed, J. W. *Chem. Commun.* **2011**, *47* (35), 9891–9893.

(3)   Perrin, A. The chemistry of low dosage clathrate hydrate inhibitors, University of Durham, 2015.

(4)   Perrin, A.; Myers, D.; Fucke, K.; Musa, O. M.; Steed, J. W. *Dalt. Trans.* **2014**, *43* (8), 3153–3161.

(5)   Teng, J.; Bates, S.; Engers, A. E.; Leach, K.; Schields, P.; Yang, Y. *J. Pharm. Sci.* **2010**, *99* (9), 3815–3825.

(6)   Kobyakov, V. V; Ovsepyan, A. M.; Panov, V. P. *Polym. Sci. U.S.S.R.* **1981**, *23* (1), 168–180.

(7)   Bryan, M. C.; Wernick, D.; Hein, C. D.; Petersen, J. V.; Eschelbach, J. W.; Doherty, E. M. *Beilstein J. Org. Chem.* **2011**, *7* (1), 1141–1149.

(8)   Clayden, J. *Nature* **2012**, *481*, 274–275.

(9)   Haldar, P.; Ray, J. K. *Tetrahedron Lett.* **2003**, *44* (45), 8229–8231.

(10)   Zhou, J.-C. *Molecules* **1990**, *4*, M117.

(11)   Menges, F. http://www.effemm2.de/spekwin: Berchetesgarden 2016.

3 Cocrystallisation of hydrate inhibitor models

3.1 Introduction

One method to study the behaviour of KHIs with water is to crystallise hydrated structures of the model compounds in Scheme 2.1. Single crystal x-ray diffraction studies of a hydrated structure would give information into the bonding behaviour between the model compounds and water, including bond length and bond angle which could be used to help explain how the polymers behave with water.

Previous attempts to create hydrate crystals of model compounds **6**-**10** have not successfully created model compound hydrates.[1] As the model compounds are based on polymers which are used for their ability for preventing water crystallising it is not unexpected that low molecular weight molecules designed to emulate hydrate inhibitors do not easily form hydrates. As simply forming hydrates from the pure model compounds from wet solutions is not effective, other methods must be explored. One such method is the formation of cocrystals.

Cocrystals are crystals with more than one distinct molecule in the structure.[2] Addition of the second component can be used as a method to crystallise difficult to crystallise products by supplying interactions between the molecules which the single component on its own is lacking. The model compounds all have the ability to accept hydrogen bonds, but have no strong hydrogen donating groups.[3,4] Adding a molecule capable of hydrogen bond donation to the crystallisation attempts with the model compounds may provide the missing supramolecular interactions required for crystal growth. Hydrates can also be formed this way, though even cocrystals which are not hydrated will give insight into how the model compounds interact with different species.

3.2 Results and Discussion

A range of crystallisation series were performed to try and create cocrystals of the model compounds with different components.

3.2.1 Macrocycles

Macrocycles, such as calixarenes, cyclodextrins and cucurbiturils, are host compounds, capable of hosting a guest in their cavities. In most cases when there is no other guest present the macrocyclic cavity is filled with water and the entropy gain associated with freeing the water molecules is a large driving force for guest incorporation.[5] Unless a guest

nearly completely fills the macrocycle, water molecules can also remain in the host along with the newly introduced guest. As this commonly occurs, finding a macrocycle that will hold both one of the model compounds and some water is a possible solution to trying to acquire hydrated crystal structures of the model compounds and thus observe the nature of the bonding between the lactam rings and water.

A range of different types and sizes of macrocycles were tested with the model compounds in an attempt to find the right combination of interactions and cavity size. Slow evaporation crystallisation experiments using 1:2, 1:1 and 2:1 molar ratios of macrocycle:model compound were performed. The macrocycles used were α, β and γ cyclodextrin, *p*-sulfonatocalix[n]arene where n = 4, 6 or 8 as a sodium salt and as the free acid, 4-tert-butylcalix[4]arene, benzyloxycalix[5]arene and mixtures of cucurbiturils 5, 6, 7 and 8. Model compounds **6**-**10** were used. The macrocycle/model compound mixtures were dissolved in water, except for the experiments using 4-tert-butylcalix[4]arene and benzyloxycalix[5]arene for which a 1:1 volume ratio of toluene:acetone was used.

Many macrocycles are difficult to crystallise due to their large size and the chance of crystallisation is greatly affected by the guest molecule. Smaller macrocycles have less conformational freedom so often crystallise more readily than their larger counterparts. Unfortunately the smaller macrocycles have much smaller cavities, so struggle to incorporate many guests of interest. This has been evident with the *p*-sulfonatocalix[n]arene salts and free acids. The n = 6 and n = 8 derivatives have failed to yield any crystals of diffraction quality in any experiment attempted, resulting in solid films which show no birefringence under polarised light. On the other hand, a 1:1 molar ratio mix of *p*-sulfonatocalix[4]arene (SC4):bisVCap produced crystals of diffraction quality. Single crystal x-ray analysis of the crystals revealed the crystals to be *p*-sulfonatocalix[4]arene pentasodium dodecahydrate. This a known crystal structure most recently reported by Fucke *et al.*[6] and does not incorporate the model compound.

The model compounds are all dimeric lactams, so their failure to crystallise in the SC4 cavity may be due to their size being too large to fit in the cavity. Smaller monomeric models, ethylpyrrolidone and ethylcaprolactam were tried to see if a smaller compound would bind into the SC4 cavity. Both ethylpyrrolidone and ethylcaprolactam used in slow evaporation crystallisation experiments using 1:2, 1:1 and 2:1 molar ratios of macrocycle:model compound were performed. The macrocycles used were α, β and γ cyclodextrin, *p*-sulfonatocalix[n]arene where n = 4, 6 or 8 as a sodium salt and as the free acid, 4-tert-butylcalix[4]arene, benzyloxycalix[5]arene and mixtures of cucurbiturils 5, 6, 7 and 8. The

macrocycle/model compound mixtures were dissolved in water, except for the experiments using 4-tert-butylcalix[4]arene and benzyloxycalix[5]arene for which a 1:1 volume ratio of toluene:acetone.

3.2.1.1   *p*-sulfonatocalix[4]arene/ethylpyrrolidone

Crystals of diffraction quality grew from the slow evaporation of a 1:1 mixture of ethylpyrrolidone and the free acid of SC4 dissolved in water over the course of 18 months, the resulting crystal structure can be seen in Figure 3.1. *P*-sulfonatocalix[n]arenes are sulfonic acids and thus are highly acid. The pH of a solution of the same SC4 concentration as the starting solution of the crystallisations was measured to have a pH of 2.1, this will experience some variance as the evaporation of the solvent increases the concentration. The low pH leads to the ethylpyrrolidone guest being protonated and a new material, crystal **1**, being formed with the formula $C_{28}H_{20}O_{16}S_4.3(C_6H_{12}NO).H_3O.4H_2O$.
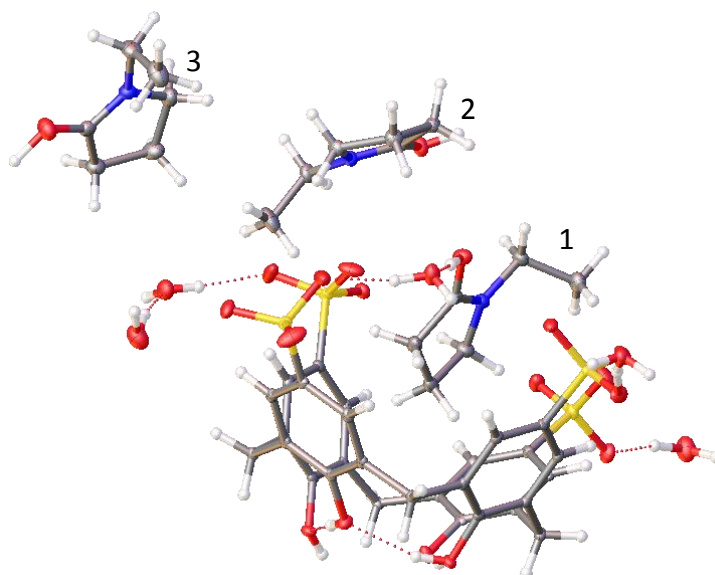
Figure 3.1 – Asymmetric unit of crystal 1 showing the SC4 macrocycle and three protonated ethylpyrrolidone molecules, EP 1 in the SC4 ring, EP 2 and EP 3. Hydrogen bonds are shown by red dotted lines.

Crystal **1** is a hydrated structure, with the unit cell containing four water molecules and a hydronium ion. The crystal structure has three distinct ethylpyrrolidone molecules EP 1, EP 2 and EP 3 as shown in Figure 3.1. EP 1 rests in the SC4 cavity and the other two lie above the upper rim of the macrocycle. To compare the different environments of the ethylpyrrolidone molecules Hirshfeld surface analyses were performed for each ethylpyrrolidone molecule. The Hirshfeld surface fingerprint plots can be found in Figure 3.2 and show the similarities and differences between the environments and interactions of the three ethylpyrrolidone molecules.

The Hirshfeld surface fingerprint plots of all three ethylpyrrolidone molecules have 'wings' in the upper left of the plot, which arise from the C-H part of a C-H…π interaction. For EP 1, the 'wing' comes from the hydrogen atoms on the carbons of the lactam ring interacting with all four of the aromatic rings of the SC4 in which it resides. The 'wing' of EP 2 arises from the C-H…π interaction between the hydrogen atoms on the carbon adjacent to the carbonyl group of the lactam ring interaction with the outside of a neighbouring SC4. Finally the 'wing' of EP 3 arises from interaction of the hydrogen atoms of the methylene group adjacent to the nitrogen in the lactam ring with a different neighbouring SC4. The centre ethylpyrrolidone molecule C-H…π bonds in an edge to face fashion, with the lactam ring approaching being perpendicular with the aromatic ring. The outer ethylpyrrolidone molecule on the other hand, C-H…π bonds in a face-face fashion, with the lactam and aromatic rings being almost parallel to one another.
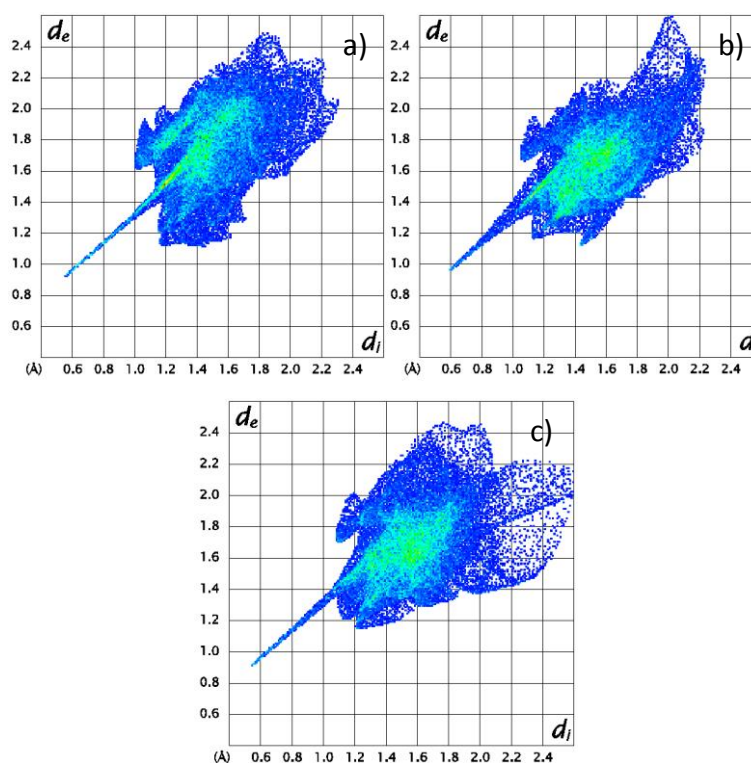
Figure 3.2 – Hirshfeld fingerprint plots for the ethylpyrrolidone molecules in crystal 1, a) EP 1, b) EP 2, c) EP 3.

Diffuse blue regions found in the top right corners of the Hirshfeld surface plots, arise from less efficient packing such as void spaces. Moving from the EP 1 to EP 2 then EP 3 this diffuse region becomes larger and more prominent. This shows that the molecule inside the SC4 cavity has very little space around it and much closer neighbours than the outer molecules.

The Hirshfeld fingerprint plot for all three ethylpyrrolidinium cations in the crystal structure show long, sharp peaks in the upper left part of the plot which are demonstrative of

hydrogen bond donating character. As the carbonyl groups of all three pyrrolidone molecules are protonated it is to be expected that they would exhibit hydrogen bond donation capability. None of the Hirshfeld surface fingerprint plots show any peaks characteristic of hydrogen bond accepting interactions, suggesting that the ethylpyrrolidone molecules are only hydrogen bond donating. EP 1 has a hydrogen bond to water with an O···O distance of 2.459(2) Å, which is classified as a strong, mostly covalent bond according to the definition by Jeffery.[7] This water molecule donates a hydrogen bond to the sulfonate group of the SC4 in which the pyrrolidone molecule resides and the sulfonate group of a neighbouring SC4 as well as accepting a hydrogen bond the hydroxyl group of another SC4 ring. EP 3 donates a hydrogen bond with a O···O of 2.430(2) Å to the nearest water molecule. This water molecule also donates hydrogen bonds to two other water molecules, which both donate hydrogen bonds to the sulfonate groups of neighbouring SC4 molecules. EP 2 does not hydrogen bond to water. Instead it donates a hydrogen bond with an O···O distance of 2.527(2) Å to a sulfonate group of a neighbouring SC4 molecule. None of the ethyl pyrrolidone molecules accept hydrogen bonds. There are also no short contact interactions between the pyrrolidone molecules, any interactions are mediated by water.

In conclusion a hydrated lactam structure was successfully created and characterised by single crystal x-ray crystallography. Instead of the hydrogen bond accepting interactions which would be expected from the lactam functionality, the acidic nature of SC4 resulted in protonated lactam groups which only donate, and do not accept, hydrogen bonds. This does not make for a realistic model of PVP in an oil pipeline where the pH is generally higher than 2, so it would be expected that the lactams would not be protonated and thus not donate hydrogen bonds. So whilst this crystal structure is interesting in its own right, it does not add anything to the knowledge of kinetic hydrate inhibition in pipelines.

3.2.2   Halogen Bonding

Halogen bonds are highly directional, relatively strong intermolecular interactions which have strong analogies to hydrogen bonds. Halogen bonds are possible due to the polarisable nature of the electron density around the later halogens, especially iodine. Attaching electron withdrawing groups to iodine results in the electron density being pulled away from one side of the atom, resulting in a δ^+ charge termed a 'sigma hole'. This charge can interact with a range of nucleophiles to from supramolecular systems. One of the most common and one of the most effective halogen bond donors is 1,4-diiodotetrafluorobenzene (pDITFB).[8–10]

The simplest halogen bonding molecules are the diatomic, elemental halogens themselves, particularly iodine due to its polarisable electron density. The electron density around I_2 can be influenced by external molecules, creating the partial charges required for supramolecular assembly. Topically, iodine also has a history of interacting with PVP. Iodine is administered as an anti-septic often in a form complexed with PVP called povidone-iodine.[11,12] As PVP has already shown affinity for iodine, it was reasoned that the model compounds studied herein will show a similar kind of interaction.

Much stronger halogen bonding compounds can be formed by covalently bonding electron withdrawing groups to the halogen instead of relying intermolecular interactions to cause the required partial charge. For example pDITFB has been used in creating a plethora of cocrystals[8–10] and even co-liquid-crystalline materials.[13,14] Part of its widespread use can be related to its commercial availability, relative stability and strength of the halogen bond it forms. The fluorinated aromatic ring is strongly electron withdrawing, resulting in a significant δ^+ charge at the tips of both of the iodine atoms. Compounds with an alkene functionality between the benzene ring and the iodine atoms, such 1-iodoethynyl-4-iodobenzene, are even stronger halogen bond donors. Unfortunately a multistep, inert conditions reaction is required to synthesise 1-iodoethynyl-4-iodobenzene , which is much less stable to air, heat and moisture than pDITFB. 1,2-diiodotetrafluorobenzene (oDITFB) is also a commercially available compound which is stable to benchtop conditions. The ortho derivative, oDITFB, is less commonly used than the para version, pDITFB, with only 30 results when searching for cocrystals in the CSD compared with 205 results for pDITFB. This is possibly due to steric reasons as both of the halogen bonding groups are adjacent on the benzene ring making interaction with multiple molecules challenging. The steric clash of having the two iodine atoms adjacent on the ring will also make it more difficult to synthesise than the para version, making it a more expensive molecule to buy, this may also contribute to the fewer recorded cocrystals of oDITFB.

Slow evaporation crystallisation experiments were performed with the model compounds **6**-**11** and the halogen bond donors: pDITFB, oDITFB, 1,4-diiodobenzene, 1-chloro-(2-iodoethynyl)benzene and iodine. All halogen bond donors were weighed out in a 1:1 ratio with compounds **6**-**11**. For crystallisations containing iodine the components were dissolved in water, whilst pDITFB, oDITFB, 1,4-diiodobenzene and 1-chloro-(2-iodoethynyl)benzene crystallisations were dissolved in a 1:1 volume ratio of acetone:DCM. The solvent was allowed to evaporate at room temperature. After one week, pDITFB with bisVCap gave crystals of diffraction quality.

3.2.2.1   1,4-diiodotetrafluorobenzene/bisVCap

Slow evaporation of a 1:1 molar ratio of pDITFB:bisVCap from a DCM/acetone 1:1 mixture gives a 1:1 pDITFB:bisVCap cocrystal, crystal **2**, with the formula $C_{16}H_{26}N_2O_2.C_6F_4I_2$. Crystal **2** was also successfully formed from a 1:1 molar ratio of pDITFB:bisVCap dissolved in acetone and allowing the solvent to evaporate at room temperature, this was verified by PXRD. Crystal **2** is the only BisVCap cocrystal isolated so far. Attempts to produce cocrystals of bisVCap usually result in crystals of bisVCap as a single component.

The x-ray crystal structure of crystal **2** can be seen in Figure 3.3. The halogen bonds are shown by red dashed lines. The halogen bonds between the oxygen atom of the carbonyl and the iodine of pDITFB have I···O distances of 2.897(6) Å and 2.916(6) Å. A search of the Cambridge structural database for cocrystals of pDITFB with a molecule containing a carbonyl group yields 23 results, 12 of which contain no halogen bond between pDITFB and the carbonyl. Of the 11 remaining structures 3 contain halogen bonds with a length shorter than 2.95 Å,[15–17] showing the halogen bond of crystal **2** to a relatively strong bond when compared to similar cocrystals.
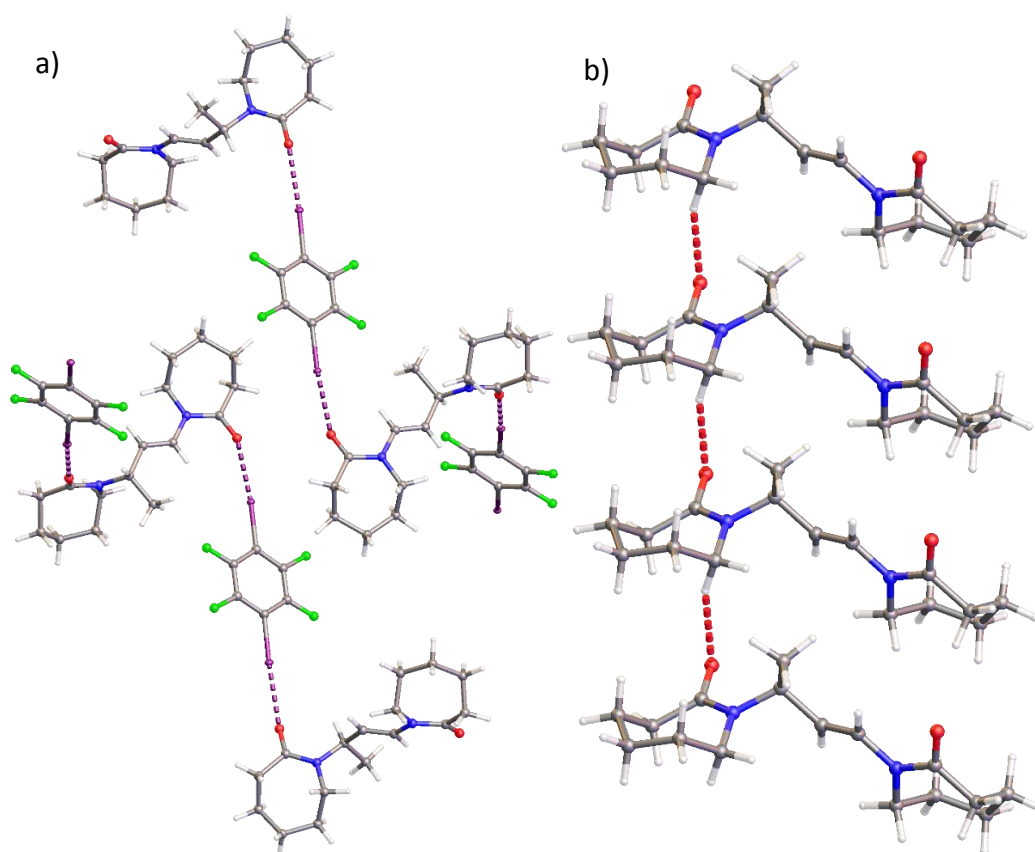
Figure 3.3 – Crystal structure of crystal 2. a) Both pDITFB and bisVCap with the halogen bonds shown by dashed purple lines, b) only bisVCap, highlighting the hydrogen bonds shown by dashed red lines.

The Hirshfeld surface fingerprint plots of pDITFB and bisVCap in crystal **2** are shown in Figure 3.4. In the left hand plot which corresponds to the pDITFB molecule, the halogen bond donor interaction is indicated by a black arrow, bottom right of the diagonal. The prominent feature along the diagonal is the H⋯F close packing, the H⋯F distance range from $2.516(4) - 2.606(5)$ Å.
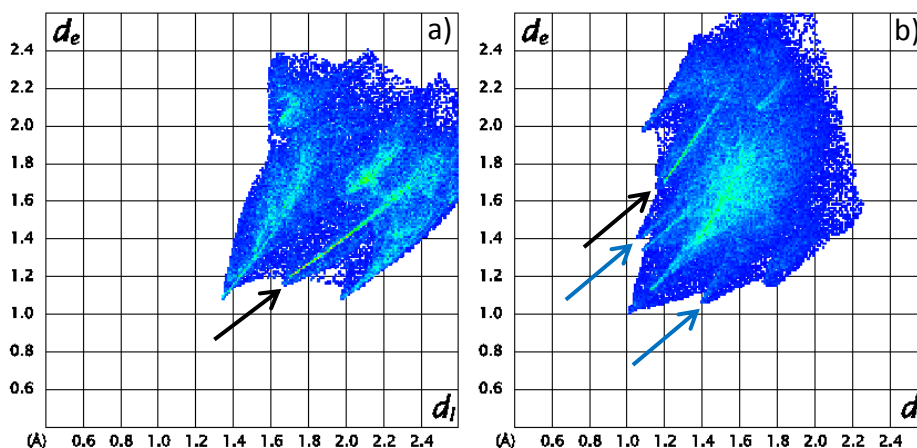
Figure 3.4 – Hirshfeld surface fingerprint plots of crystal 2, a) pDITFB and b) bisVCap. Halogen bonds are indicated by black arrows and CH⋯O hydrogen bonds are indicated by blue arrows.

The H⋯F close packing is also apparent along the diagonal of the Hirshfeld surface fingerprint plot of bisVCap, pictured right in Figure 3.3. The plot for bisVCap also has the halogen bond interaction indicated by a black arrow. For bisVCap the halogen bonding interaction appears to the top left of the diagonal, showing that is the halogen bond accepting interaction. The two blue arrows show the C-H⋯O hydrogen bond interactions between the bisVCap molecules. The hydrogen bonds occur between the carbonyl group of a lactam ring and the C-H adjacent to the nitrogen of a lactam of a neighbouring bisVCap as shown in Figure 3.3b The C⋯O distance of these hydrogen bonds is 3.493(9) Å.

It has been suggested that halogen bonds are often too weak to be observed in solution, though in some cases NMR titrations have successfully shown halogen bonds in solution.[18,19] To test if this holds true for this system an NMR titration was performed. Acetonitrile was chosen as the solvent as it successfully dissolves both bisVCap and pDITFB, but does not have any hydrogen bonding interaction with bisVCap which competes with the halogen bonds. BisVCap was dissolved in d$_3$-acetonitrile and pDITFB was added in 10 mol equivalent portions to the solution until a large excess of pDITFB. As there are no hydrogen atoms in pDITFB, a large excess can be added without obscuring the bisVCap signals as no peaks for pDITFB can be observed in a ^{1}H NMR spectrum. After 50 equivalents of pDITFB a new product was seen to begin forming. Remaking a fresh sample at the same concentration showed no sign of this

product however, leaving a sample standing for 2 hours showed the gradual formation of the new compound.

To test if this product was due to a reaction between pDITFB and bisVCap, or with residual acid in the sample of pDITFB, a bisVCap/dilute HCl/acetonitrile mixture, a pDITFB/bisVCap/acetonitrile mixture and a bisVCap/acetontrile mixture were heated at 60 °C for three days in acetonitrile. The bisVCap/acetonitrile sample showed no sign of the new product. Both the pDITFB/bisVCap/acetonitrile and bisVCap/dilute HCl/acetonitrile samples showed the same unknown product. This suggests that the reaction occurs dues to a small amount of residual acid present in pDITFB, not because of the pDITFB itself. Electrospray time of flight mass spectroscopic analysis of the unknown product gave a peak with mass 227 which has not successfully been assigned and as it is an acid catalysed decomposition product, not a reaction between pDITFB and bisVCap, no further investigation was undertaken.

To prevent this acid decomposition product forming, an NMR titration was performed with fresh samples prepared after every three spectra were recorded. There is no change in the chemical shift of the bisVCap up to 50 equivalents of pDITFB, at which point the solubility of the pDITFB becomes the limiting factor. This suggests that the halogen bonding is not strong enough to be observed in solution.

The cocrystal and individual components were characterised by differential scanning calorimetry (DSC) to acquire information on the melt behaviour and screen for any polymorph changes. DSC experiments were run at 10 °C/min in a heat/cool/heat cycle. Hot stage microscope experiments, emulating the DSC experiments, were performed to clarify any unexplained features.

The DSC thermograph of pDITFB itself, shown in Figure 3.5, shows a variety of features. During the first heating cycle, a small endothermic peak at 84 °C is seen. This has previously been attributed to a polymorph change, with the high temperature polymorph being reported by Chaplot *et al*.[20] A small endothermic peak is also observed at 105 °C before the main melt endotherm at 108 °C. When heated above 150 °C pDITFB begins to decompose as is characterised by a multitude of ill-defined peaks, so DSC experiments were run past 120 °C. During the cooling cycle a large loop occurs at 96 °C. This feature often arises from a sublimation event, with the compound vaporising and recrystallising on the lid of the pan. The second heating cycle shows only the melt peak at 108 °C.
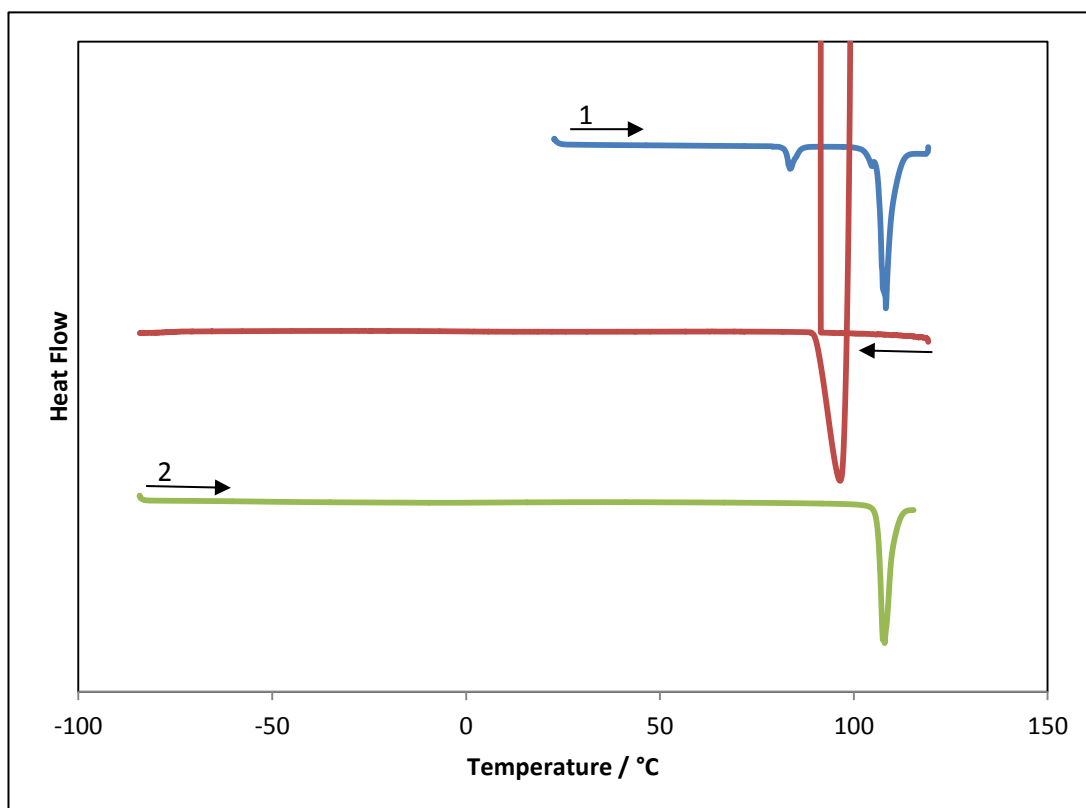
Figure 3.5 – DSC heat/cool/heat thermograph of pDITFB. Exotherm up.

A hot stage microscope experiment was performed to elucidate the cause of the peak at 105 °C and verify the other features as shown in Figure 3.6. As the glass slide is much thicker than the pans used for DSC, the exact temperatures at which events occur are slightly from those observed in the DSC experiment. During heating cycles events occur at a higher temperature than seen in the DSC thermograph and in cooling cycles the events often occur at a lower temperature. This reflects the slower change in temperature of the microscope sample.

A change in crystal morphology is seen after 85 °C, as would be expected from a polymorph change. At 106 °C a there is a sudden and notable change in morphology, quickly followed by melting by 108 °C. Judging from the morphology of this new phase, it seems to be liquid crystalline in nature. Heating a sample of pDITFB on the hot stage microscope to 100.5 °C and holding at this temperature for half an hour results in a slow conversion to this liquid crystal phase. The phase has a mosaic texture, with parts which some parts change to black when the polarising filter is crossed whilst some parts which remain unchanged. From these observations it is possible to say that it is one of the more ordered smectic liquid crystal phases such as $S_{b(cry)}$,[21] though any further investigation into the liquid crystal phase is beyond the scope of this project. The formation of this liquid crystal phase does explain the peak at 105 °C in the DSC thermogram. The sample had completely melted by 110 °C. As the cooling

cycle began, crystals began forming on the underside of the hot stage window. This is deposition of the vaporous pDITFB. This process occurs at a lower temperature in the DSC experiment, 93 °C instead of 109 °C. The hot stage window does not significantly heat up during the course of an experiment, so the deposition can occur whenever the sample evaporates. In the DSC pan, deposition can only occur when the pan has cooled enough to not immediately evaporate or sublime the sample.
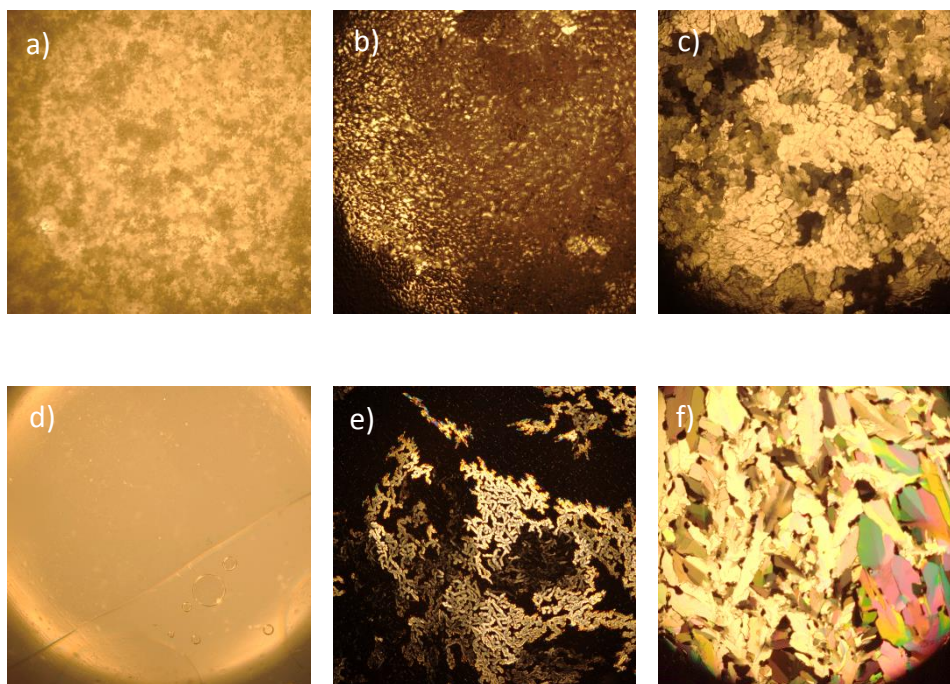
Figure 3.6 - Hot stage microscope experiment heating then cooling pDITFB: a) 20 °C, b) 90 °C, held for 30 min to allow full conversion of morphology, c) 106 °C, held for 30 min to allow full conversion of morphology, d) 110 °C, e) 109 °C, sample formed on the inside of the hot stage window from evaporation and deposition of pDITFB, f) 103 °C, crystals formed from cooling of the melt.

The DSC plot for bisVCap can be seen in Figure 3.7. During the first heating cycle the only feature is an endothermic peak at 145 °C corresponding to the sample melting. During the cooling cycle there is no recrystallisation peak or features of any kind. The second heat cycle shows a glass transition at -11 °C and an endothermic, melt peak, which is smaller than the melt peak from the first heating cycle, at 139 °C. If there was truly no recrystallisation there would be no melt peak on the second heating cycle. This gives two options. The first is that there is a recrystallisation on cooling, but it occurs over such a long time scale that no peak was observable in the DSC plot. The second is that there is a recrystallisation event on heating, which is either over a long time frame or obscured by the melt peak. To visualise what is happening, the DSC experiment was reproduced using a hot stage microscope. The sample was heated at 10 °C min^{-1} to 150 °C at which sample had melted completely, then cooled at the same rate to -100 °C then heated again to 150 °C also at the same rate. The pictures from the experiment can be found in Figure 3.8.
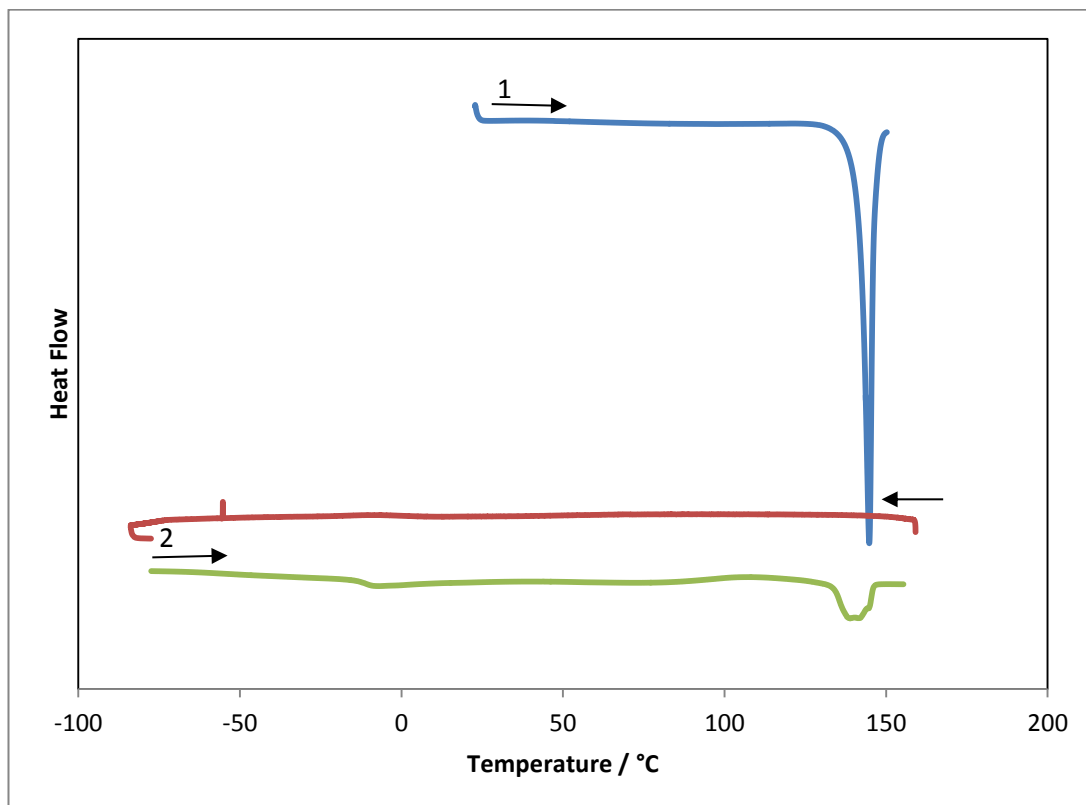
Figure 3.7 – DSC heat/cool/heat experiment of bisVCap at a rate of 10 °C/min. Exotherm up.

The microscope experiment shows all of the sample to have melted when heated to 150 °C. No change was observed at temperatures down to the DSC instrument limit of -90 °C. As glass transitions are very rate dependant and the hot stage microscope cools slower than the DSC below 0 °C, the sample was cooled further to find visual evidence of a glass transition. At -100 °C the sample suddenly cracked, which is a common sign that a glass has been formed, as the glass becomes brittle when cooled too far and thermal shrinkage caused the sample to crack.[22,23] On heating all the cracks had disappeared by 10 °C, suggesting the glass transition had been passed. Further heating to 100 °C resulted in small crystals beginning to form, these crystals continued growing until 150 °C where they began to melt. All of the crystals had completely melted by 154 °C. As can be seen by the pictures in Figure 3.8, compared to the amount of material at the beginning of the experiment, very little of the material has chance to recrystallise at this rate of heating before melting occurs. This would account for the reduction in size of the melt peak in the second heating cycle. As the recrystallisation occurs over a range of 50 °C and not all of the sample recrystallises, the lack of observable recrystallisation peak is due to the heat capacity of the recrystallisation being small and the recrystallisation being long, resulting in a peak too broad and too weak to observe.
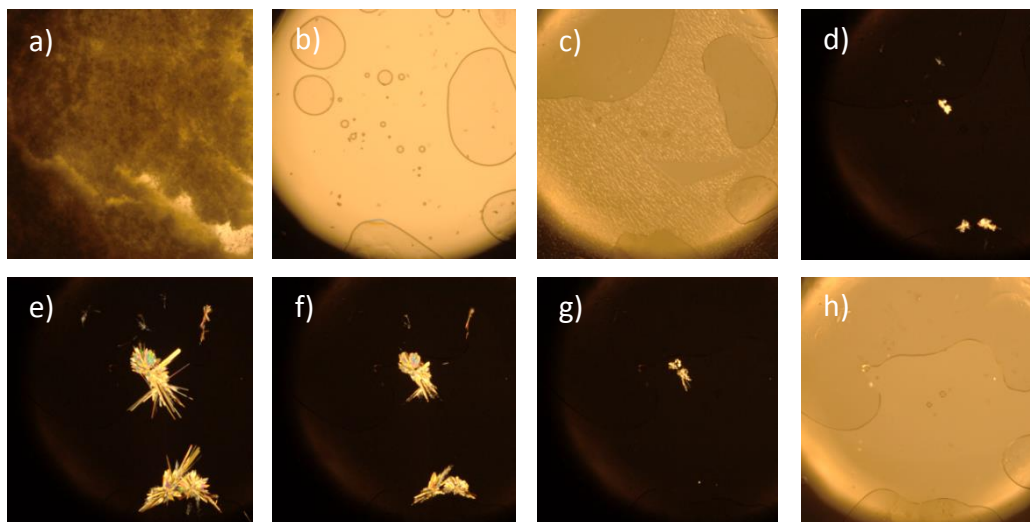
Figure 3.8 – Hot stage microscope heat/cool/heat experiment of bisVCap at a rate of 10 °C/min: a) start experiment at 18 °C, b) 150 °C, everything has melted, c) -100 °C cracks form, d) 100 °C small crystals begin to form, e) 145 °C crystals still continue to grow, f) 150 °C crystals begin to melt whilst crystals are still growing, g) 152 °C, melting continues h) 154 °C all crystals have melted.

The DSC of crystal **2** is similar to the DSC of bisVCap. Upon the first heating cycle the cocrystal melts at 109 °C, as shown by an endothermic peak in the DSC thermograph. Heating above 150 °C quickly leads to decomposition, most probably of the pDITFB as heating the single component above 150 °C leads to similar decomposition. In a DSC where decomposition has not occurred, such as Figure 3.9, the molten cocrystal can be cooled again, upon which it would be expected that a recrystallisation peak would be evident. There is no recrystallisation of crystal **2** on cooling. The second heat cycle reveals a glass transition at 9 °C and another, albeit much smaller, endothermic, melting peak at 109 °C. The second melt is at the same temperature as the first within error, suggesting it does not arise from either single component or a decomposition product, but from the melting of crystal **2**. The smaller peak suggests that there is much less material in the second melt than the first melt, similar to bisVCap. Again the lack obvious crystallisation peak in the DSC could either be because the recrystallisation is too slow to be easily observed or it is obscured by the melt.
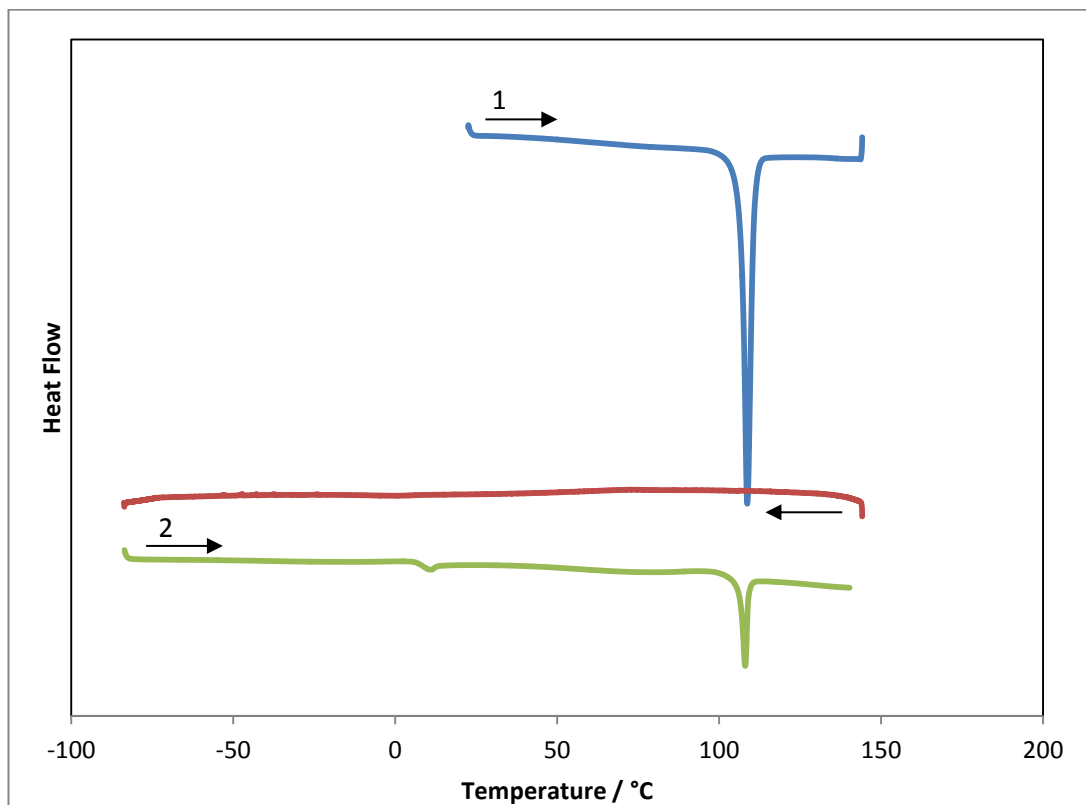
Figure 3.9 – DSC heat/cool/heat experiment of crystal 2 at a rate of 10 °C/min. Exotherm up.

To test if the slow crystallisation theory holds true, the method of the DSC experiment (10 °C/min, heat to 150 °C, cool to -90 °C, heat to 150 °C) was reproduced on the hot stage microscope, the pictorial results of which can be seen in Figure 3.10. The cocrystal melts at 110 °C in the hot stage microscope instead of 108 °C in the DSC, as previously mentioned this is due to slower temperature changes on the thicker glass slide when compared to the thin, metal DSC pans. The next event to occur is upon cooling to -62 °C, when the sample suddenly cracks, which is typical of a super cooled glass. More cracks appear as the sample is cooled further. During the second heating cycle the cracks start to disappear around 10 °C with all having disappeared by 15 °C. Again, this is later than the glass transition in the DSC which is at 9 °C and also takes much longer due to the rate of heating on the much thicker glass slide. With further heating to 77 °C small crystals appear. These crystal continue to grow as the sample is heated. By 106 °C the crystals are still growing but are also starting to melt again. Judging by the microscope slide, the crystallisation process occurs over a broad temperature range and all not all of the material recrystallises. The smaller amount of crystalline material formed in the second heating cycle is in keeping with the smaller second melt peak in the DSC. The recrystallisation occurs over a range of 39 °C and not all of the sample recrystallises resulting in a broad and weak recrystallisation peak which is not observable in the DSC thermograph.
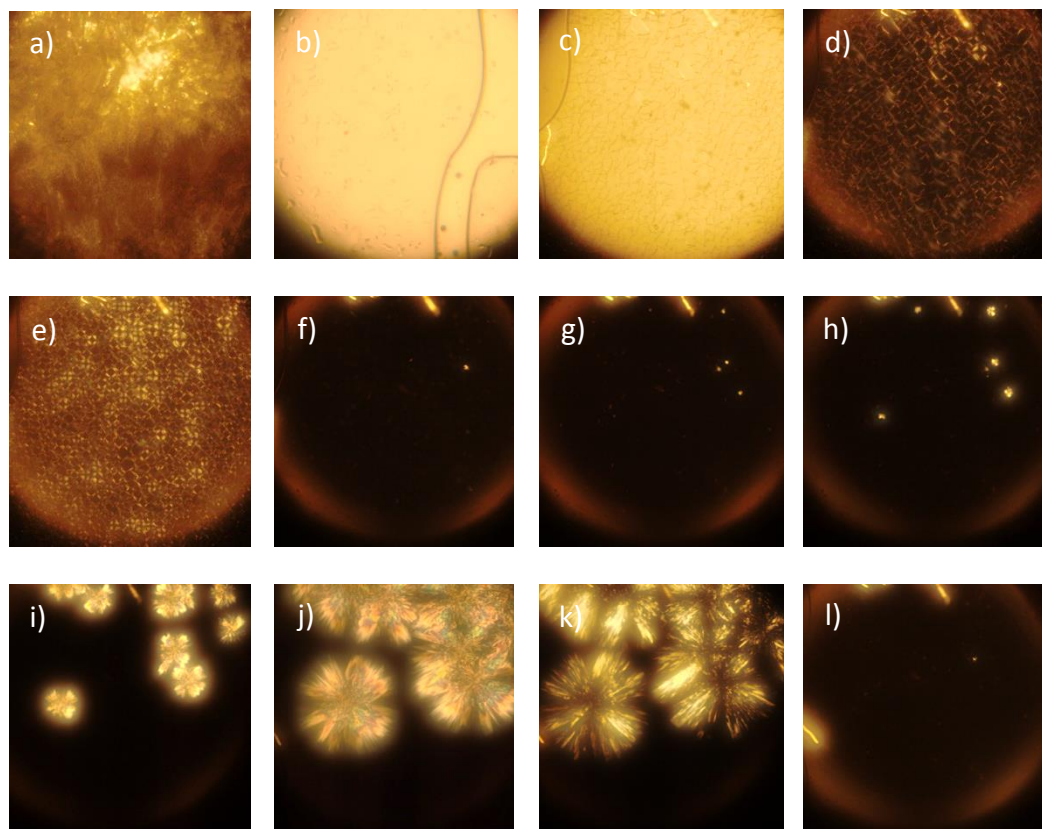
Figure 3.10 - Hot stage microscope heat/cool/heat experiment of crystal 2 at a rate of 10 °C/min: a) start at 15 °C, b) 110 °C, all material has melted, c) -62 °C, cracks form, d) -77 °C, polarising filter changed to crossed, cracks continue to form, e) -90 °C, more cracks have formed, end of cooling, f) 15 °C cracks disappeared, g) 77 °C, crystals appearing, h) 80 °C, crystal growth, i) 90 °C, crystals continue growing, j)106 °C, crystal growth halts, smaller crystals begin to melt, k) 114 °C, melting becomes quicker, affecting the larger crystals, l) 115 °C all crystals melted.

It is not uncommon for a compound to exhibit a metastable amorphous form and a crystalline form, but it is much more uncommon for a cocrystal to exhibit a coamorphous form, as usually the second component will stabilise one form or the other and thus not allow both. Quasi-isothermal DSC measurements can be used to calculate the heat capacity of a material and thus compare the relative stability of crystalline and amorphous forms.[24,25]

As can be seen from Figure 3.11, pDITFB has the lowest heat capacity of all the samples tested. As expected from the previous DSC thermograph, Figure 3.5, showing pDITFB to have a melting point of 108 °C, there is a peak in the heat capacity plot around 380 K from the sample melting. After melting the heat capacity is slightly higher as liquids are not as thermodynamically stable as crystals.

The crystals of bisVCap have higher heat capacity than the cocrystal. It is a possibility that difference in heat capacity between bisVCap and crystal **2** could be a major part of the driving force for the cocrystal formation, as the difference in heat capacity shows crystal **2** to be more thermodynamically stable than bisVCap. Both crystals show melting points approximately where one would expect from the the previous DSC plots, Figure 3.7 and

Figure 3.9. The heat capacity of the liquids is higher than the crystal for both bisVCap and crystal **2**.[26]

The amorphous form of bisVCap has a higher capacity than the crystalline form. There is a large change in heat capacity of the amorphous form as it goes through the glass transition. The heat capacity starts decreasing again at 318 K, where during the microscope experiment it was seen that crystallisation started. The heat capacity of the amorphous form in the quasi-isothermal DSC never reached the level of the crystalline form as never at any point does the whole of the sample crystallise. The amorphous bisVCap after the glass transition has a similar heat capacity to the melt of the crystalline bisVCap. This is in keeping with the fact that amorphous forms are super cooled liquids, so should have a very similar heat capacity to the melt.[26]

The coamorphous form of crystal **2** has higher heat capacity than the cocrystalline form. Similar to bisVCap, the amorphous form of crystal **2** after the glass transition has a similar heat capacity to the melt. Before the glass transition the heat capacity of the coamorphous material is very low, approaching that of the crystal, showing the coamorphous form to be particularly stable so there is little driving force for recrystallisation.
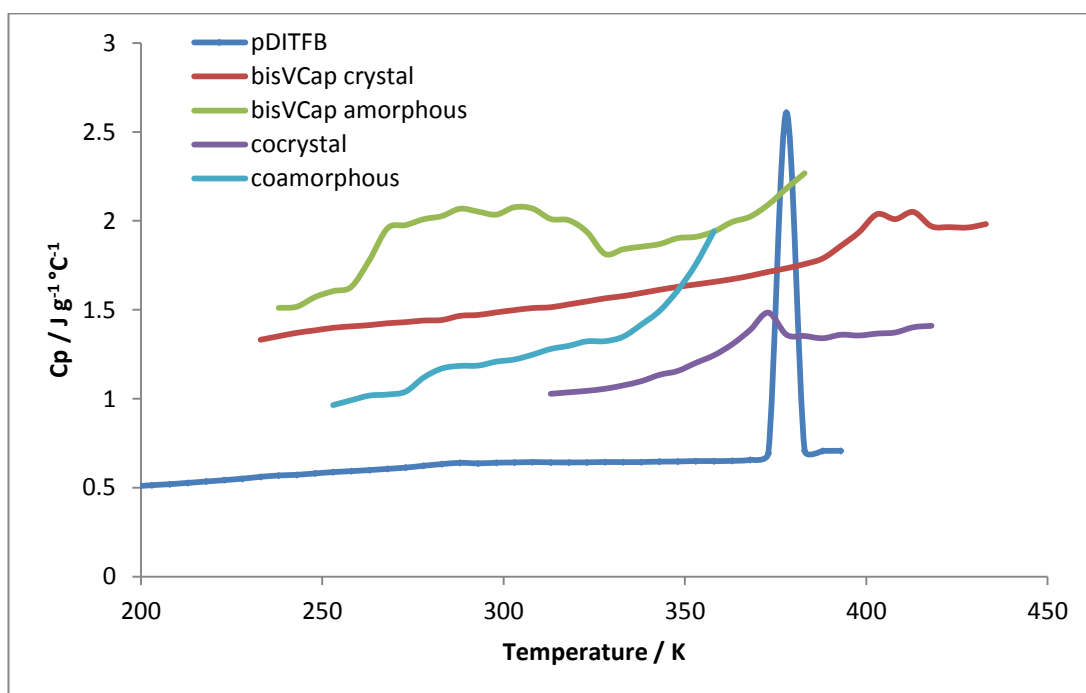
Figure 3.11 – Heat capacity against temperature from the quasi-isothermal DSC for pDITFB, crystalline bisVCap, amorphous bisVCap, crystalline bisVCap/pDITFB and amorphous bisVCap/pDITFB.

Addition of pDITFB to bisVCap gave a novel cocrystal of a model compound which has previously proven challenging to crystallise. The cocrystal is rare as it is also stable as a coamorphous form as well as a cocrystalline form. Further investigation into the heat

capacity and molecular mobility would give insight into the interactions which dictate the stability of the crystalline and amorphous forms of bisVCap and the cocrystal, though more in depth analysis is beyond the scope of this thesis.

3.2.3 Metal cocrystals and complexes

BisHEP has previously shown the ability to form metal complexes with a zinc and the s-block metals[1,27] and H_2bisVP has been reported in a complex with sodium.[27] The model compounds **6**-**9** have shown no such capacity for metal binding with the s-block elements or zinc. Searching the CSD reveals multiple structures of rare earth metals surrounded by 4 to 8 pyrrolidone, piperidone or caprolactam molecules. For example, Evans *et al.*[28] reported crystal structures of the form shown in Scheme 3.1 with cerium, praseodymium and neodymium. This suggests that the lactam functionality might have a higher affinity for the rare earth metals than the s-block metals and thus complex more readily. Attempts to form metal complexes of model compounds **6**-**10** with terbium, gadolinium, yttrium, ytterbium, lanthanum, aluminium and vanadium were performed. Model compounds and metal salts were mixed in a 3:1 molar ratio of model compound:metal salt and dissolved in water. The solvent was allowed to evaporate at room temperature. From these experiments a single complex was formed. $CdCl_2$ and compound **5**, HEPVCap, resulted in a coordination polymer discussed in section 3.2.3.1.
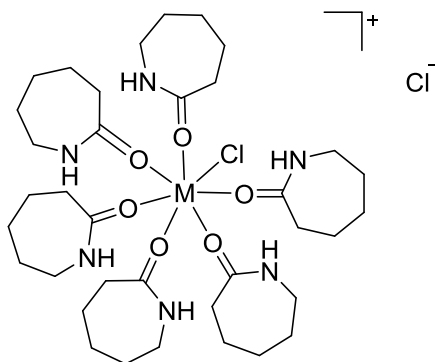
Scheme 3.1 – General form of the caprolactam metal complexes reported by Evans *et al.*[28]

As the complexation experiments model compounds **6**-**10** only resulted in a single novel crystal structures compounds **11**-**16** the structures of which can be seen in Scheme 2.1. The details of their synthesis can be found in chapter 2. Compounds **14**-**16** have major impurities of the dimeric model compounds bisVP or bisVCap. The crude products were still tested in crystallisation experiments as the potential for tetradentate chelation from the new products may result in preferred chelation over the bidentate chelation possible by the side products of bisVP and bisVCap.

The model compounds **13**-**16** were mixed with a wide range of metal salts from the s, d and f block as well as $Al(NO_3)_3$ in water; the full list of metal salts can be found in the experimental section 3.3.3. A very large majority of these crystallisation attempts resulted in crystals of the metal salt without any ligand complexed or oily mixtures. $CdCl_2$ with $Et(OVCap)_2$ gave a novel product which is discussed in section 3.2.3.2. The crude $Et(OVP)_2$/bisVP mixture with $Y(CF_3SO_3)_3$ also gave a novel complex which is detailed in section 3.2.3.3.

3.2.3.1   Caprolactam/HEP/CdCl₂

In the presence of $CdCl_2$ HEPVCap decomposes to HEP and ε-caprolactam. The decomposition of the ether linkage of HEPVCap in the presence of $CdCl_2$ suggests the ether link to be unstable to Lewis acids. The fragments then coordinate to the cadmium centres giving a crystal, crystal **3**, with the formula $3(CdCl_2).2(C_6H_{11}NO).2(C_6H_{11}NO_2)$. The crystal structure of crystal **3** is shown in Figure 3.12.

Figure 3.12 – Crystal structure of crystal 3. Hydrogen bonds between the ligands are shown by red dashed lines.

The cadmium centres are linked together into chains by bridging chloride ligands, two shared between two metal centres. The $CdCl_2$ chains are linked by two bridging HEP molecules to

the same two cadmium centres. Going along a cadmium chain there are three distinct cadmium centres. The first has two ε-caprolactam ligands, one above and one below the line of the chain. The next along has two HEP ligands bridging to the next chain below, the next and final cadmium centre has two HEP ligands bridging to the chain above. After this final bridged cadmium centre, the pattern repeats, returning to cadmium with two ε-caprolactam ligands.

There are hydrogen bonds between the carbonyl groups of the ε-caprolactam ligands and the hydroxyl groups of the nearest HEP ligands. These hydrogen bonds have O⋯O distances which vary between 2.644(6) - 2.719(7) Å. The Cd-Cl bonds range from 2.542(2) – 2.642(1) Å, with all four Cd-Cl bond of each metal centre being different from one another. The distances between the cadmium atoms in the chain varies from 2.786 – 3.857 Å with the shorter distances occurring between centres ε-caprolactam and centres with HEP and the longer distances occurring between to HEP bound centres. The organic ligands demonstrate shorter metal-ligand distances than the Cd-Cl bonds, with Cd-ε-caprolactam distances being between 2.396(5) – 2.427(5) Å, bonds between cadmium and the carbonyl group of HEP being 2.278(4) – 2.338(4) Å and bonds between cadmium and the hydroxyl group of HEP being 2.341(4) – 2.356(4) Å.

3.2.3.2 Caprolactam/ethylene glycol/CdCl$_2$

Et(OVCap)$_2$ in the presence of CdCl$_2$ decomposes to ε-caprolactam and ethylene glycol. The fragments all coordinate to the cadmium metal centres to form crystal **4** with the formula 2CdCl$_2$, 2(C$_6$H$_{11}$NO), C$_2$H$_6$O$_2$. The crystal structure of crystal **4** as can be seen in in Figure 3.13. The cadmium metal centres are joined to one another by two bridging chloride ions to form a chain. The Cd-Cl bond distance vary between 2.548(1) – 2.632 (6) Å with all four bonds to each metal centre being of different length. The Cd-Cd distances in the chain are either 3.725(1) Å or 3.789(1) Å. From the cadmium with the ε-caprolactam ligands, the distance to the next two cadmium centres is the same, whilst for cadmium atoms with ethylene glycol ligands, the nearest two cadmium centres are different distances away.
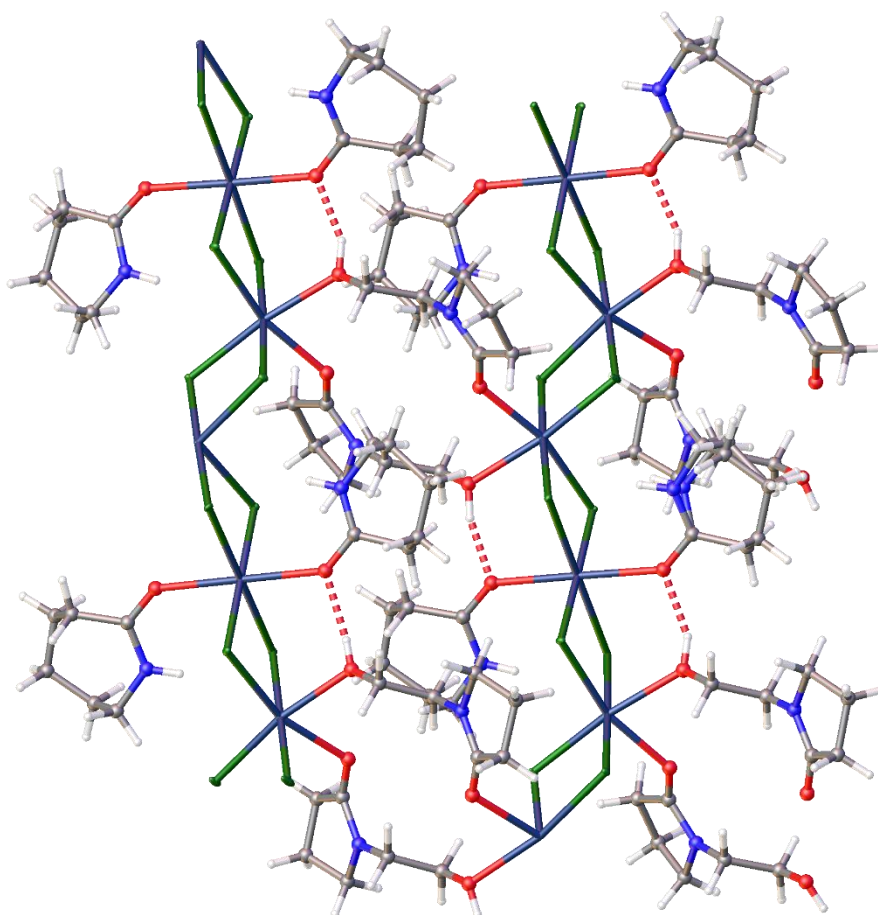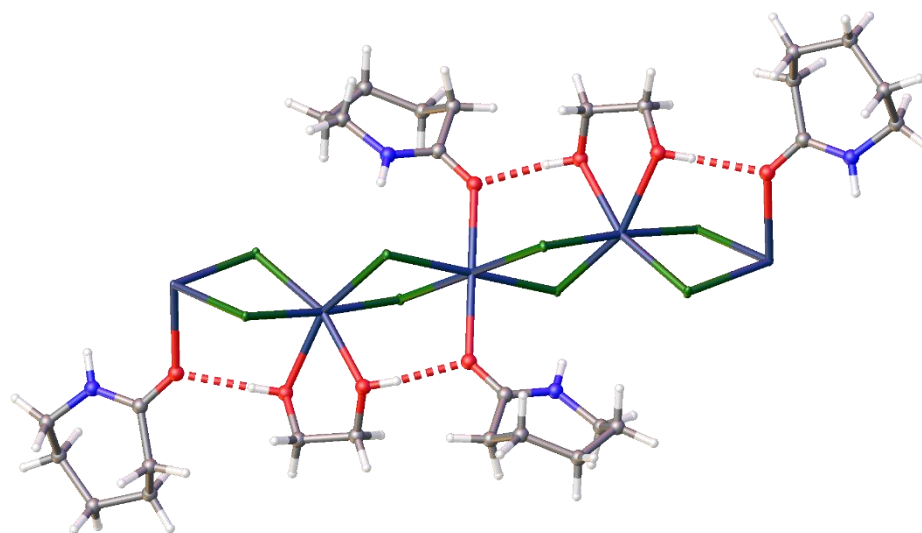
Figure 3.13 - Crystal structure of crystal 4. Hydrogen bonds between the ligands are shown by red dashed lines.

Going along the cadmium chain, the pendant groups alternate between cadmium with a bidentate ethylene glycol ligand and cadmium with two ε-caprolactam ligands. The ε-caprolactam ligands lie equidistant above and below the chain, though there are two different ε-caprolactam coordinated cadmium centres, one with Cd-ε-caprolactam bond lengths of 2.417(2) Å and the other with Cd-ε-caprolactam bond lengths of 2.332(2) Å. the ethylene glycol binds asymmetrically with one end exhibiting a Cd-O bond length of 2.382(2) Å and the other a Cd-O bond length of 2.337(2) Å. There are hydrogen bonds between the carbonyl of the ε-caprolactam molecules and the hydroxyl groups of the ethylene glycol. The shorter Cd-ε-caprolactam bond, 2.332(2) Å, hydrogen bonds to the side of the ethylene glycol with the shorter Cd-O bond, 2.337(2) Å, by a hydrogen bond with an O···O distance of 2.679(2) Å. The hydrogen bond between the ε-caprolactam with the longer Cd-ε-caprolactam bond, 2.417(2) Å and the side of the ethylene glycol with the longer Cd-O bond, 2.372(2) Å, exhibits a longer hydrogen bond with an O···O distance of 2.729(2) Å.

The ether linkages in both Et(OVCap)$_2$ and HEPVCap are not stable to Lewis acids. In Lewis acidic conditions, such as in solution with the Lewis acidic metals used in the crystallisation experiments, the ether linkages undergo cleavage, resulting in ε-caprolactam and an alcohol. There is no proposed theory for what happens to the two carbon atoms from VCap which are not present in the crystal structures.

3.2.3.3   1,1,3-tri-2-pyrrolidonylbutane/Y(CF$_3$SO$_3$)$_3$

The crude mixture of Et(OVP)$_2$ and bisVP when mixed with Y(CF$_3$SO$_3$)$_3$ in water resulted in crystals of diffraction quality from slow evaporation of the solvent. A complex of Et(OVP)$_2$

coordinated to a metal was again not what was achieved, but to differ from the $CdCl_2$ crystal structures $Y(CF_3SO_3)_3$ did not complex with the fragments of a decomposed molecule. Instead a completely new ligand had been formed in-situ, the structure of which can be seen in Scheme 3.2. The resulting crystal, crystal **5** has the formula $C_{16}H_{35}N_3O_8.3(CF_3SO_3).H_2O$ and the crystal structure of crystal **5** is shown in Figure 3.14 From the two $CdCl_2$ structures, it has been seen that the presence of a Lewis acid can break down the ether-VCap links to give free ε-caprolactam, thus it is reasonable to assume that Lewis acids could also break down an ether-VP link to free pyrrolidone. This free pyrrolidone could then attack the double bond of the bisVP resulting in the product in Scheme 3.2.
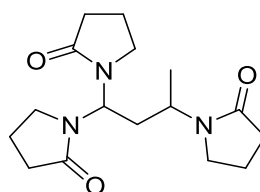
Scheme 3.2 – Tridentate pyrrolidone ligand from crystal 5.

The yttrium metal centre is 8-coordinate, with 5 water ligands and two 1,1,3-tri-2-pyrrolidonylbutane ligands, one bound mono dentate and one bound bidentate. The ligands are bound asymmetrically with no ligand being directly opposite another. The bidentate ligand O-Y distances are 2.305(3) and 2.315(3) Å whilst the monodentate ligand has an O-Y length of 2.277(3) Å. The water ligands O-Y distances range from 2.329(3) – 2.390(3) Å. The crystal structure contains chains of 1,1,3-tri-2-pyrrolidonylbutane and yttrium, with the 1,1,3-tri-2-pyrrolidonylbutane binding bidentate to one yttrium centre then binding monodentate to the next yttrium centre. The 1,1,3-tri-2-pyrrolidonylbutane ligand does not exhibit any carbonyl based hydrogen bonding as the carbonyls are already taken up by the ligand-yttrium coordination bond. The three triflate anions accept hydrogen bonds to their sulfonate groups from the water molecules coordinated to the yttrium centre. These hydrogen bonds have O⋯O lengths ranging from 2.686(6) – 2.792(4) Å.
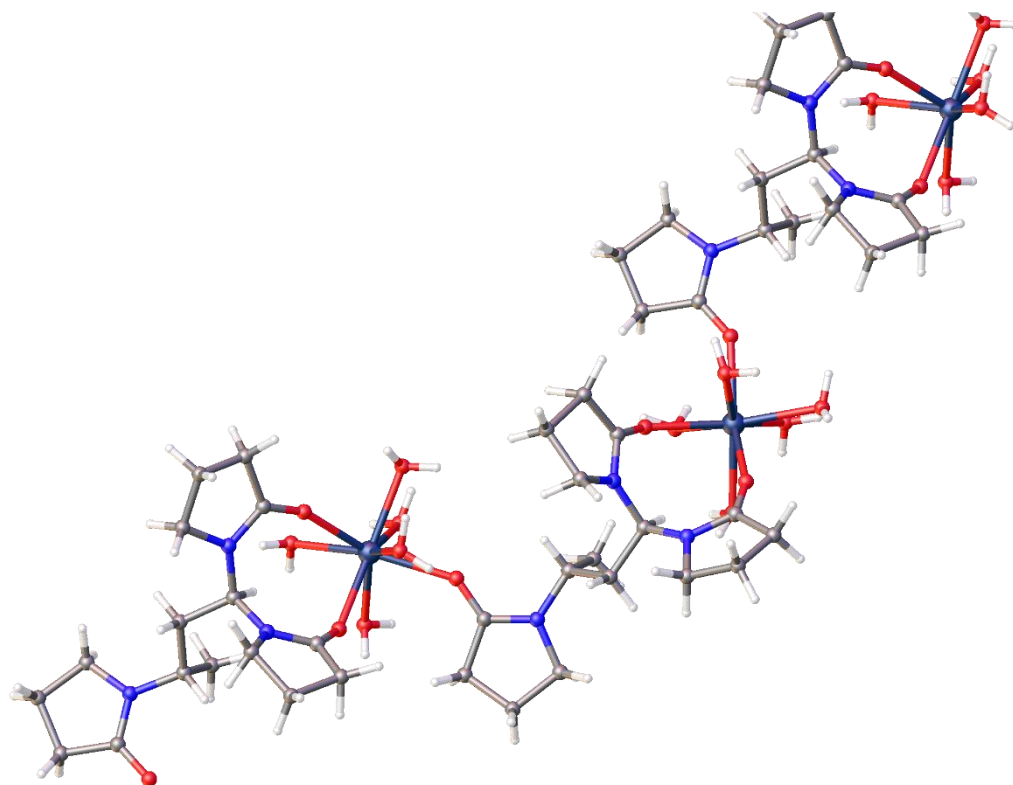
Figure 3.14 – Crystal structure of crystal 5, showing the chain of yttrium centres held together by 1,1,3-tri-2-pyrrolidonylbutane ligands binding to on yttrium centre in a bidentate fashion and another yttrium centre in a monodentate fashion. The triflate anions are omitted for clarity.

In conclusion the ether-lactam link, whilst stable in aqueous solution, is not stable when in the presence of certain metal compounds. Mild Lewis acid catalysts with the ability to coordinate the lactam carbonyl groups and any resulting alcohols can result in the degradation of the ether link. The exact nature of the metal salt does have a notable effect on the metal's efficiency at degrading the ether link as Et(OVCap)$_2$ successfully crystallised as a pure organic crystal from solutions containing Cd(CH$_3$COO)$_2$ and Cs(CH$_3$COO)$_2$, though CdCl$_2$ resulted in its degradation. Whilst disappointing that the ligands did not function as intended, the unexpected reaction of Et(OVP)$_2$ with Y(CF$_3$SO$_3$)$_3$ may introduce new opportunities by way of creating new compounds to model PVP and PVCap, containing three and not two rings, which would allow for more confirmations and opportunity to chelate in a more than bidentate fashion.

3.2.4   Other crystals

3.2.4.1   The GRAS list

In the pharmaceutical industry there is a list of additives which are safe for human consumption called the generally regarded as safe (GRAS) list. This list is used to help look for cocrystals of drugs that do not need extensive toxicity studies before going to clinical

trials. This reduces the chances of making a biologically incompatible cocrystal and increases the chance of a drug being accepted for human consumption. As the GRAS list is commonly used for cocrystal screening, it was a logical choice for some initial experiments. As PVP is commonly used for drug delivery, from being a simple pill binder,[29–31] to potentially helping controlled release formulations by formulating thermoresponsive delivery systems,[32–35] it is possible that there are suitable interactions between the models of PVP and drug molecules or additives to form cocrystals.

The potential coformers with the ability to donate hydrogen bonds chosen were (+)-tartaric acid, 4-aminobenzoic acid, citric acid, glutamic acid, nicotinamide, nicotinic acid, fumaric acid, malonic acid, succinic acid and oxalic acid. All are carboxylic acids so have the ability to accept as well as donate hydrogen bonds. This unfortunately increases the chance of single component crystallisation as the component has sufficient interaction with itself to make its crystallisation favourable. This did not seem to be the case. All crystallisation attempts resulted in thick oils. No crystals formed over the course of two years.

3.2.4.2 Hydrogen bond donors

All of the model compounds are capable of accepting hydrogen bonds, but not donating them to any significant degree. Thus a compound which is hydrogen bond donating, but not accepting, should be capable of supplying the lacking hydrogen bond donation interactions and form cocrystals with the model compounds. The compounds studied in this context were: guanidine, metformin, tannic acid, telluric acid, boric acid and a range of other boronic acids.

Guanidine and metformin (the pharmaceutical name for 1,1-dimethylbiguanide) are both available as HCl salts. Chloride ions are strongly hydrogen bond accepting, so exchange to a much less hydrogen bond accepting counter ion was undertaken. Hexafluorophosphate is not significantly hydrogen bond accepting and is a large and diffuse ion so was chosen as it may aid solubility of the salts in non-aqueous solvents and thus allow for a wider solvent choice and limit the possible hygroscopicity of the products. The ion exchange was performed using $AgPF_6$, as insoluble AgCl is formed and can simply be filtered away, preventing reverse ion exchange. Even with an anion as diffuse as hexafluorophosphate, both metformin and guanidine were still only soluble in water to any meaningful extent, so crystallisations were performed in water. Both coformers with mixed in 1:1 ratios with **6-11** and allowed to crystallise by evaporation from water. All attempted crystallisations gave plate-like and twinned crystals. Recrystallisation by heating and cooling and by redissolving

and evaporating slower did not result in crystals of quality suitable for single crystal x-ray diffraction.

Tannic acid is a large polyphenol which is an acid derivative of tannin which is found naturally in oak leaves and bark. Whilst the carbonyls of the ester group could technically accept hydrogen bonds, the steric bulk of the molecule would make accessing them difficult. Taking this into consideration, tannic acid falls into the category of hydrogen bond donor which does not accept hydrogen bonds. The large molecular mass of tannic acid makes crystallisation challenging, though ease of availability makes it attractive. Tannic acid was mixed with compounds **6**-**11** in a 1:1 molar ratio and then dissolved in water. Solvent evaporation resulted in very viscous, brown liquids. No crystal formed over the course of two years.

Boric acid has previously been reported to cocrystallise with the one of the model compounds, bisHEP, as a 1:1 bisHEP:boric acid cocrystal.[1] However, no further boric acid based co crystals were achieved by crystallisation attempts with boric acid and the other model compounds **6**-**10**.

Telluric acid is analogous in form to boric acid. Instead of boron which is surrounded by three hydroxyl groups, telluric acid contains tellurium and is surrounded by six hydroxyl groups. As boric acid has shown such promise by crystallising with bisHEP, a similar acid may also prove useful. Telluric acid was mixed in a 1:1 ratio with compound **6**-**10**, dissolved in water and the solvent was left to evaporate. After 8-9 months, low quality crystals of telluric acid are eventually formed in all attempted crystallisations with no trace of any model compound.

Taking a boronic acid to be of the form RR'BOH where R and R' can be any group, boric acid is the simplest boronic acid. Again, as boric acid can form a cocrystal with bisHEP, it is possible that other boronic acids may also cocrystallise with the model compounds. A range of monoboronic acids were chosen based on availability: 2-chloropyradine boronic acid, 4-formylphenyl boronic acid, 2-fluoropyradine, 4-pyradinylphenyl boronic acid, 3-pyridyl boronic acid, 4-pyridyl boronic acid, 3-furyl boronic acid, 3-thiophenyl boronic acid, 1,4-phenyldiboronic acid and tetrahydroxydiboron. All were mixed with compounds **6**-**11**, dissolved in water and the solvent was left to evaporate. Two cocrystals were formed by 1,4-phenyldiboronic acid with bisHEP and tetrahydroxydiboron with bisVCap which are detailed in section 4. The crystallisation containing 3-furyl boronic acid and bisHEP gave crystals of pure 3-furyl boronic acid which have not been reported in the CSD so the crystal structure of 3-furanyl boronic acid is shown here in Figure 3.15.
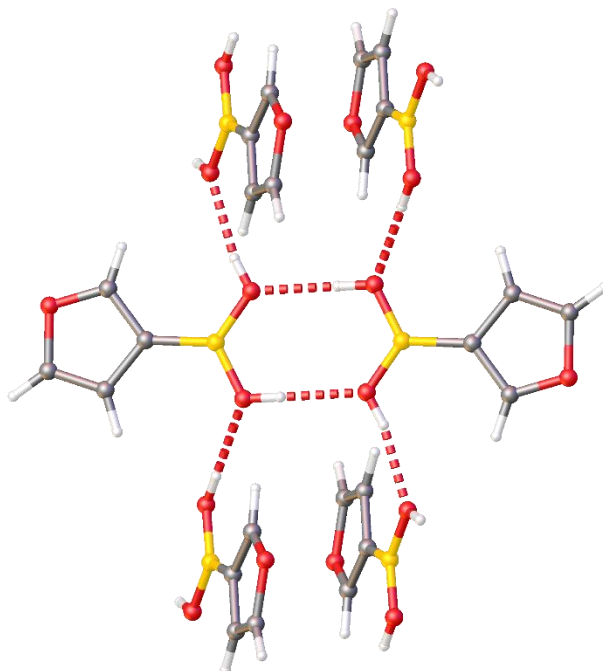
Figure 3.15 – Crystal structure 3-furanyl boronic acid, showing the 3-furyl boronic acid dimer and bond to the nearest dimers on either side. Hydrogen bonds are shown by red dotted lines.

The 3-furyl boronic acid molecules are held together in dimers by a cyclic hydrogen bond pattern between the hydroxy groups of the boronic acid groups, with each molecule donating and accepting a hydrogen bond, these hydrogen bonds have an O···O distance of 2.7334(2) Å. These dimers are planar. The next dimer along is held close by O-H···O hydrogen bonds between the boronic acid groups with O···O distances of 2.726(2) Å. The planes of two neighbouring dimers are at 64.78° to each other.

The hydrogen bonds are easily observable and highlighted by black arrows in the Hirshfeld surface fingerprint plot in Figure 3.16. Further out from the trailing diagonal there are two more peaks, highlighted by blue arrows, arise from hydrogen bonding interactions. Where one dimer donates a hydrogen bond to the neighbouring dimer, the same hydroxyl group accepts a hydrogen bond from a C-H of the furan ring. This hydrogen bond has a C···O length of 3.366(3) Å which is significantly longer than the O-H···O hydrogen bond so thus appears further from the diagonal.
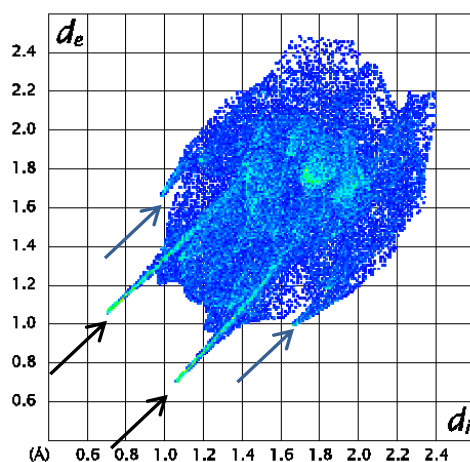
Figure 3.16 – Hirshfeld surface fingerprint plot of 3-furyl boronic acid, black arrows point to O-H...O hydrogen bond interactions, blue arrows point to C-H...O hydrogen bond interactions.

3.2.4.3   Peroxide

In mildly sour systems (pipelines containing small amounts of H_2S) hydrogen peroxide can be added along with the KHI to interact with the H_2S and remove it from the pipeline. Hydrogen peroxide is loaded into the polymer mix and it is possible that the hydrogen peroxide interacts strongly enough with the polymer that it may crystallise with the model compounds.

A range of crystallisation attempts with compounds **6-9** with molar peroxide ratios 1:2, 1:1 and 2:1 were performed. A small volume of warm water was used to dissolve any model compound which had not dissolved in the peroxide solution and the crystallisation were left in the fridge at 5 °C. All bisVCap crystallisations returned solids though none of diffraction quality. The other model compounds remained liquid after two years. Whilst an interesting concept, interaction with peroxide is not a strong enough driving force to cocrystallise with the model compounds.

3.2.4.4   Analogous compounds

As the model compounds based on hydrate inhibitors have proven difficult to crystallise, it became of interest to try analogous compounds, such as similar ring based carbonyls with different heteroatoms as shown in Scheme 3.3. The goal is to find conceptually similar molecules that will crystallise quicker and with a higher rate of success at forming cocrystals but still have similar functionality and shape. Compounds **18-23** are commercially available. Compound **17** was synthesised from thionyl chloride and butanediol by the procedure outlined by Gao *et al.*[36]

2,7-dioxathiephene-1-oxide (17) caprolactone (18) dihydrothiophen-3-one (19) dihydrofuran-3(2H)-one (20)

2(5H)-thiophenone (21) 6-hydroxybenzo[d][1,3] oxathiol-2-one (22) 3-methyl-2(3H)-benzothiazolone (23)
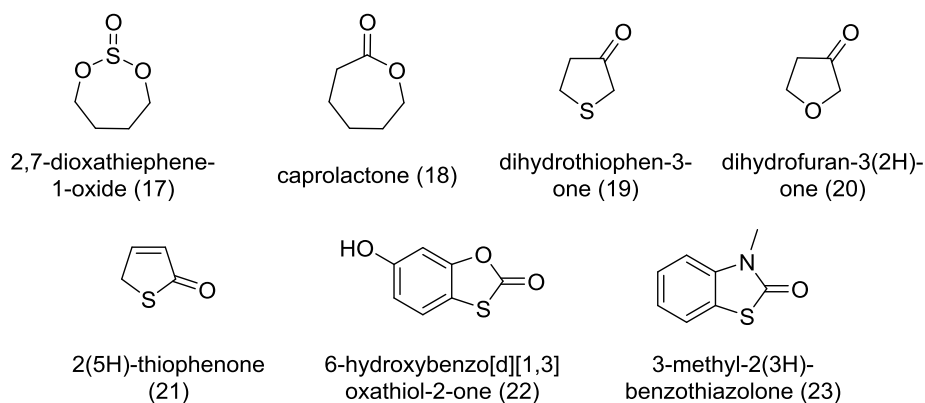
Scheme 3.3 – Structure of the compounds analogous to the model compounds based on PVP and PVCap.

A relatively small range of second components were chosen to attempt to cocrystallise with compounds **17-23**. Those selected for their hydrogen bond donation: boric acid, tetrahydroxydiboron, metformin, guanidine and telluric acid, and the halogen bonding compounds: pDITFB, oDITFB, 1,4-diiodobenzene and 1-chloro-(2-iodoethynyl)benzene. All crystallisations were performed using a 1:1 molar ratio of components. All halogen bonding experiments were performed in a 1:1 volume ratio of acetone:DCM. The boric acid, tetrahydroxydiboron, metformin, guanidine and telluric acid crystallisation of compounds **18-23** were performed in water, whilst compounds 12 was performed in a 1:1 volume ratio of acetone:water as **17** is not water soluble.

Unfortunately no cocrystals were formed. Compound **23** often crystallised as low quality single component crystals and pDITFB and 1,4-diiodobenzene also gave crystals of the single components. Whilst an interesting idea the right components to form cocrystals with **17-23** was not found in this short screen. Future work would benefit from a more through screen of potential second components, ratios and solvent choices. Though the cost and quantity of the compounds may be a barrier to a truly broad cocrystal screen.

3.2.5 Grinding

Grinding is a method commonly used in cocrystal screens. The two desired coformers are ground together and analysed by PXRD, Raman spectroscopy or IR spectroscopy, to determine whether the resulting powder is just a simple mixture with no strong interactions between the components or a new material different from its constituent parts.[3,37,38] Grinding is usually performed using a mortar and pestle or a mill, such as a ball mill. It is sometimes advantageous to add a small amount of solvent to maximise surface area and aid cocrystal formation, this process is called solvent drop grinding or liquid assisted grinding.[39] As the model compounds interact mainly through the carbonyl moiety of the lactam ring, IR spectroscopy is ideal to study if the model compounds form new species when ground with

a second component. The carbonyl stretch in IR spectroscopy is strong and sensitive to changes such as hydrogen bonding and metal coordination so if a cocrystal or other new species is formed, the hydrogen bonding interaction of the carbonyl group should be readily apparent from the shift in the IR carbonyl peak.

Compounds **6**-**8** and **10**-**12** were used in grinding experiments. As purification of compound **9** has not been possible it was not chosen for grinding, as the crude mixture results in multiple peaks in the carbonyl region, making clear analysis difficult. Compounds **6**-**8** and **10**-**12** were ground together in a 1:1 molar ratio with aluminium nitrate, boric acid, pDITFB, guanidinium tetrafluoroborate, nicotinamide, tartaric acid and telluric acid. Grinding was performed by hand using a mortar and pestle until a visibly homogeneous mixture was formed. The samples were then analysed by IR spectroscopy using an ATR attachment. Spectra of the mixtures were overlaid with a spectrum of the pure model compound and the position of the carbonyl peaks were compared. The overlay of bisHEP and the ground bisHEP samples can be found in Figure 3.17.
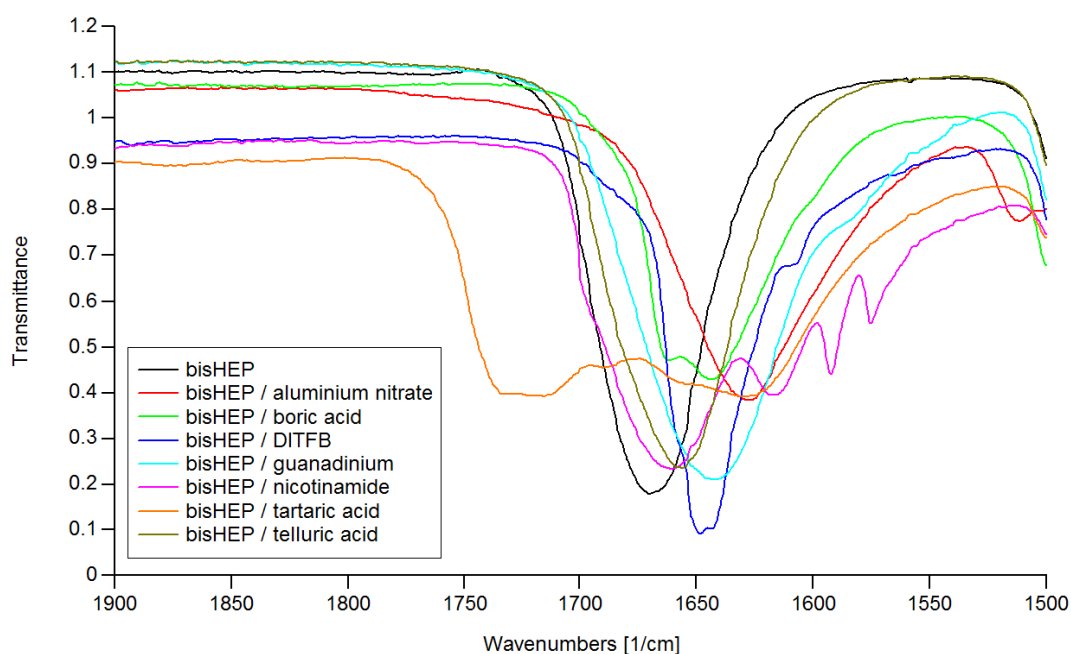
Figure 3.17 – Overlay of the IR spectra of bisHEP and bisHEP ground in a 1:1 ratio aluminium nitrate, boric acid, DITFB, guanidinium BF$_4$, nicotinamide, tartaric acid and telluric acid.

The IR carbonyl peak shifts for compounds **6**-**8** and **10**-**12** alone and when ground are shown in Table 3.1. BisVCap shows no change in the carbonyl peak when ground with any of the selected chemicals. To check is the lack of change in the carbonyl peak is truly from a lack of interaction or inadequate mixing, bisVCap and aluminium nitrate were mixed in a 1:1 molar ratio and ground together using a ball mill. The mixture was milled in 10 min bursts at 20 Hz and an IR spectrum recorded after every 10 min milling. The milling was performed for a total

of 50 min. As seen in Figure 3.18, even after 50 min of milling, there is no change in the carbonyl peak of bisVCap in the IR spectra. This suggests that there is no significant interaction between bisVCap and aluminium chloride and the lack of carbonyl peak shift did not arise from inadequate mixing.
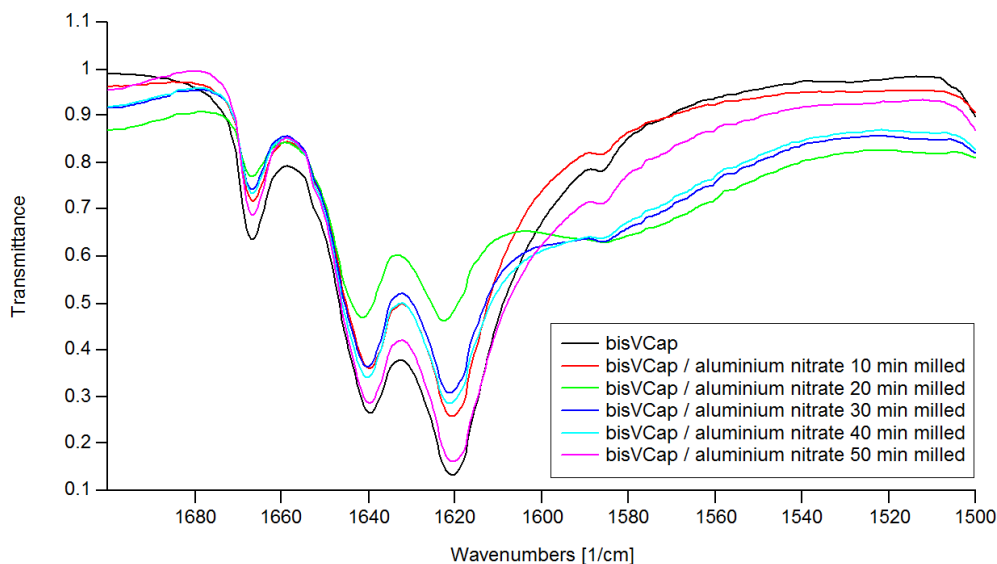
Figure 3.18 – IR spectra of bisVCap with aluminium nitrate after milling in 10 min increments.

MEP also showed no significant change in the carbonyl peak with any of the compounds tried. Suggesting that there is no significant interaction between MEP and aluminium nitrate, boric acid, pDITFB, guanidinium tetrafluoroborate, nicotinamide, tartaric acid or telluric acid. There is no carbonyl shift reported for MEP with nicotinamide of guanidinium BF_4 as the nicotinamide carbonyl peaks and the guanidinium imine peak obscure the MEP carbonyl peak.

HEPVCap did not show any peak shifts larger enough to represent the formation of hydrogen bond. When ground with aluminium nitrate the carbonyl peaks broaden too much to accurately pick out the signals from both carbonyls, whilst this suggests some interaction, compared to the large shifts cause by aluminium nitrate with bisVP, H_2bisVCap and bisHEP, the broadening of the HEPVCap carbonyl peak is not significant. When ground with tartaric acid and nicotinamide the HEPVCap signals are obscured by the carbonyl peaks of tartaric acid and nicotinamide so cannot be recorded.

The carbonyl peak of bisVP show no change within error when ground with telluric acid. With boric acid, pDITFB, guanidinium BF_4, nicotinamide and tartaric acid there are significant shifts between 7-20 cm^{-1} and with aluminium nitrate there is a large peak shift of 45 cm^{-1}. This suggests with tested chemicals, except telluric acid, there is interaction between bisVP and

the chemical. BisVP is an oil at room temperature and upon grinding with any of the tested compounds thick oils form. These show no birefringence under polarised light and no crystals formed over the course of three days.

	bisVCap		bisVP	H$_2$bisVCap	HEPVCap		bisHEP	MEP
model compound	1667	1640	1673	1631	1647	1629	1671	1632
aluminium nitrate	1667	1641	1628	1588	-	1627	1627	1633
boric acid	1667	1641	1652	1617	1642	1624	1662	1632
DITFB	1667	1641	1653	1614	1647	1624	1648	1632
guanidinium BF$_4$	1666	1640	1666	1598	1643	-	1643	-
nicotinamide	1667	1641	1657	1614	-	-	1661	-
tartaric acid	1667	1641	1657	1592	-	-	1629	1632
telluric acid	1667	1641	1676	1627	1644	1629	1657	1633

Table 3.1 –Carbonyl peak positions in cm^{-1} for model compound 1-3 and 5-7 alone and ground in a 1:1 molar ratio with aluminium nitrate, boric acid, DITFB, guanidinium BF$_4$, nicotinamide, tartaric acid and telluric acid. Dashed indicated that the peak of interest was either obscured or too broad to measure.

H$_2$bisVCap shows no shift with telluric acid, moderate shifts of 14-17 cm^{-1} with boric acid, nicotinamide and pDITFB and large shifts of 32-42 cm^{-1} with aluminium nitrate, guanidinium BF$_4$ and tartaric acid. This suggests that there is significant interaction between H$_2$bisVCap and boric acid, nicotinamide and pDITFB and strong interactions between H$_2$bisVCap and aluminium nitrate, guanidinium BF$_4$ and tartaric acid. H$_2$bisVCap is usually an oil at room temperature due to absorbed water,[40] when ground with any of the chosen chemicals, a thick paste which shows no birefringence under polarised light was formed. Even leaving in a vacuum desiccator under vacuum for three days did not form any solids.

The carbonyl peak for bisHEP changes with addition of all of the tested compounds. A moderate shift between 9-13 cm^{-1} is seen with boric acid, nicotinamide and telluric acid, a larger shift of 23-28 cm^{-1} is seen with pDITFB and guanidinium BF$_4$ and large shifts of 42-44 cm^{-1} were seen with aluminium nitrate and tartaric acid. This suggests that bisHEP interacts with all the compounds tested. BisHEP is a liquid at room temperature and all the ground mixtures were also liquids and no solids were observed over the course of three days.

Slow evaporation experiments of 1:1 ratios compounds **6**-**8** and **10**-**12** with aluminium nitrate, boric acid, guanidinium tetrafluoroborate, nicotinamide, tartaric acid and telluric acid from water and compounds **6**-**8** and **10**-**12** with pDITFB in 1:1 volume ratio acetone:DCM did not result in any solid product. All remained liquids after six months.

Whilst grinding experiments do show that interactions between the compounds **7**, **8**, **10** and **11** with aluminium nitrate, boric acid, pDITFB, guanidinium tetrafluoroborate, nicotinamide,

tartaric acid and telluric acid, it does not guarantee cocrystal formation. Coamorphous materials or even solvation of one compound in the other, is driven by intermolecular interaction such as hydrogen bonds the same as cocrystal formation. The models of crystallisation inhibitors do interact with other compounds, but often inhibit their crystallisation, resulting in oils. Whilst meaning cocrystal formation is challenging, the difficulty of forming crystals shows the model compounds to exhibit similar crystallisation inhibition properties to the polymers, making them good models to study.

3.3 Experimental

3.3.1 Macrocycles

Crystallisation experiments were performed in 2 cm^3 glass vials with plastic screw lids. The model compounds along with a second component, defined in Table 3.2, were weighed into the vial and the vial was filled with 1.5 cm^3 of the appropriate solvent. The sample was heated and sonicated until everything had dissolved. Crystallisations containing water were left open whilst other solvents were left with the lid resting on top of the vial. The samples were checked every couple of weeks until either crystals formed, non-crystalline solids formed or a thick oil which did not change over the course of a few months was formed.

Model compound	Model compound weight / g	Macrocycle	Macrocycle weight / g	Solvent
ethyl caprolactam	0.0047	SC4	0.050	water
	0.0095	SC4	0.050	water
	0.0190	SC4	0.050	water
	0.0032	SC6	0.050	water
	0.0063	SC6	0.050	water
	0.0130	SC6	0.050	water
	0.0024	SC8	0.050	water
	0.0047	SC8	0.050	water
	0.0095	SC8	0.050	water
	0.0053	SC4 Na salt	0.050	water
	0.0107	SC4 Na salt	0.050	water
	0.0213	SC4 Na salt	0.050	water
	0.0036	SC6 Na salt	0.050	water
	0.0071	SC6 Na salt	0.050	water
	0.0146	SC6 Na salt	0.050	water
	0.0027	SC8 Na salt	0.050	water
	0.0053	SC8 Na salt	0.050	water
	0.0107	SC8 Na salt	0.050	water
	0.0067	benzyloxycalix [5]arene	0.050	toluene/ acetone

	0.0087	4-tert-butyl calix[4]arene	0.050	toluene/ acetone
	0.0100	cucurbiturils 5, 6	0.050	dilute HCl
	0.0100	cucurbiturils 6, 7, 8	0.050	dilute HCl
	0.0088	α-cyclodextrin	0.050	water
	0.0103	β-cyclodextrin	0.050	water
	0.0117	γ-cyclodextrin	0.050	water
ethyl pyrrolidone	0.0038	SC4	0.050	water
	0.0075	SC4	0.050	water
	0.0150	SC4	0.050	water
	0.0025	SC6	0.050	water
	0.0050	SC6	0.050	water
	0.0100	SC6	0.050	water
	0.0020	SC8	0.050	water
	0.0037	SC8	0.050	water
	0.0075	SC8	0.050	water
	0.0043	SC4 Na salt	0.050	water
	0.0084	SC4 Na salt	0.050	water
	0.0169	SC4 Na salt	0.050	water
	0.0028	SC6 Na salt	0.050	water
	0.0056	SC6 Na salt	0.050	water
	0.0112	SC6 Na salt	0.050	water
	0.0022	SC8 Na salt	0.050	water
	0.0042	SC8 Na salt	0.050	water
	0.0084	SC8 Na salt	0.050	water
	0.0053	benzyloxycalix [5]arene	0.050	toluene/ acetone
	0.0109	4-tert-butyl calix[4]arene	0.050	toluene/ acetone
	0.0100	cucurbiturils 5, 6	0.050	dilute HCl
	0.0100	cucurbiturils 6, 7, 8	0.050	dilute HCl
	0.0071	α-cyclodextrin	0.050	water
	0.0083	β-cyclodextrin	0.050	water
	0.0095	γ-cyclodextrin	0.050	water
bisVCap	0.0090	SC4	0.050	water
	0.0190	SC4	0.050	water
	0.0370	SC4	0.050	water
	0.0070	SC6	0.050	water
	0.0120	SC6	0.050	water
	0.0250	SC6	0.050	water
	0.0050	SC8	0.050	water
	0.0900	SC8	0.050	water
	0.0190	SC8	0.050	water
	0.0101	SC4 Na salt	0.050	water

	0.0213	SC4 Na salt	0.050	water
	0.0416	SC4 Na salt	0.050	water
	0.0079	SC6 Na salt	0.050	water
	0.0135	SC6 Na salt	0.050	water
	0.0281	SC6 Na salt	0.050	water
	0.0056	SC8 Na salt	0.050	water
	0.1011	SC8 Na salt	0.050	water
	0.0213	SC8 Na salt	0.050	water
	0.0131	benzyloxycalix [5]arene	0.050	toluene/ acetone
	0.0214	4-tert-butyl calix[4]arene	0.050	toluene/ acetone
	0.0200	cucurbiturils 5, 6	0.050	dilute HCl
	0.0200	cucurbiturils 6, 7, 8	0.050	dilute HCl
	0.0175	α-cyclodextrin	0.050	water
	0.0204	β-cyclodextrin	0.050	water
	0.0233	γ-cyclodextrin	0.050	water
H$_2$bisVCap	0.0380	SC4	0.050	water
	0.0750	SC4	0.050	water
	0.0150	SC4	0.050	water
	0.0250	SC6	0.050	water
	0.0500	SC6	0.050	water
	0.1000	SC6	0.050	water
	0.0190	SC8	0.050	water
	0.0330	SC8	0.050	water
	0.0750	SC8	0.050	water
	0.0427	SC4 Na salt	0.050	water
	0.0843	SC4 Na salt	0.050	water
	0.0169	SC4 Na salt	0.050	water
	0.0281	SC6 Na salt	0.050	water
	0.0562	SC6 Na salt	0.050	water
	0.1124	SC6 Na salt	0.050	water
	0.0213	SC8 Na salt	0.050	water
	0.0371	SC8 Na salt	0.050	water
	0.0843	SC8 Na salt	0.050	water
	0.0132	benzyloxycalix [5]arene	0.050	toluene/ acetone
	0.0216	4-tert-butyl calix[4]arene	0.050	toluene/ acetone
	0.0200	cucurbiturils 5, 6	0.050	dilute HCl
	0.0200	cucurbiturils 6, 7, 8	0.050	dilute HCl
	0.0176	α-cyclodextrin	0.050	water
	0.0206	β-cyclodextrin	0.050	water
	0.0235	γ-cyclodextrin	0.050	water
bisVP	0.0300	SC4	0.050	water

0.0600	SC4	0.050	water
0.1190	SC4	0.050	water
0.0200	SC6	0.050	water
0.0400	SC6	0.050	water
0.0790	SC6	0.050	water
0.0150	SC8	0.050	water
0.0300	SC8	0.050	water
0.0600	SC8	0.050	water
0.0337	SC4 Na salt	0.050	water
0.0674	SC4 Na salt	0.050	water
0.1337	SC4 Na salt	0.050	water
0.0225	SC6 Na salt	0.050	water
0.0449	SC6 Na salt	0.050	water
0.0888	SC6 Na salt	0.050	water
0.0169	SC8 Na salt	0.050	water
0.0337	SC8 Na salt	0.050	water
0.0674	SC8 Na salt	0.050	water
0.0105	benzyloxycalix[5]arene	0.050	toluene/ acetone
0.0171	4-tert-butyl calix[4]arene	0.050	toluene/ acetone
0.0200	cucurbiturils 5, 6	0.050	dilute HCl
0.0200	cucurbiturils 6, 7, 8	0.050	dilute HCl
0.0140	α-cyclodextrin	0.050	water
0.0163	β-cyclodextrin	0.050	water
0.0186	γ-cyclodextrin	0.050	water

H_2bisVP	0.0350	SC4	0.050	water
	0.0710	SC4	0.050	water
	0.1400	SC4	0.050	water
	0.0230	SC6	0.050	water
	0.0470	SC6	0.050	water
	0.0950	SC6	0.050	water
	0.0180	SC8	0.050	water
	0.0360	SC8	0.050	water
	0.0710	SC8	0.050	water
	0.0393	SC4 Na salt	0.050	water
	0.0798	SC4 Na salt	0.050	water
	0.1573	SC4 Na salt	0.050	water
	0.0258	SC6 Na salt	0.050	water
	0.0528	SC6 Na salt	0.050	water
	0.1067	SC6 Na salt	0.050	water
	0.0202	SC8 Na salt	0.050	water
	0.0405	SC8 Na salt	0.050	water
	0.0798	SC8 Na salt	0.050	water
	0.0106	benzyloxycalix[5]arene	0.050	toluene/ acetone

	0.0173	4-tert-butyl calix[4]arene	0.050	toluene/ acetone
	0.0200	cucurbiturils 5, 6	0.050	dilute HCl
	0.0200	cucurbiturils 6, 7, 8	0.050	dilute HCl
	0.0141	α-cyclodextrin	0.050	water
	0.0164	β-cyclodextrin	0.050	water
	0.0188	γ-cyclodextrin	0.050	water
HepVCap	0.0375	SC4	0.050	water
	0.0761	SC4	0.050	water
	0.1500	SC4	0.050	water
	0.0246	SC6	0.050	water
	0.0504	SC6	0.050	water
	0.1018	SC6	0.050	water
	0.0193	SC8	0.050	water
	0.0386	SC8	0.050	water
	0.0761	SC8	0.050	water
	0.0421	SC4 Na salt	0.050	water
	0.0855	SC4 Na salt	0.050	water
	0.1685	SC4 Na salt	0.050	water
	0.0277	SC6 Na salt	0.050	water
	0.0566	SC6 Na salt	0.050	water
	0.1144	SC6 Na salt	0.050	water
	0.0217	SC8 Na salt	0.050	water
	0.0433	SC8 Na salt	0.050	water
	0.0855	SC8 Na salt	0.050	water
	0.0126	benzyloxycalix [5]arene	0.050	toluene/ acetone
	0.0206	4-tert-butyl calix[4]arene	0.050	toluene/ acetone
	0.0200	cucurbiturils 5, 6	0.050	dilute HCl
	0.0200	cucurbiturils 6, 7, 8	0.050	dilute HCl
	0.0151	α-cyclodextrin	0.050	water
	0.0176	β-cyclodextrin	0.050	water
	0.0201	γ-cyclodextrin	0.050	water

Table 3.2 – Macrocycle crystallisation values and solvents.

3.3.2 Halogen bonding

Crystallisation experiments were performed in 2 cm^3 glass vials with plastic screw lids. Both components were weighed into the vial and the vial was filled with 1.5 cm^3 of the appropriate solvent. The sample was heated and sonicated until everything had dissolved. Crystallisations containing water were left open whilst other solvents were left with the lid resting on top of the vial. The samples were checked every couple of weeks until either crystals formed, non-crystalline solids formed or a thick oil which did not change over the course of a few months

was formed. The crystallisation containing the halogen bond donating compounds can be found in Table 3.3 .

Model compound	Model compound weight / g	Halogen bond donor	Halogen bond donor weight / g	Solvent
bisVCap	0.047	pentafluoro iodobenzene	0.050	acetone/DCM
	0.035	pDITFB	0.050	acetone/DCM
	0.025	oDITFB	0.050	acetone/DCM
	0.042	1,2-diiodobenzene	0.050	acetone/DCM
	0.017	3-chloro-(2-iodoethynyl) benzene	0.050	acetone/DCM
	0.050	iodine	0.046	ethanol
H$_2$bisVCap	0.048	pentafluoro iodobenzene	0.050	acetone/DCM
	0.035	pDITFB	0.050	acetone/DCM
	0.025	oDITFB	0.050	acetone/DCM
	0.042	1,4-diiodobenzene	0.050	acetone/DCM
	0.018	3-chloro-(2-iodoethynyl)benzene	0.050	acetone/DCM
	0.050	iodine	0.045	ethanol
bisVP	0.038	pentafluoro iodobenzene	0.050	acetone/DCM
	0.028	pDITFB	0.050	acetone/DCM
	0.025	oDITFB	0.050	acetone/DCM
	0.034	1,4-diiodobenzene	0.050	acetone/DCM
	0.018	3-chloro-(2-iodoethynyl) benzene	0.050	acetone/DCM
	0.050	iodine	0.057	ethanol
H$_2$bisVP	0.038	pentafluoro iodobenzene	0.050	acetone/DCM
	0.028	pDITFB	0.050	acetone/DCM
	0.025	oDITFB	0.050	acetone/DCM
	0.034	1,4-diiodobenzene	0.050	acetone/DCM
	0.018	3-chloro-(2-iodoethynyl) benzene	0.050	acetone/DCM
	0.050	iodine	0.057	ethanol
HepVCap	0.046	pentafluoro iodobenzene	0.050	acetone/DCM
	0.033	pDITFB	0.050	acetone/DCM
	0.025	oDITFB	0.050	acetone/DCM

	0.041	1,4-diiodobenzene	0.050	acetone/DCM
	0.022	3-chloro-(2-iodoethynyl) benzene	0.050	acetone/DCM
	0.050	iodine	0.053	ethanol
bisHEP	0.035	pentafluoro iodobenzene	0.050	acetone/DCM
	0.025	pDITFB	0.050	acetone/DCM
	0.025	oDITFB	0.050	acetone/DCM
	0.031	1,4-diiodobenzene	0.050	acetone/DCM
	0.017	3-chloro-(2-iodoethynyl)benzene	0.050	acetone/DCM
	0.050	iodine	0.053	ethanol
MEP	0.024	pentafluoro iodobenzene	0.050	acetone/DCM
	0.018	pDITFB	0.050	acetone/DCM
	0.018	oDITFB	0.050	acetone/DCM
	0.022	1,4-diiodobenzene	0.050	acetone/DCM
	0.027	3-chloro-(2-iodoethynyl) benzene	0.050	acetone/DCM

Table 3.3 – Halogen bond crystallisation values and solvents.

3.3.3   Metal complexes

Crystallisation experiments were performed in 2 cm^3 glass vials with plastic screw lids. Both components were weighed into the vial and the vial was filled with 1.5 cm^3 of the appropriate solvent. The sample was heated and sonicated until everything had dissolved. Crystallisations containing water were left open whilst other solvents were left with the lid resting on top of the vial. The samples were checked every couple of weeks until either crystals formed, non-crystalline solids formed or a thick oil which did not change over the course of a few months was formed. The crystallisation containing metal salts can be found in Table 3.4.

Model compound	Model compound weight / g	Metal salt	Metal salt weight / g	Solvent
bisVCap	0.067	terbium (III) chloride	0.150	water
	0.078	terbium (III) nitrate	0.150	water
	0.022	gadolinium (III) chloride	0.050	water
	0.027	gadolinium (III) nitrate	0.050	water
	0.032	yttrium triflouromethane sulfonate	0.050	water

	0.037	ytterbium trifluoromethane sulfonate	0.050	water
	0.021	yttrium (III) carbonate	0.050	water
	0.026	lanthanum (II) nitrate	0.050	water
	0.021	lanthanum chloride	0.050	water
	0.030	terbium carbonate	0.050	water
H₂bisVCap	0.067	terbium (III) chloride	0.150	water
	0.078	terbium (III) nitrate	0.150	water
	0.022	gadolinium (III) chloride	0.050	water
	0.027	gadolinium (III) nitrate	0.050	water
	0.032	yttrium triflouromethane sulfonate	0.050	water
	0.037	ytterbium trifluoromethane sulfonate	0.050	water
	0.021	yttrium (III) carbonate	0.050	water
	0.026	lanthanum (II) nitrate	0.050	water
	0.021	lanthanum chloride	0.050	water
	0.030	terbium carbonate	0.050	water
bisVP	0.084	terbium (III) chloride	0.150	water
	0.098	terbium (III) nitrate	0.150	water
	0.028	gadolinium (III) chloride	0.050	water
	0.034	gadolinium (III) nitrate	0.050	water
	0.040	yttrium triflouromethane sulfonate	0.050	water
	0.047	ytterbium trifluoromethane sulfonate	0.050	water
	0.027	yttrium (III) carbonate	0.050	water
	0.033	lanthanum (II) nitrate	0.050	water
	0.027	lanthanum chloride	0.050	water
	0.037	terbium carbonate	0.050	water
H₂bisVP	0.083	terbium (III) chloride	0.150	water

	0.097	terbium (III) nitrate	0.150	water
	0.028	gadolinium (III) chloride	0.050	water
	0.034	gadolinium (III) nitrate	0.050	water
	0.040	yttrium triflouromethane sulfonate	0.050	water
	0.046	ytterbium trifluoromethane sulfonate	0.050	water
	0.027	yttrium (III) carbonate	0.050	water
	0.032	lanthanum (II) nitrate	0.050	water
	0.026	lanthanum chloride	0.050	water
	0.037	terbium carbonate	0.050	water
bisHEP	0.078	terbium (III) chloride	0.150	water
	0.091	terbium (III) nitrate	0.150	water
	0.026	gadolinium (III) chloride	0.050	water
	0.031	gadolinium (III) nitrate	0.050	water
	0.037	yttrium triflouromethane sulfonate	0.050	water
	0.043	ytterbium trifluoromethane sulfonate	0.050	water
	0.025	yttrium (III) carbonate	0.050	water
	0.030	lanthanum (II) nitrate	0.050	water
	0.025	lanthanum chloride	0.050	water
	0.035	terbium carbonate	0.050	water
HEPVCap	0.050	cadmium accetate	0.043	water
	0.050	cadmium chloride	0.034	water
	0.050	cadmium sulphate	0.039	water
	0.050	caesium acetate	0.036	water
	0.050	caesium carbonate	0.061	water
	0.050	caesium chloride	0.031	water
	0.050	caesium hydroxide	0.031	water

0.050	cobalt (II) chloride	0.024	water
0.050	cobalt (II) nitrate	0.034	water
0.050	cobalt (II) sulphate	0.052	water
0.050	copper (II) acetate	0.034	water
0.050	copper (II) bromide	0.042	water
0.050	copper (II) chloride	0.025	water
0.050	copper (II) tetrafluoroborate	0.044	water
0.050	ferric chloride	0.030	water
0.050	iron (II) bromide	0.040	water
0.050	lead (II) nitrate	0.062	water
0.050	lithium bromide	0.016	water
0.050	lithium iodide	0.025	water
0.050	magnesium nitrate	0.028	water
0.050	manganese (II) acetate	0.032	water
0.050	nickel (II) acetate	0.046	water
0.050	nickel (II) chloride	0.024	water
0.050	nickel (II) nitrate	0.054	water
0.050	ytterbium trifluoromethanesulfonate	0.116	water
0.050	yttrium (III) carbonate	0.067	water
0.050	lanthanum (II) nitrate	0.081	water
0.050	manganese sulfate	0.032	water
0.050	lanthanum chloride	0.066	water
0.050	terbium carbonate	0.093	water
0.050	chromium (III) nitrate	0.075	water
0.050	chromium (III) sulphate	0.073	water
0.050	terbium (III) chloride	0.070	water

92

0.050	gadolinium (III) chloride	0.069	water
0.050	gadolinium (III) nitrate	0.084	water
1.050	praseodymium (III) nitrate	0.081	water
2.050	erbium (III) chloride	0.071	water
3.050	europium (III) chloride	0.068	water
0.030	lanthanum (II) nitrate	0.145	water
0.030	ytterbium trifluorometha nesulfonate	0.208	water
0.030	yttrium (III) carbonate	0.120	water
0.030	terbium carbonate	0.167	water
0.050	sodium chloride	0.019	water
0.050	neodymium (III) nitrate	0.147	water
0.050	potassium bromide	0.040	water
0.050	potassium carbonate	0.046	water
0.050	potassium chloride	0.025	water
0.050	potassium hexaflurophosp hate	0.062	water
0.050	potassium nitrate	0.034	water
0.050	sodium carbonate	0.036	water
0.050	sodium hydrogen carbonate	0.028	water
0.050	sodium hydrogen sulphate	0.040	water
0.050	sodium nitrate	0.029	water
0.050	strontium nitrate	0.071	water
0.050	zinc chloride	0.046	water
0.050	zinc acetate	0.061	water
0.050	zinc nitrate	0.063	water
0.050	calcium nitrate	0.055	water
0.050	strontium carbonate	0.067	water

	0.050	caesium carbonate	0.109	water
	0.050	cerium nitrate	0.146	water
MEP	0.013	cadmium acetate	0.050	water
	0.011	cadmium chloride	0.050	water
	0.012	cadmium sulphate	0.050	water
	0.011	caesium acetate	0.050	water
	0.019	caesium carbonate	0.050	water
	0.010	caesium chloride	0.050	water
	0.010	caesium hydroxide	0.050	water
	0.008	cobalt (II) chloride	0.050	water
	0.011	cobalt (II) nitrate	0.050	water
	0.011	copper (II) acetate	0.050	water
	0.013	copper (II) bromide	0.050	water
	0.008	copper (II) chloride	0.050	water
	0.006	calcium chloride	0.050	water
	0.014	copper (II) tetrafluoroborate	0.050	water
	0.010	sodium hexafluorophosphate	0.050	water
	0.009	ferric chloride	0.050	water
	0.013	iron (II) bromide	0.050	water
	0.019	lead (II) nitrate	0.050	water
	0.005	lithium bromide	0.050	water
	0.004	lithium nitrate	0.050	water
	0.009	magnesium nitrate	0.050	water
	0.010	manganese (II) acetate	0.050	water
	0.015	nickel (II) acetate	0.050	water
	0.008	nickel (II) chloride	0.050	water
	0.017	nickel (II) nitrate	0.050	water

0.031	yttrium trifluoromethanesulfonate	0.050	water
0.006	sodium tetrafluoroborate	0.050	water
0.020	lanthanum (II) nitrate	0.050	water
0.010	manganese sulfate	0.050	water
0.021	lanthanum chloride	0.050	water
0.025	terbium nitrate	0.050	water
0.023	chromium (III) nitrate	0.050	water
0.003	sodium chloride	0.050	water
0.022	terbium (III) chloride	0.050	water
0.022	gadolinium (III) chloride	0.050	water
0.026	gadolinium (III) nitrate	0.050	water
0.025	praseodymium (III) nitrate	0.050	water
0.009	erbium (III) chloride	0.020	water
0.009	europium (III) chloride	0.020	water
0.010	lanthanum (II) nitrate	0.020	water
0.021	yttrium (III) carbonate	0.050	water
0.014	ytterbium trifluoromethanesulfonate	0.020	water
0.029	terbium carbonate	0.050	water
0.016	cobalt (II) sulphate	0.050	water
0.026	neodymium (III) nitrate	0.050	water
0.007	potassium bromide	0.050	water
0.008	potassium carbonate	0.050	water
0.004	potassium chloride	0.050	water
0.011	potassium hexaflurophosphate	0.050	water
0.006	potassium nitrate	0.050	water

	0.006	sodium carbonate	0.050	water
	0.005	sodium hydrogen carbonate	0.050	water
	0.007	sodium hydrogen sulphate	0.050	water
	0.005	sodium nitrate	0.050	water
	0.012	strontium nitrate	0.050	water
	0.008	zinc chloride	0.050	water
	0.011	zinc acetate	0.050	water
	0.011	zinc nitrate	0.050	water
	0.010	calcium nitrate	0.050	water
	0.012	strontium carbonate	0.050	water
	0.019	caesium carbonate	0.050	water
	0.025	cerium nitrate	0.050	water
	0.023	chromium (III) sulfate	0.050	water
Et(OVCap)$_2$	0.034	cadmium acetate	0.050	water
	0.027	cadmium chloride	0.050	water
	0.031	cadmium sulphate	0.050	water
	0.028	caesium acetate	0.050	acetone
	0.048	caesium carbonate	0.050	water
	0.025	caesium chloride	0.050	water
	0.025	caesium hydroxide	0.050	acetone
	0.019	cobalt (II) chloride	0.050	acetone
	0.027	cobalt (II) nitrate	0.050	acetone
	0.027	copper (II) acetate	0.050	water
	0.033	copper (II) bromide	0.050	water
	0.020	copper (II) chloride	0.050	acetone
	0.016	calcium chloride	0.050	water
	0.035	copper (II) tetrafluoroborate	0.050	acetone

0.025	sodium hexafluorophosphate	0.050	water
0.024	ferric chloride	0.050	acetone
0.032	liron (II) bromide	0.050	acetone
0.049	lead (II) nitrate	0.050	water
0.013	lithium bromide	0.050	acetone
0.010	lithium nitrate	0.050	acetone
0.022	magnesium nitrate	0.050	acetone
0.025	manganese (II) acetate	0.050	water
0.037	nickel (II) acetate	0.050	water
0.019	nickel (II) chloride	0.050	water
0.043	nickel (II) nitrate	0.050	acetone
0.079	yttrium trifluoromethanesulfonate	0.050	acetone
0.016	sodium tetrafluoroborate	0.050	acetone
0.051	lanthanum (II) nitrate	0.050	acetone
0.025	manganese sulfate	0.050	water
0.052	lanthanum chloride	0.050	water
0.064	terbium nitrate	0.050	acetone
0.059	chromium (III) nitrate	0.050	acetone
0.009	sodium chloride	0.050	water
0.055	terbium (III) chloride	0.050	water
0.055	gadolinium (III) chloride	0.050	water
0.066	gadolinium (III) nitrate	0.050	acetone
0.064	praseodymium (III) nitrate	0.050	acetone
0.022	erbium (III) chloride	0.020	water
0.022	europium (III) chloride	0.020	water
0.025	lanthanum (II) nitrate	0.020	acetone

	0.053	yttrium (III) carbonate	0.050	water
	0.036	ytterbium trifluorometha nesulfonate	0.020	acetone
	0.073	terbium carbonate	0.050	water
	0.041	cobalt (II) sulphate heptahydrate	0.050	water
	0.064	neodymium (III) nitrate	0.050	acetone
	0.018	potassium bromide	0.050	water
	0.020	potassium carbonate	0.050	water
	0.011	potassium chloride	0.050	water
	0.015	potassium nitrate	0.050	water
	0.027	potassium hexaflurophosp hate	0.050	acetone
	0.016	sodium carbonate	0.050	water
	0.018	sodium hydrogen sulphate	0.050	acetone
	0.012	sodium hydrogen carbonate	0.050	water
	0.013	sodium nitrate	0.050	water
	0.031	strontium nitrate	0.050	water
	0.020	zinc chloride	0.050	acetone
	0.027	zinc acetate	0.050	water
	0.028	zinc nitrate	0.050	acetone
	0.024	calcium nitrate	0.050	acetone
	0.029	strontium carbonate	0.050	water
	0.048	caesium carbonate	0.050	water
	0.064	cerium nitrate	0.050	water
	0.058	chromium (III) sulfate	0.050	water
	0.055	aluminium nitrate	0.050	water
	0.050	vanadium chloride	0.023	water
	0.050	vanadium oxide	0.027	water
Pr(OVP)$_2$	0.033	cadmium acetate	0.050	water

0.026	cadmium chloride	0.050	water
0.029	cadmium sulphate	0.050	water
0.027	caesium acetate	0.050	water
0.046	caesium carbonate	0.050	water
0.024	caesium chloride	0.050	water
0.024	caesium hydroxide	0.050	water
0.018	cobalt (II) chloride	0.050	water
0.026	cobalt (II) nitrate	0.050	water
0.026	copper (II) acetate	0.050	water
0.031	copper (II) bromide	0.050	water
0.019	copper (II) chloride	0.050	water
0.016	calcium chloride	0.050	water
0.033	copper (II) tetrafluoroborate	0.050	water
0.024	sodium hexafluorophosphate	0.050	water
0.023	ferric chloride	0.050	water
0.030	Iron (II) bromide	0.050	water
0.047	lead (II) nitrate	0.050	water
0.012	lithium bromide	0.050	water
0.010	lithium nitrate	0.050	water
0.021	magnesium nitrate	0.050	water
0.024	manganese (II) acetate	0.050	water
0.035	nickel (II) acetate	0.050	water
0.018	nickel (II) chloride	0.050	water
0.041	nickel (II) nitrate	0.050	water
0.076	yttrium trifluoromethanesulfonate	0.050	water

0.016	sodium tetrafluorobora te	0.050	water
0.049	lanthanum (II) nitrate	0.050	water
0.024	manganese sulfate	0.050	water
0.050	lanthanum chloride	0.050	water
0.061	terbium nitrate	0.050	water
0.056	chromium (III) nitrate	0.050	water
0.008	sodium chloride	0.050	water
0.053	terbium (III) chloride	0.050	water
0.053	gadolinium (III) chloride	0.050	water
0.064	gadolinium (III) nitrate	0.050	water
0.061	praseodymium (III) nitrate	0.050	water
0.022	erbium (III) chloride	0.050	water
0.021	europium (III) chloride	0.020	water
0.024	lanthanum (II) nitrate	0.020	water
0.051	yttrium (III) carbonate	0.020	water
0.035	ytterbium trifluorometha nesulfonate	0.050	water
0.070	terbium carbonate	0.020	water
0.040	cobalt (II) sulphate heptahydrate	0.050	water
0.062	neodymium (III) nitrate	0.050	water
0.017	potassium bromide	0.050	water
0.019	potassium carbonate	0.050	water
0.011	potassium chloride	0.050	water
0.014	potassium nitrate	0.050	water
0.026	potassium hexaflurophosp hate	0.050	water
0.015	sodium carbonate	0.050	water

	0.017	sodium hydrogen sulphate	0.050	water
	0.012	sodium hydrogen carbonate	0.050	water
	0.012	sodium nitrate	0.050	water
	0.030	strontium nitrate	0.050	water
	0.019	zinc chloride	0.050	water
	0.026	zinc acetate	0.050	water
	0.027	zinc nitrate	0.050	water
	0.023	calcium nitrate	0.050	water
	0.028	strontium carbonate	0.050	water
	0.046	caesium carbonate	0.050	water
	0.061	cerium nitrate	0.050	water
	0.055	chromium (III) sulfate	0.050	water
	0.053	aluminium nitrate	0.050	water
	0.022	vanadium chloride	0.050	water
	0.026	vanadium oxide	0.050	water
Et(OVP)$_2$	0.041	cadmium acetate	0.050	water
	0.032	cadmium chloride	0.050	water
	0.037	cadmium sulphate	0.050	water
	0.034	caesium acetate	0.050	acetone
	0.057	caesium carbonate	0.050	water
	0.030	caesium chloride	0.050	water
	0.030	caesium hydroxide	0.050	water
	0.023	cobalt (II) chloride	0.050	water
	0.032	cobalt (II) nitrate	0.050	acetone
	0.032	copper (II) acetate	0.050	water
	0.039	copper (II) bromide	0.050	water
	0.024	copper (II) chloride	0.050	acetone
	0.020	calcium chloride	0.050	water

0.042	copper (II) tetrafluoroborate	0.050	acetone
0.030	sodium hexafluorophosphate	0.050	acetone
0.029	ferric chloride	0.050	acetone
0.038	Iiron (II) bromide	0.050	acetone
0.058	lead (II) nitrate	0.050	water
0.015	lithium bromide	0.050	acetone
0.012	lithium nitrate	0.050	acetone
0.026	magnesium nitrate	0.050	water
0.030	manganese (II) acetate	0.050	water
0.044	nickel (II) acetate	0.050	water
0.023	nickel (II) chloride	0.050	water
0.051	nickel (II) nitrate	0.050	acetone
0.094	yttrium trifluoromethanesulfonate	0.050	acetone
0.019	sodium tetrafluoroborate	0.050	acetone
0.061	lanthanum (II) nitrate	0.050	water
0.030	manganese sulfate	0.050	water
0.062	lanthanum chloride	0.050	water
0.077	terbium nitrate	0.050	water
0.070	chromium (III) nitrate	0.050	water
0.010	sodium chloride	0.050	water
0.066	terbium (III) chloride	0.050	water
0.065	gadolinium (III) chloride	0.050	water
0.079	gadolinium (III) nitrate	0.050	water
0.077	praseodymium (III) nitrate	0.050	acetone
0.027	erbium (III) chloride	0.020	water
0.026	europium (III) chloride	0.020	water

0.030	lanthanum (II) nitrate	0.020	water
0.063	yttrium (III) carbonate	0.050	water
0.044	ytterbium trifluoromethanesulfonate	0.020	water
0.088	terbium carbonate	0.050	water
0.049	cobalt (II) sulphate heptahydrate	0.050	water
0.077	neodymium (III) nitrate	0.050	water
0.021	potassium bromide	0.050	water
0.024	potassium carbonate	0.050	water
0.013	potassium chloride	0.050	water
0.018	potassium nitrate	0.050	water
0.032	potassium hexaflurophosphate	0.050	acetone
0.019	sodium carbonate	0.050	water
0.021	sodium hydrogen sulphate	0.050	water
0.015	sodium hydrogen carbonate	0.050	water
0.015	sodium nitrate	0.050	water
0.037	strontium nitrate	0.050	water
0.024	zinc chloride	0.050	water
0.032	zinc acetate	0.050	water
0.033	zinc nitrate	0.050	water
0.029	calcium nitrate	0.050	water
0.035	strontium carbonate	0.050	water
0.057	caesium carbonate	0.050	water
0.076	cerium nitrate	0.050	water
0.069	chromium (III) sulfate	0.050	water
0.066	aluminium nitrate	0.050	water
0.050	vanadium chloride	0.028	water
0.050	vanadium oxide	0.032	water

Pr(OVP)$_2$	0.039	cadmium acetate	0.050	water
	0.031	cadmium chloride	0.050	water
	0.035	cadmium sulphate	0.050	water
	0.032	caesium acetate	0.050	acetone
	0.055	caesium carbonate	0.050	water
	0.028	caesium chloride	0.050	water
	0.028	caesium hydroxide	0.050	water
	0.022	cobalt (II) chloride	0.050	water
	0.031	cobalt (II) nitrate	0.050	acetone
	0.030	copper (II) acetate	0.050	water
	0.037	copper (II) bromide	0.050	water
	0.023	copper (II) chloride	0.050	acetone
	0.019	calcium chloride	0.050	water
	0.040	copper (II) tetrafluoroborate	0.050	acetone
	0.028	sodium hexafluorophosphate	0.050	acetone
	0.027	ferric chloride	0.050	acetone
	0.036	liron (II) bromide	0.050	acetone
	0.056	lead (II) nitrate	0.050	water
	0.015	lithium bromide	0.050	acetone
	0.012	lithium nitrate	0.050	acetone
	0.025	magnesium nitrate	0.050	water
	0.029	manganese (II) acetate	0.050	water
	0.042	nickel (II) acetate	0.050	water
	0.022	nickel (II) chloride	0.050	water
	0.049	nickel (II) nitrate	0.050	acetone
	0.090	yttrium trifluoromethanesulfonate	0.050	acetone

3: Cocrystallisation of hydrate inhibitor models

0.018	sodium tetrafluoroborate	0.050	acetone
0.059	lanthanum (II) nitrate	0.050	water
0.028	manganese sulfate	0.050	water
0.059	lanthanum chloride	0.050	water
0.073	terbium nitrate	0.050	water
0.067	chromium (III) nitrate	0.050	water
0.010	sodium chloride	0.050	water
0.063	terbium (III) chloride	0.050	water
0.062	gadolinium (III) chloride	0.050	water
0.076	gadolinium (III) nitrate	0.050	water
0.073	praseodymium (III) nitrate	0.050	acetone
0.026	erbium (III) chloride	0.020	water
0.025	europium (III) chloride	0.020	water
0.029	lanthanum (II) nitrate	0.020	water
0.060	yttrium (III) carbonate	0.050	water
0.042	ytterbium trifluoromethanesulfonate	0.020	water
0.084	terbium carbonate	0.050	water
0.047	cobalt (II) sulphate heptahydrate	0.050	water
0.073	neodymium (III) nitrate	0.050	water
0.020	potassium bromide	0.050	water
0.023	potassium carbonate	0.050	water
0.013	potassium chloride	0.050	water
0.017	potassium nitrate	0.050	water
0.031	potassium hexaflurophosphate	0.050	acetone
0.018	sodium carbonate	0.050	water

0.020	sodium hydrogen sulphate	0.050	water
0.014	sodium hydrogen carbonate	0.050	water
0.014	sodium nitrate	0.050	water
0.036	strontium nitrate	0.050	water
0.023	zinc chloride	0.050	water
0.031	zinc acetate	0.050	water
0.032	zinc nitrate	0.050	water
0.028	calcium nitrate	0.050	water
0.034	strontium carbonate	0.050	water
0.055	caesium carbonate	0.050	water
0.073	cerium nitrate	0.050	water
0.066	chromium (III) sulfate	0.050	water
0.063	aluminium nitrate	0.050	water
0.050	vanadium chloride	0.026	water
0.050	vanadium oxide	0.031	water

Table 3.4 – Metal crystallisation values and solvents.

3.3.4 Other cocrystals

3.3.4.1 The GRAS list

Crystallisation experiments were performed in 2 cm^3 glass vials with plastic screw lids. Both components were weighed into the vial and the vial was filled with 1.5 cm^3 of the appropriate solvent. The sample was heated and sonicated until everything had dissolved. Crystallisations containing water were left open whilst other solvents were left with the lid resting on top of the vial. The samples were checked every couple of weeks until either crystals formed, non-crystalline solids formed or a thick oil which did not change over the course of a few months was formed. The crystallisation containing the GRAS list compounds can be found in Table 3.5.

Model compound	Model compound weight / g	GRAS chemical	GRAS chemical weight / g	Solvent
bisVCap	0.05	oxalic acid	0.023	water
	0.05	nicotinamide	0.022	water
	0.05	(+) tartaric acid	0.027	water
	0.05	citric acid	0.035	water
	0.05	glutamic acid	0.026	water

	0.05	4-aminobenzoic acid	0.025	water
	0.05	caffeine	0.035	water
	0.05	citric acid	0.035	water
	0.05	fumaric acid	0.021	water
	0.05	malonic acid	0.019	water
	0.05	succinic acid	0.021	water
	0.05	nicotinic acid	0.022	water
H_2bisVCap	0.05	oxalic acid	0.023	water
	0.05	nicotinamide	0.022	water
	0.05	(+) tartaric acid	0.027	water
	0.05	citric acid	0.034	water
	0.05	glutamic acid	0.026	water
	0.05	4-aminobenzoic acid	0.024	water
	0.05	caffeine	0.035	water
	0.05	citric acid	0.035	water
	0.05	fumaric acid	0.021	water
	0.05	malonic acid	0.019	water
	0.05	succinic acid	0.021	water
	0.05	nicotinic acid	0.022	water
bisVP	0.05	oxalic acid	0.028	water
	0.05	nicotinamide	0.027	water
	0.05	(+) tartaric acid	0.034	water
	0.05	citric acid	0.043	water
	0.05	glutamic acid	0.033	water
	0.05	4-aminobenzoic acid	0.031	water
	0.05	caffeine	0.028	water
	0.05	citric acid	0.028	water
	0.05	fumaric acid	0.017	water
	0.05	malonic acid	0.015	water
	0.05	succinic acid	0.017	water
	0.05	nicotinic acid	0.018	water
H_2bisVP	0.05	oxalic acid	0.028	water
	0.05	nicotinamide	0.027	water
	0.05	(+) tartaric acid	0.033	water
	0.05	citric acid	0.043	water
	0.05	glutamic acid	0.033	water
	0.05	4-aminobenzoic acid	0.031	water
	0.05	caffeine	0.028	water
	0.05	citric acid	0.028	water
	0.05	fumaric acid	0.017	water
	0.05	malonic acid	0.015	water
	0.05	succinic acid	0.017	water
	0.05	nicotinic acid	0.018	water

Table 3.5 – GRAS list crystallisation values and solvents.

3.3.4.2 Hydrogen bond donors

Crystallisation experiments were performed in 2 cm³ glass vials with plastic screw lids. Both components were weighed into the vial and the vial was filled with 1.5 cm³ of the appropriate solvent. The sample was heated and sonicated until everything had dissolved. Crystallisations containing water were left open whilst other solvents were left with the lid resting on top of the vial. The samples were checked every couple of weeks until either crystals formed, non-crystalline solids formed or a thick oil which did not change over the course of a few months was formed. The crystallisation containing the hydrogen bond donating compounds can be found in Table 3.6.

Model compound	Model compound weight / g	Hydrogen bond donor	Hydrogen bond donor weight / g	Solvent
bisVCap	0.040	boric acid	0.009	water
	0.040	boric acid	0.018	water
	0.040	boric acid	0.009	ethanol
	0.040	boric acid	0.018	ethanol
	0.040	boric acid	0.009	methanol
	0.040	boric acid	0.018	methanol
	0.050	borax	0.064	water
	0.040	tetrahydroxy diboron	0.008	water
	0.040	benzenedi boronic acid 2-chloro	0.019	water
	0.040	pyradine boronic acid 4-formylphenyl	0.023	water
	0.040	boronic acid 2-fluoro	0.022	water
	0.040	pyradine 4-pyradinyl	0.020	water
	0.040	phenyl boronic acid 3-pyridyl	0.030	water
	0.040	boronic acid 4-pyridyl	0.018	water
	0.040	boronic acid 3-furyl boronic	0.018	water
	0.040	acid 3-thiophenyl	0.016	water
	0.040	boronic acid	0.018	water
	0.020	tannic acid	0.122	water
	0.050	telluric acid metformin tetrafluoro	0.041	water
	0.050	borate	0.039	water

	0.050	guanadinium tetrafluoro borate	0.026	water
H_2bisVCap	0.044	boric acid	0.010	water
	0.043	boric acid	0.019	water
	0.039	boric acid	0.009	ethanol
	0.046	boric acid	0.020	ethanol
	0.052	boric acid	0.012	methanol
	0.054	boric acid	0.024	methanol
	0.046	borax	0.070	water
	0.045	tetrahydroxy diboron	0.009	water
	0.045	benzene diboronic acid	0.021	water
	0.032	2-chloro pyradine boronic acid	0.018	water
	0.040	4-formylphenyl boronic acid	0.021	water
	0.037	2-fluoro pyradine	0.019	water
	0.030	4-pyradinyl phenyl boronic acid	0.023	water
	0.043	3-pyridyl boronic acid	0.019	water
	0.042	4-pyridyl boronic acid	0.020	water
	0.044	3-furyl boronic acid	0.018	water
	0.042	3-thiophenyl boronic acid	0.019	water
	0.020	tannic acid	0.121	water
	0.050	telluric acid	0.041	water
	0.050	metformin tetrafluoro borate	0.039	water
	0.050	guanadinium tetrafluoro borate	0.026	water
bisVP	0.058	boric acid	0.016	water
	0.092	boric acid	0.051	water
	0.084	boric acid	0.023	ethanol
	0.084	boric acid	0.047	ethanol
	0.084	boric acid	0.023	methanol
	0.115	boric acid	0.064	methanol
	0.040	borax	0.055	water
	0.041	tetrahydroxy diboron	0.029	water
	0.053	1,4-phenyl diboronic acid	0.013	water

	0.055	2-chloro pyradine boronic acid	0.033	water
	0.035	4-formylphenyl boronic acid	0.024	water
	0.038	2-fluoro pyradine	0.024	water
	0.042	4-pyradinyl phenyl boronic acid	0.040	water
	0.042	3-pyridyl boronic acid	0.023	water
	0.050	4-pyridyl boronic acid	0.023	water
	0.041	3-furyl boronic acid	0.025	water
	0.041	3-thiophenyl boronic acid	0.024	water
	0.020	tannic acid	0.153	water
	0.050	telluric acid	0.052	water
	0.050	metformin tetrafluoro borate	0.049	water
	0.050	guanadinium tetrafluoro borate	0.033	water
H$_2$bisVP	0.110	boric acid	0.030	water
	0.061	boric acid	0.034	water
	0.120	boric acid	0.033	ethanol
	0.123	boric acid	0.068	ethanol
	0.079	boric acid	0.022	methanol
	0.110	boric acid	0.061	methanol
	0.046	borax	0.07	water
	0.045	tetrahydroxy diboron	0.009	water
	0.045	1,4-phenyl diboronic acid	0.0212	water
	0.032	2-chloro pyradine boronic acid	0.018	water
	0.04	4-formylphenyl boronic acid	0.021	water
	0.037	2-fluoro pyradine	0.019	water
	0.03	4-pyradinyl phenyl boronic acid	0.023	water
	0.043	3-pyridyl boronic acid	0.019	water
	0.042	4-pyridyl boronic acid	0.02	water

	0.044	3-furyl boronic acid	0.0176	water
	0.042	3-thiophenyl boronic acid	0.019	water
	0.020	tannic acid	0.153	water
	0.050	telluric acid	0.052	water
	0.050	metformin tetrafluoro borate	0.049	water
	0.050	guanadinium tetrafluoro borate	0.033	water
HepVCap	0.046	boric acid	0.012	water
	0.048	boric acid	0.012	water
	0.045	boric acid	0.012	ethanol
	0.040	boric acid	0.010	ethanol
	0.039	boric acid	0.010	methanol
	0.041	boric acid	0.011	methanol
	0.043	borax	0.059	water
	0.052	tetrahydroxydi boron	0.012	water
	0.051	1,4-phenyl diboronic acid	0.028	water
	0.036	2-chloro pyradine boronic acid	0.024	water
	0.050	4-formylphenyl boronic acid	0.031	water
	0.049	2-fluoro pyradine	0.029	water
	0.044	4-pyradinyl phenyl boronic acid	0.031	water
	0.042	3-pyridyl boronic acid	0.022	water
	0.041	4-pyridyl boronic acid	0.021	water
	0.044	3-furyl boronic acid	0.021	water
	0.035	3-thiophenyl boronic acid	0.019	water
	0.020	tannic acid	0.142	water
	0.050	telluric acid	0.048	water
	0.050	metformin tetrafluoro borate	0.045	water
	0.050	guanadinium tetrafluoro borate	0.031	water
bisHEP	0.046	borax	0.07	water

	0.045	tetrahydroxydi boron	0.009	water
	0.045	1,4-phenyl diboronic acid	0.0212	water
	0.032	2-chloro pyradine boronic acid	0.018	water
	0.04	4-formylphenyl boronic acid	0.021	water
	0.037	2-fluoro pyradine	0.019	water
	0.03	4-pyradinyl phenyl boronic acid	0.023	water
	0.043	3-pyridyl boronic acid	0.019	water
	0.042	4-pyridyl boronic acid	0.02	water
	0.044	3-furyl boronic acid	0.0176	water
	0.042	3-thiophenyl boronic acid	0.019	water
	0.020	tannic acid	0.142	water
	0.050	telluric acid	0.048	water
	0.050	metformin tetrafluoro borate	0.045	water
	0.050	guanadinium tetrafluoro borate	0.031	water
MEP	0.022	boric acid	0.050	water
	0.031	tetrahydroxydi boron	0.050	water
	0.058	1,4-phenyl diboronic acid	0.050	water
	0.080	telluric acid	0.050	water
	0.086	metformin tetrafluoro borate	0.050	water
	0.051	guanadinium tetrafluoro borate	0.050	water

Table 3.6 – Hydrogen bond crystallisation values and solvents.

3.3.4.3   Analogous compounds

Crystallisation experiments were performed in 2 cm^3 glass vials with plastic screw lids. Both components were weighed into the vial and the vial was filled with 1.5 cm^3 of the appropriate solvent. The sample was heated and sonicated until everything had dissolved. Crystallisations containing water were left open whilst other solvents were left with the lid resting on top of the vial. The samples were checked every couple of weeks until either crystals formed, non-

crystalline solids formed or a thick oil which did not change over the course of a few months was formed. The crystallisation containing the analogous compounds can be found in Table 3.7.

Analogous compound	Analogous compound weight / g	Second component	Second component weight / g	Solvent
2,7-dioxathiephene-1-oxide	0.017	pentafluoro iodobenzene	0.050	acetone/DCM
	0.012	pDITFB	0.050	acetone/DCM
	0.012	oDITFB	0.050	acetone/DCM
	0.015	1,4-diiodobenzene	0.050	acetone/DCM
	0.019	3-chloro-(2-iodoethynyl) benzene	0.050	acetone/DCM
	1.310	boric acid	0.023	acetone/water
	1.310	tetrahydroxydi boron	0.033	acetone/water
	1.310	1,4-phenyl diboronic acid	0.061	acetone/water
	0.025	telluric acid	0.042	acetone/water
	0.025	guanadinium tetrafluoro borate	0.027	acetone/water
	0.025	metformin tetrafluoro borate	0.045	acetone/water
caprolactone	0.019	pentafluoro iodobenzene	0.050	acetone/DCM
	0.014	pDITFB	0.050	acetone/DCM
	0.014	oDITFB	0.050	acetone/DCM
	0.017	1,4-diiodobenzene	0.050	acetone/DCM
	0.022	3-chloro-(2-iodoethynyl) benzene	0.050	acetone/DCM
	0.050	boric acid	0.027	water
	0.050	tetrahydroxy diboron	0.039	water
	0.050	1,4-phenyl diboronic acid	0.073	water
	0.050	telluric acid	0.101	water
	0.025	guanadinium tetrafluoro borate	0.032	water
	0.025	metformin tetrafluorobora te	0.054	water

dihydrothiophen-3-one	0.017	pentafluoro iodobenzene	0.050	acetone/DCM
	0.012	pDITFB	0.050	acetone/DCM
	0.012	oDITFB	0.050	acetone/DCM
	0.015	1,4-diiodobenzene	0.050	acetone/DCM
	0.019	3-chloro-(2-iodoethynyl) benzene	0.050	acetone/DCM
	0.050	boric acid	0.036	water
	0.050	tetrahydroxy diboron	0.052	water
	0.050	1,4-phenyl diboronic acid	0.097	water
	0.050	telluric acid	0.134	water
	0.025	guanadinium tetrafluoro borate	0.042	water
	0.025	metformin tetrafluoroborate	0.071	water
dihydrofuran-3(2H)-one	0.017	pentafluoro iodobenzene	0.050	acetone/DCM
	0.013	pDITFB	0.050	acetone/DCM
	0.013	oDITFB	0.050	acetone/DCM
	0.015	1,4-diiodobenzene	0.050	acetone/DCM
	0.019	3-chloro-(2-iodoethynyl) benzene	0.050	acetone/DCM
	0.050	boric acid	0.036	water
	0.050	tetrahydroxydi boron	0.052	water
	0.050	1,4-phenyldi boronic acid	0.097	water
	0.050	telluric acid	0.113	water
	0.025	guanadinium tetrafluoro borate	0.036	water
	0.025	metformin tetrafluoro borate	0.060	water
2(5H)-thiophenone	0.017	pentafluoro iodobenzene	0.050	acetone/DCM
	0.012	pDITFB	0.050	acetone/DCM
	0.012	oDITFB	0.050	acetone/DCM
	0.015	1,4-diiodobenzene	0.050	acetone/DCM
	0.019	3-chloro-(2-iodoethynyl) benzene	0.050	acetone/DCM
	0.050	boric acid	0.031	water

114

	0.050	tetrahydroxy diboron	0.045	water
	0.050	1,4-phenyl diboronic acid	0.083	water
	0.050	telluric acid	0.115	water
	0.025	guanadinium tetrafluoro borate	0.037	water
	0.025	metformin tetrafluoro borate	0.061	water
6-hydroxybenzo [d][1,3]oxathiol -2-one	0.029	pentafluoro iodobenzene	0.050	acetone/DCM
	0.021	pDITFB	0.050	acetone/DCM
	0.021	oDITFB	0.050	acetone/DCM
	0.025	1,4-diiodobenzene	0.050	acetone/DCM
	0.032	3-chloro-(2-iodoethynyl) benzene	0.050	acetone/DCM
	0.050	boric acid	0.018	water
	0.050	tetrahydroxy diboron	0.027	water
	0.050	1,4-phenyl diboronic acid	0.049	water
	0.050	telluric acid	0.068	water
	0.025	guanadinium tetrafluoro borate	0.022	water
	0.025	metformin tetrafluoro borate	0.036	water
3-methyl-2(3H)-benzo thiazolone	0.028	pentafluoro iodobenzene	0.050	acetone/DCM
	0.021	pDITFB	0.050	acetone/DCM
	0.021	oDITFB	0.050	acetone/DCM
	0.025	1,4-diiodobenzene	0.050	acetone/DCM
	0.031	3-chloro-(2-iodoethynyl) benzene	0.050	acetone/DCM
	0.050	boric acid	0.019	water
	0.050	tetrahydroxy diboron	0.027	water
	0.050	1,4-phenyl diboronic acid	0.050	water
	0.050	telluric acid	0.070	water

	0.025	guanadinium tetrafluoro borate	0.022	water
	0.025	metformin tetrafluoro borate	0.037	water

Table 3.7 – Analogous compound crystallisation values and solvents.

3.3.4.4 Hydrogen peroxide

Hydrogen peroxide was mixed with the dimers in a 1:1 and 1:2 H_2O_2 to dimer ratios. The minimum amount of water to dissolve or disperse the dimer was added to the mixture. Samples were left to slow evaporate or cool in the fridge or freezer. Samples in the freezer had 0.2 cm^3 of ethanol added to prevent freezing of the water. All combinations are shown in Table 3.8.

Model compound	Model compound / g	30% H_2O_2 / cm^3	Crystallisation type
bisVCap	0.092	0.037	cooling 5 °C
	0.088	0.072	cooling 5 °C
bisVP	0.102	0.052	cooling 5 °C
	0.098	0.099	cooling 5 °C
H2bisVCap	0.073	0.030	cooling 5 °C
	0.082	0.066	cooling 5 °C

Table 3.8 - Hydrogen peroxide/model compound crystallisations.

3.3.5 Differential scanning calorimetry

Differential scanning calorimetry scans were recorded on a TA Q2000. The heat/cool/heat cycles were performed using standard aluminium pans containing 3 – 12 mg of sample. Standard mode was used. The heat/cool/heat cycles began with a heating cycle at a rate of 10 °C min^{-1}, then cooling cycle at 50 °C min^{-1} and finally a second heating cycle at 10 °C min^{-1}. The quasi-isothermal experiments were performed using t-zero aluminium pans with hermetic lids containing 6 – 25 mg of sample. A sapphire was run before each sample to allow calibration.

Sapphire experiments were started at 6.85 °C with a ± 1.00 °C modulation every 120 sec. The temperature was held isothermal for 5 min before being raised by 20.00 °C increments to a value of 326.85 °C.

Sample experiments were performed with a ± 1.00 °C modulation every 60 sec. Samples were held isothermally for 10 min at each temperature before being raised by 5.00 °C. For amorphous material runs, the sample was first heated beyond the melting point and cooled

to form the amorphous material. Heating was at a rate of 10 °C min^{-1} with the sample held at the higher temperature for 5 min and cooling at a rate of 10 °C min^{-1} to the start temperature of the experiment. The samples were heated to 150 °C and 120 °C for amorphous bisVCap and the coamorphous material respectively. The start and end temperatures of the samples can be found in Table 3.9. All experiments were carried out twice with fresh samples.

Sample	Start temp. / °C	End temp. / °C
bisVCap crystal	-40	160
bisVCap amorphous	-35	160
pDITFB	-80	120
cocrystal	40	145
coamorphous	-15	85

Table 3.9 – Start and end temperature for the quasi-isothermal DSC experiments.

3.3.6 IR Spectroscopy

Experiments were performed on a Perkin Elmer FTIR spectrum 100 with an attenuated total reflectance (ATR) attachment. Data were recorded at a resolution of 2 cm^{-1} for 16 runs over the range 4000 – 600 cm^{-1}. Samples were prepared by grinding together a 1:1 molar ratio of the two components using a mortar and pestle for one minute before placing on the ATR crystal, applying pressure using the side arm and running the FTIR spectrum. The single components were ran for comparison by placing the compound on the ATR crystal applying pressure using the side arm and running the FTIR spectrum. Spectral analysis was performed using SpekWin32.[41] The combinations of chemicals tried can be found in Table 3.10.

Model compound	Second component
bisVCap	aluminium nitrate
	guanadinium tetrafluoroborate
	metformin tetrafluoroborate
	telluric acid
	nicotinamide
	tartaric acid
	SC4
H2bisVCap	aluminium nitrate
	telluric acid
	oxalic acid
	α-cyclodextrin
	β-cyclodextrin
	γ-cyclodextrin
HEPVCap	aluminium nitrate
	guanadinium tetrafluoroborate
	metformin tetrafluoroborate
	telluric acid

	sodium tetraphenylborate
	sodium hexafluorophosphate
	zinc chloride
	tetrahydroxyboron
MEP	pDITFB
	oDITFB
	boric acid
	calcium nitrate
	sodium chloride
	telluric acid
bisHEP	aluminium nitrate
	guanadinium tetrafluoroborate
	metformin tetrafluoroborate
	telluric acid

Table 3.10 – Combinations of chemicals for grinding and IR analysis.

3.3.7   Crystallographic data

Powder x-ray diffraction was performed using a Bruker AXS D8 Advance diffractometer, with a Lynxeye Soller PSD Detector and CuKα radiation at a wavelength of 1.5406 Å by Mr Gary Oswald.

Single crystal crystallographic analysis were performed on a Bruker Photon D8 Venture diffractometer (ImuS microsource, λMoKα, λ = 0.71073 Å) equipped with a Cryostream (Oxford Cryosystems) open-flow nitrogen cryostat, at 120 K. The data collection and refinement was kindly carried out by Dr Dmitry S. Yufit.

Ethyl pyrrolidone/p-sulfonatocalix[4]arene crystal data: Empirical formula $C_{28}H_{20}O_{16}S_4$, $3(C_6H_{12}NO)$, H_3O, $4H_2O$, space group $P\overline{1}$, a = 10.8924(7) Å, b = 16.0836(10) Å, c = 16.7429(11) Å, α = 116.186(2)°, β = 94.591(3)°, γ = 94.434(2)°, volume = 2603.2(3) Å^3, Z = 2, F(000) = 1240.0, MoKα (λ = 0.71073) 2θ range for data collection = 4.75 - 58°, data = 13824, parameters = 773, goodness-of-fit on F^2 = 1.017, R_1 = 0.0686, wR_2 = 0.1049

BisVCap/1,4-diiodotetrafluorobenzene crystal data: Empirical formula $C_{16}H_{26}N_2O_2$, $C_6F_4I_2$, space group $P2_1/n$, a = 21.8250 Å, b = 5.2275(3) Å, c = 23.0386 Å, α = 90.00°, β = 114.280(7)°, γ = 90.0°, volume = 2396.0(2)) Å^3, Z = 4, F(000) = 1320.0, MoKα (λ = 0.71073) 2θ range for data collection = 4.16 - 52°, data = 4716, parameters = 290, goodness-of-fit on F^2 = 1.005, R_1 = 0.0895, wR_2 = 0.1006

HEP/ε-caprolactam/CdCl₂ crystal data: Empirical formula $3(CdCl_2)$, $2(C_6H_{11}NO)$, $2(C_6H_{11}NO_2)$, space group *Cc*, a = 21.4093(9) Å, b = 35.3293(15) Å, c = 18.7193(8) Å, α = 90.00°, β = 100.388(2)°, γ = 90.0°, volume = 13926.7(10) Å^3, Z = 16, F(000) = 8160.0, MoKα (λ = 0.71073)

2θ range for data collection = 4.36 - 60°, data = 40562, parameters = 1562, goodness-of-fit on F^2 = 1.009, R_1 = 0.06049, wR_2 = 0.0936

CdCl$_2$/ε-caprolactam/ethylene glycol crystal data: Empirical formula $2CdCl_2$, $2(C_6H_{11}NO)$, $C_2H_6O_2$, space group $P2_1/c$, a = 13.6049(2) Å, b = 14.4911(2) Å, c = 11.9047(2) Å, α = 90.00°, β = 110.162(2)°, γ = 90.00°, volume = 2203.19(6) Å^3, Z = 4, F(000) = 1288.0, MoKα (λ = 0.71073) 2θ range for data collection = 4.252 − 60.000°, data = 6412, parameters = 244, goodness-of-fit on F^2 = 1.033, R_1 = 0.0301, wR_2 = 0.0511

1,1,3-tri-2-pyrrolidonylbutane/Y(CF$_3$SO$_3$)$_3$ crystal data: Empirical formula $C_{16}H_{35}N_3O_8$, $3(CF_3SO_3)$, H_2O, space group $P2_1/n$, a = 11.1216(9) Å, b = 23.5054(19) Å, c = 14.4218(12) Å, α = 90.00°, β = 91.688(3)°, γ = 90.00°, volume = 3768.5(5) Å^3, Z = 4, F(000) = 1928.0, MoKα (λ = 0.71073) 2θ range for data collection = 4.472 - 58°, data = 10015, parameters = 484, goodness-of-fit on F^2 = 1.047, R_1 = 0.0832, wR_2 = 0.1582

2-Furanylboronic acid crystal data: Empirical formula $C_4H_6BO_3$, space group $P2_1/n$, a = 9.1128(9) Å, b = 6.9860(7) Å, c = 9.1402(9) Å, α = 90.00°, β = 116.623(4)°, γ = 90.00°, volume = 320.19(9) Å^3, Z = 4, F(000) =236.0, MoKα (λ = 0.71073) 2θ range for data collection = 4.98 - 56°, data = 1256, parameters = 82, goodness-of-fit on F^2 = 1.061, R_1 = 0.0444, wR_2 = 0.1113

3.4 References

(1)   Perrin, A. The chemistry of low dosage clathrate hydrate inhibitors, University of Durham, 2015.

(2)   Grothe, E.; Meekes, H.; Vlieg, E.; Ter Horst, J. H.; De Gelder, R. *Cryst. Growth Des.* **2016**, *16* (6), 3237–3243.

(3)   Trask, A. V; Jones, W. *Top. Curr. Chem.* **2005**, *254*, 41–70.

(4)   Najar, A. A.; Azim, Y. *J. Indian Inst. Sci.* **2014**, *94*, 45–67.

(5)   Connors, K. A. *Binding constants: the measurement of molecular complex stability*; John Wiley & Sons: New York, Chichester, Brisbane, Toronto, Singapore, 1987.

(6)   Fucke, K.; Anderson, K. M.; Filby, M. H.; Henry, M.; Wright, J.; Mason, S. A.; Gutmann, M. J.; Barbour, L. J.; Oliver, C.; Coleman, A. W.; Atwood, J. L.; Howard, J. A. K.; Steed, J. W. *Chem. Eur. J.* **2011**, *17* (37), 10259–10271.

(7)   Jeffrey, G. A. *An Introduction to Hydrogen Bonding*; Oxford University Press: Oxford, 1997.

(8)   Gilday, L. C.; Robinson, S. W.; Barendt, T. A.; Langton, M. J.; Mullaney, B. R.; Beer, P. D. *Chem. Rev.* **2015**, 7118–7195.

(9)   Metrangolo, P.; Meyer, F.; Pilati, T.; Resnati, G.; Terraneo, G. *Angew. Chem. Int. Ed. Engl.* **2008**, *47* (33), 6114–6127.

(10)   Aakeröy, C. B.; Baldrighi, M.; Desper, J.; Metrangolo, P.; Resnati, G. *Chem. - A Eur. J.* **2013**, *19* (48), 16240–16247.

(11)   Schenck, H.-U.; Simak, P.; Haedicke, E. *J. Pharm. Sci.* **1979**, *68*, 1505–1509.

(12)   Khan, M. N.; Naqvi, A. H. *J .Tissue Viability* **2006**, *16*, 6–10.

(13)   Bruce, D. W.; Metrangolo, P.; Meyer, F.; Prasang, C.; Resnati, G.; Terraneo, G.; Whitwood, A. C.; Praesang, C.; Resnati, G.; Terraneo, G.; Whitwood, A. C. *New J. Chem.* **2008**, *32*, 477–482.

(14)   Präsang, C.; Nguyen, H. L.; Horton, P. N.; Whitwood, A. C.; Bruce, D. W. *Chem. Commun.* **2008**, 6164–6166.

(15)   Hursthouse, M. B.; Gelbrich, T.; Plater, M. J. *CSD Priv. Commun.* **2003**, CCDC 223298.

(16) Aakeroy, C. B.; Desper, J.; Fasulo, M.; Hussain, I.; Levin, B.; Schultheiss, N. *Cryst. Eng. Comm.* **2008**, *10* (12), 1816–1821.

(17) Takemura, A.; McAllister, L. J.; Hart, S.; Pridmore, N. E.; Karadakov, P. B.; Whitwood, A. C.; Bruce, D. W. *Chem. Eur. J.* **2014**, *20* (22), 6721–6732.

(18) Caballero, A.; White, N. G.; Beer, P. D. *Angew. Chem. Int. Ed.* **2011**, *50* (8), 1845–1848.

(19) Raatikainen, K.; Cavallo, G.; Metrangolo, P.; Resnati, G.; Rissanen, K.; Terraneo, G. *Cryst. Growth Des.* **2013**, *13* (2), 871–877.

(20) Chaplot, S. L.; McIntyre, G. J.; Mierzejewski, A.; Pawley, G. S. *Acta Cryst.* **1981**, *B37*, 2210–2214.

(21) Singh, S. *Liquid Crystal Fundamentals*; World Scientific Publishing Co. Pte. Ltd. New: New Jersey, London, Singapore, Hong Kong, 2002.

(22) Schoff, C. K. *Purity Determinations by Thermal Methods: A Symposium*; ASTM International: Philadelphia, 1984.

(23) Morris, M. D. *Microscopic and Spectroscopic Imaging of the Chemical State*; Morris, M. D., Ed.; CRC Press: New York, Basel, Hong Kong, 1993.

(24) Nurzyńska, K.; Booth, J.; Roberts, C. J.; McCabe, J.; Dryden, I.; Fischer, P. M. *Mol. Pharm.* **2015**, *12* (9), 3389–3398.

(25) Wunderlich, B. *Pure Appl. Chem.* **2009**, *81* (10), 1931–1952.

(26) Taylor, L. S.; Shamblin, S. L. In *Polymorphism in Pharmaceutical Solids*; Brittain, H. G., Ed.; Informa Healthcare: New York, 2016.

(27) Perrin, A.; Myers, D.; Fucke, K.; Musa, O. M.; Steed, J. W. *Dalt. Trans.* **2014**, *43* (8), 3153–3161.

(28) Evans, W. J.; Fujimoto, C. H.; Greci, M. A.; Ziller, J. W. *Eur. J. Inorg. Chem.* **2001**, 745–749.

(29) Bailly, N.; Thomas, M.; Klumperman, B. *Biomacromol.* **2012**, *13* (12), 4109–4117.

(30) Macleod, G. S.; Fell, J. T.; Collett, J. H. *Int. J. Pharm.* **1999**, *188* (1), 11–18.

(31) Wilken, C. Poly (N -Vinylpyrrolidone) based biomimetic hydrogels, University of Stellenbosch, 2012.

(32)   Beija, M.; Marty, J.-D.; Destarac, M. *Chem. Commun.* **2011**, *47* (10), 2826–2828.

(33)   Liang, X.; Kozlovskaya, V.; Chen, Y.; Zavgorodnya, O.; Kharlampieva, E. *Chem. Mater.* **2012**, *24* (19), 3707–3719.

(34)   Vihola, H.; Laukkanen, A.; Valtola, L.; Tenhu, H.; Hirvonen, J. *Biomater.* **2005**, *26* (16), 3055–3064.

(35)   Vihola, H.; Laukkanen, A.; Tenhu, H.; Hirvonen, J. *J. Pharm. Sci.* **2008**, *97* (11), 4783–4793.

(36)   Gao, Y.; Sharpless, K. B. *J. Am. Chem. Soc* **1988**, *110*, 7538–7539.

(37)   Friščić, T.; Jones, W. *Cryst. Growth Des.* **2009**, *9* (3), 1621–1637.

(38)   Shan, N.; Toda, F.; Jones, W. *Chem. Commun.* **2002**, No. 20, 2372–2373.

(39)   Trask, A. V; Motherwell, W. D. S.; Jones, W. *Chem. Commun.* **2004**, No. 7, 890–891.

(40)   Davenport, J. R.; Musa, O. M.; Paterson, M. J.; Piepenbrock, M.-O. M.; Fucke, K.; Steed, J. W. *Chem. Commun.* **2011**, *47* (35), 9891–9893.

(41)   Menges, F. http://www.effemm2.de/spekwin: Berchetesgarden 2016.

4 Gelling guar

4.1 Introduction

Guar is a plant cultivated in India, Pakistan and any other warm climate with a low chance of frost. The beans produced from guar are edible, though the gum extracted from them has many more uses. Guar gum is a straight chain galactomannan, whose suggested repeat unit is shown in Scheme 4.1. Guar gum is used to reduce ice crystal size in ice cream, improve the texture of cheese, thicken face creams and toothpastes, bind pills for drug delivery and improving the wear of paper to name but a small fraction of its uses.[1] In the oil industry guar is used to thicken mud to help with drilling, as a surfactant to maintain slurries, as a lubricant for a variety of parts and to minimise water loss in certain geological formations.[2–4]
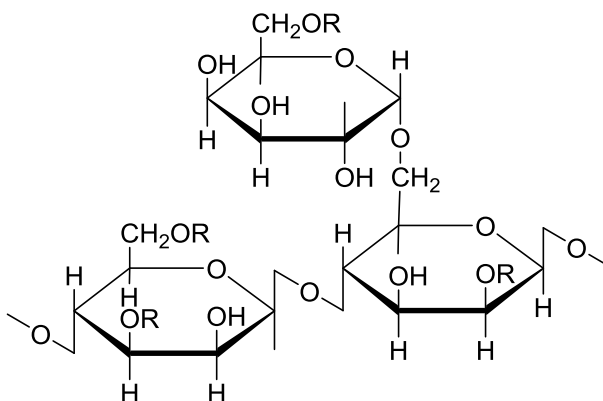
Scheme 4.1 - Repeat unit of guar gum.[5]

For many applications, especially as a thickening agent, the guar gum is crosslinked. In the presence of water crosslinked guar gum readily swells to form a hydrogel.[6] Crosslinking is often performed by borate ions either by using boric acid at high pH or borax. Hydroxyl groups in the guar gum react reversibly with the borate ions, losing water and forming a guar-borate complex. When this complex reacts with a second chain of guar a crosslink is formed, Scheme 4.2. As the steps to form the crosslinks are reversible this is a dynamically crosslinked system, so the gel can be broken and reformed easily. New methods of crosslinking are of industrial interest, either to reduce cost, vary the properties of the final product or change the rate of the crosslinking reaction.
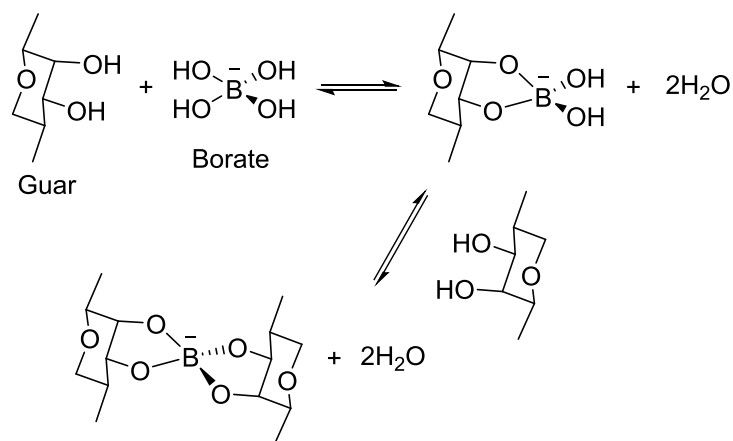
Scheme 4.2 - Crosslinking of guar by borate ions.

As boric acid is a well-established, effective crosslinker of guar,[1,6–9] it stands to reason that analogous compounds, such as boronic acids and other comparable Lewis acids, like telluric acid, may also show similar behaviour. Cocrystals of established crosslinkers, such as boric acid cocrystals, may also be capable of crosslinking guar. Perrin[10] reported a 2:1 boric acid:bisHEP cocrystal, crystal **6**. The crystal structure of crystal **6** is shown in Figure 4.1. Crystal **6** is made up of two zigzagging, hydrogen bonded boric acid chains with bisHEP molecules hydrogen bonded between the two chains every alternating boric acid molecule. Crystal **6** should release boric acid in solution which will be able to crosslink guar. The hydrogen bonds which hold the cocrystal together could possibly slow the release and availability of the boric acid molecules, slowing the rate of gelation. A longer gelation time resulting in a similar strength of gel to the normal boric acid crosslinked guar would be of great interest in any situation where the gel is required to be shaped using a mould, as the solution could be poured before the gel has formed.
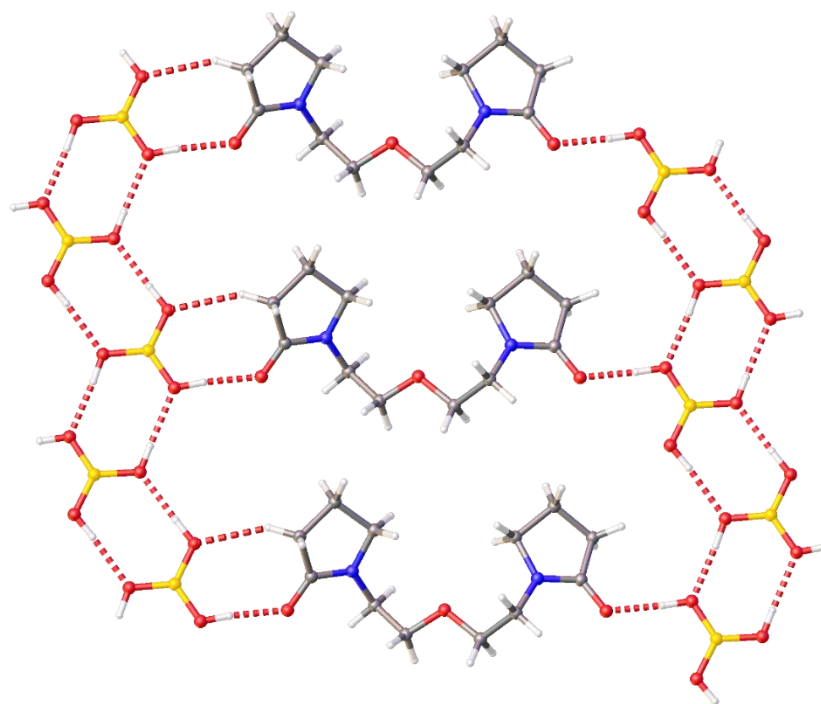
Figure 4.1 – Crystal packing of crystal 6. Hydrogen bonds are shown by red dashed lines.[11]

4.2 Results and Discussion

4.2.1 Preparing crystal 6

Crystal **6** was successfully prepared by the grinding method outlined by Perrin[10] and the structure was confirmed by comparing the experimental powder x-ray pattern of the ground sample to a powder x-ray pattern calculated from the single crystal x-ray structure using Mercury,[12] Figure 4.2. The calculated and experimental patterns do not look the same by eye, but a computational fit performed by Prof John Evans, Durham University, revealed the experimental pattern to be what would be expected from the crystal with strong orientational preference. As crystal **6** forms flat, plate-like needles, Figure 4.3, orientational preference in the PXRD pattern is to be expected. As the PXRD pattern for the ground sample is what could be expected from the cocrystal and does not show any similarity to the PXRD patterns calculated from the crystal structures of boric acid,[13,14] the powder was used in gelation experiments without further preparation.
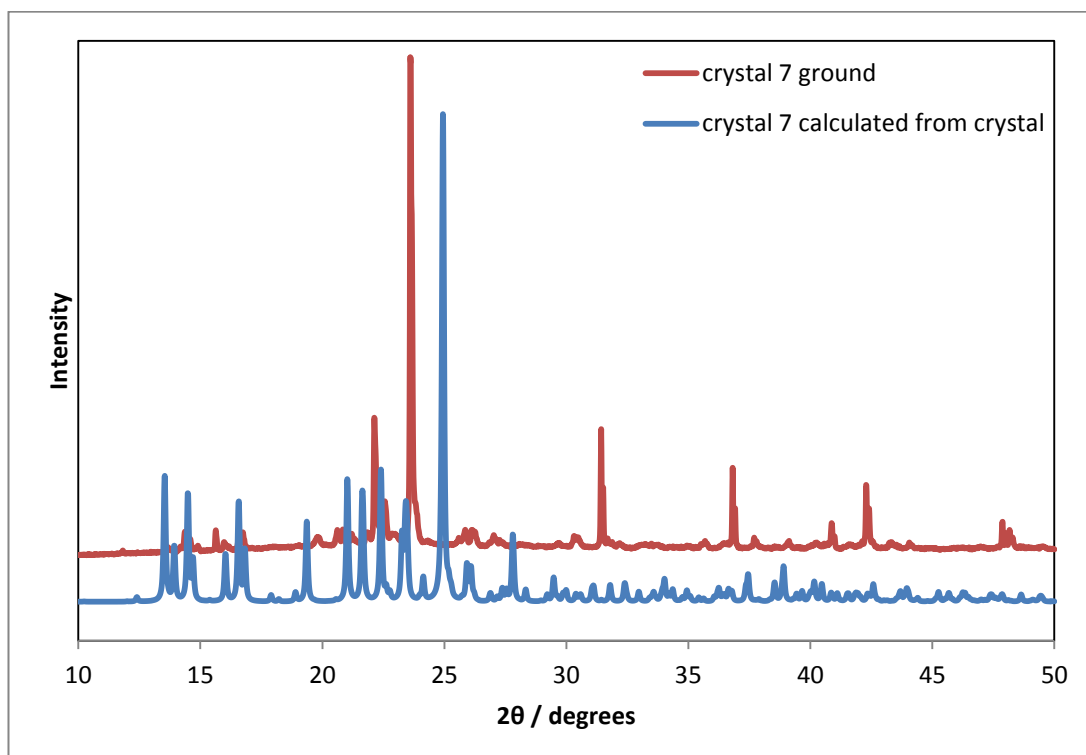
Figure 4.2 – PXRD plot of the experimental data of crystal 6 made by grinding and the calculated from the crystal structure of crystal 6.
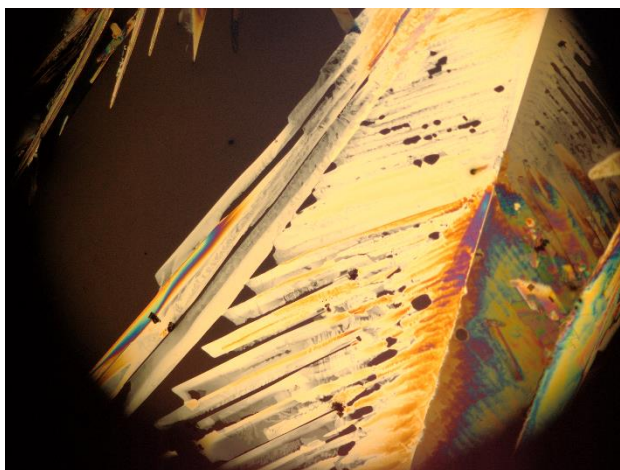
Figure 4.3 – Crystals of crystal 6.

4.2.2   1,4-phenylenediboronic acid/bisHEP cocrystal

A 1:1 molar ratio of bisHEP and 1,4-phenylenediboronic acid was dissolved in water and the solvent was allowed to slowly evaporate over the course of four weeks to give diffraction quality crystals of a 1:1 1,4-phenylenediboronic acid:bisHEP cocrystal, crystal **7**, with the formula $C_6H_8B_2O_4 \cdot C_{12}H_{20}N_2O_3$. The crystal packing of crystal **7** is shown in Figure 4.4.

The 1,4-phenylenediboronic acid molecules form chains with the bisHEP molecules bridging between two chains by accepting hydrogen bonds from the boronic acid groups. In the 1,4-phenylenediboronic acid chain the torsion between the benzene ring and the boronic acid

moiety is 28.35(16)° on the side hydrogen bonding to the bisHEP and 10.48(15)° on the side hydrogen bonding to the next 1,4-phenylenediboronic acid molecule. The hydrogen bonds between the 1,4-phenylenediboronic acid molecules have O···O distances of 2.810(2) Å and 2.754(2) Å. In comparison, in pure 1,4-phenylenediboronic acid[15] the hydrogen bond O···O distances between the 1,4-phenylenediboronic acid molecules are both the same at 2.761(3) Å and the torsions at both ends of the 1,4-phenylenediboronic acid molecule are much more similar to each other with values of 23.5° and 25.0°. The inclusion of bisHEP decreases the symmetry of the 1,4-phenylenediboronic acid molecules seen in the structure of pure 1,4-phenylenediboronic acid resulting in one longer bond and a twisted 1,4-phenylenediboronic acid conformation.
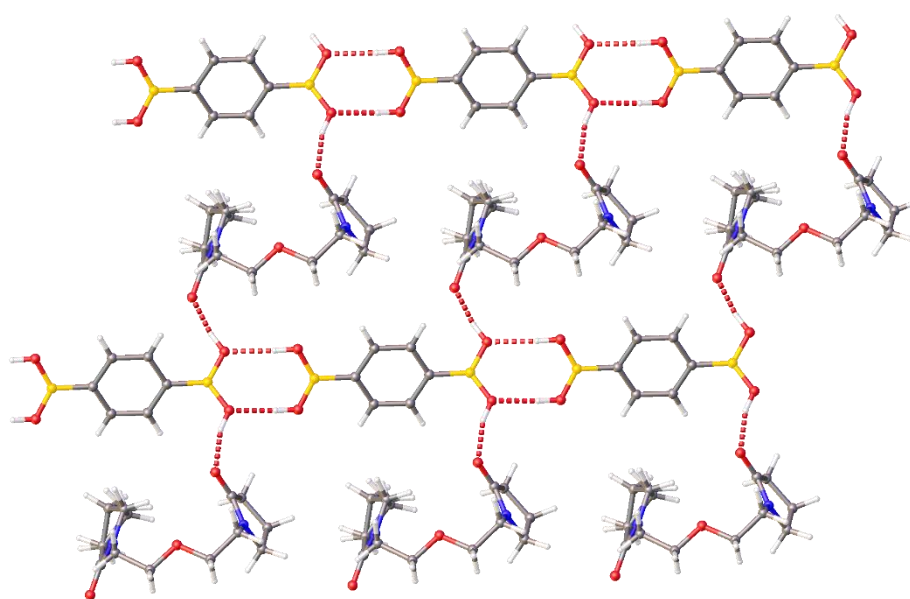
Figure 4.4 – Crystal packing of crystal 7 with hydrogen bonds shown by red dashed lines.

The hydrogen bonds between the bisHEP and 1,4-phenylenediboronic acid molecules have O···O distances of 2.626(2) Å and 2.699(1) Å. These are slightly longer than the lengths of the hydrogen bonds between the carbonyl group of bisHEP and boric acid in crystal **6** which have O···O bond lengths of 2.6583(13) Å and 2.6045(13) Å. As the difference in bond length is not large, it suggests the strength of the hydrogen bonds between bisHEP with 1,4-phenylenediboronic acid and boric acid is similar. Crystal **6** and crystal **7** both have bisHEP bridging the chains formed be the boronic acids, though the conformation of the bisHEP molecules are distinctly different. In crystal **6** the bisHEP molecules are much more U-shaped in than the bisHEP molecules in crystal **7**. In crystal **7** the pyrrolidone rings are held close to parallel, with the carbonyl groups pointing away from each other, one forward and one back from the plane of the molecule shown in Figure 4.5a. In crystal **6** the pyrrolidone rings lie

almost flat to one another within the plane of the molecule shown in Figure 4.5b, with the carbonyl groups pointing out to the left and right of the molecule.
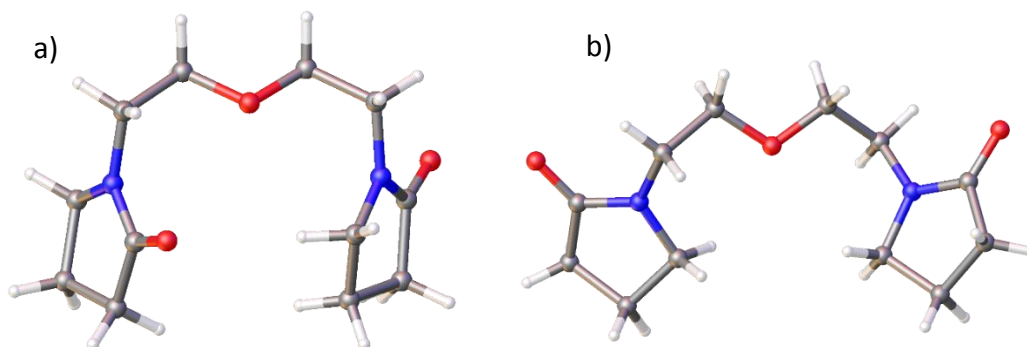
Figure 4.5 – Conformation of bisHEP in a) crystal 7 and b) crystal 6.

The Hirschfeld surface fingerprint plots of bisHEP for both crystal **6** and crystal **7** can be found in Figure 4.6. Both plots exhibit a sharp peak in the lower right half of the plot. This is characteristic of hydrogen bond accepting behaviour from the carbonyl of the lactam which makes bisHEP a strong hydrogen bond acceptor. There are two main differences between the Hirshfeld surface fingerprint plots of crystal **6** and crystal **7**. The first of which is the larger amount of diffuse blue area in the top right of the plot for crystal **7**. This arises from more space around the molecule as crystal **7** is less densely packed around the bisHEP molecules than crystal **6**. The second difference it that the plot of crystal **6** also has a small, but significant, peak in the top right, which is indicative of hydrogen bond donating behaviour. In crystal **6** the bisHEP molecule donates a single C-H···O hydrogen bond to the boric acid molecules of left hand side boric acid chain as illustrated in Figure 4.1. This hydrogen bond donating interaction is absent in crystal **7**.
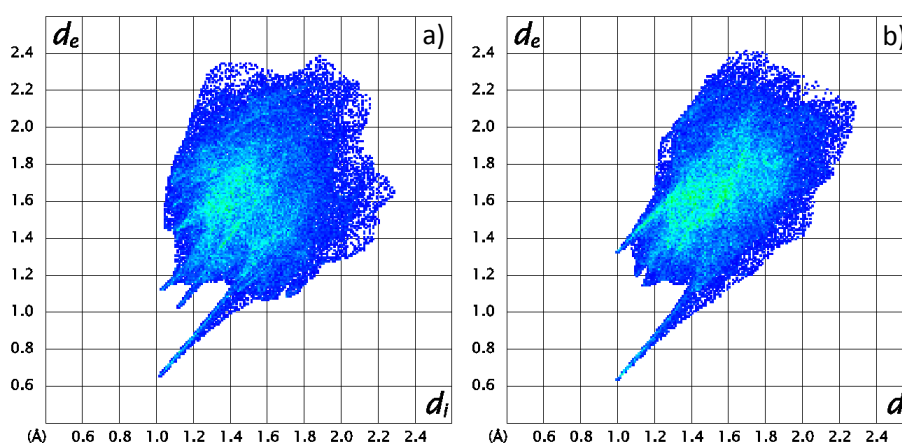
Figure 4.6 – Hirshfeld surface fingerprint plots of bisHEP in a) crystal 7 and b) crystal 6.

IR spectra of bisHEP and crystal **7** showed the carbonyl peak of bisHEP to shift from 1668 cm^{-1} to 1647 cm^{-1} upon formation of the cocrystal. The significant decrease in wavenumber

arises from the formation of hydrogen bonds forming between the carbonyl group of bisHEP and 1,4-phenylenediboronic acid as can be seen in the crystal structure in Figure 4.4.

DSC of crystal **7** shows small sharp endothermic peaks beginning at 55 °C, which are attributed to decomposition of the sample. The decomposition peaks get larger and more frequent until 150 °C which was the maximum temperature tested. The decomposition is probably due to the unstable nature of the lactam rings in bisHEP.

Crystal **7** is a novel crystal structure with strong parallels to the previously reported crystal **6**. Though of a similar composition, containing bisHEP and a boronic acid, crystal **6** and crystal **7** have different stoichiometry and conformation of the bisHEP molecules. The strong hydrogen bonds between bisHEP and 1,4-phenylenediboronic acid in crystal **7** may be able to delay the availability of 1,4-phenylenediboronic acid to react in solution, affording delayed onset reactions.

4.2.3   ε-caprolactam/boric acid cocrystal

Slow evaporation of a 1:1 mixture of tetrahydroxydiboron and bisVCap did not result in a tetrahydroxydiboron/bisVCap cocrystal, but instead both components underwent Lewis acid catalysed cleavage resulting in a ε-caprolactam/boric acid cocrystal, crystal **8**, with the formula $C_6H_{11}NO \cdot B(OH)_3$. The crystal structure of crystal **8** is shown in Figure 4.7. The boric acid molecules form a zigzagging, hydrogen-bonded chain, with ε-caprolactam molecules hydrogen bonding to the outside. These chains lie parallel to each other forming layers. The chains in same layers have no short contact interactions with each other, with the closest C⋯C distance between the pendant ε-caprolactam groups being 4.274(2) Å. Between the layers there are short contact interactions between boric acid and ε-caprolactam with C⋯H distances of 3.595(1) Å and 3.519(1) Å. There are no ε-caprolactam to ε-caprolactam or boric acid to boric acid short contact interactions between the layers.

The boric acid to ε-caprolactam hydrogen bonds have a O⋯O length of 2.564(1) Å and a N⋯O length of 3.035(1) Å. The O-H⋯O of crystal **8** is particularly short with most similar ε-caprolactam to hydroxyl group hydrogen bonds in the CSD having O⋯O lengths of 2.66 – 2.67 Å.[16,17] A sulfonamide benzoic acid/ε-caprolactam cocrystal reported by Bolla *et al.*[18] exhibits a very comparable O⋯O length between the carbonyl of the ε-caprolactam molecule and the hydroxyl group of sulfonamide benzoic acid of length 2.556(10) Å. The boric acid chain in crystal **8** is held together by two hydrogen bonds, one donating, one accepting, between each pair of boric acid molecules. Both hydrogen bonds to the same boric acid molecule along have the same length, with different lengths of hydrogen bond to the different boric

acid molecules. The O⋯O length of the hydrogen bonds are 2.657(1) Å to one boric acid molecule and 2.707(1) to the other. When compared to the boric acid chain in crystal **6**, crystal **8** has less variation in bond lengths in the boric acid chain, as crystal **6** has 4 different boric acid to boric acid hydrogen bond lengths, ranging from 2.683(1) to 2.750(12) Å. The crystal structure of pure boric acid[19] also shows more variation in boric acid to boric acid hydrogen bond length, with the O⋯O hydrogen bond distances varying between 2.688(7) Å and 2.740(6) Å and no two being the same. In crystal **8** the boric acid molecules are more symmetrically bound to one another than in either pure boric acid or crystal **6**.
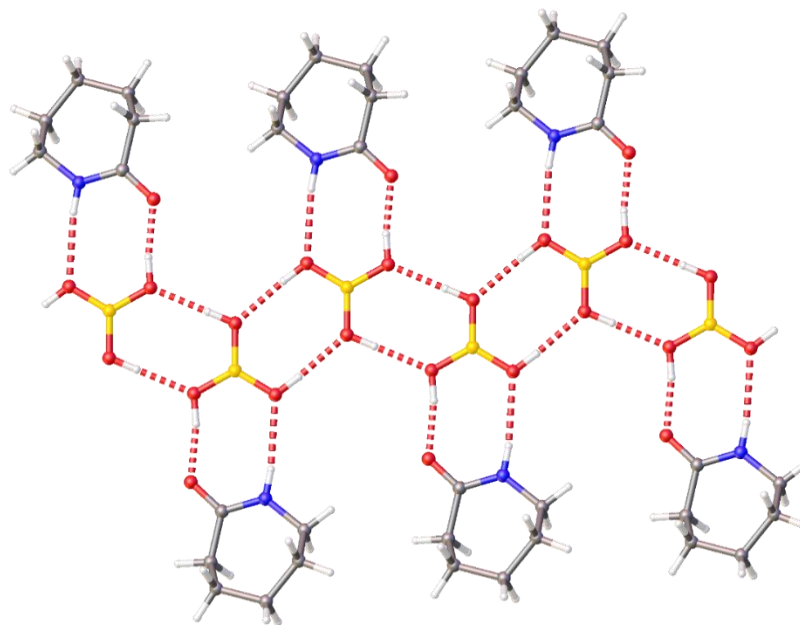
Figure 4.7 - Crystal packing of crystal 8 with hydrogen bonds shown in red.

The Hirschfeld surface fingerprint plot of ε-caprolactam in crystal **8** can be seen in Figure 4.8. There is a strong hydrogen bond accepting peak in the bottom right of the diagram, relating to the carbonyl group accepting a hydrogen bond from boric acid. The top left of the graph shows a hydrogen bond donating peak, arising from the N-H of the ε-caprolactam donating a hydrogen bond to an oxygen atom of the boric acid. The small diffuse blue region between the two hydrogen bonding peaks is indicative of a cyclic hydrogen bonding moiety. In this case the cyclic hydrogen bonding between the boric acid molecule and the ε-caprolactam molecule, as can be seen in Figure 4.7
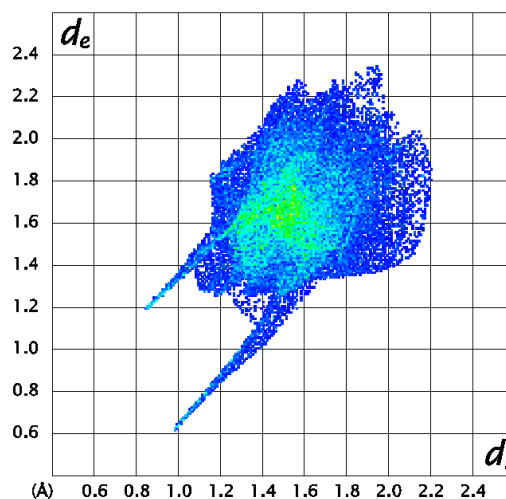
Figure 4.8– Hirschfeld surface analysis of ε-caprolactam in crystal 8.

DSC of crystal **8** showed the crystal to decompose on heating, as the DSC plot showed many overlapping, endothermic peaks. Both boric acid and ε-caprolactam show the beginnings of decomposition on heating, so meaningful DSC of analysis is crystal **8** is not possible. IR spectroscopy shows the carbonyl peak of ε-caprolactam to shift from 1653 cm^{-1} to 1623 cm^{-1} upon forming the cocrystal. The large shift in the IR carbonyl peak to a lower wavenumber is indicative of strong hydrogen bonding behaviour, as was observed in the crystal structure.

It is preferable to be able to produce crystal **8** directly from its constituent parts, ε-caprolactam and boric acid, so a larger amount of pure product can be formed and to verify reproducibility, as the cleavage of bisVCap and tetrahydroxydiboron may not be complete. To attempt direct acquisition of crystal **8**, ε-caprolactam and boric acid were accurately weighed out in a 1:1 molar ratio and ground together using a ball mill until a homogenous powder was formed. This powder was analysed by PXRD, the results of which can be seen in Figure 4.9. A powder x-ray pattern of crystal **8** was calculated from the single crystal structure using Mercury[12] and compared to the experimental PXRD pattern achieved from the ground structure. Allowing for a small shift in peaks due to the difference in the temperatures of the measurements, single crystal data was recorded at 120 K whilst PXRD was performed at room temperature, and changes in intensity due to preferred orientations in the powder the calculated and experimental powder patterns are consistent, confirming that grinding is an adequate method of forming crystal **8**.
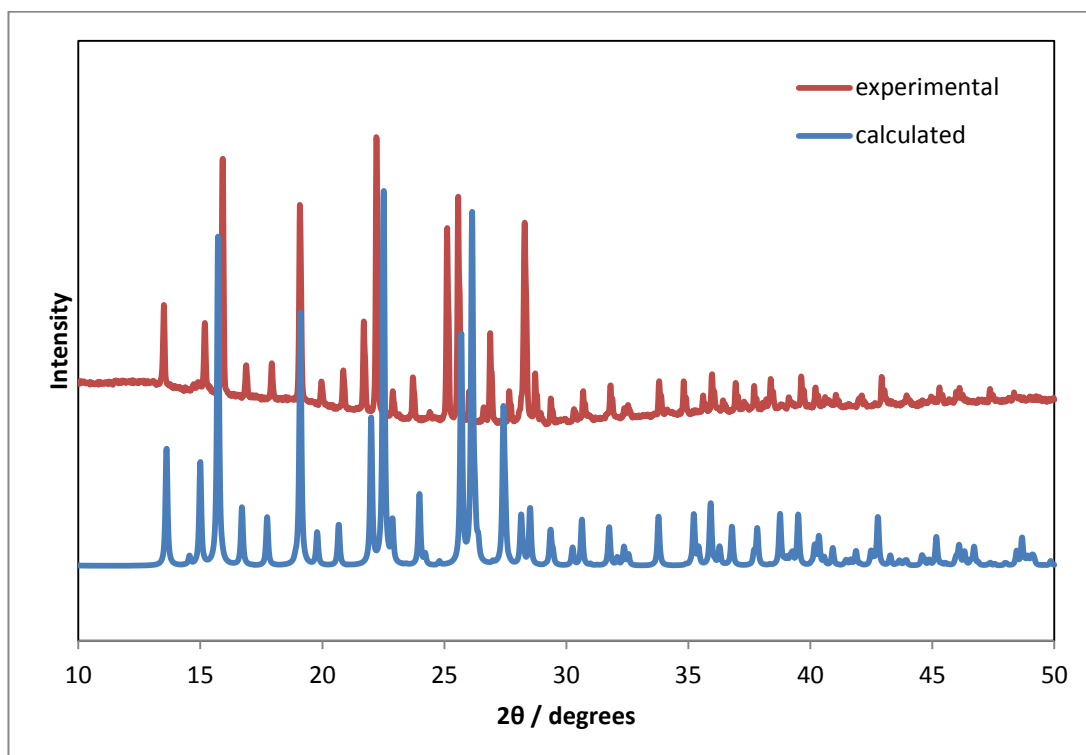
Figure 4.9– PXRD of crystal 8 calculated from the crystal structure and formed by grinding of the two components.

4.2.4   Gelling guar

4.2.4.1   Gel tests

As boric acid is already well researched as a crosslinker of guar, it is used as the control experiment to which all others are compared. Bishop *et al.*[7] found that a 10:2000:1 wt/wt/wt ratio of guar:water:boric acid with a small amount of NaOH to raise the pH above 9, to be an effective recipe to achieve a robust guar gel. For a gel made of 20 cm^3 of water, 0.1 g of guar and 0.01 g of boric acid, 0.1 cm^3 of 2 M NaOH raises the pH enough for gelling to occur. To allow direct comparison to the control experiment which uses boric acid as the crosslinker, all other potential crosslinking additives were added in 1:1 molar ratio of active component:boric acid. The active component for the cocrystals is the boronic acid component, other acids are simply added in a 1:1 molecular ratio compared to boric acid.

Readily available diboronic acids, tetrahydroxydiboron and 1,4-phenylenediboronic acid, were tested for their ability to gel guar. Monoboronic acids were not tested as they would not be effective in gelling guar. As seen in Scheme 4.2, the boronic acid must react with two guar chains to form a crosslink and monoboronic acids only have one reactive group so are not capable of creating both sides of the crosslink. Telluric acid was also tested; whilst not a boronic acid, it is a Lewis acid of an analogous form to boric acid with a pKa$_1$ of 7.7 compared

with boric acid which has a pKa$_1$ of 9.3.[20] The three cocrystals, crystals **6**-**8**, were also tested for crosslinking ability.

As expected, the control experiment using boric acid readily formed a gel when mixed with a guar/water mixture after 0.01 cm^3 of 2 M NaOH was added. Tetrahydroxydiboron and telluric acid did not show any capacity for crosslinking. For both tetrahydroxydiboron and telluric acid a second experiment using 5 M NaOH, instead of the usual 2 M NaOH, was performed to ensure that the compound has been deprotonated. This was not successful with either the tetrahydroxydiboron or the telluric acid. Neither tetrahydroxydiboron nor telluric acid gelled guar under the conditions tested, so are not effective crosslinkers for guar and are not included in any further gelation experiments. On the other hand, 1,4-phenylenediboronic acid and crystals **6**-**8** all readily formed a gel upon the standard gelling conditions of guar, water and 0.01 cm^3 of 2 M NaOH.

4.2.4.2   Gelation time

To test if use of a cocrystal instead of just the boronic acid affects the gelation time an inversion test was used. The inversion test is a common visual test for gel formation, if a material can support its own weight when the vial the sample is in is inverted, then a gel is said to have formed. To make a timed experiment of the inversion test the samples were inverted every 30 seconds. When the gel could support itself without collapse for 30 seconds it was taken to be fully formed. At first it seemed that the cocrystals **6** and **8** gave a delayed crosslinking, as it took the samples containing crystal **6** or crystal **8** longer to pass the inversion test than the samples containing pure boric acid. Repeats of the experiment showed this observation not to be reproducible, with boric acid containing samples sometimes having a long onset time and cocrystals samples sometimes having a short onset time. The samples were prepared, without NaOH as this starts the gelation process, directly one after another in the same lab, so there is no notable difference in temperature and the mixing procedures, length of shaking and sonication, were kept as similar as possible. The only difference is how long the sample had been stood before the NaOH was added. Experiments varying how long after the water, crosslinker and guar had been mixed the NaOH was added were undertaken. For the first sample, NaOH was added as soon as the crosslinker and guar had all completely dissolved in the water. This point is taken to be 0 min. For the subsequent samples NaOH was added 10, 20, 30, 40, 50 and 60 min after the dissolution of guar and boric acid. The experiments were repeated for boric acid, 1,4-phenylenediboronic acid and crystals **6**-**8**. For boric acid, crystal **6** and crystal **8**, the 0 min addition of NaOH noticeably thickened the mixture but did not result in a gel capable of

passing the inversion test. The gelation times for the samples containing boric acid, crystal **6** or crystal **8** decreased with the time waited before NaOH addition until 50 min, where the gelation time for all sample was approximately 2 min. The experiments were repeated twice and the averaged data of gelation time against time before NaOH was added for boric acid, crystal **6** and crystal **8** is shown in Figure 4.10.
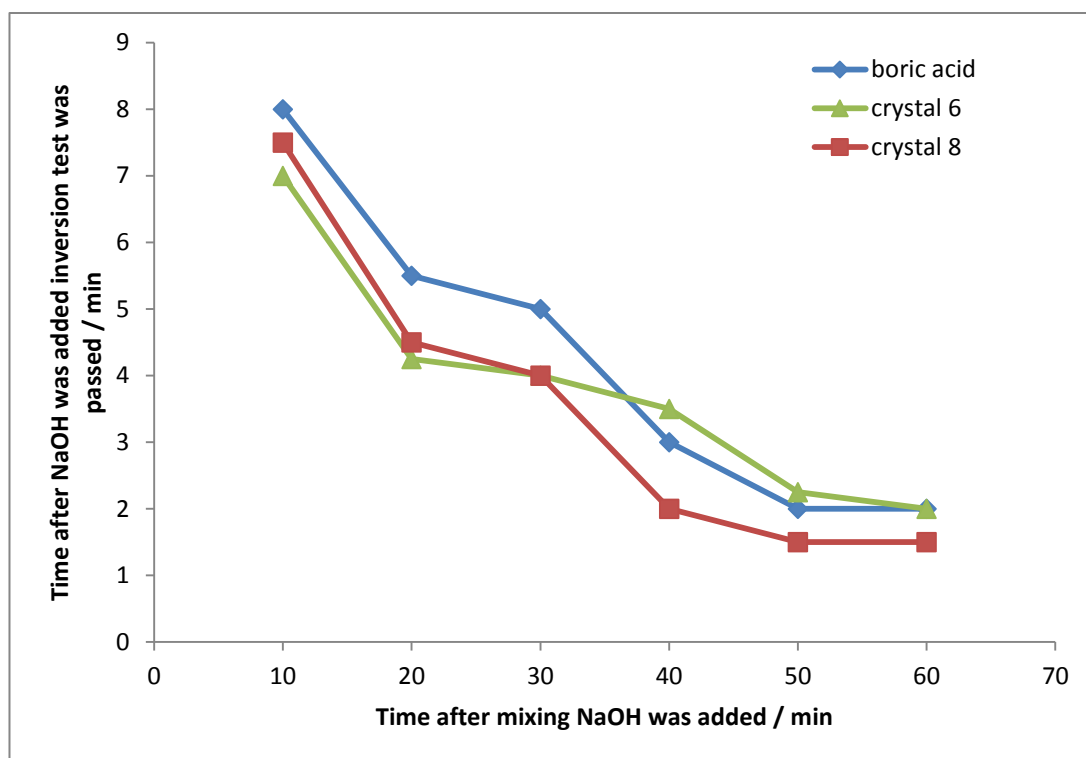
Figure 4.10 – Average gelation time over two experiments of samples containing boric acid, crystal 6 or crystal 8 with varying times before addition of NaOH.

For samples containing 1,4-phenylenediboronic acid or crystal **7** gelation occurred in under a minute regardless of time between mixing and NaOH addition. Samples which had been stood for an hour do gel noticeably faster than those at 0 min, as it is difficult to mix the sample thoroughly before gelation occurs, resulting in a gel surrounded by unreacted solution. Both 1,4-phenylenediboronic acid and crystal **8** behave the same within the scope of these experiments.

The dependency of gelation on the time which NaOH is added is possibly due to entanglement of the guar chains in solution, this entanglement would add a further degree of physical crosslinking to the chemical crosslinks formed by the boric acid, strengthening the gel and shortening the time before the inversion test is passed. Further investigation into the time dependence of gelation is beyond the scope of this project. Within the error of the experiment there is no difference in gelation time between the cocrystals and boronic acids, suggesting that the supramolecular bonds which form the cocrystal are not persistent

enough in solution to significantly slow the gelation process. Any differences there may be are small and not within the scope of potential utilization in an industry setting for any delayed gelation applications.

4.2.4.3 Gel strength

Oscillatory stress sweep rheology was used to test the relative strength of the guar gels formed with boric acid, 1,4-phenylenediboronic acid and crystals **6**-**8**. Oscillatory stress sweeps were performed using a smooth 25 mm steel geometry and 60 mm smooth Peltier steel plate with a gap of 1000 μm. The frequency was fixed at 1 Hz and the stress sweep was performed from 0 – 1000 Pa. The samples for rheology were prepared by mixing water, guar and crosslinker an hour before adding NaOH to avoid any variations in the gel which may arise from the differences in gelation time caused by earlier addition of NaOH. As the samples are shaken to thoroughly mix in the NaOH, the gels often have air bubbles, which can lead to erratic rheology results. To help reduce errors due to bubbles, multiple samples of the same gel were run until reproducible results were produced.

The plot of the oscillatory stress sweeps for boric acid, crystal **6** and crystal **8** can be found in Figure 4.11. All three samples start with a storage modulus between 20.9 and 22.6 log(Pa). When compared to the multiple runs of the same samples, this is within the expected variance and not a significant difference. The storage modulus for all three samples decreases and eventually crosses over with the loss modulus between 225 and 283 Pa. Again the difference between repeats of the same sample is greater than the difference between samples, so within error the crossing point is the same. The crossover of the storage and loss modulus shows a change from a gel with significant solid like character to a sol which behaves much more like a liquid. When enough stress is applied the bonds of the crosslinks readily break and reform due to the dynamic, non-covalent nature of the crosslinks formed by guar and the boronic acids, causing the gel to collapse. After the stress has been removed, the gel reforms.
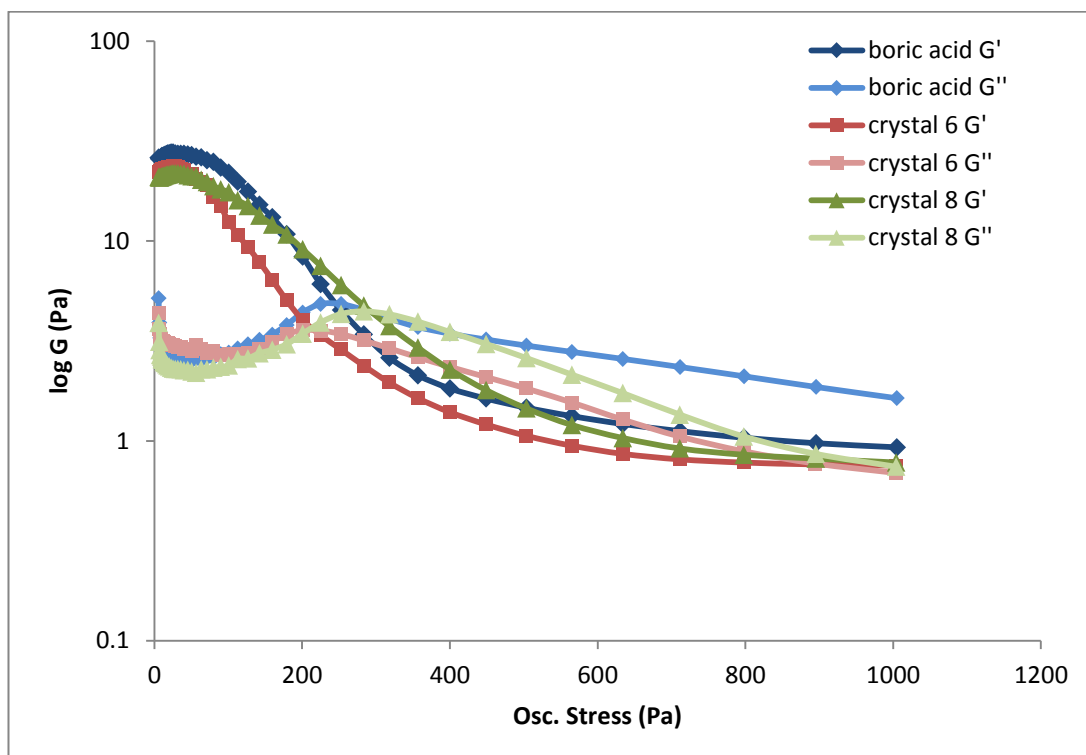
Figure 4.11 – Oscillatory stress sweep plot of boric acid, crystal 6 and crystal 8.

Crystal **7** and 1,4-phenylenediboronic acid also show almost identical behaviour. The oscillatory stress sweep plot, Figure 4.12, shows both gels to start at a storage modulus of 27 log(Pa) and then decrease, crossing the loss modulus at approximately 565 Pa. As seen with the boric acid based crosslinkers, there is no difference between 1,4-phenylenediboronic acid and its crystal **7** outside of experimental error.
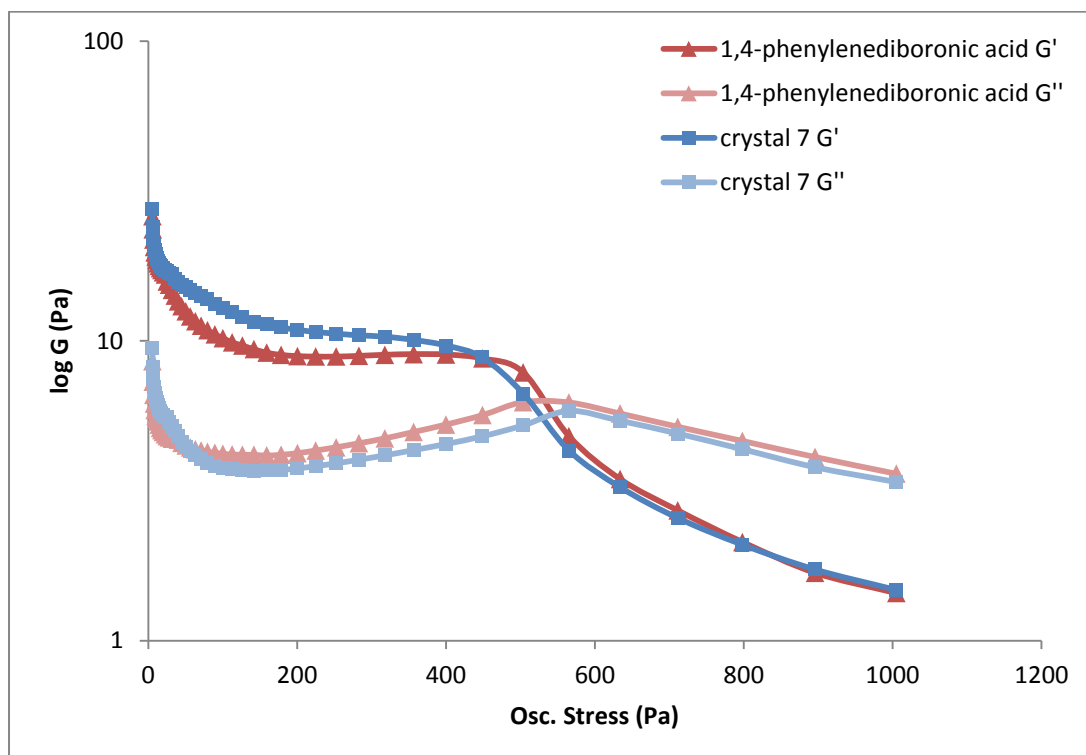
Figure 4.12 – Oscillatory stress sweep plot of 1,4-phenylenediboronic acid and crystal 7.

In conclusion the interactions between the components of the cocrystals that promote the formation of the cocrystals are not significant enough in solution to affect the boronic acids' ability to gel guar, either in gelation time, or strength of gel. On the other hand 1,4-phenylenediboronic acid does give stronger gels than boric acid which require more stress to go through the gel-sol transition. This could have potential applications where stronger guar gels are requires, though the greater expense and less favourable toxicity of 1,4-phenylenediboronic acid would probably hamper the use of 1,4-phenylenediboronic acid in many situations where guar gel is used.

4.3 Experimental

4.3.1 Cocrystal synthesis

Crystal **6** was made by grinding a 1:1 bisHEP:boric acid mixture in a mortar and pestle for one minute. Excess bisHEP was removed by pressing the mixture between dry filter papers until only an off white solid remained. The sample was characterised by PXRD.

Crystal **7** was made by dissolving 0.021 g 1,4-phenylenediboronic and 0.045 g bisHEP together in water and allowing the water to evaporate at room temperature. Crystals of diffraction quality formed within three weeks and analysed by single crystal x-ray crystallography. A second sample was formed made by grinding a 1:1 bisHEP:1,4-

phenylenediboronic acid in a mortar and pestle for one minute. The sample was analysed by IR spectroscopy.

Crystal **8** was made by dissolving 0.008 g of tetrahydroxydiboron and 0.04 g of bisVCap together in water and allowing the water to evaporate at room temperature. Single crystals of diffraction quality were achieved within three weeks and analysed by single crystal x-ray crystallography. A second sample was formed by grinding a 1:1 ratio of ε-caprolactam:boric acid in a Retsch MM200 ball mill at 20 Hz for 30 min. The sample was characterised by PXRD.

IR spectra were performed using a Perkin Elmer FTIR spectrum 100 with an attenuated total reflectance (ATR) attachment. Data were recorded at a resolution of 2 cm^{-1} for 16 runs over the range $4000 - 600$ cm^{-1}.

Powder x-ray diffraction was performed using a Bruker AXS D8 Advance diffractometer, with a Lynxeye Soller PSD Detector and CuKα radiation at a wavelength of 1.5406 Å by Mr Gary Oswald.

Single crystal crystallographic analyses were performed on a Bruker Photon D8 Venture diffractometer (ImuS microsource, λMoKα, λ = 0.71073 Å) equipped with a Cryostream (Oxford Cryosystems) open-flow nitrogen cryostat, at 120 K. The data collection and refinement was kindly carried out by Dr Dmitry S. Yufit.

ε-caprolactam/boric acid crystal data: Empirical formula $C_6H_{11}NO$, $B(OH)_3$, space group $P2_1/n$, a = 6.9008(3) Å, b = 18.7679(8) Å, c = 7.4385(3) Å, α = 90.00°, β = 111.3340(10)°, γ = 90.00°, volume = 897.37(7) $Å^3$, Z = 4, F(000) = 376.0, MoKα (λ = 0.71073) 2θ range for data collection = 4.34 - 60°, data = 2628, parameters = 165, goodness-of-fit on F^2 = 1.056, R_1 = 0.0436, wR_2 = 0.0903

BisHEP/1,4-phenylenediboronic crystal data: Empirical formula $C_6H_8B_2O_4$, $C_{12}H_{20}N_2O_3$, space group $P\overline{1}$, a = 10.0731(4) Å, b = 10.2343(4) Å, c = 12.1312(5) Å, α = 112.5470(10)°, β = 111.5550(10)°, γ = 90.5390(10)°, volume = 1038.42(7) $Å^3$, Z = 2, F(000) = 432.0, MoKα (λ = 0.71073) 2θ range for data collection = $4.04 - 60$°, data = 6065, parameters = 325, goodness-of-fit on F^2 = 1.064, R_1 = 0.0684, wR_2 = 0.1682

4.3.2 Gel experiments

Gelling mixtures were prepared in a 10:2000:1 wt/wt/wt ratio. For the different acids, the acid was added in the same molar amount as boric acid. Cocrystals were added to result in the same number of moles of boronic acid. The compositions can be found in Table 4.1.

Guar and either boric acid, 1,4-phenylenediboronic acid, crystals **6**-**8**, telluric acid or tetrahydroxydiboron were dissolved in water, compositions outlined in Table 4.1, by shaking for 30 seconds followed by 30 seconds of sonication after which 0.01 cm^3 of 2 M NaOH was added then the mixture was vigorously shaken for a further 20 seconds. Samples were inverted to test for gel formation.

Guar and either telluric acid or tetrahydroxydiboron were dissolved in water, compositions outlined in Table 4.1, by shaking for 30 seconds followed by 30 seconds of sonication after which 0.01 cm^3 of 5 M NaOH was added then the mixture was vigorously shaken for a further 20 seconds. Samples were inverted to test for gel formation.

Crosslinker	Crosslinker / g	Guar / g	Water / cm^3	2 M NaOH / cm^3	5 M NaOH / cm^3
boric acid	0.0010	0.010	2.00	0.01	0
crystal **7**	0.0024	0.010	2.00	0.01	0
1,4-phenylenediboronic acid	0.0027	0.010	2.00	0.01	0
crystal **8**	0.0065	0.010	2.00	0.01	0
crystal **9**	0.0045	0.010	2.00	0.01	0
tetrahydroxydiboron		0.010	2.00	0.01	0
telluric acid		0.010	2.00	0.01	0
tetrahydroxydiboron		0.010	2.00	0	0.01
telluric acid		0.010	2.00	0	0.01

Table 4.1 - Composition of guar gelling experiments.

Guar and either boric acid, 1,4-phenylenediboronic acid, crystals **6**, **7** or **8** were dissolved in water, compositions outlined in Table 4.1, by shaking for 30 seconds followed by 30 seconds of sonication. 0.01 cm^3 of 2 M NaOH was added 0, 10, 20, 30, 40, 50 or 60 minutes after the sonication and the sample was vigorously shaken for a further 20 seconds. The vials were inverted every thirty seconds after addition of NaOH until the sample could hold its own weight for at least 5 seconds or half an hour had passed with no gel forming.

Samples for rheology were prepared by dissolving guar and either boric acid, 1,4-phenylenediboronic acid, crystals **6**, **7** or **8** in water, compositions outlined in Table 4.1, by shaking for 30 seconds followed by 30 seconds of sonication. After one hour 0.1 cm^3 of NaOH was added and the sample was vigorously shaken for a further 20 seconds. Oscillatory stress sweep experiments were performed on a TA Discovery HR-2 hybrid rheometer equipped with a smooth 25 mm steel geometry and 60 mm smooth Peltier steel plate. 2 cm^3 of gel was positioned on the steel plate below the geometry using a spatula. The geometry was lowered

to a distance 1000 μm from the plate. The frequency was set at 1 Hz and the stress sweep was performed from 0.1 - 1000 Pa at 25 °C. Data was recorded using TRIOS v4.1.0.31739.

4.4 References

(1)   Chudzikowski, R. J. *J. Soc. Cosmet. Chem.* **1971**, *22*, 43–60.

(2)   Juppe, H. L.; Marchant, R. P.; Melbouci, M. Environmentally Acceptable Fluid Polymer Suspension for Oil Field Services. US6620769, 2003.

(3)   Dino, D. J. Modified Polygalactomannans as Oil Field Shale Inhibitors. US5646093, 1990.

(4)   Mahto, V.; Sharma, V. P. *J. Pet. Sci. Eng.* **2004**, *45* (1–2), 123–128.

(5)   Rafique, C. M.; Smith, F. *J. Am. Chem. Soc* **1950**, *72*, 4634–4637.

(6)   Kesavan, S.; Prudhomme, R. K. *Macromolecules* **1992**, *25* (7), 2026–2032.

(7)   Bishop, M.; Shahid, N.; Yang, J.; Barron, A. R. *Dalt. Trans.* **2004**, No. 17, 2621–2634.

(8)   Kinsey, E. W. I.; Sharif, S.; Harry, D. N. Method of Gelling a Guar or Derivated Guar Polmer Solution Utilized to Perform a Hydraulic Fracturing Operation. US5488083, 1996.

(9)   Subrahmanyam, P. J. *J. Chem. Pharm. Res.* **2012**, *4* (2), 1052–1060.

(10)   Perrin, A. The chemistry of low dosage clathrate hydrate inhibitors, University of Durham, 2015.

(11)   Perrin, A.; Myers, D.; Fucke, K.; Musa, O. M.; Steed, J. W. *Dalt. Trans.* **2014**, *43* (8), 3153–3161.

(12)   Macrae, C. F.; Bruno, I. J.; Chisholm, J. A.; Edgington, P. R.; McCabe, P.; Pidcock, E.; Rodrigues-Monge, L.; Taylor, R.; van de Streek, J.; Wood, P. A. *J. Appl. Cryst.* **2008**, *41*, 466–470.

(13)   Kurakevych, O. O.; Solozhenko, V. L. *Acta Crystallogr., Sect. C Cryst. Struct. Commun.* **2007**, *63*, i80–i82.

(14)   Freyhardt, C. C.; Wiebcke, M.; Felsche, J. *Acta Crystallogr., Sect. C Cryst. Struct. Commun.* **2000**, *56*, 276–278.

(15)   Rodríguez-Cuamatzi, P.; Vargas-Díaz, G.; Maris, T.; Wuest, J. D.; Höpfl, H. *Acta Crystallogr. Sect. E Struct. Rep. Online* **2004**, *60* (8), 1316–1318.

(16)   Bis, J. A.; McLaughlin, O. L.; Vishweshwar, P.; Zaworotko, M. J. *Cryst. Growth Des.*

2006, *6* (12), 2648–2650.

(17)   Sanphui, P.; Bolla, G.; Nangia, A.; Chernyshev, V. *IUCrJ* **2014**, *1*, 136–150.

(18)   Bolla, G.; Nangia, A. *Chem. Commun.* **2015**, *51*, 15578–15581.

(19)   Shuvalov, R. R.; Burns, P. C. *Acta. Cryst.* **2003**, *C59*, i47–i49.

(20)   Reger, D. L.; Goode, S. R.; Ball, D. W. *Chemistry : Principles and Practice*, Third Edit.; Brooks/Cole, Cengage Learning: Belmont, 2010.

5   Interactions of sour gas with KHIs

5.1   Introduction

Desirable natural gases, such as methane, are found mixed with gases such as hydrogen sulfide and carbon dioxide which are referred to as acid gases. After a certain threshold of H_2S the gas is then classed as a sour gas. This threshold varies by company but the sales specification is often 4 ppm of H_2S.[1,2] Sour gas is often sweetened, in other words the acidic elements are removed, before being transported through pipes.[3] The presence of acidic gases causes corrosion of the pipeline,[4] as well as promoting the formation of hydrates.[5]

H_2S forms hydrates at the lowest partial pressure of all the components in sour gas, at least partially due to its size being correct to fit in the hydrate cavities.[6] The favourability of H_2S clathrate formation brings added danger to the system. As well as the health hazards which are always associated with natural gas clathrates, such as flammability and pipe blockages, hydrates formed in a sour system are rich in H_2S.[6] This poses a significant health risk, as H_2S high acute toxicity, even at low concentrations, so avoiding a significant concentration of H_2S is necessary to ensure safe working conditions.[7]

The presence of H_2S changes the polarity of the system and increases the level of moisture in the gas.[8] The more water there is in the system, the higher the likelihood of it crystallising and hydrates forming. There is plenty of evidence that hydrates are more likely to form in sour systems than sweet ones. H_2S apparently makes the formation of hydrates more favourable, though no reason for this, except for favourable size, has been proposed, and it seemingly contradicts the theory that more polar molecules make less stable clathrate hydrates,[9] as well as helping introduce water to form the hydrates. Though there has been no research into if there is any effect on the inhibitors. Insight into the interactions between sour gas and KHIs could lead to the development of more effect products for use in sour systems.

There has long been a theory in the oil field industry that acid gas interacts with KHI effectively inhibiting the inhibitor.[6] This theory is based on the observation that in sour systems more KHI is required to achieve the desired level of hydrate inhibition. Though often taken as fact, no data has been published proving this to be true, making it a topical and worthwhile avenue of study.

5.2   Results and discussion

The goal of this chapter is to explore whether the presence of acid gases adversely affects KHIs' ability to inhibit clathrate hydrate formation. For ease of analysis model compounds **6-9** and compound **11** were studied as well as the KHI polymers **1**, **3** and **5**. Interactions between the model compounds and the acids gases were explored by attempted cocrystallisation with acid gases, NMR titrations and IR titrations.

5.2.1   Crystallisations

One possibility for the seeming inhibition of the KHIs in sour conditions is that the acid gases interact more strongly, or at least comparably, with the KHI than the water does creating competitive inhibition. If the interaction is stronger it may be possible to create cocrystals of the model compound with the acid gases. Cocrystals of gases have been reported before, the most prevalent of which probably being the clathrate hydrates which the KHIs are designed to inhibit.[5,9,10] Unfortunately the methods to form lab synthesised clathrate hydrates require high pressure and thus specialised equipment,[11–13] so looking to clathrate hydrates as an example of how to form new clathrate structures is not viable. Other clathrate structures can be formed in much less demanding conditions. For example hydroquinone exhibits clathrate structures with both CO_2 and H_2S which are formed by bubbling gas through a warm supersaturated solution of hydroquinone then allowing the solution to slowly cool to room temperature.[14,15]

To test the efficiency of the experimental setup a hydroquinone/CO_2 crystallisation was performed. Hydroquinone and water were placed in a glass vial stoppered with a Suba seal. The solution was heated until all of the hydroquinone was dissolved. CO_2 was generated by allowing dry ice to warm in a sidearm flask, attached to a rubber tube with a syringe and needle. The needle was submerged in the hydroquinone solution and an exit needle was introduced to allow the gas to bubble through the solution. The exit needle was removed before the gas inlet needle to leave the sample under an atmosphere of CO_2. The sample was placed in a dewar flask filled with boiling water and allowed to cool to room temperature over the course of three days. Large needle shaped crystals of hydroquinone/CO_2 clathrate, crystal **9**, were successfully created and analysed by single crystal x-ray diffraction, matching the crystal structure found in the literature.[14,15] The structure of crystal **9** is shown in Figure 5.1, showing the hexagonal, hydrogen bonded channels of hydroquinone containing CO_2 molecules. This confirms the experimental setup is adequate to form clathrate structures.
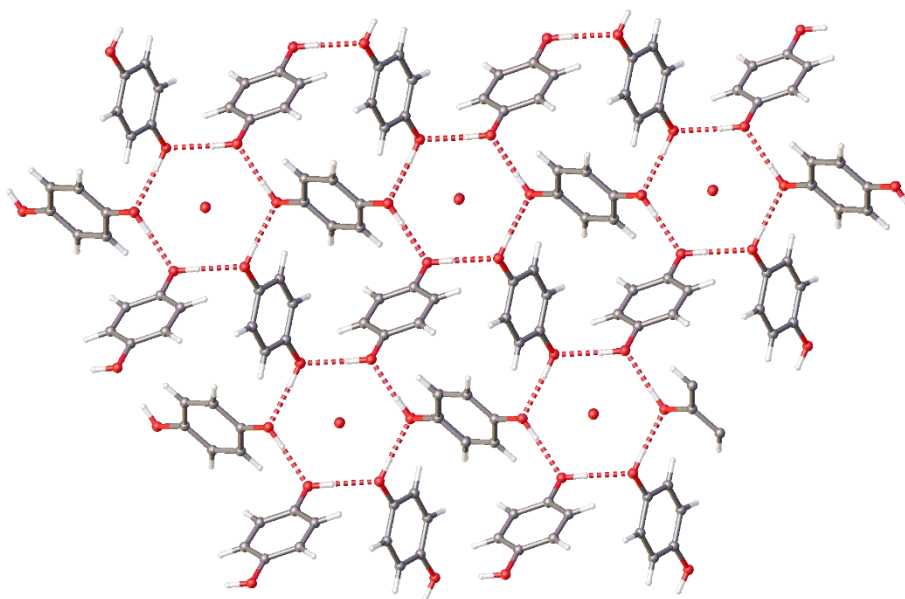
Figure 5.1 - Crystal structure of crystal 9 showing hexagonal channels of hydroquinone filled with CO_2. Hydrogen bonds are shown by red dashed lines.

Crystallisations were attempted with compounds **6-9** and **11** and the acid gases CO_2 and H_2S. The model compounds, ca. 0.05 g, were dissolved in 0.5 cm^3 of acetone, ethanol, methanol propan-1-ol, propan-2-ol, acetonitrile and 90 % ethanol in water. The vials were stoppered with a Suba seal. CO_2 was produced by allowing dry ice to warm in a sidearm flask and H_2S was produced by dropping HCl into a sidearm flask containing FeS. The acid gases were bubbled through the solutions using a rubber tube attached to a syringe and needle by the method described for the hydroquinone clathrate. The crystallisations were left in the freezer at -20 °C under an atmosphere of acid gas for up to two and a half years. Only one sample gave a new crystalline product. After 8 months bisVP in acetone with CO_2 formed large yellow needle shaped crystals. The crystals were solely bisVP without any CO_2 and do not further the study into the effects of sour gases on KHIs. The crystal structure of bisVP is discussed in further detail in section 2.2.2.

The interactions between CO_2 and H_2S and compounds **6-9** and **11** are not sufficient to form a clathrate structure of the model compound with a sour gas. In conclusion, crystallisation is not an effective method with which to study the interactions between KHIs and their models and the acid gases.

5.2.2   IR and NMR Studies

To test if there is any significant interaction between the acid gases and the models a series of IR spectroscopy studies were carried out. The main functionality in the polymers and their models are the lactam rings. The carbonyl groups of the lactam rings are strongly hydrogen

bond accepting and the compounds contain no strong hydrogen bond donor groups. This allows easy observation by IR spectroscopy of the KHIs and model compounds interacting with hydrogen bond donors, as upon hydrogen bonding the carbonyl double bond gains more single bond like character, lengthening the bond and shifting the carbonyl stretch band to a lower wavenumber. Stronger interactions result in larger changes in the carbonyl stretch peak.

Acetonitrile was chosen as the solvent for these experiments as it is polar enough for relatively easy dissolution of the polymers and model compounds, but the lack of a hydrogen bond donating group means it will not cause a significant shift in the carbonyl stretch band of the studied compounds. IR spectra of the model compounds were recorded in fresh acetonitrile and two sour solutions, one containing CO_2 and the other H_2S, to see if the acid gases directly affect the extent of hydrogen bonding interactions of the model compounds in water. No quantitative analysis of the exact amount of acid gas dissolved in the sour solutions has been possible. Qualitatively IR spectra of the CO_2 containing solutions show a distinctive and very strong peak at 2343 cm^{-1} which is characteristic of the asymmetric stretch of CO_2[16,17] and the ^{1}H NMR spectrum of the sour acetonitrile shows a peak at 1.07 ppm from the H_2S. Comparison of the IR spectra of the models in acetonitrile without gas, with CO_2 and with H_2S shows that addition of the acid gases did not shift the carbonyl stretch bands within the resolution of the experiment. The carbonyl shifts of the model compound with and without sour components are shown in Table 5.1. This suggests that the acids gases do not directly interact with the model compounds. Though there is no evidence for direct interaction, it is possible that the presence of acid gas could affect the interactions of the model compounds with water.

	Carbonyl peak / cm^{-1}		
Dimer	No gas	H_2S	CO_2
bisVCap		1651	1651	1651
		1632	1632	1632
H_2bisVCap		1637	1638	1638
bisVP		1681	1681	1681
H_2bisVP		1682	1682	1682
bisHep		1684	1684	1684

Table 5.1 - Positions of the carbonyl peaks in the IR spectra of the compounds 6-9 and 11 dissolved in acetonitrile without gas, with CO_2 and with H_2S.

To test if the presence of acid gas affects the interactions of the KHIs and model compounds with water a series of IR and NMR titrations were performed, involving increasing the amount of water in the system and monitoring how the IR and NMR spectra change. IR and

NMR titrations have previously been utilised to show the validity of the model compounds as models for the KHIs, showing the model compounds to exhibit similar changes in their NMR and IR spectra to the polymers when water is added.[18,19] To avoid obscuring the peaks of interest in the IR spectra Davenport *et al.*[18] chose to use D_2O was used instead of H_2O. D_2O was added to an acetonitrile solution of PVCap and a solution of bisVCap. Comparison of the changes in carbonyl stretch band showed the model compound, bisVCap, to react in a similar manner to the KHI, leading to the conclusion that bisVCap is a suitable model for PVCap. If the presence of acid gases affects the KHIs' interaction with water, a change in the IR and NMR titrations should be evident.

Samples were prepared by dissolving of 0.01 g **1**, **3**, **5-9** and **11** in acetonitrile. Compounds **1**, **3**, **5-9** and **11** were all tested without any gas added, with CO_2 and with H_2S. For the experiments containing either CO_2 of H_2S, the required gas was bubbled through the solution for 1 min before the first spectrum and for 1 min after every three spectra were recorded to minimise loss of gas over time. D_2O was added at from 0 up to 500 equivalents for the experiments with compounds **6-9** and **11** and at 0 up to 250 equivalents of D_2O per carbonyl group for the experiments with **1**, **3** and **5**. The carbonyl shifts of the lactam rings were followed and plotted against the number of equivalents of water added. There was no difference between the sweet and sour systems for any compound that was not within error. Note that later points in the titration become more inaccurate as broadening of the carbonyl peak makes accurate peak position data difficult. The carbonyl shifts for PVP and PVCap without gas, with CO_2 and with H_2S are shown in Figure 5.2.
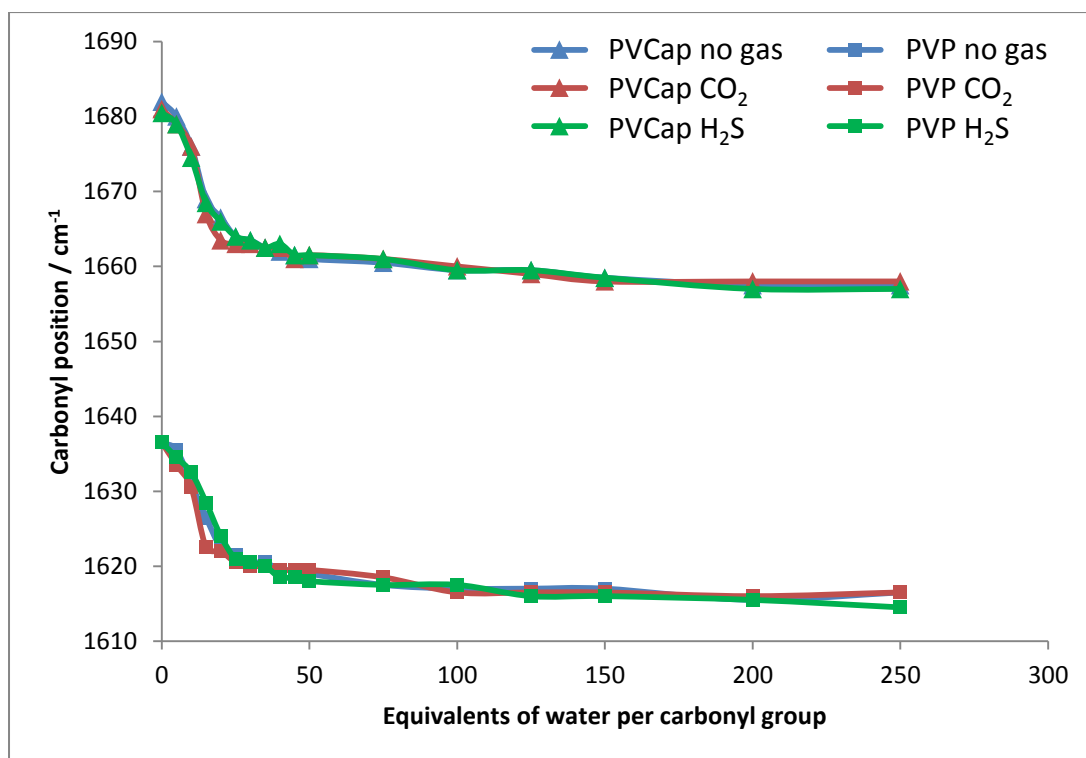
Figure 5.2 – Positions of the carbonyl peaks of PVP and PVCap upon addition of D_2O with and without sour gas.

As D_2O is titrated into the KHI or model compound solution the carbonyl band does not simply shift but also broadens and changes shape. This peak asymmetry can give information on the different levels of hydration of the carbonyl groups as not all will hydrate at the same time.[20] Band asymmetry of the sweet system was extensively explored by Perrin.[19] When overlaid the sweet and sour systems show no significant change in peak shape or position, PVCap is shown as an example in Figure 5.3. This further suggests that there is no change in the interaction of KHIs or the model compounds in sour systems. As there is no difference between the sweet and sour systems and in depth analysis of the peak asymmetry of the sour systems would not supply any further information so was not undertaken.
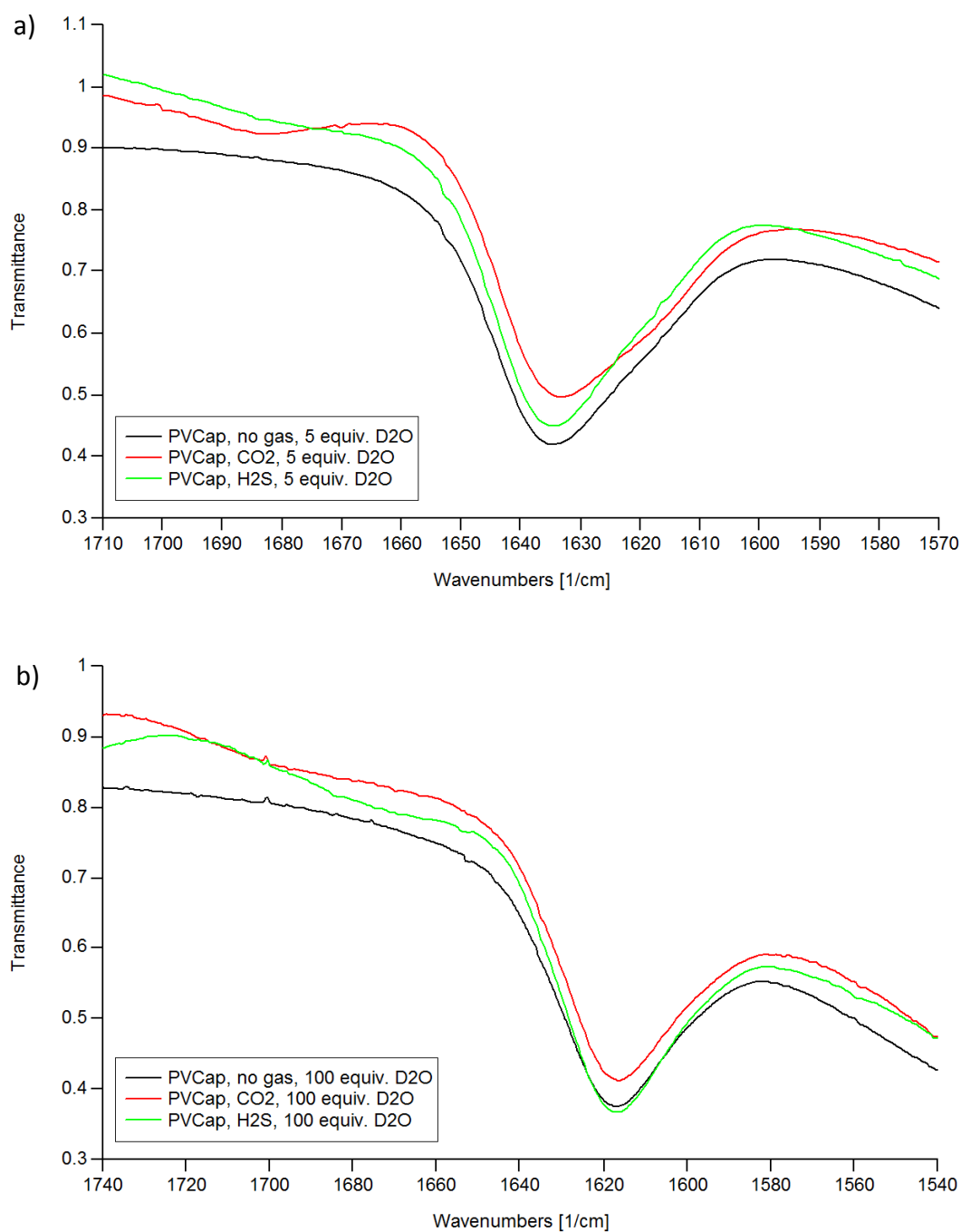
Figure 5.3 - Carbonyl peak of PVCap in acetonitrile without acid gas, with CO₂ and with H₂S with a) 5 equivalents of water per carbonyl group and b) 100 equivalents of water per carbonyl group.

As the IR titrations strongly suggest that acid gases do not affect the KHIs' interaction with water, a single series of NMR titrations was performed to check for any differences which may have been missed by the IR experiments. BisVCap was chosen for the NMR titrations as it is the easiest model compound to synthesise, purify and, as the only solid, the easiest to accurately weigh out. The polymers were not chosen as they give much more complicated NMR spectra than their low molecular weight models, making analysis by NMR difficult. The samples were prepared by dissolving 0.006 g of bisVCap in 0.75 m³ of deuterated acetonitrile.

D_2O was added from 0 to 500 equivalents, with a spectrum being recorded after every addition. The spectra of the NMR titration of bisVCap without gas is shown in Figure 5.4. For the sample containing CO_2, CO_2 was bubble through the solution before the first spectrum and after every three spectra to avoid loss of gas.
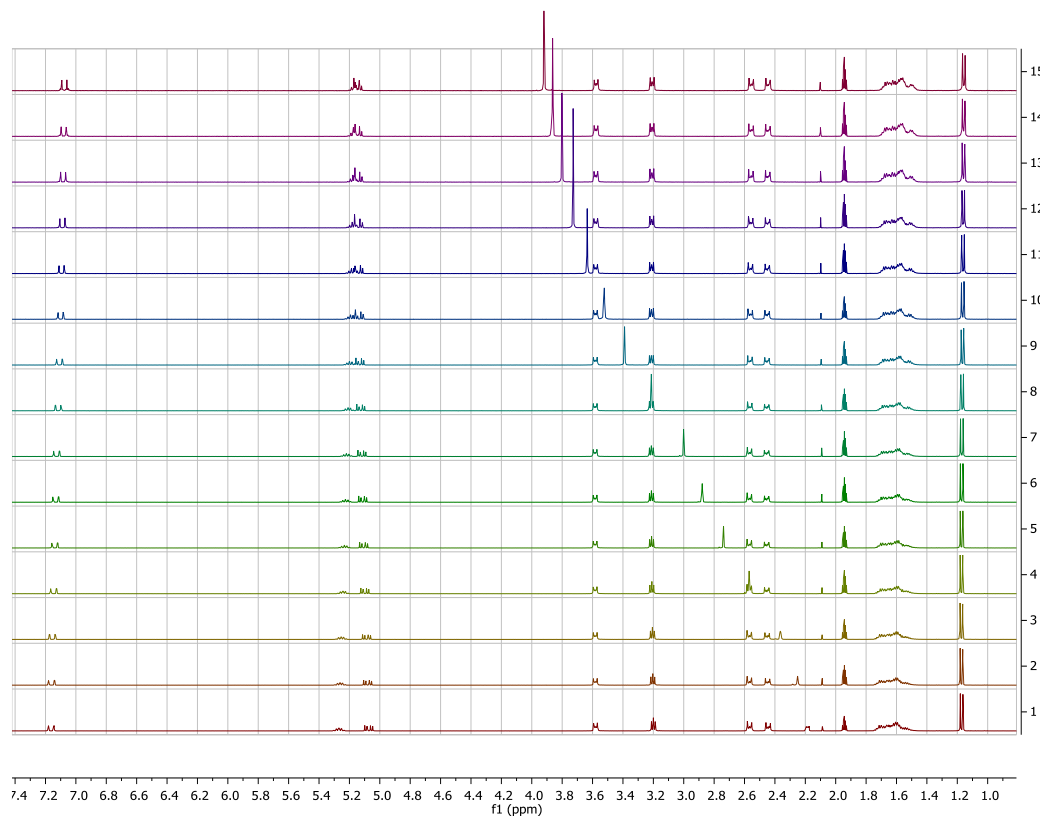
Figure 5.4 - NMR spectra of bisVCap in acetonitrile with increasing amounts of D_2O from bottom to top.

For the titration with H_2S, the same method was initially used as for CO_2, bubble gas through before the first spectrum and every three thereafter. The spectra for the titration with H_2S show extra peaks, one from the H_2S itself at 1.07 ppm, and some small ill-defined peaks from the production method of H_2S. As the titration continued and more H_2S was added more peaks appeared eventually obscuring parts of the spectrum and a black powder appeared in the sample, possibly FeS which had been pushed into the sample by the flow of gas. To prevent this issue, a new sample of bisVCap and acetonitrile was made every three spectra, the appropriate amount of D_2O was added, then H_2S was bubbled through before finally recording the next spectrum.

To check that extra peaks were not caused by the H_2S reacting with bisVCap a sample of bisVCap in a d-acetonitrile/D_2O mix had H_2S bubbled through every half hour over a period of 2.5 hours to mimic the conditions in the titration. No change was observed in the peaks corresponding to the bisVCap and no extra peaks appeared over the course of the

experiment. As no reaction seems to be occurring between the bisVCap and H_2S and the impurities in the NMR do not seem to affect the outcome of the titration, no further action was taken.

As seen in Figure 5.4 a multitude of peaks shift upon addition of D_2O, the most significant shifts happen to the peaks at 5.27 and 7.16 ppm. The chemical shift in ppm of these peaks throughout the titrations with no gas, CO_2 and H_2S can be found in Figure 5.5. There is no significant change between the sweet and sour systems that is not within measurement error, suggesting that the acid gases do not affect the interactions of bisVCap with water as far as can be observed by NMR. As no significant change was observed in the NMR spectra of bisVCap and all IR titrations showed no change upon the addition of acid gas, no further NMR titrations were performed.
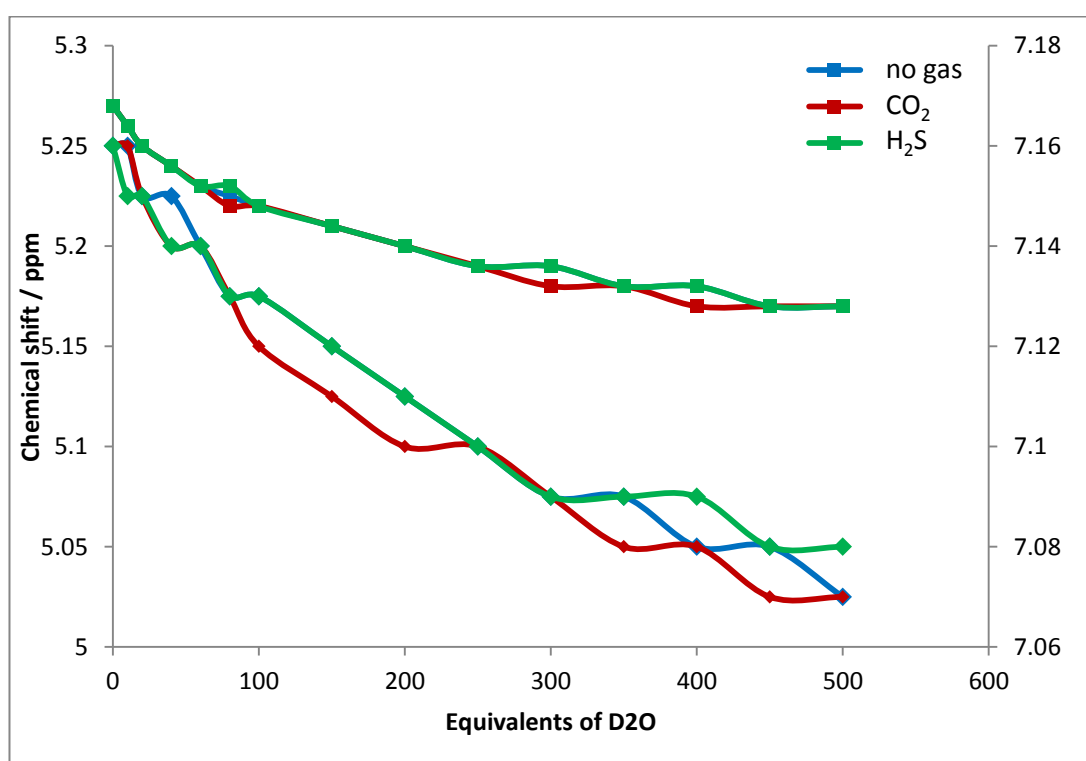
Figure 5.5 - Chemical shift of the peaks at 5.27 and 7.16 during NMR titrations of bisVCap without acid gas, with CO_2 and with H_2S.

To summarise, there is no interaction between compounds **6**-**9** and **11** or the KHIs tested with CO_2 or H_2S observable by IR and NMR spectroscopy. This suggests that the acid gases do not affect the way in which KHIs interact with water, so it is likely that sour systems do not retard their hydrate inhibiting ability. Acid gases, especially H_2S, have long been known to promote the formation of clathrate hydrates.[5] H_2S is commonly referred to as a help gas,[21,22] even allowing molecules which do not normally form clathrates to do so. H_2S forms

clathrates at the lowest pressure and highest temperature of any component in natural gas. In conclusion, sour gas systems do not inhibit the inhibitor, instead they promote the problem. As clathrates form more readily in sour systems more KHI is required to achieve a desirable level of hydrate inhibition. This also explains why anti-agglomerants (AAs) are generally referred to as unaffected by gas composition.[6] AAs do not prevent the formations of clathrates but just keep them flowing as a slurry,[23] thus faster clathrate formation does not greatly change the AA mode of action.

5.3 Experimental

5.3.1 Producing sour gas

Carbon dioxide was produced by placing approximately 5 g of dry ice in a side arm flask and covering the top with a rubber bung. Rubber tubing was used to connect the side arm of the flask and a syringe and needle. The needle was submerged in the solutions requiring CO_2, allowing the gas to bubble through the solution. The bung was regularly removed to release any build-up of pressure.

Hydrogen sulfide was produced by slowly dropping dilute hydrochloric acid onto iron (II) sulfide. This was done using a dropping funnel full of HCl and side arm flask containing ca. 0.5 g of FeS. Rubber tubing was used to connect the side arm of the flask and a syringe and needle. The needle was submerged in the solutions requiring H_2S, allowing the gas to bubble through the solution. The bung was regularly removed to release any build-up of pressure. All equipment was thoroughly cleaned with bleach before removal from the fume cupboard.

5.3.2 Crystallisations

0.1 g of hydroquinone was dissolved in 0.5 cm^3 of hot water. The sample was stoppered with Suba seals which were pierced with an exit needle and the needle from the CO_2 generator. The needle from the CO_2 generator was submerged in the solution and CO_2 was bubbled through the solutions 1 min. The exit needle was then removed, followed by the needle from the CO_2 generator. The sample was left in a Dewar filled with boiling water for three days. Large, needle shaped crystals were formed and analysed by single crystal x-ray crystallography.

Single crystal crystallographic analysis was performed on a Bruker Photon D8 Venture diffractometer (ImuS microsource, λMoKα, λ = 0.71073 Å) equipped with a Cryostream (Oxford Cryosystems) open-flow nitrogen cryostat, at 120 K. The data collection and refinement was kindly carried out by Dr Dmitry S. Yufit.

Hydroquinone/CO₂ crystal data: Empirical formula $C_6H_6O_2$, 1/12 CO_2, space group *R-3*, *a* = 16.4400(14) Å, *b* = 16.440(14) Å, *c* = 5.4822(5) Å, *α* = 90.00°, *β* = 90.00°, *γ* = 120.00°, volume = 1283.18(19) Å^3, Z = 9, F(000) = 538.0, MoKα (λ = 0.71073) 2θ range for data collection = 4.96 – 0.1320°, data = 901, parameters = 52, goodness-of-fit on F^2 = 1.079, R$_1$ = 0.0583, wR$_2$ = 0.1320

Compounds **6**-**9** and **11** were dissolved in 0.5 mL of acetone, ethanol, methanol propan-1-ol, propan-2-ol, acetonitrile and 90 % ethanol in water. Details of compounds weight and solvent can be found in Table 5.2. The samples were stoppered with Suba seals which were pierced with an exit needle and the needle from the CO_2 generator. The needle from the CO_2 generator was submerged in the solution and CO_2 was bubbled through the solutions 1 min. The exit needle was then removed, followed by the needle from the CO_2 generator. All were placed in the freezer -20 °C and checked for crystals on a monthly basis over the course of 36 months.

Dimer	Dimer / g	Solvent
bisVCap	0.16	ethanol
	0.15	methanol
	0.14	acetone
	0.15	90% ethanol in water
	0.15	propan-2-ol
	0.15	propan-1-ol
	0.15	acetonitrile
H₂bisVCap	0.34	ethanol
	0.33	methanol
	0.37	acetone
	0.33	90% ethanol in water
	0.35	propan-2-ol
	0.31	propan-1-ol
	0.37	acetonitrile
bisVP	0.41	ethanol
	0.36	methanol
	0.37	acetone
	0.37	90% ethanol in water
	0.42	propan-2-ol
	0.45	propan-1-ol
	0.44	acetonitrile
H₂bisVP	0.43	ethanol
	0.38	methanol
	0.37	acetone
	0.38	90% ethanol in water
	0.35	propan-2-ol
	0.43	propan-1-ol

	0.44	acetonitrile
bisHep	0.13	methanol
	0.12	ethanol
	0.11	acetone
	0.12	90% ethanol in water
	0.11	propan-2-ol
	0.12	propan-1-ol
	0.18	acetonitrile

Table 5.2 – Composition of CO_2 containing crystallisation attempts.

Compounds **6**-**9** and **11** were dissolved in 0.5 mL of acetone, ethanol, methanol propan-1-ol, propan-2-ol, acetonitrile and 90 % ethanol in water. Details of compounds weight and solvent can be found in Table 5.3. The samples were stoppered with Suba seals which were pierced with an exit needle and the needle from the H_2S generator. The needle from the H_2S generator was submerged in the solution and H_2S was bubbled through the solutions 1 min. The exit needle was then removed, followed by the needle from the H_2S generator. All were placed in the freezer -20 °C and checked for crystals on a monthly basis over the course of 36 months.

Dimer	Dimer / g	Solvent
bisVCap	0.19	ethanol
	0.17	methanol
	0.15	acetone
	0.16	90% ethanol in water
	0.15	propan-2-ol
	0.16	propan-1-ol
	0.13	acetonitrile
H_2bisVCap	0.36	ethanol
	0.34	methanol
	0.35	acetone
	0.38	90% ethanol in water
	0.33	propan-2-ol
	0.31	propan-1-ol
	0.31	acetonitrile
bisVP	0.45	ethanol
	0.57	methanol
	0.68	acetone
	0.34	90% ethanol in water
	0.37	propan-2-ol
	0.53	propan-1-ol
	0.32	acetonitrile
H_2bisVCap	0.32	ethanol
	0.32	methanol
	0.35	acetone
	0.34	90% ethanol in water

	0.37	propan-2-ol
	0.41	propan-1-ol
	0.37	acetonitrile
bisHep	0.11	methanol
	0.11	ethanol
	0.13	acetone
	0.10	90% ethanol in water
	0.15	propan-2-ol
	0.17	propan-1-ol
	0.14	acetonitrile

Table 5.3 - Composition of H₂S containing crystallisation attempts.

5.3.3 IR studies

Experiments were performed on a Perkin Elmer FTIR spectrum 100 using a liquid IR cell with CaF_2 windows and a 0.05 mm spacer. Data were recorded at a resolution of 1 cm^{-1} for 16 runs over the range 2800 – 1400 cm^{-1}. Spectral analysis was performed using Spekwin32.[24] Two batches of sour acetonitrile were made, one by bubbling CO_2 through the solvent, the other by bubbling H_2S through the solvent. The acid gases were made as described in section 5.3.1.

IR titrations with H_2S, CO_2 and without sour gas, were performed for compounds **1**, **3**, **5**-**9** and **11**. 0.01 g of compound was dissolved in 1 cm^3 of acetonitrile. For compounds **6**-**10** water was added at 0, 10, 20, 40, 60, 80, 100, 150, 200, 250, 300, 350, 400, 450 and 500 equivalents of D_2O and spectra were recorded after each addition. For **1**, **3** and **5** water was added at 0, 5, 10, 20, 30, 40, 50, 75, 100, 125, 150, 175, 200, 225 and 250 equivalents of D_2O per carbonyl group and spectra were recorded after each addition.

For the sour titrations 0.01 g of **1**, **3**, **5**-**9** and **11** were dissolved in 1 cm^3 of acetonitrile. H_2S or CO_2 were bubbled through the solution for 1 min before the first spectrum was recorded. For compounds **6**-**9** and **11** water was added at 0, 10, 20, 40, 60, 80, 100, 150, 200, 250, 300, 350, 400, 450 and 500 equivalents of D_2O and spectra were recorded after each addition. For **1**, **3** and **5** water was added at 0, 5, 10, 20, 30, 40, 50, 75, 100, 125, 150, 175, 200, 225 and 250 equivalents of D_2O per carbonyl group and spectra were recorded after each addition. After every 5 spectra the acid gas was again bubbled through the solution.

5.3.4 NMR study

NMR spectra were recorded on a Varian-Mercury spectrometer, operating at 400 MHz, chemical shifts are reported in ppm (δ) relative to residual solvent.

0.006 g of bisVCap was dissolved in 0.75 cm^3 of deuterated acetonitrile. D_2O was titrated directly into the NMR tube and the tube was inverted to ensure mixing of the D_2O. Spectra

were recorded at 0, 10, 20, 40, 60, 80, 100, 150, 200, 250, 300, 350, 400, 450 and 500 equivalents of D_2O.

0.006 g of bisVCap was dissolved in 0.75 cm^3 of deuterated acetonitrile. CO_2 was bubbled through the solution for 1 min before the first spectrum was recorded and after every 3 spectra. D_2O was titrated directly into the NMR tube and the tube was inverted to ensure mixing of the D_2O. Spectra were recorded at 0, 10, 20, 40, 60, 80, 100, 150, 200, 250, 300, 350, 400, 450 and 500 equivalents of D_2O.

0.006 g of bisVCap was dissolved in 0.75 cm^3 of deuterated acetonitrile. D_2O was titrated directly into the NMR tube and the tube was inverted to ensure mixing of the D_2O. H_2S was bubbled through the solution for 1 min. A fresh sample of 0.006 g bisVCap in 0.75 cm^3 of deuterated acetonitrile with H_2S bubbled through was prepared after ever 3 spectra. Spectra were recorded at 0, 10, 20, 40, 60, 80, 100, 150, 200, 250, 300, 350, 400, 450 and 500 equivalents of D_2O.

5.4   References

(1)   Amosa, M. K.; Mohammed, I. A.; Yaro, S. A. *Naft. Sci. J.* **2010**, *61* (2), 85–92.

(2)   Tusiani, M. D.; Shearer, G. *LNG : A Nontechnical Guide*; PennWell Books: Tulsa, 2007.

(3)   Goodwin, M. J.; Musa, O. M.; Steed, J. W. *Energy Fuels* **2015**, *29* (8), 4667–4682.

(4)   Li, L.; Jiang, Z.; Chen, Y.; Xiao, F. *J. Chem. Pharm. Res.* **2014**, *6* (4), 288–293.

(5)   Sloan, E. D.; Koh, C. *Clathrate Hydrates of Natural Gases*, Third Edit.; CRC Press, 2007.

(6)   Thieu, V.; Frostman, L. M. In *SPE International Symposium on Oilfield Chemistry*; 2005.

(7)   Beauchamp Jr, R. O.; Bus, J. S.; Popp, J. A.; Boreiko, C. J.; Andjelkovich, Dragana, A. *Crit. Rev. Toxicol.* **1984**, *13* (1), 25–97.

(8)   Carroll, J. J. In *Annual GPA Convention*; 2002.

(9)   Alavi, S.; Udachin, K.; Ripmeester, J. A. *Chem. Eur. J.* **2010**, *16* (3), 1017–1025.

(10)   Chazallon, B.; Focsa, C.; Charlou, J.-L.; Bourry, C.; Donval, J.-P. *Chem. Geol.* **2007**, *244* (1–2), 175–185.

(11)   Clarke, M. A.; Bishnoi, P. R. *Chem. Eng. Sci.* **2005**, *60* (3), 695–709.

(12)   Dartois, E.; Duret, P.; Marboeuf, U.; Schmitt, B. *Icarus* **2012**, *220* (2), 427–434.

(13)   Noaker, L. J.; Katz, Donald, L. *J. Pet. Technol.* **1954**, *6* (9), 135–137.

(14)   Ukegawa, H.; Matsuo, T.; Suga, H. *J. Incl. Phenom.* **1985**, *3*, 261–267.

(15)   Mak, T. C. W.; Tse, J. S.; Tse, C.; Lee, K.; Chong, Y. *J. Chem. Soc., Perkin Trans. 2* **1976**, 1959–1962.

(16)   Falk, M.; Miller, A. G. *Vib. Spectrosc.* **1992**, *4*, 105–108.

(17)   Martin, P. E.; Barker, E. F. *Phys. Rev.* **1932**, *41*, 291–303.

(18)   Davenport, J. R.; Musa, O. M.; Paterson, M. J.; Piepenbrock, M.-O. M.; Fucke, K.; Steed, J. W. *Chem. Commun.* **2011**, *47* (35), 9891–9893.

(19)   Perrin, A. The chemistry of low dosage clathrate hydrate inhibitors, University of Durham, 2015.

(20)   Spěváček, J.; Dybal, J.; Starovoytova, L.; Zhigunov, A.; Sedláková, Z. *Soft Matter* **2012**, *8* (22), 6110–6119.

(21)   Mohammadi, A. H.; Richon, D. *J. Chem. Thermodyn.* **2012**, *48*, 36–38.

(22)   Mohammadi, A. H.; Richon, D. *J. Chem. Eng. Data* **2010**, *55* (1), 566–569.

(23)   Perrin, A.; Musa, O. M.; Steed, J. W. *Chem. Soc. Rev.* **2013**, *42* (5), 1996–2015.

(24)   Menges, F. http://www.effemm2.de/spekwin: Berchetesgarden 2016.

6 Neutron study of PVCap and butoxyethanol

6.1 Introduction

Neutron scattering is a technique comparable to x-ray diffraction. Samples diffract either the x-rays or neutrons and structural information about the system can be obtained from the diffraction pattern.[1] Often x-ray diffraction will be chosen over neutron diffraction as x-rays have higher flux and are scattered more strongly since neutrons must hit the nucleus of the atom to be diffracted. Moreover x-ray diffraction instrumentation is readily available in the home laboratory setting. The amount by which x-rays are diffracted is related to the number of electrons of the atom which it hits and hence the atomic number; the higher the atomic number of the atom, the stronger the diffraction. This means light atoms, such as hydrogen, diffract very weakly and are subject to systematic errors, making analysis requiring hydrogen atoms more difficult. In contrast, the amount which neutrons are diffracted is not dependant on the mass of that atom. As can be seen in Figure 6.1, the ability to diffract neutrons has no correlation with atomic mass. Hydrogen and deuterium in particular, have greatly different coherent scattering lengths, hydrogen's being negative, -3.74 fm, whilst deuterium's positive, 6.67 fm.[2] This allows analysis of high hydrogen systems, by using isotopic substitution of hydrogen and deuterium to change the level of contrast and collect multiple datasets of the same chemical composition. So whilst less convenient than x-ray diffraction, high hydrogen systems, such as studying water, are much more readily studied by neutron diffraction.
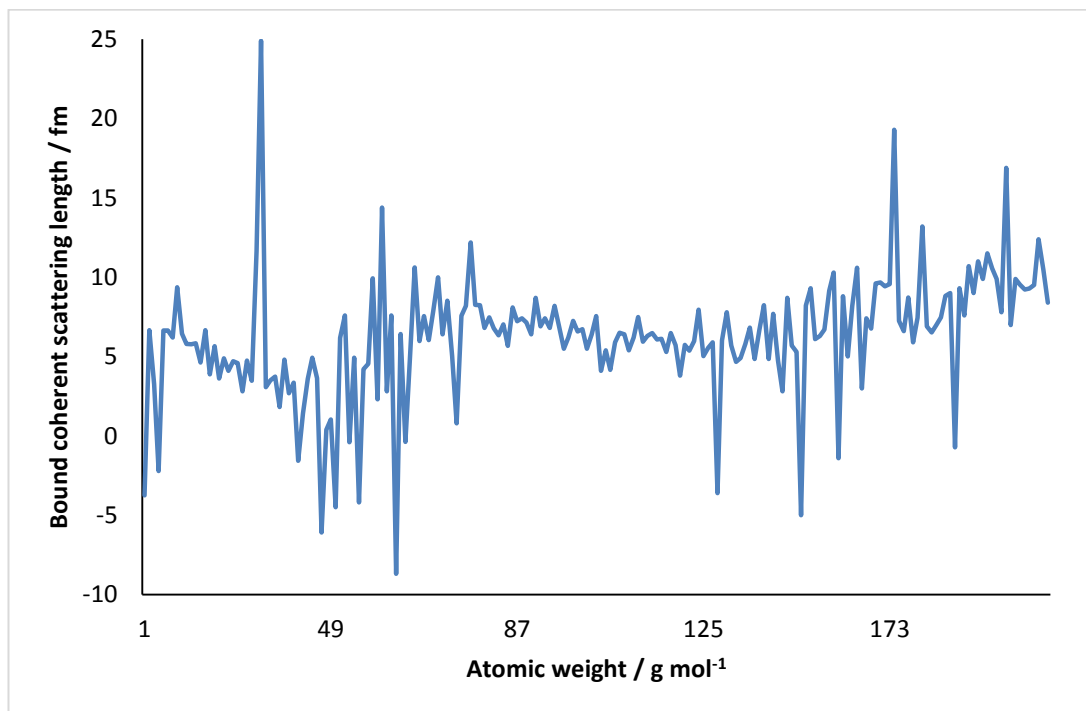
Figure 6.1 – Coherent scattering of atoms sorted by their molecular mass. Plotted from the data of Sears.[2]

In a single crystal, a motif is repeated infinitely in all directions which allows for a definitive structure to be determined. Defects and disorder in a crystal complicate this process, but the order and regularity in the crystal make it possible to solve the structure. By definition disordered systems do not have the three dimensional order present in crystals, being either amorphous solids or fluids. As there is no order in any direction and as fluid systems are dynamic and so constantly changing, no exact structure determination can be achieved. Instead an average, statistical overview of the system can be produced, giving information on the average nearest neighbours and whether any long range order is present.[3] This is done by creating a model of the system then refining it against the experimental data. This process is often done using modified Monte Carlo based simulations,[4] though use of molecular dynamic has also been explored.[5] Once the modelled data fits the experimental data as precisely as possible, the model can be analysed to extract information about the system. One such useful plot is the g(r) plot. The g(r) plot shows variations in atomic density at a distance r from an atom, giving information on the nearest neighbours in the system as well as any longer range structure which may exist. For example, g(r) plots have shown the average length of the hydrogen bond between methanol and water,[6] the differences in intermolecular interactions in different densities of water upon increasing the pressure,[7,8] interactions between the ions in ionic liquids[9,10] and how much liquid-like behaviour supercritical materials exhibit.[11]

Whilst statistically significant conclusions can be draw from the neutron scattering of disordered systems the dynamic nature of the system can make accurate interpretation difficult. For example 2-butoxyethanol in water has previously been the focus of a collection of small angle neutron studies by D'Arrigo et al.[12–14] which resulted in different conclusions from analysing the same system. D'Arrigo et al. used a non-linear least-squares fit between the simulated and experimental data. For the calculated data they assume that any formed micelles would be spherical and that not all of the butoxyethanol would be involved in micelle formation. They then calculated how the SANS data would look for different sizes of micelle and compared this data to the data from the SANS experiment, adjusting the size of the micelles and amount of free butoxyethanol until the calculated and experimental data were as close to the same as possible. In all their analyses an acceptable goodness-of-fit was achieved. In their earlier papers it was concluded that butoxyethanol does form micelles, with a radius corresponding to the length of the butoxyethanol 17 Å.[13] The number of micelles were at a maximum around 40 °C, but formed as low as 4 °C.[13] In a later paper, D'Arrigo et al. state that they do not believe that butoxyethanol forms true micelles but 'fluctuating micelle-like molecular groupings'.[14] This shows that similar analyses of the same system do not necessarily give the same results as simulations are not guaranteed to give the same result twice and the continuously fluctuating nature of liquid samples makes finding a single, definite answer much more challenging than solid systems.

6.2 Results and discussion

Previous work in the group[15] used neutron diffraction to look at the interactions of bisVCap with water in an attempt to glean insight into KHI's hydration behaviour in solution. To further this study it was proposed that neutron diffraction experiments could offer information about the synergistic effect that butoxyethanol has on PVCap. Butoxyethanol is a weak anti-agglomerant hydrate inhibitor but when added to a pipeline with PVCap the resulting hydrate inhibition is greater than the sum of hydrate inhibition of butoxyethanol and PVCap alone.[16] Two systems were studied: the control system of butoxyethanol/water and butoxyethanol/water/PVCap. PVCap is sold for pipeline applications in a 50 wt% solution in butoxyethanol so PVCap was added in a 1:1 weight ratio to butoxyethanol to maximise the industrial relevance.

KHIs are added to a pipeline at typically 0.01-5 wt%.[17] Whilst a higher concentration of butoxyethanol and PVCap is further from industrial relevance, it is necessary for neutron diffraction experiments as lower concentrations will make the data impossible to distinguish from pure water, especially as neutron diffraction is very highly sensitive to hydrogen so

water diffracts strongly. Butoxyethanol was added in 5 mol% to water, which is the highest concentration which allows both the butoxyethanol and PVCap to fully dissolve at 6 °C. This temperature was chosen to try and avoid micelle formation of butoxyethanol[12–14] and aid dissolution of larger amounts of PVCap. PVCap is Flory-Huggins type I polymer[18] leading it to precipitate out of solution at higher temperatures due to the entropy gain in freeing up ordered water molecules along the length of the polymer chain. In the system studied this resulted in the amount of polymer used is not being fully soluble at room temperature and cooling below 3 °C also resulted in a large enough decrease in solubility to also cause precipitation. This leaves a relatively small temperature window, 3-10 °C, in which the polymer remains in solution and 6 °C falls in the middle of this temperature range.

Experiments were run on NIMROD (Near and InterMediate Range Order Diffractometer) at the ISIS neutron source with Dr Sam Callear as the local contact. NIMROD is a wide angle neutron diffractometer which records data from low to high Q. A wide Q range gives information on local environment of a molecule as well as any long range order which may occur. Because of its ability to go to a 2θ angle as low as 0.5°, NIMROD is classed as small angle neutron scattering (SANS) instrument.[19] It is important to have as many data sets to fit the simulation to as possible to get a more accurate simulation possible. To do this a range of chemically same but isotopically different composition were used. As the systems studied were in water, three isotopic versions of water were used, H_2O, D_2O and HDO. Whilst deuterating the polymer is not possible, it was possible to purchase 2-butoxythanol-1,1,2,2-d_4 from QMX Laboratories Ltd. This gave a total of six different combinations of deuterated and non-deuterated water and butoxyethanol, all of which were used for the butoxyethanol/water experiments as detailed in Table 6.1. Only four combinations of deuterated water and butoxyethanol were used for the butoxyethanol/water/PVCap experiments due to limited beam time at the neutron source.

Water	Butoxyethanol	PVCap
H_2O	H	-
HDO	H	-
D_2O	H	-
H_2O	D	-
HDO	D	-
D_2O	D	-
H_2O	H	yes
D_2O	H	yes
HDO	D	yes
D_2O	D	yes

Table 6.1 – Composition of the NIMROD experiments performed. Where D means 2-butoxythanol-1,1,2,2-d₄ was used and H means that fully protic butoxyethanol was used.

6.2.1　The simulation process

Whilst the large difference in scattering lengths between hydrogen and deuterium makes neutron scattering ideal to study organic systems, the inelastic scattering of hydrogen adds a level of complexity.[20] Most elements have small or no inelastic scattering, neutrons hit the sample with a certain amount of energy and exit the sample with the same amount of energy. Hydrogen on the other hand has a high degree of inelastic scattering, meaning that many neutrons which are diffracted by hydrogen either gain or lose energy.[21] This changes the recorded diffraction pattern and is especially troublesome in the low Q region where the inelastic scattering causes a significant increase in f(Q) which obscures the elastic scattering at low Q. Thus for meaningful analysis of the data to be performed, the inelastic scattering from hydrogen must be removed. The inelastic scattering from hydrogen was removed using Gudrun.[22] The program uses the composition of the sample, input by the user, to calculate the amount of inelastic scattering which should occur and then subtract the calculated inelastic scattering from the raw data. This is an iterative process that is repeated until there is no change in the output data. A majority of parameters are instrument specific and supplied by the Gudrun program itself. Iterations of inelastic scattering removal were carried out one at a time until there was not visible change in the output data. This adjusted data was then used to refine a model of the system.

The models of the systems were created using Empirical Potential Structure Refinement (EPSR).[23,24] Models for the molecules in a system are created and the structure minimised using Jmol,[25] creating .ato files. The .ato files contain the information on the atoms types and

bonding of the molecule, including partial charges, which bonds are capable of rotation, bond lengths and the positions of a low energy starting conformation. The starting partial charges for the atoms in a molecule are either generated by a program such as MOPAC[26] or, in the case of the simulations in study, input by hand from the work of Jorgensen *et al.*[27] on conformation energetics of organic liquids. The partial charges are refined during the iterative process of the simulation, so the exact starting value is only important in as far as avoid local energy minima and minimising the time required for the system to equilibrate. The molecules are then put in a box in the correct ratio for the sample being analysed using the mixato function in EPSR to create a .ato file for the box. The size of the box depends on the desired number of molecules and the density, EPSR creates a box which gives the correct density with the number of molecules provided. Initially all the molecules are stacked on top of one another in the centre of the box, the molecules are then randomised, moved at random to somewhere in the box. A function called fmole is then used to 'shake' the box, reducing the number of molecules which are still occupying the same space.

EPSR uses a Monte Carlo based simulation, where atoms are moved a random distance in a random direction. If the random move increases the energy of the system too greatly, the move is rejected, if only a small increase or a decrease in energy is seen, then the move is accepted.[28] Unlike a purely computational simulation, EPSR has experimental data to compare to. The diffraction pattern which would be expected from the model is calculated by ESPR and then compared to the experimental diffraction pattern and a goodness-of-fit is calculated. As well as measuring the energy of the model and aiming for the lowest energy possible, as is done in a standard Monte Carlo simulation, there is also a measure of how well the model fits the experimental data. This gives further information on if the model is a reasonable representation of reality, as in a pure simulation the chemical intuition of the user is relied on, with no experimental data to verify correctness of the model. The more different isotopic substitutions which were recorded, the more data there is to refine to, resulting in a more accurate model.

After a few hundred iterations of the Monte Carlo method, the model reaches a stable goodness-of-fit and a stable energy level. When the model is stable, the ereq, the energy which the system has, can be raised. This inputs energy into the system, allowing the molecules to move more and fit better to the experimental data. Older versions of EPSR, such as EPSR24, required the ereq to be input by the user, though the most recent version of EPSR, EPSR25, increases the ereq automatically, stopping the increase when no further

improvement of the goodness-of-fit and energy can be gained. Both EPSR24 and EPSR25 were tested in this study.

After the energy level of the simulated data is stable and the goodness-of-fit shows no further improvement, the data is then accumulated into an append.xyz file. The append.xyz file records the position of every atom in the box for each iteration of the simulation. A minimum file size of 3 GB is required for the simulation to be of statistical significance, resulting in data from thousands of iterations. The next step is to create a .HISU file from the append.xyz file using the xyz2hisu function of the dputils package from Project Aten.[29] The .HISU file gives the average positions from all of the iterations recorded. The dputils tool, pdens, can then be used to make this .HISU file into data readable by the Aten program which can used to graphically represent the data. The pdens tool creates two files, a .avg which is the average position of the molecule chosen to be the centre of the analysis and a .pdens file which gives information on the density of surrounding molecules of a chosen type. The .avg file requires three atoms to be picked as the axis of the model. The numbering of the atoms are determined upon the creation of the molecule in Jmol and are found in the .ato file for the molecule, the numbering for butoxyethanol in the simulations are shown in Figure 6.2. The chosen axis atoms are the centre of the analysis. Using butoxyethanol in water as an example, atoms 18, 21 and 22, as labelled in Figure 6.2 were chosen as the axis atoms. The resulting .avg file can be plot to give Figure 6.3a. The three axis atoms remain still at the centre of the model, whilst the rest of the butoxyethanol molecule is free to change conformation. The multiple conformations over thousands of iterations are all plot simultaneously. The reference atoms in every iteration are perfectly superimposed and the rest of the chain is the superimposition of every conformation which occurred in the simulation.
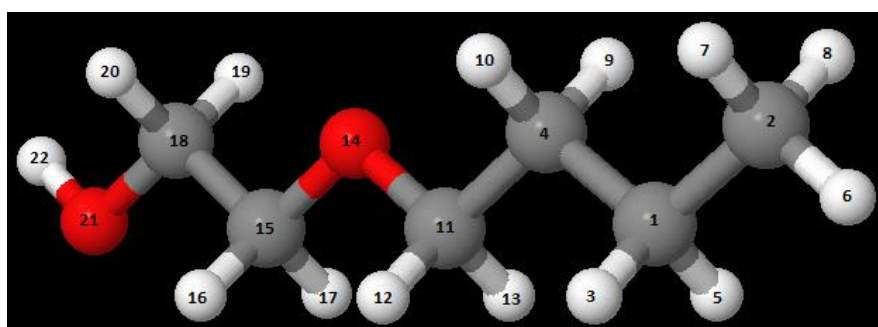
Figure 6.2 – Numbering of the butoxyethanol atom file.

To form a .pdens file, a second molecule type must be chosen. Still using the butoxyethanol/water system as an example, either butoxyethanol or water can be chosen as the second molecule depending on which interactions are of interest to visualise. For this

example water was chosen. As butoxyethanol was chosen as the central molecule and water was chosen as the interacting molecule, this will give information on the water surrounding butoxyethanol. The .pdens file is plot as translucent blue regions, representing the density of the chosen molecule surrounding the axis atoms. The pdens plot of water surrounding butoxyethanol is shown in Figure 6.3b. As the whole box is filled with water the .pdens would appear as a translucent cube if the data did not cut off at a certain density. The cut off parameters in Aten are in terms of density and can be adjusted to show hydration spheres arising from a higher density of water surrounding the hydrophilic parts of a molecule.
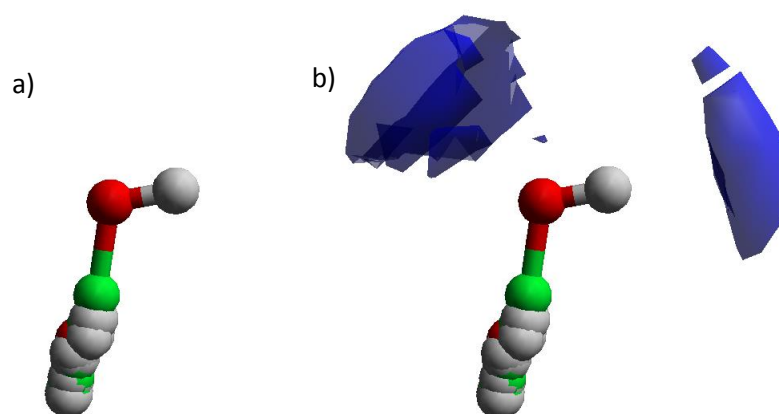
Figure 6.3 – a) Visualisation of the .avg file of butoxyethanol, showing the alcohol taken as the axis and the range of positions of the rest of the molecule, b) visualisation of the .avg file of butoxyethanol with the .pdens file containing information on density of the surrounding water plot as areas of translucent blue.

6.2.2   Model of butoxyethanol/water

The model of water was created and minimised using Jmol.[25] The model of butoxyethanol was created and minimised using Jmol and given full freedom to rotate around every bond. The model consists of a cubic box with side measuring 34.96 Å on each side filled with 1045 water molecules and 55 butoxyethanol molecules with a density of 0.102 atoms Å^{-3}. The model can be seen in Figure 6.4.
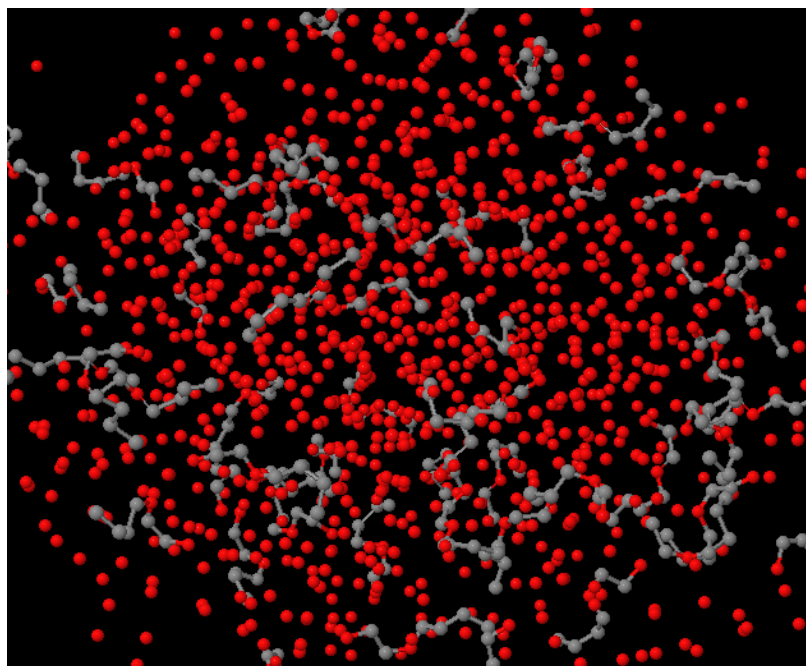
Figure 6.4 – Simulation box for the butoxyethanol/water simulation with hydrogen atoms omitted for clarity.

Both EPSR24 and EPSR25 were used to refine the data in two separate simulations. In EPSR24 the ereq is input by hand and in EPSR25 the ereq is adjusted automatically. Both versions gave acceptable energy, -37 kJ mol^{-1} for both simulations and an acceptable goodness-of-fit, R = 0.1 for both simulations. The output data from EPSR25 gave very noisy data for the partial atomic distribution functions, g(r) plot, whilst EPSR24 gives smooth curves, as shown in Figure 6.5. Noisy partial distributions are usually a result of the simulation not being given long enough to equilibrate. Even after two weeks more run time, the EPSR25 data does not become any less noisy. This seems to be an issue with this version of EPSR, which at the time of writing is still in the beta testing phase. Further analysis of the butoxyethanol/water system was performed on the smoother data created by EPSR24.
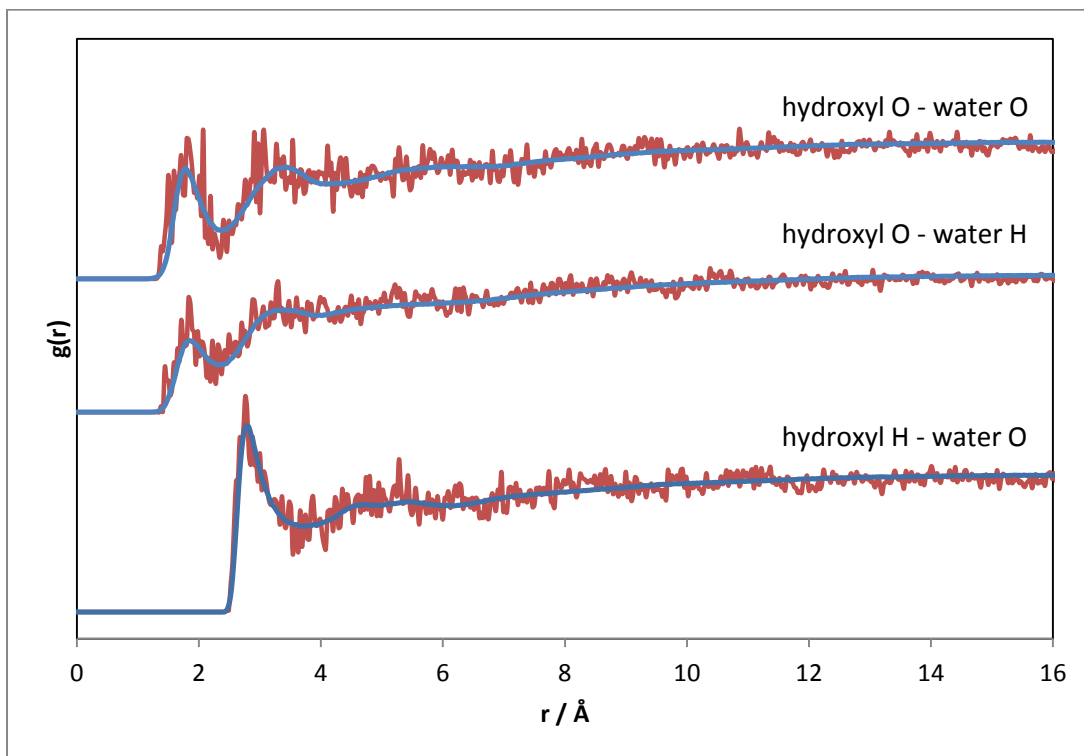
Figure 6.5 – Partial interactions of the hydrogen of the hydroxyl group of butoxyethanol with water and the oxygen of the hydroxyl group of butoxyethanol with water. Data refined using EPSR24 is shown in blue, data refined by EPSR25 is shown in red.

After the point at which increasing the ereq no longer improves the goodness-of-fit or the energy of the simulation and both remained stable, the fit of the simulation to the experimental data was acceptable. Comparison of the experimental data and simulated data are shown in Figure 6.6. Only four data sets are shown to allow for direct comparison to the butoxyethanol/water/PVCap data. At low Q, Figure 6.6a, the peaks around 2.5 $Å^{-1}$ in the H_2O H-butoxyethanol and HDO H-butoxyethanol data are shifted higher in the simulation than the experimental data. The D_2O D-butoxyethanol simulation also fails to exhibit the ripples in the experimental data. The problems in the low Q data arise from the beginnings of agglomeration.[30,31] Whilst the temperature was chosen to minimise the chances of micelle formation, the sample was also made to be as concentrated as possible, which favours butoxyethanol forming micelles. EPSR is not designed to study micelle formation, so a better fit of the low Q data is not possible with this program. As the real space data, Figure 6.6b, has been fitted well and the low Q data is not completely unreasonable, this simulation has been taken as the best model for the system which can be made with the current technology.
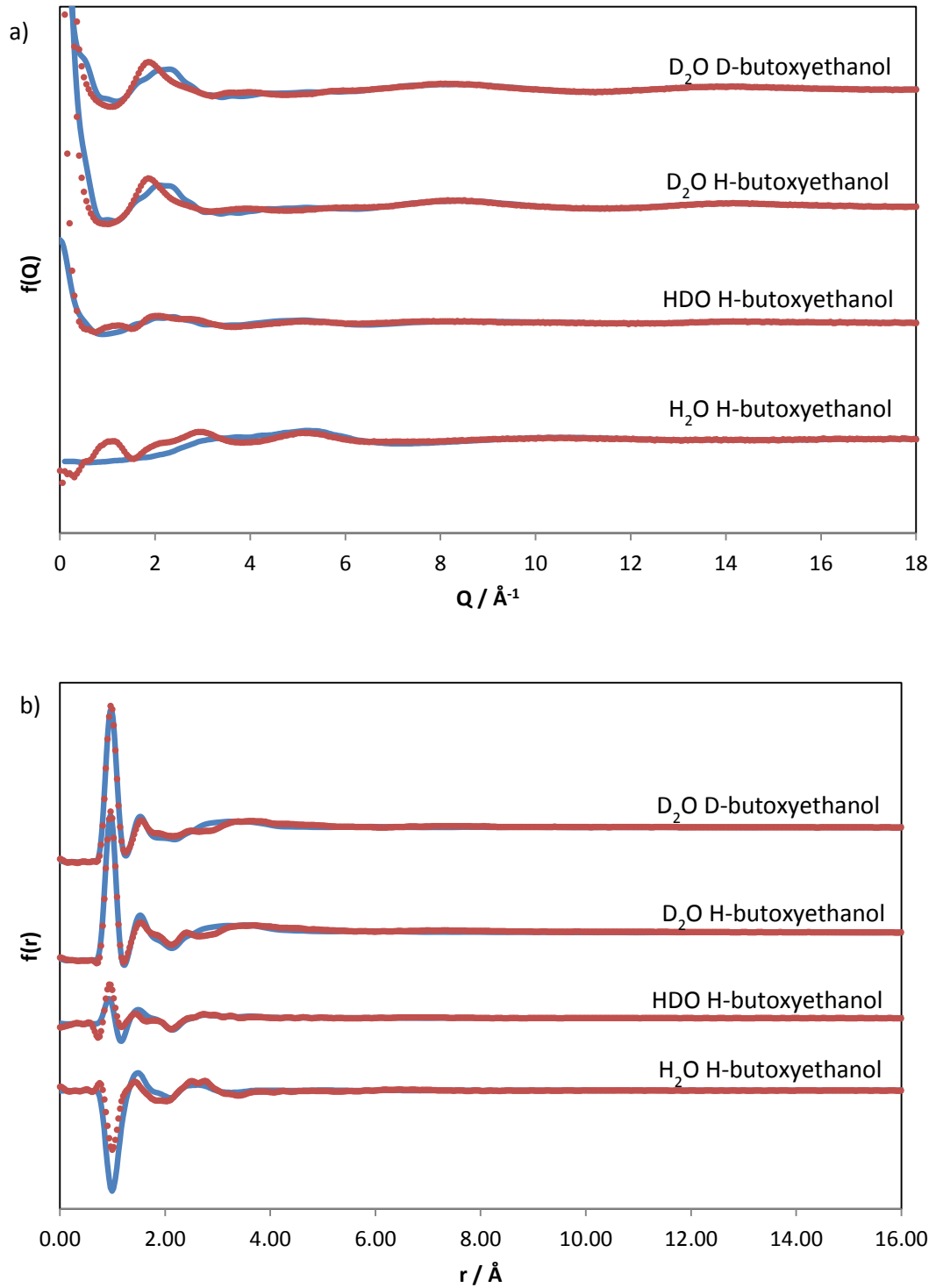
Figure 6.6 – Quality of fit for the EPSR simulation of butoxyethanol/water shown in a) reciprocal space and b) real space. The experimental data are shown by dotted red lines whilst the simulated data are shown by solid blue lines.

Figure 6.7 shows the .avg and .pdens analyses of the butoxyethanol/water data. In Figure 6.7a the centre of the analysis is the hydroxyl group of the butoxyethanol, atoms 18, 21 and 22. Two hydration spheres can be seen, a larger partial ellipsoid around the oxygen side of the hydroxyl group and a smaller partial ellipsoid around the hydrogen side. This shows the hydrogen bonding nature of the alcohol group, resulting in a higher density of water around the hydrogen bond donating and hydrogen bond accepting sides of the hydroxyl group. In Figure 6.7b the ether group of the butoxyethanol is taken as the centre of the model, atoms 11, 14 and 15. By the time the density cut offs have been expanded far enough to see a hydration sphere around the oxygen of the ether, the hydration sphere around the hydroxyl group is already visible. This shows that the ether group in butoxyethanol is much less efficient than the alcohol group at ordering the surrounding water molecules. This is because the ether group is much less polar and less capable of hydrogen bonding.
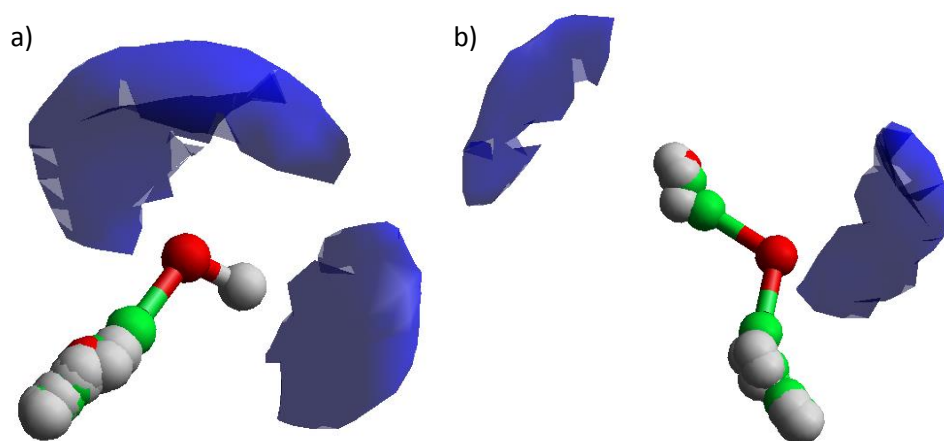
Figure 6.7 – Hydration sphere around butoxyethanol in the butoxyethanol/water simulation plotted using Aten with the axis set as a) the hydroxyl group, atoms 18, 21 and 22 and b) the ether group, atoms 11, 14 and 15.

Whilst the low Q data was not fit perfectly using EPSR, the EPSR model of butoxyethanol in water resulted in a graphic representation of the hydration of butoxyethanol which makes chemical sense. The hydroxyl group is proven to be more hydrophilic that the ether group as would be expected and smooth hydration spheres were created similar to previous work on methanol.[6]

6.2.3   Model of butoxyethanol/water/PVCap

The butoxyethanol and water molecules from the butoxyethanol/water simulation were used for the simulation of the butoxyethanol/water/PVCap system and a model of PVCap was created using Jmol. As Jmol cannot minimise a structure as large as PVCap, a monomer unit was made, minimised and attached to 21 other monomer units. Capping methyl groups were added to the ends of the polymer. This gave a polymer with a molecular weight of 3082

Da which is within the molecular weight range of the sample of PVCap used as specified by the supplier. The model of PVCap was given freedom to rotate along the backbone and the side groups were able to rotate. Rotations in the rings were not included. The fused nature of the rings and the Monte Carlo system used by EPSR would result in a large majority of moves being rejected, leading to almost no movement whilst greatly increasing the computational cost of the simulation.

A cubic box filled with 1045 water molecules and 55 butoxyethanol molecules and 2 PVCap molecules was created. The sides of the box are 37.02 Å and the simulation has a density of 0.106 atoms Å^{-3}. The model can be seen in Figure 6.8. A larger box, containing more than two polymer atoms, would be more statistically significant but the initial untangling of the polymer chains was not possible when more than two polymer chains were present, leaving two as the maximum number of polymer chains which could be simulated.
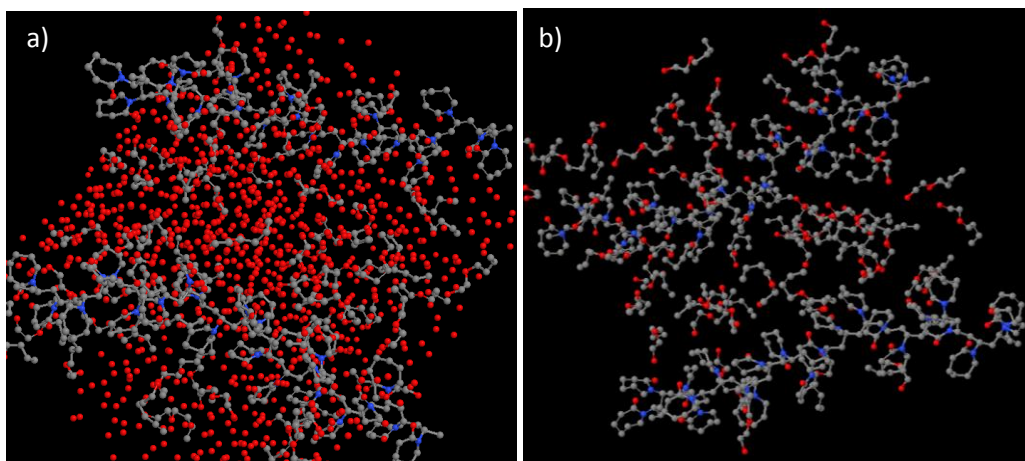
Figure 6.8 - Simulation box for the butoxyethanol/water/PVCap simulation, a) with hydrogen atoms omitted for clarity, b) with hydrogen atoms and water molecules omitted for clarity.

Using EPSR24 where the ereq was increased by hand there was an issue that as the goodness-of-fit improved, the energy of the system would increase massively, typically the energy increased to a value greater than 500 kJ mol^{-1}, for comparison the butoxyethanol/water data had an energy value of -37 kJ mol^{-1}. This is possibly due to the beginnings of phase separation of the system at higher ereq. Attempts to apply restrictions on the distance between water atoms based on previous data gathered on water[24] to allow a lower increase in ereq did not solve the problem as it did not reduce the required ereq. The automated ereq increase in EPSR25 successfully achieved an acceptable goodness-of-fit, R = 0.02, without the energy increasing an unreasonable amount, the energy of the system equilibrated at -40 kJ mol^{-1}. During the accumulation of the append.xyz file the energy does start to increase, but does not reach into the positive and the fit of the simulation to the experimental data is acceptable

as seen in Figure 6.9. Similarly to what was seen in for the butoxyethanol/water partial distribution data from EPR25 in Figure 6.5, the partial distribution data of butoxyethanol/water/PVCap is noisy. As a reasonable fit and energy level has not been possible with EPSR24, the EPSR25 data was used, even though the partial distribution data is not as clean as would be preferable.

The simulated low Q data in Figure 6.9a is much closer to the experimental data than it was for the butoxyethanol/water simulation. The peak around 2.5 $Å^{-1}$ in the H_2O H-butoxyethanol and HDO H-butoxyethanol data are still shifted slightly higher in the simulation than the experimental data, but by much less than the butoxyethanol/water simulation. The D_2O D-butoxyethanol simulation shows fewer peaks than the experimental data, but does exhibit some ripples which is closer to the experimental data than the butoxyethanol/water simulation. In the real space data in Figure 6.9b the peaks at 1 Å in the simulated data are not exactly the same, with variances in intensity unlike the butoxyethanol/water simulation where the simulated data matched the experimental data very well. Ever though the low r data of the butoxyethanol/water/PVCap data seems less well fit than the butoxyethanol/water data, all over, the fit looks slightly better than that of the butoxyethanol/water simulation which is reflected in the lower R value.

a)

b)
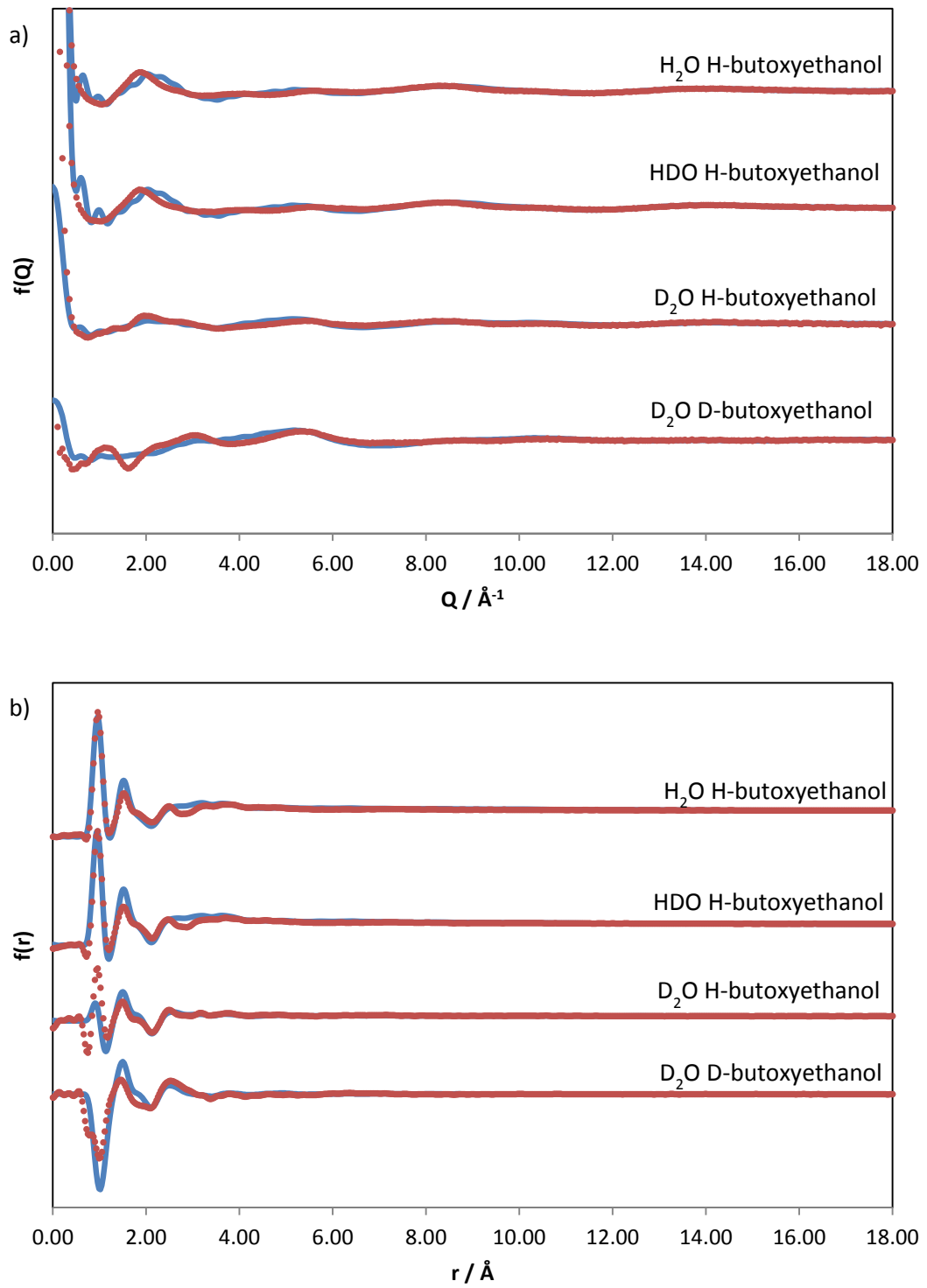
Figure 6.9 - Quality of fit for the EPSR simulation of butoxyethanol/water/PVCap shown in a) reciprocal space and b) real space. The experimental data are shown by dotted red lines whilst the simulated data are shown by solid blue lines.

To allow comparison to the butoxyethanol/water simulation, the pdens analyses were performed using butoxyethanol as the central molecule with either the hydroxyl or ether groups set as the axis atoms and water was selected as the molecule for the .pdens. As seen in Figure 6.10, the smooth hydration spheres apparent in the butoxyethanol/water simulation did not occur. There is no way to adjust the cut-off parameters to create a meaningful hydration sphere. When the alcohol is set as the axis, Figure 6.10a, either the box is completely filled with blue, or when the cut-off parameters are adjusted fragmented blue polygons are seen a long distance from the central butoxyethanol. When the ether group is set as the axis, there is no change to the hydration sphere when the cut off parameters are adjusted, it continues to be a complete shell. Neither scenario is chemically reasonable and, as one shows all of the water molecules to be far away from the central butoxyethanol molecule and the other shows the water molecules to be very close, the plots are not even consistent with each other. Even though an acceptable goodness-of-fit was reached with the simulation, the simulation is not made to deal with polymers and this is reflected in the output data.
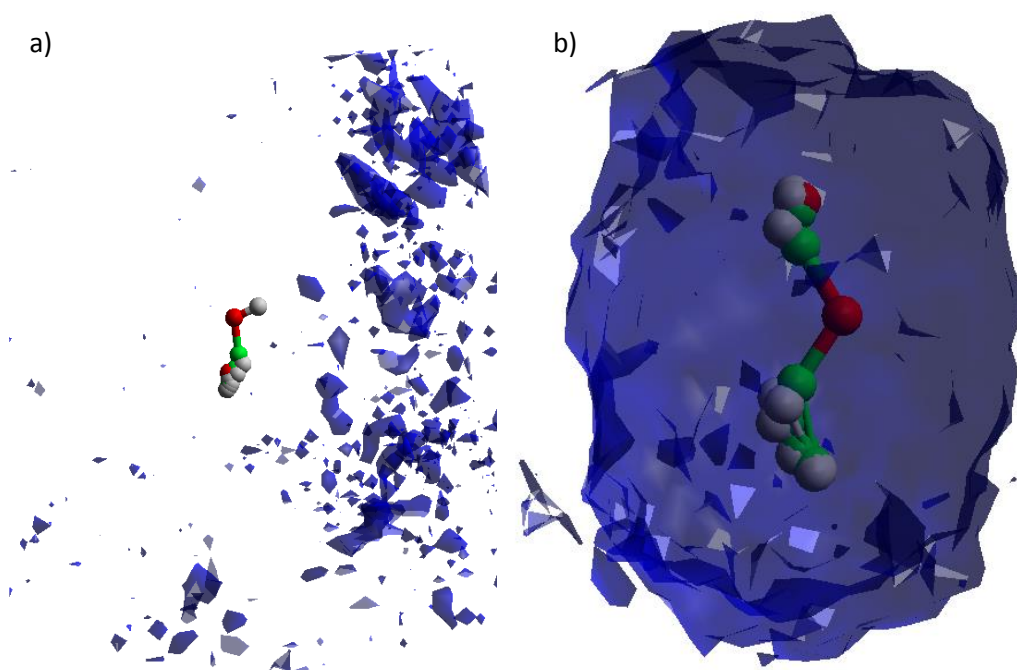
Figure 6.10 - Hydration sphere around butoxyethanol in the butoxyethanol/water/PVCap simulation plotted using Aten with the axis set as a) the hydroxyl group, atoms 18, 21 and 22 and b) the ether group, atoms 11, 14 and 15.

6.2.4 Partial atomic distribution functions

Partial atomic distribution functions give information on the distances between two selected atom types. The plot consists of g(r) against radius (r). A peak in g(r) indicates a large number of atoms at that distance and often indicates bond. For example in water, as can be seen in

Figure 6.11, the O-H line shows a peak at 1.8 Å which is the O⋯H length of the hydrogen bond between two water molecules.[32] The next broad peak along, at 3.3 Å is the second hydration sphere of water.

Compared to the neutron diffraction work on water by Soper[6–8] the partial distribution function between the H-H, O-H and O-O for the water molecules for both the butoxyethanol/water and butoxyethanol/water/polymer data are both what would be expected from a system mainly comprising of water. The peaks below 4 Å are quite well defined and typical of the hydrogen bonding in water. In the butoxyethanol/water data, at 4 Å and above, the peaks seen by Soper are still present, yet relatively broad. This would indicate that the there is less order in the second hydration sphere of water when butoxyethanol is present than when it is absent. The butoxyethanol/water/PVCap data has a peak in the O-O plot at 5.5 Å instead of the expected 4.5 Å. This could possibly be due to the second hydration sphere being further disrupted by the presence of the polymer, though as there is no shift in the peaks in either the H-H or H-O plot is it more likely that it is an inaccuracy in the simulation.
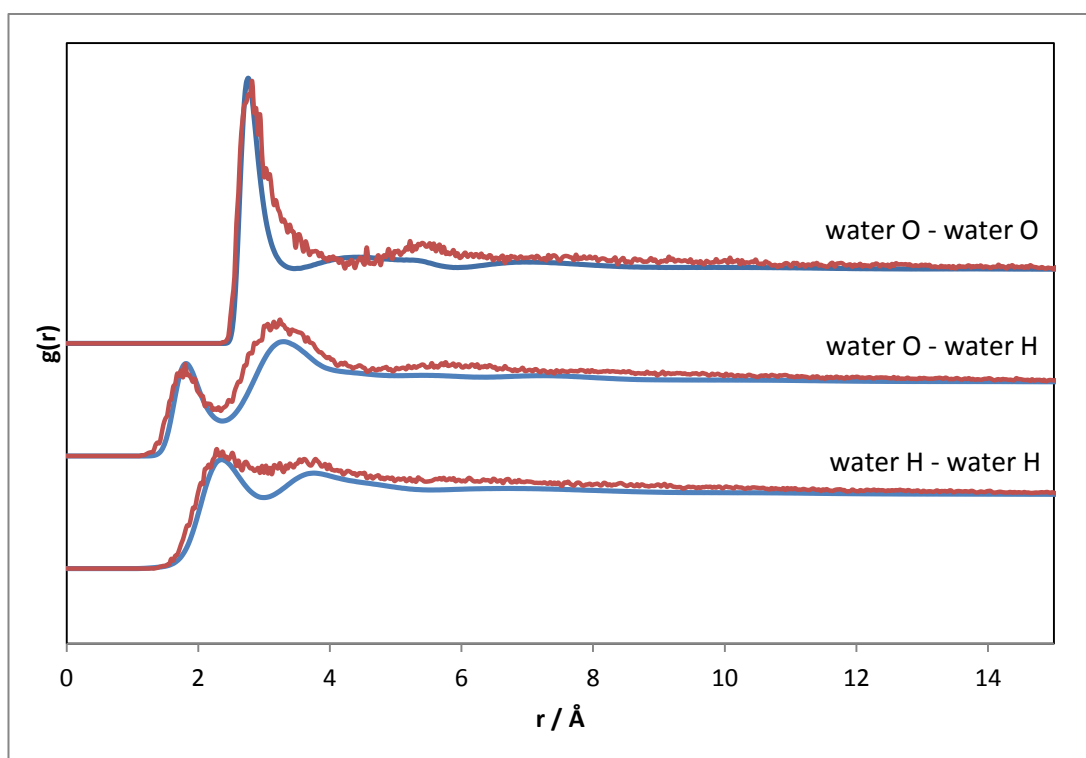
Figure 6.11 - Partial interactions of water with water. Data for the butoxyethanol/water simulation is shown in blue and data for the butoxyethanol/water/PVCap simulation is shown in red.

Comparison of the partial distributions of the alcohol and ether groups of butoxyethanol with water in both the butoxyethanol/water and butoxyethanol/water/PVCap simulations can be found in Figure 6.12. Both data sets are identical, apart from the spikes resulting from the

rough fit of the butoxyethanol/water/PVCap data from EPSR25, suggesting that within the limitations of the techniques used, there is no observable difference between the interactions between butoxyethanol and water with or without the addition of PVCap suggesting there is no change in the interactions between butoxyethanol with water within the scope of the technique and analysis used. The hydroxyl group of butoxyethanol exhibits hydrogen bonding with and O···O length of 2.8 Å to the first hydration shell of water. This is slightly longer than the 2.7 Å observed between water molecules, suggesting that the hydroxyl group of the butoxyethanol interacts with water with similar strength as water molecules interacting with each other. The ether oxygen atom shows weak bonding to the surrounding water, showing shoulders in the plot opposed to peaks, which are often indicative of little or no bonding network between the species.[7]
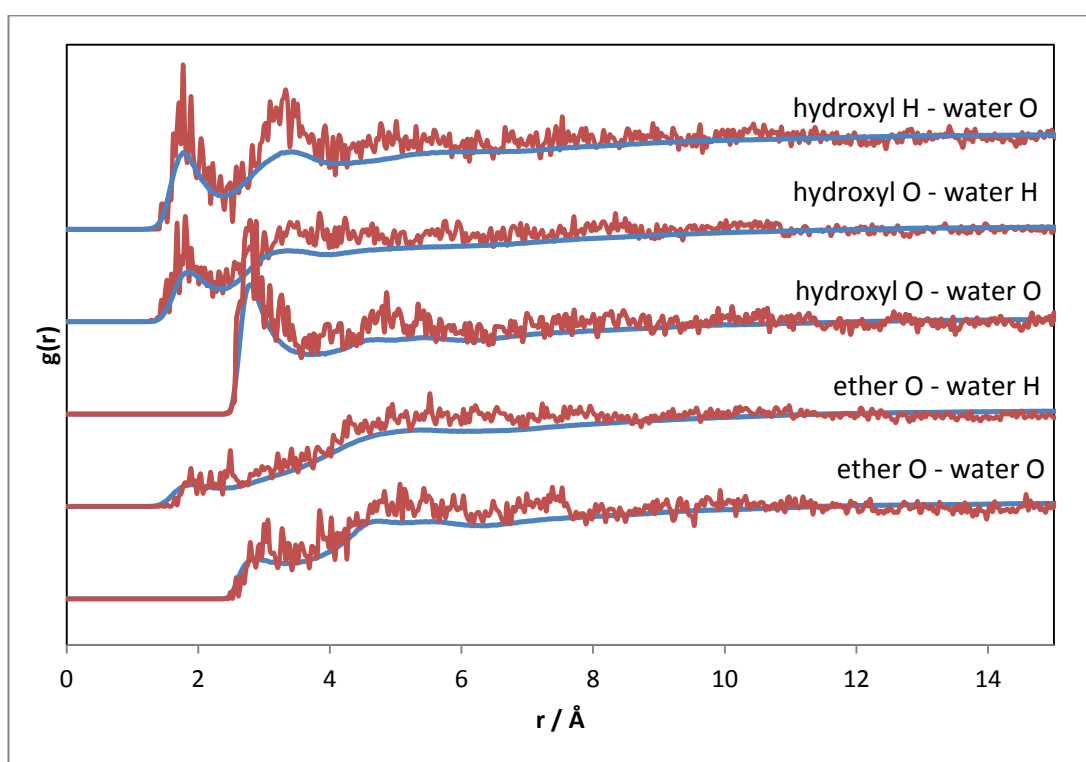
Figure 6.12 - Partial interactions of the oxygen atom of the ether of butoxyethanol with water, the hydrogen of the hydroxyl group of butoxyethanol with water and the oxygen of the hydroxyl group of butoxyethanol with water. Data for the butoxyethanol/water simulation is shown in blue and data for the butoxyethanol/water/PVCap simulation is shown in red.

Figure 6.13 shows the partial distribution functions of the carbonyl oxygen atoms with water and the lactam nitrogen atoms with water. There is no strong interactions observable in the plot. There is a small shoulder at 2.8 Å in the polymer O – water O plot, but it is much too weak to conclude that it arises from any significant hydrogen bonding behaviour.
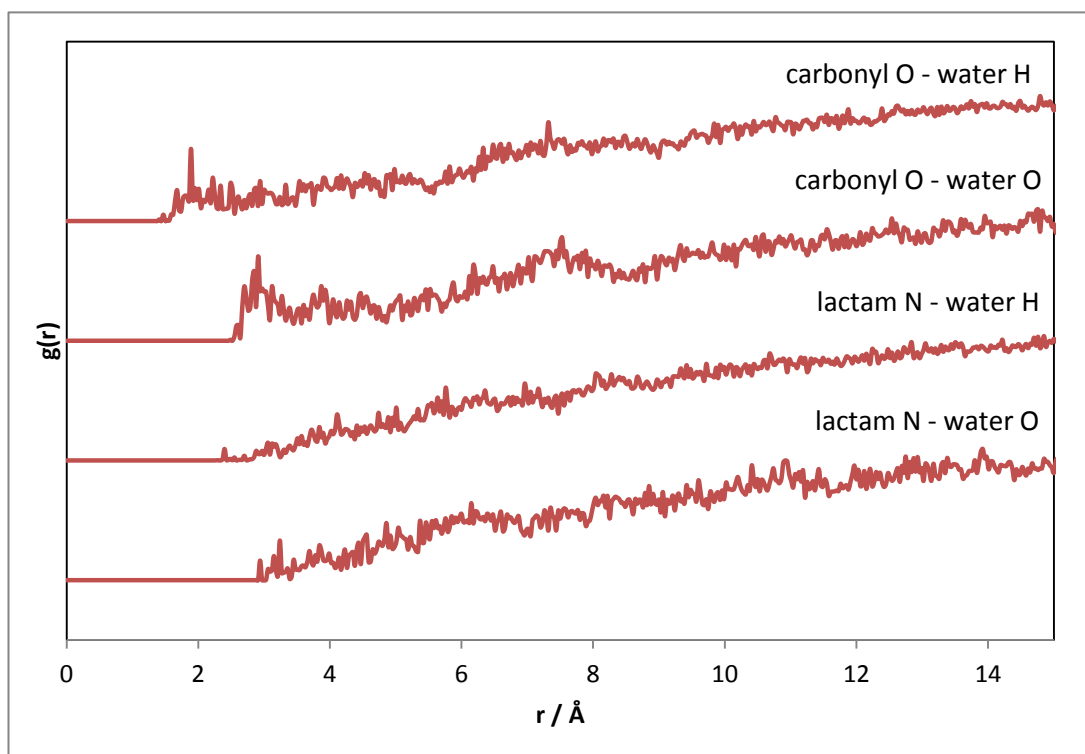
Figure 6.13 – Partial interactions of the oxygen atom of the carbonyls of PVCap with water and the nitrogen atoms of the lactam rings with water.

In conclusion SANS is not a viable method to look at this system. The concentration of polymer is too low to significantly differentiate the sample from pure water and the Monte Carlo based simulation technique is inadequate to analyse polymers. Simulations containing the polymer resulted in meaningless polygons in the pdens analysis of density and noisy data in the g(r) vs r plots. The butoxyethanol/water data gave chemically intuitive hydration spheres showing how it interacts with water in solution, though it was not at a high enough concentration to reliably conclude if the broadening of the peaks related to the second hydration sphere of water in the g(r) vs r plot of water are evident of the structure of bulk water being disrupted.

6.3   Experimental

Small angle neutron scatting experiments were performed on the Near and InterMediate Range Order Diffractometer (NIMROD) at the ISIS spallation source, in collaboration with Dr Samantha Callear. The beam size was set to 30 mm by 30 mm and titanium/zirconium cans with a 1 mm wide cavity were used along with a sample changer.

Water, D_2O and 2-butoxyethanol were purchased from Sigma Aldrich and the 2-butoxythanol-1,1,2,2-d_4 was bought from QMX Laboratories Ltd., all were used as supplied. The PVCap (Mw ~3000 Da) was supplied by Ashland Inc. in a 1:1 weight ratio solution with

butoxyethanol. The PVCap was extracted from the butoxyethanol by repeated washing with ether until a white powder was achieved and seen to be pure by ^{1}H NMR spectroscopy.

The 2-butoxyethanol was added at 5 mol% with respect to the water. The amount of PVCap used was the same weight as the non-deuterated 2-butoxyethanol, to get as close to industrial relevance as possible. The same weight of PVCap was used with the deuterated 2-butoxyethanol to keep the number of moles the same.

Compositions, temperature and time of collection are detailed below in Table 6.2, where H represents fully protic 2-butoxyethanol and D represents 2-butoxythanol-1,1,2,2-d$_4$.

Water	Butoxyethanol	PVCap	Hours of Data Collected
H_2O	H	-	6
HDO	H	-	6
D_2O	H	-	6
H_2O	D	-	6
HDO	D	-	6
D_2O	D	-	6
H_2O	H	yes	5
D_2O	H	yes	5
HDO	D	yes	6
D_2O	D	yes	6

Table 6.2 - Composition, deuteration and hours of data collect of the NIMROD experiments.

Samples were syringed into the cans to avoid any air bubbles. Samples were prepared in a water bath maintained between 3 and 10 °C by careful monitoring and addition of small amounts of ice to prevent the precipitation which occurs above and below these temperatures. All syringes and sample cans were cooled to this temperature to prevent precipitation in the equipment. The 2-butoxyethanol and PVCap sample was slowly syringed in parts whilst being held in hot water to reduce viscosity. The samples were then screwed onto the sample changer and lowered into the beam.

Analysis of the raw data was completed using Gudrun4. Simulations and modelling were performed using EPSR24 and EPSR25. Modelling of the simulations was performed using Project Aten.[29]

6.4   References

(1)   *Thermal Neutron Scattering*; Egelstaff, P. A., Academic Press: London, New York, 1965.

(2)   Sears, F. *Neutron News* **1992**, *3* (3), 26–37.

(3)   Feigin, L. A.; Svergun, D. I.; Taylor, G. W. In *Structure Analysis by Small-Angle X-Ray and Neutron Scattering*; Taylor, G. W., Ed.; Springer US: Boston, 1987; 25–55.

(4)   McGreevy, R. L.; Pusztai, L. *Mol. Simul.* **1988**, *1* (6), 359–367.

(5)   Tavagnacco, L.; Brady, J. W.; Bruni, F.; Callear, S.; Ricci, M. A.; Saboungi, M. L.; Cesàro, A. *J. Phys. Chem. B* **2015**, *119* (42), 13294–13301.

(6)   Dixit, S.; Soper, A. K.; Finney, J. L.; Crain, J. *Eur. Lett.* **2002**, *59* (3), 377–383.

(7)   Soper, A. K. *Chem. Phys.* **2000**, *258* (2–3), 121–137.

(8)   Soper, A. K.; Ricci, M. A. *Phys. Rev. Lett.* **2000**, *84* (13), 2881–2884.

(9)   Norman, S. E.; Turner, A. H.; Youngs, T. G. A. *RSC Adv.* **2015**, *5* (82), 67220–67226.

(10)   Hardacre, C.; Holbrey, J. D.; Mullan, C. L.; Youngs, T. G. a; Bowron, D. T. *J. Chem. Phys.* **2010**, *133*, 1–7.

(11)   Bernabei, M.; Ricci, M. A. *J. Phys. Cond. Matt.* **2008**, *20*, 1–8.

(12)   D'Arrigo, G.; Teixeira, J.; Giordano, R.; Mallamace, F. *J. Chem. Phys.* **1991**, *95* (4), 2732-2737.

(13)   D'Arrigo, G.; Giordano, R.; Teixeira, J. *Phys. Scr.* **1992**, *T45*, 248–250.

(14)   D'Arrigo, G.; Giordano, R.; Teixeira, J. *J. Mol. Struct.* **1997**, *404*, 319–334.

(15)   Perrin, A. The chemistry of low dosage clathrate hydrate inhibitors, University of Durham, 2015.

(16)   Cohen, J. M.; Wolf, P. F.; Young, W. D. *Energy Fuels* **1998**, *12*, 216–218.

(17)   Perrin, A.; Musa, O. M.; Steed, J. W. *Chem. Soc. Rev.* **2013**, *42* (5), 1996–2015.

(18)   Meeussen, F.; Nies, E.; Berghmans, H.; Verbrugghe, S.; Goethals, E.; Prez, F. Du. *Polymer* **2000**, *41*, 8597–8602.

(19)   Bowron, D. T.; Soper, A. K.; Jones, K.; Ansell, S.; Birch, S.; Norris, J.; Perrott, L.; Riedel, D.; Rhodes, N. J.; Wakefield, S. R.; Botti, A.; Ricci, M.; Grazzi, F.; Zoppi, M. *Rev. Sci. Instrum.* **2010**, *81* (3), 33905.

(20)   Wignall, G. D.; Bates, F. S. *J. Appl. Cryst.* **1987**, *20* (1), 28–40.

(21)   Hauser, W.; Feshbach, H. *Phys. Rev.* **1952**, *87* (2), 366–373.

(22)   McLain, S. E.; Bowron, D. T.; Hannon, A. C.; Soper, A. K. Oxford 2014.

(23)   Soper, A. K. *Phys. Rev. B* **2005**, *72* (10), 104204.

(24)   Soper, A. K. *Mol. Phys.* **2001**, *99* (17), 1503–1516.

(25)   Hanson, R. M.; Prilusky, J.; Renjian, Z.; Nakane, T.; Sussman, J. L. *Isr. J. Chem.* **2013**, *53*, 207–216.

(26)   Stewart, J. J. P. Stewart Computational Chemistry: Glasgow 2016.

(27)   Jorgensen, W. L.; Maxwell, D. S.; Tirado-Rives, J. *J. Am. Chem. Soc.* **1996**, *118* (15), 11225–11236.

(28)   Mooney, C. Z. *Monte Carlo Simulation.*; Sage Publications: Thousand Oaks, London, New Delhi, 1997.

(29)   Youngs, T. G. A. *J. Comput. Chem.* **2009**, *31* (3), 239–648.

(30)   Gapiński, J.; Szymański, J.; Wilk, A.; Kohlbrecher, J.; Patkowski, A.; Hołyst, R. *Langmuir* **2010**, *26* (12), 9304–9314.

(31)   Lin, Y.; Alexandridis, P. *J. Phys. Chem. B* **2002**, *106* (47), 12124–12132.

(32)   Soper, A.; Benmore, C. *Phys. Rev. Lett.* **2008**, *101* (6), 65502.

7 Coamorphous materials

7.1 Introduction

A major challenge in the development of drugs is the bioavailability of the active pharmaceutical ingredient. One of the main issues affecting bioavailability is the solubility of the drug in water.[1] Cocrystals, salt formation and metastable polymorphs have been among the methods employed to help drug solubility.[2] Another method is to prevent the drug from crystallising, keeping it in an amorphous state. As the amorphous state is less thermodynamically stable than the crystal, this often can lead to an increase in solubility in a range of solvents, most importantly for drugs, water.[3]

Often trying to create an amorphous state of a pure compound is challenging, with either crystals forming regardless of preparation method, or conversion to the more stable crystal structure over time.[4] One way to help prevent this is the addition of a second component to create a coamorphous mixture. Similar in concept to cocrystals,[5,6] coamorphous materials introduce a second component to change the drug's interactions, but unlike cocrystals, the goal is to disrupt favourable interactions which promote crystal formation instead of introducing more interactions to help crystals form.[7]

One of the many applications of PVP has been in drug formulation.[8–10] Often as a binding and bulking agent when making pills or for potentially creating delayed release formulation based on its thermal behaviour. Another use of PVP in drug formulation is its ability to stabilise amorphous forms of drugs.[11,12] Though PVP is effective at stabilising the amorphous form of a range of drugs, polymer stabilisers are often used in high loading.[13] Whilst high loading isn't necessarily a problem for drugs with a small therapeutic index, drugs which require a larger dosage would either need pills too large to easily swallow or multiple pills per dose, neither of which are preferable for the patient. The other main disadvantage of PVP is that it is hygroscopic.[14] This reduces the shelf life of the product, either by water promoted degradation of the drug, or because water can cause a plasticising effect in pills, aiding molecular mobility and crystallisation.[15] So whilst PVP is perfectly adequate, a less hygroscopic, lower loading alternative would be preferable. Pyrogallol,[16] amino acids[17,18] and mixtures of two drugs[19–21] have all been previously been shown to be effective in stabilising the amorphous form of pharmaceuticals. The model compounds of PVP and PVCap shown in Scheme 2.1, may be also prove effective as low molecular weight alternatives to PVP in amorphous drug formulations.

7.2   Results and Discussion

7.3   Coamorphous screening

7.3.1   ROY

ROY (5-methyl-2-[(2-nitrophenyl)amino]-3-thiophenecarbonitrile, Scheme 7.1) is a highly polymorphic compound which is a precursor for the antipsychotic drug olanzapine. ROY is named after the colours of its polymorphs: red, orange and yellow. Due to its large number of polymorphs, ROY has been the focus of much study with significant effort expended in seeking new polymorphs or controlling solid form using novel methods of crystallisation.[22,23] Whilst of academic interest, the high crystallinity of compounds such as ROY can be disadvantageous in a pharmaceutical setting do to the low solubility of its crystal forms. Corner *et al.*[16] found pyrogallol to be a suitable candidate to stabilise the amorphous form of ROY offering a small molecule alternative to the commonly used PVP. As the model compounds of the KHIs have shown themselves to be particularly apt at preventing a wide range of substances crystallising, it is possible that they may make coamorphous phases with ROY.

Compounds **1**, **3**, **6-11** and VCap were all ground using a mortar and pestle in a 1:1 molar ratio with ROY. The grinding ensures that both components were thoroughly mixed, as differences in melting point can make mixing difficult in the melt. The samples were placed on a microscope slide and covered with a thin, glass cover slide then heated in the hot stage microscope until all material had melted. The samples were then removed from the hot stage and allowed to cool at room temperature overnight. The cooled samples were examined under a microscope fitted with cross polarising filters to check if any crystals had formed on cooling. Pictures of the microscope slides and crossed polarised microscope images can be found in Figure 7.1.

As expected the reference sample of ROY without any second compound readily crystallises. It is interesting to note that under the conditions used, ROY crystallises into three distinctive blocks of different colour suggesting that at least three different forms can be made from cooling the melt in this way. The cross polarised microscope image shows there is possibly more than three forms in the sample. This has been previously reported by Chen *et al.*[24] who observed that cooling ROY from the melt results in four polymorphs forming. They reported the Y04 forms first and cross-nucleates allowing different, faster growing forms to crystallise,

resulting in a mixture of polymorphs from the same cooling crystallisation. Further analysis into the polymorphism of ROY is beyond the scope of this study.
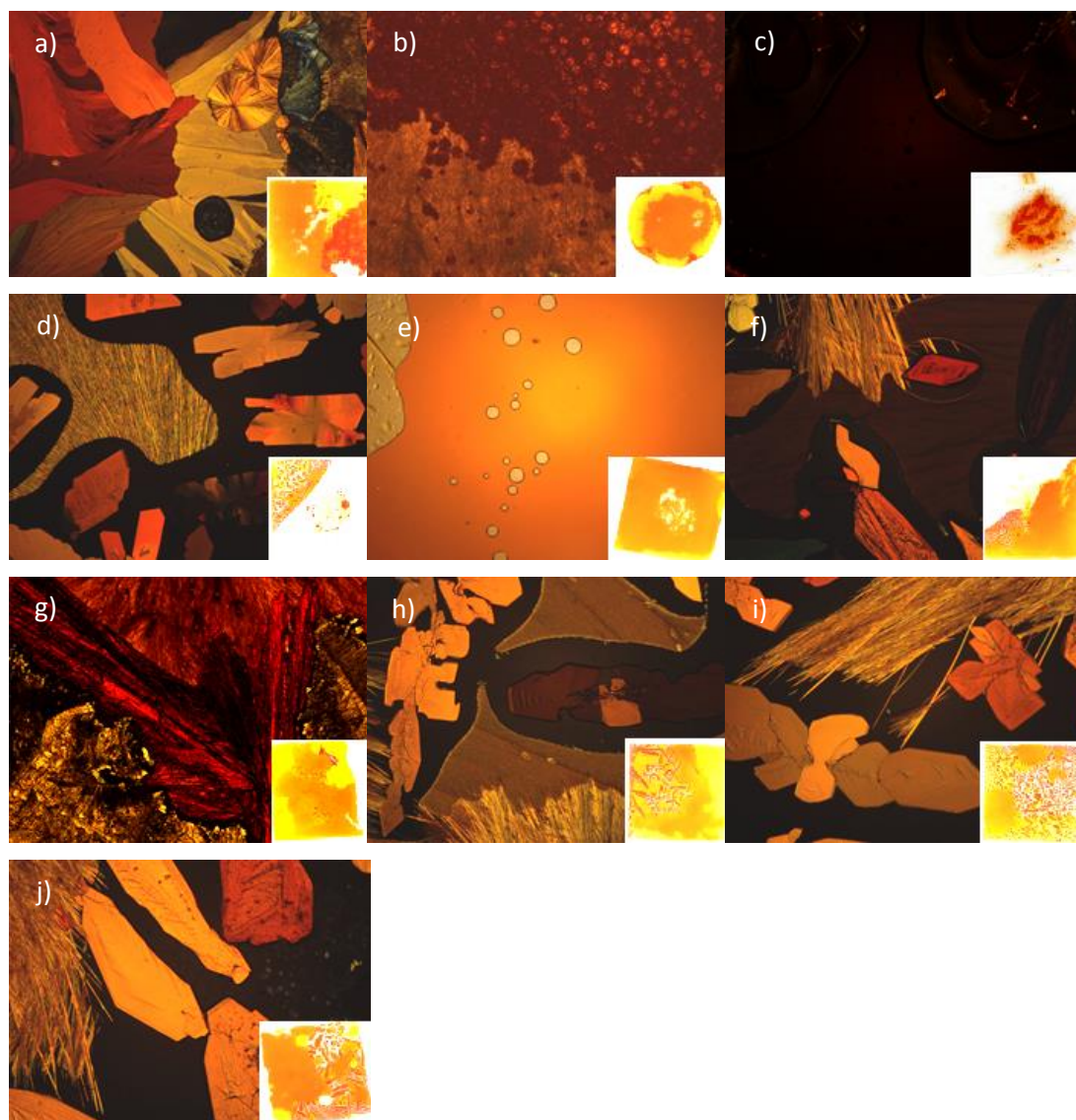
Figure 7.1 – Polarised light microscope images of ROY samples cooled overnight with photos of the microscope slide in the bottom right corner. Samples are: a) ROY, b) ROY and PVP, c) ROY and PVCap, d) ROY and VCap, e) ROY and bisVCap, f) ROY and H₂bisVCap, g) ROY and bisVP, h) ROY and H₂bisVCap, i) ROY and bisHEP, j) ROY and HEPVCap.

PVP with ROY was tested as an example of what, according to literature,[11,12] should be an effective coamorphous material. There are areas of different colours suggesting that different phases may exist, though none of the phases show birefringence so are not crystalline. PVCap is not used as an amorphous stabiliser in the pharmaceutical industry. This is possibly due to the fact that PVP is an adequate and affordable amorphous stabiliser whilst PVCap is more expensive. As PVP is known to prevent drug recrystallisation,[11,12] it stands to reason that PVCap may also be effective. The PVCap/ROY sample does remain amorphous

and of a single phase, similarly the unsaturated model for PVCap, bisVCap, also gives an amorphous mixture.

Apart from bisVCap, the other model compounds do not seem to be effective in preventing ROY crystallising over time. Though no quantitative analysis has been performed, it is worth noting that ROY shows a very significant amount of crystallisation within a couple of minutes of being removed from the heat whilst all model compounds slowed the crystallisation. BisHEP slowed down the crystallisation the least, with crystals beginning to form within half an hour whilst the other models did not show any signs of crystallisation within the next couple of hours. After 22 hours however, there were crystals present in all the samples which include compounds **7**-**11**. Compounds **7**-**11** resulted in different combinations of crystal habitats and amorphous regions. In depth analysis of which polymorphs form is beyond the scope of this project, whilst interesting to note that the crystallisation behaviour is changed by the additive, the fact that the additives did not successfully stabilise the amorphous phase is the important information for this study.

None of the samples changed any further after two months of storage at room temperature, suggesting all crystallisation was complete within the first 24 hours and those which did not crystallise are stable at least on a two month time scale.

7.3.2 BisVCap and bisVP with a range of drugs

As bisVCap showed potential as an amorphous phase stabiliser for ROY, further experiments were performed with other drugs. Even though bisVP did not effectively prevent ROY from crystallising, as the equivalent model to bisVCap of PVP, which is the commercially used stabiliser, bisVP was also screened with the same range of drugs. Thirteen drugs were chosen based on easy availability and relative heat stability, for example no β-lactam rings, for initial screening to see if any would form a coamorphous phase with bisVCap or bisVP. The drugs chosen, shown in Scheme 7.1, were benzocaine, caffeine, carbamazepine, carisoprodol, dopamine, ethionamide, ibuprofen, isoniazid, metformin, mexiletine, tolfenamic acid, valsartan and ROY is included here for completeness.

benzocaine   caffeine   carbamazepine   carisoprodol

dopamine   ethionamide   ibuprofen   isoniazid

metformin   mexiletine   tolfenamic acid

valsartan   ROY
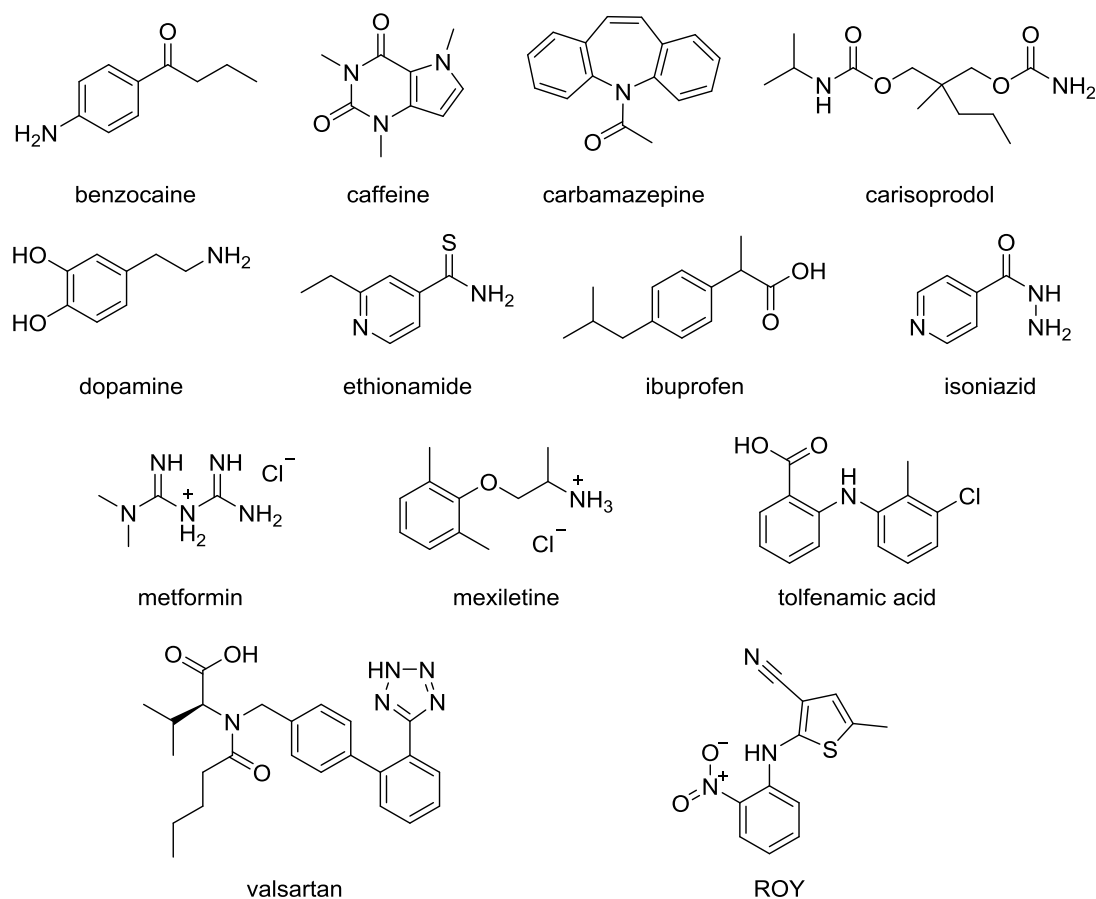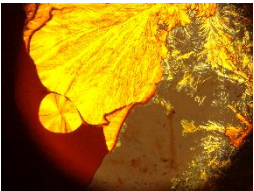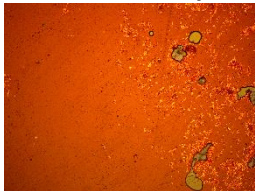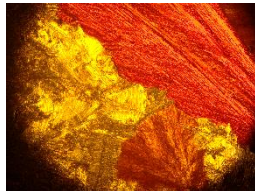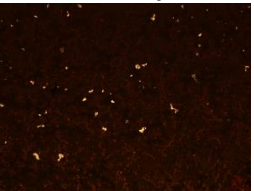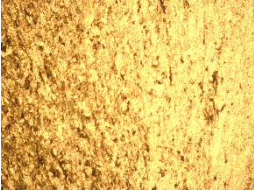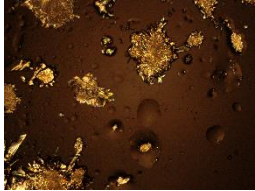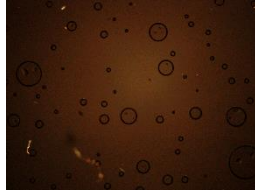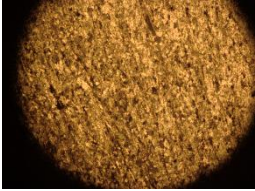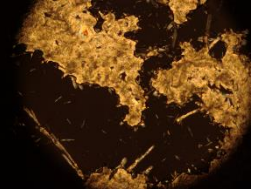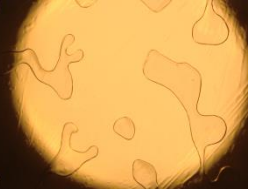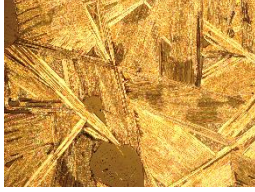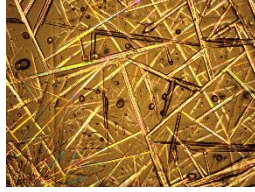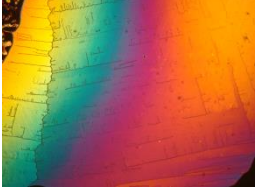
Scheme 7.1 – Structures of the drug molecules.
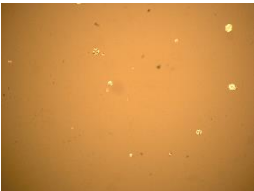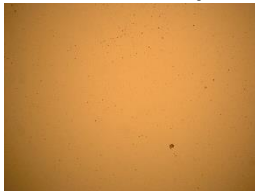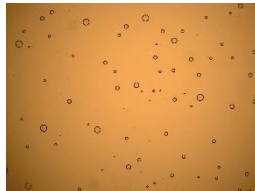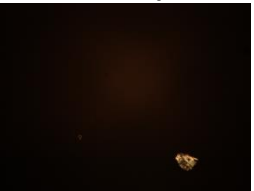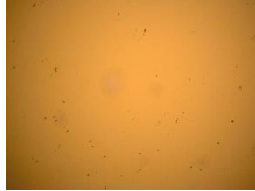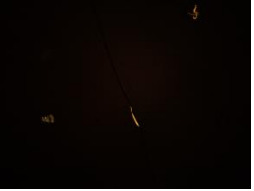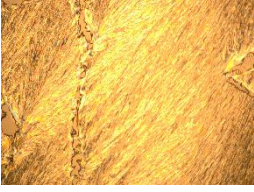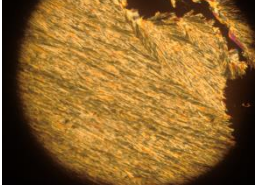
The drugs were ground together in a 1:1 mol ratio using a mortar and pestle with bisVCap and with bisVP before being heated in a hot stage microscope until all material had melted and allowed to cool at room temperature. Pictures were taken using a camera attached to a polarised light microscope the next morning and two weeks after melting to see if any crystallisation had occurred. The pictures can be found in Figure 7.2. One of the first samples which can be rejected as a candidate of interest is valsartan, which even on its own, remains amorphous, suggesting that it is either not heat stable, particularly hydroscopic when in the melt or forms a stable amorphous form on its own. The amorphous samples using bisVP all become viscous fluids, like bisVP itself, creating what could be described as a solution, not as an amorphous solid. As creating a solution was not the aim, bisVP is rejected as a potential stabiliser. Out of the remaining samples, bisVCap with benzocaine, caffeine and metformin can be rejected from this experiment alone, as they crystallise overnight. BisVCap with carbamazepine, carisoprodol, dopamine, ethionamide, ibuprofen, isoniazid, mexiletine and tolfenamic acid all result in materials which appear amorphous by polarised light microscopy after 18 hours at room temperature.

Drug	Overnight cooling	Overnight cooling with bisVCap	Overnight cooling with bisVP	2 weeks	2 weeks with bisVCap	2 weeks with bisVP
ROY						
Benzocaine						
Caffeine						
Carbamazepine						

Drug	Overnight cooling	Overnight cooling with bisVCap	Overnight cooling with bisVP	2 weeks	2 weeks with bisVCap	2 weeks with bisVP
Carisoprodol						
Dopamine						
Ethionamide						
Ibuprofen						
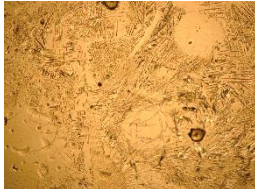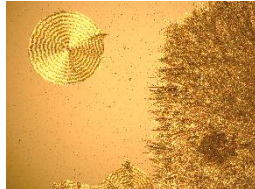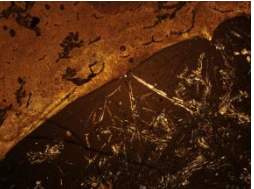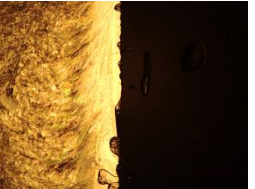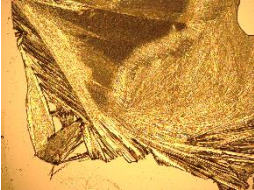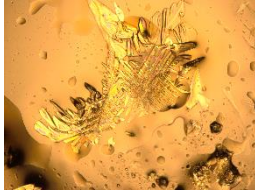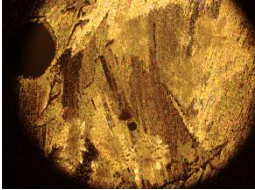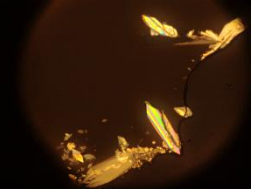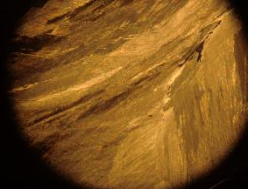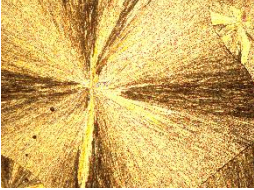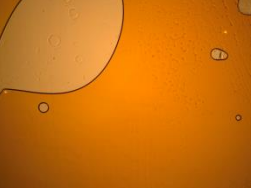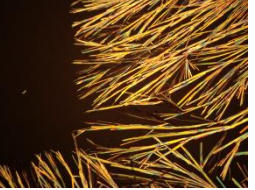
Drug	Overnight cooling	Overnight cooling with bisVCap	Overnight cooling with bisVP	2 weeks	2 weeks with bisVCap	2 weeks with bisVP
Isoniazid						
Metformin						
Mexiletine						
Tolfenamic Acid						

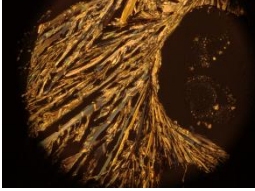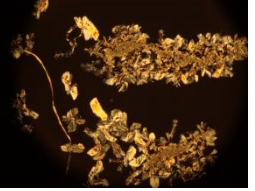| Drug	Overnight cooling	Overnight cooling with bisVCap	Overnight cooling with bisVP	2 weeks	2 weeks with bisVCap	2 weeks with bisVP
Valsartan						

Figure 7.2 – Cooling of the melts of a range of drugs with and without bisVCap and bisVP overnight and after two weeks

7.4   Differential scanning calorimetry

DSC is commonly employed to establish if a melted material recrystallises when cooled and reheated. The components are mixed in the desired ratio and then heated until everything has melted. The molten mixture is then cooled, often to the limits of the machine being used, before being heated past the melting point again. On the first heating cycle either one or more endothermic peaks corresponding to the melting of the sample should be observed. Two peaks would occur at the melting points of the two separate components. A single melting point happens if both of the components share a melting point, form intermolecular interaction upon mixing such as cocrystalline materials or if the higher melting component is soluble in the molten lower melting component. More than two peaks corresponding to melting points may also be possible if one or both of the components have multiple polymorphs as polymorphs can have different melting points to one another. For an amorphous mixture there should be no exothermic peak from recrystallisation upon cooling or reheating. The second heating cycle should show a glass transition of the amorphous material and no melting peak, as there should be no crystalline material present to melt.

Out of the drug/bisVCap combinations which appeared amorphous by polarised light microscopy, more failed as this stage. Dopamine shows an endothermic peak in the second heating cycle corresponding to melting. As no recrystallisation was observed in the hot stage microscope experiment which only heated the sample once, it is possible that recrystallisation occurred during the second heating cycle. As dopamine recrystallises during the heat/cool/heat DSC experiment, it is not a suitable material for a coamorphous drug formulation with bisVCap. Ethionamide, tolfenamic acid, mexilitine and ibuprofen show collections of sharp and overlapping endothermic peaks on heating, which arise from decomposition of the sample. Ethionamide and mexilitine both decompose soon after their melting points as seen in the DSC thermographs of the individual components, so decomposition of these two samples is not surprising. Ibuprofen and tolfenamic acid on the other hand are stable significantly above their melting points as was observed in the DSC thermographs of the single components. The decomposition of the ibuprofen/bisVCap and tolfenamic acid/bisVCap mixtures on heating whilst the single components do not decompose on heating to the same temperature suggests that the interaction with bisVCap promotes degradation of the sample. The exact nature of this decomposition has not been explored further, though it is sufficient to say that bisVCap is not an appropriate additive for these drugs. The DSC plot of tolfenamic acid and bisVCap/tolfenamic acid are shown in Figure 7.3 to highlight the decomposition upon heating bisVCap/tolfenamic acid.
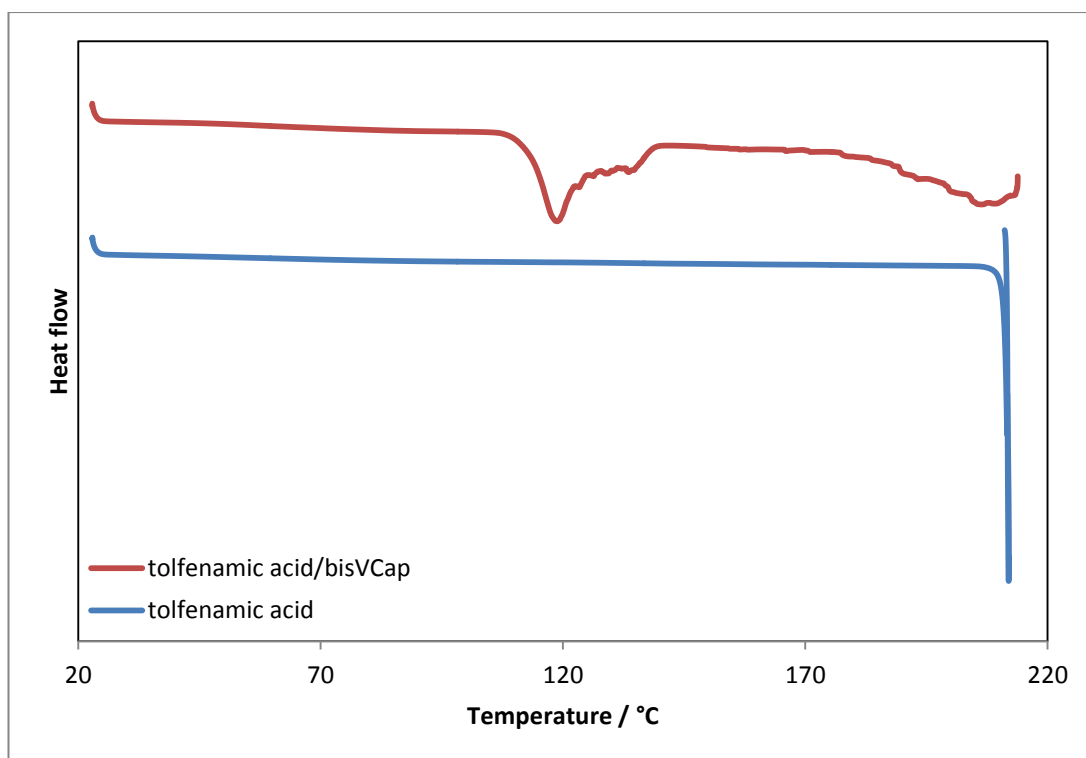
Figure 7.3 – The first heating cycles of the heat/cool/heat DSC thermographs of tolfenamic acid and bisVCap/tolfenamic acid, exotherm up.

Carisoprodol, carbamazepine, isoniazid and ROY all had DSC thermographs lacking decomposition, recrystallisation or endothermic peaks in the second heating cycle corresponding to the melting of a crystalline material. The DSC thermographs can be seen in Figure 7.4. All four thermographs show an endothermic peak on heating which corresponds to the sample melting. On cooling there are not exothermic peaks which would arise from recrystallisation of the sample, suggesting that no recrystallisation on cooling occurs. During the second heating cycle all the thermographs show an exothermic step which relates to the glass transition. No other feature is visible in the second heating cycle. The lack of exothermic peak from a recrystallisation event and the lack of endothermic peak in the second heating cycle shows carisoprodol, carbamazepine, isoniazid and ROY in 1:1 ratios with bisVCap to be amorphous within the scope of the DSC experiment.
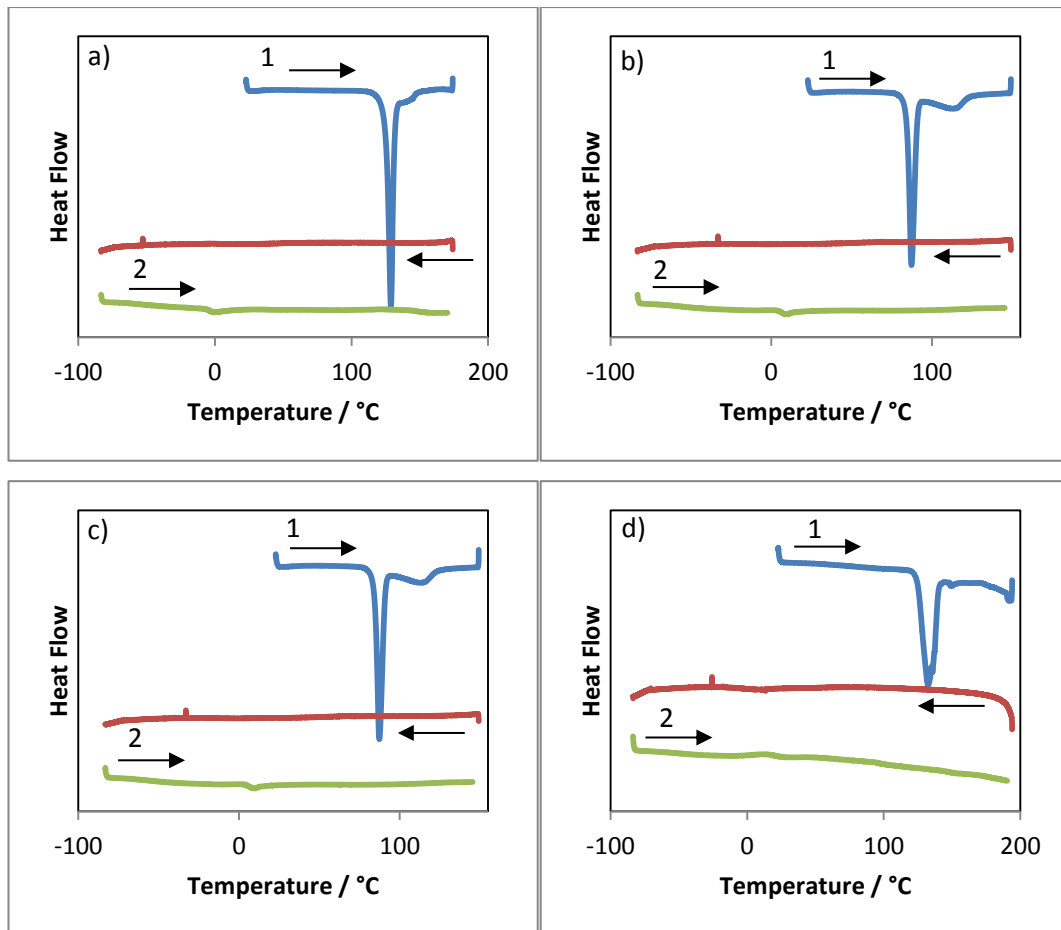
Figure 7.4 – Heat/cool/heat DSC plots of a) bisVCap/carbamazepine, b) bisVCap/carisoprodol, c) bisVCap/isoniazid and d) bisVCap/ROY, exotherm up.

To further verify the DSC results, the same heat/cool/heat cycles which were performed in the DSC experiments were reproduced using a hot stage attached to a polarised light microscope. This adds visual verification that no crystallisation has occurred when carisoprodol, carbamazepine, isoniazid and ROY were mixed in a 1:1 molar ratio with bisVCap. The results of the microscope experiments can be seen in Figure 7.5, Figure 7.6, Figure 7.7 and Figure 7.8. No crystallisation was seen in any sample in the microscope images further evidencing the formation of an amorphous phase.
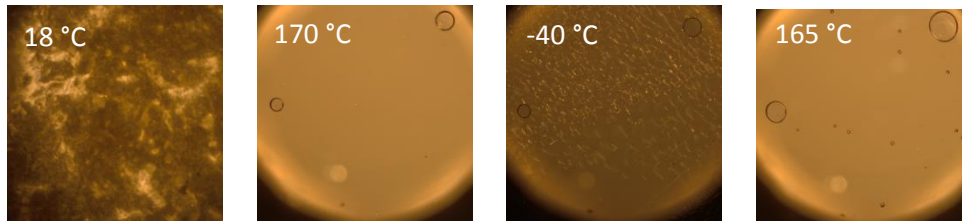
Figure 7.5 – Heat cool heat cycle of bisVCap and carbamazepine in a 1:1 ratio under a cross polarised filter
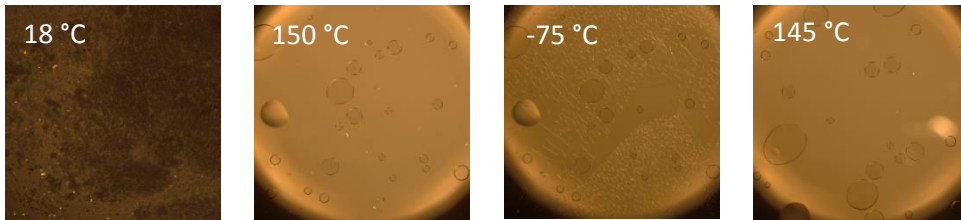

Figure 7.6 – Heat cool heat cycle of bisVCap and carisoprodol in a 1:1 ratio under a cross polarised filter
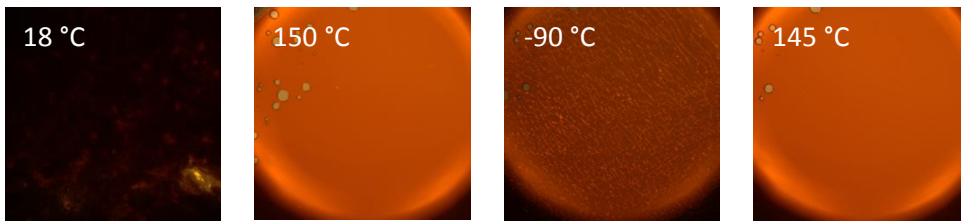

Figure 7.7 – Heat cool heat cycle of bisVCap and ROY in a 1:1 ration under a cross polarised filter
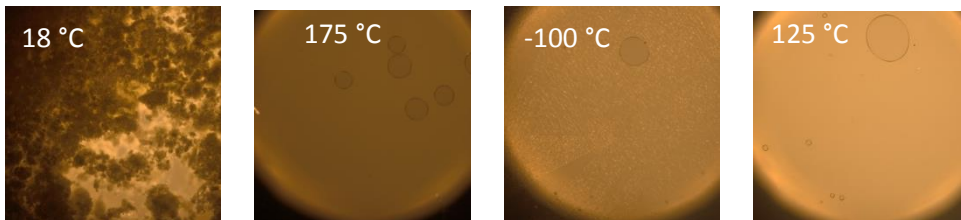

Figure 7.8 - Heat cool heat cycle of bisVCap and isoniazid in a 1:1 ration under a cross polarised filter

7.5   Effective ratio

One major problem with PVP as an amorphous stabiliser is the large amount required for stabilisation of the amorphous phase. This often leads to very large pills or dosages which consist of multiple tablets. This is not ideal for the end user. If an amorphous stabiliser can work with a lower loading it could help the development of pills which are much easier to swallow. Thus further hot stage microscope and DSC experiments of the short listed drugs, carisoprodol, carbamazepine, isoniazid and ROY, were performed with increasing drug:bisVCap ratios to determine the highest effective ratio.

For the microscope experiments the drugs and bisVCap were ground in the desired ratio, heated until all the sample had melted then cooled back to room temperature and analysed by polarised light microscopy. Carbamazepine, carisoprodol, isoniazid and ROY all showed no visible crystallisation at a 2:1 drug:bisVCap molar ratio. Carisoprodol also did not show any visible crystallisation at a 3:1 carisoprodol:bisVCap ratio. At 3:1 drug:bisVCap ratio carbamazepine, isoniazid and ROY all formed crystals overnight and carisoprodol formed crystals overnight from a 4:1 ratio. Heat/cool/heat DSC experiments were performed for the ratios which did not form crystals in the hot stage microscope experiments. Similar to the 1:1 ratios, no recrystallisation event or melt during the second heating cycle is present in the DSC plots for 3:1 carisoprodol:bisVCap, 2:1 carbamazepine:bisVCap, 2:1 isoniazid:bisVCap or 2:1 ROY:bisVCap. This suggests that bisVCap is still an effective crystallisation inhibitor at these ratios.

The final experiment to prove amorphousness is PXRD, which should show no Bragg peaks as there should be no crystalline material to diffract. The amorphous samples were prepared 18 hours before the PXRD experiments were run by melting the two components together and allowing the samples to cool to room temperature overnight. Carbamazepine:bisVCap 2:1 and 1:1 and carisoprodol:bisVCap 3:1, 2:1 and 1:1 showed no Bragg peaks in the powder patterns, Figure 7.9, showing that these materials are amorphous by x-ray diffraction. The 1:1 ratio of ROY:bisVCap did not exhibit any Bragg peaks so is amorphous by x-ray diffraction. The 2:1 ratio of ROY:bisVCap on the other hand is largely amorphous but has some small Bragg peaks and the material has begun to crystallise overnight.
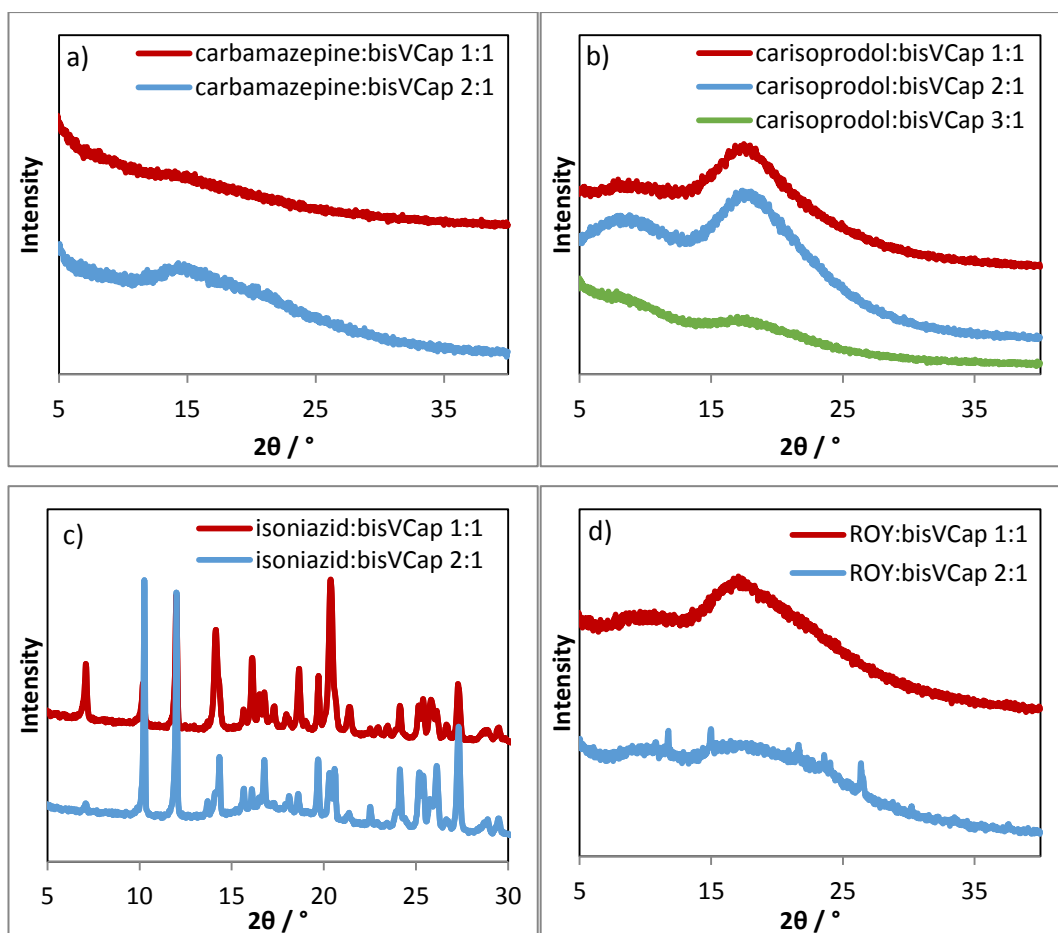
Figure 7.9 – PXRD plot of a) carbamazepine with bisVCap in a 1:1 and 2:1 molar ratio, b) carisoprodol with bisVCap in a 1:1 and 2:1 molar ratio, c) isoniazid with bisVCap in a 1:1 and 2:1 molar ratio, d) ROY with bisVCap in a 1:1 and 2:1 molar ratio.

Neither isoniazid:bisVCap 2:1 or isoniazid:bisVCap 1:1 are amorphous by PXRD as both exhibit Bragg peaks in their PXRD plots. Both the 2:1 and 1:1 ratios gave powder patterns consistent with being the same crystal form to one another. Comparison to powder patterns calculated from the literature crystal structures of isoniazid[25] and bisVCap[26] using Mercury[27] shows the crystalline material to be a mixture of isoniazid and bisVCap, Figure 7.10.
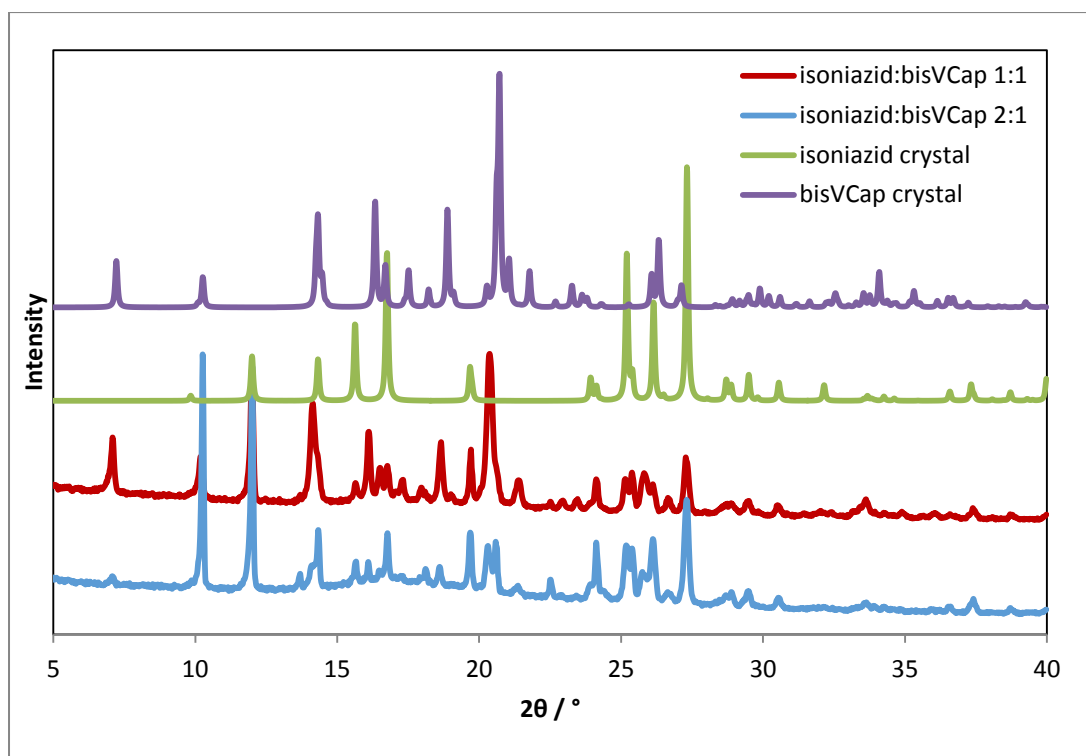
Figure 7.10 – PXRD plot of isoniazid with bisVCap in a 1:1 and 2:1 molar ratios and the powder diffraction patterns calculated from the crystal structures of isoniazid[25] and bisVCap.[26]

After four weeks of being stored at room temperature, all samples except for 1:1 carisoprodol:bisVCap showed Bragg peaks in their PXRD plots, showing that over time they revert to the more thermodynamically stable crystalline forms. The coamorphous form of 1:1 carisprodol:bisVCap is stable over the course of a month, which shows great promise for drug formulation.

7.6 IR spectroscopy

To see if any insight could be gleaned into how the amorphous form is stabilised, IR spectra were recorded of carisoprodol, carbamazepine, isoniazid, ROY and bisVCap, as well as the 1:1, 2:1 and for carisoprodol 3:1 drug:bisVCap mixtures ground and melted together. As carisoprodol, carbamazepine, isoniazid and bisVCap all contain carbonyl groups, the carbonyl region was focused upon to look for any changes. ROY contains a nitrile group and ROY and isoniazid contain amine groups, which were also focused on to look for any significant interactions.

For all four drugs, when just ground with bisVCap, no significant changes in the IR spectra were observed, with the spectra being a mix of the spectra of the single components with no shifts in the peaks of interest, as highlighted in Figure 7.11 and Figure 7.12. Upon melting and cooling there are observable changes for carbamazepine, carisoprodol and isoniazid. For carisoprodol, Figure 7.11, when the sample is melted and cooled the carbonyl peaks of

bisVCap at 1622 cm^{-1} and 1640 cm^{-1} become much broader and less well defined. This is indicative of amorphous materials as there are many different conformations and environments in which the molecules reside, creating broad peaks which are an average of all the possible environments in the amorphous material.[17,20,28,29] The carbonyl peak for the carisoprodol broadens and also shifts from 1690 cm^{-1} to 1708 cm^{-1}. This suggests that the carbonyl bonds are becoming stronger so less involved in any intermolecular bonding and that the hydrogen bonding which normally holds the crystal structure together is being disrupted. The bands between 3475 – 3180 cm^{-1} which are associated with the N-H stretches of the carbamate groups, become a single broad peak in the spectrum of the cooled sample after melting, where in pure carisoprodol there were four sharp, distinct peaks, which suggests a change in bonding. Upon increasing the ratio of carisoprodol:bisVCap from 1:1 to 2:1 to 3:1 there is no significant change in the wavenumber of any of the peaks. From the changes in the IR spectra of carisoprodol with bisVCap, it can be said that there are changes in the local environment and interaction of the carisoprodol molecules which affect the crystallisation.
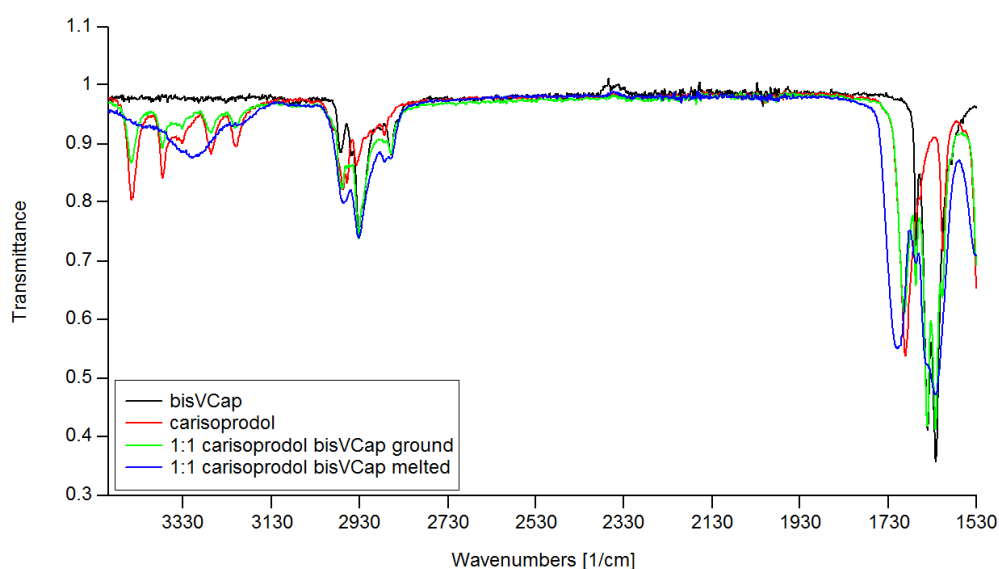
Figure 7.11 – IR spectra of bisVCap, carisoprodol and a 1:1 molar ratio of carisoprodol:bisVCap ground and melted.

Similarly both carbamazepine and isoniazid, Figure 7.12 and Figure 7.13 respectively, show a large degree of broadening of the carbonyl peaks in the spectra of the cooled samples after melting and no change in the ground sample. The spectra of cooled melts of samples of carbamazepine:bisVCap and isoniazid:bisVCap showed no change between the 1:1 and 2:1 ratios. On the other hand, ROY exhibits no change in peaks in the IR spectra in the ground or melted samples at either a 1:1 or 2:1 ROY:bisVCap ratio. Even when melted and cooled, the spectrum for ROY/bisVCap is a mixture of the bisVCap and ROY spectra, with no shifts in the

peaks of interest. This suggests that unlike carbamazepine, carisoprodol and isoniazid, which see significant changes to the local environment, the stabilisation of the amorphous form in ROY/bisVCap arises from a bulk property, not from local intermolecular interactions.
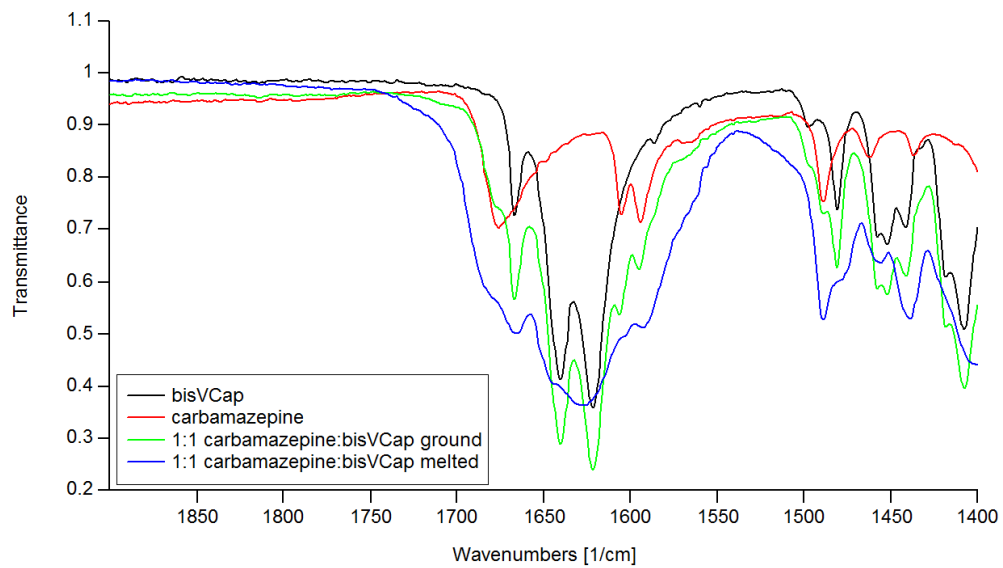
Figure 7.12 - IR spectra of bisVCap, carbamazepine and a 1:1 molar ratio of carbamazepine:bisVCap ground and melted and cooled.
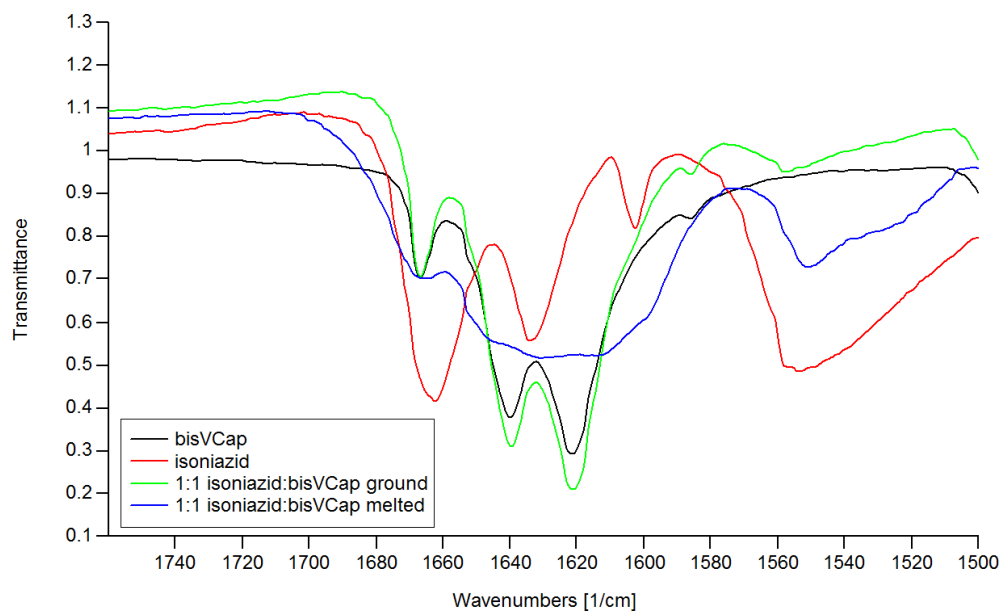
Figure 7.13 - IR spectra of bisVCap, isoniazid and a 1:1 molar ratio of isoniazid:bisVCap ground and melted.

7.7   Dynamic vapour sorption

One of the biggest issues with PVP as an amorphous stabiliser is its hydroscopicity.[14] If bisVCap is significantly less hydroscopic than PVP, then it is a promising candidate for future pharmaceutical applications. DVS was used to compare the water uptake of bisVCap and PVP and the data is presented in section 2.2.1. As seen in Figure 2.2, bisVCap is not hydroscopic, absorbing only 0.05 water molecules per molecule of bisVCap, or 0.0025 water molecules per carbonyl moiety at 90 %RH. PVP on the other hand, absorbs 2.5 water molecules per carbonyl group which is orders of magnitude more than bisVCap. This suggests bisVCap may be a desirable amorphous stabiliser which will not absorb much atmospheric water.

As amorphous forms are more soluble than crystal forms due to their thermodynamic instability, it is possible that the amorphous form of bisVCap could absorb much more water than the crystalline form. The DVS plot for crystalline bisVCap, Figure 7.14a, shows a mass increase of 0.35 %. The amorphous bisVCap, Figure 7.14b, shows a larger mass increase of 1.2 % which corresponds to 0.18 water molecules per molecule of bisVCap. Whilst the amorphous bisVCap does absorb more water than the crystalline bisVCap, the small increase in mass and lack of hysteresis in the DVS plot suggest that amorphous bisVCap is also not hydroscopic. Amorphous bisVCap absorbs much less water than PVP, making it an acceptable additive to stabilise amorphous materials whilst avoiding plasticisation due to water.
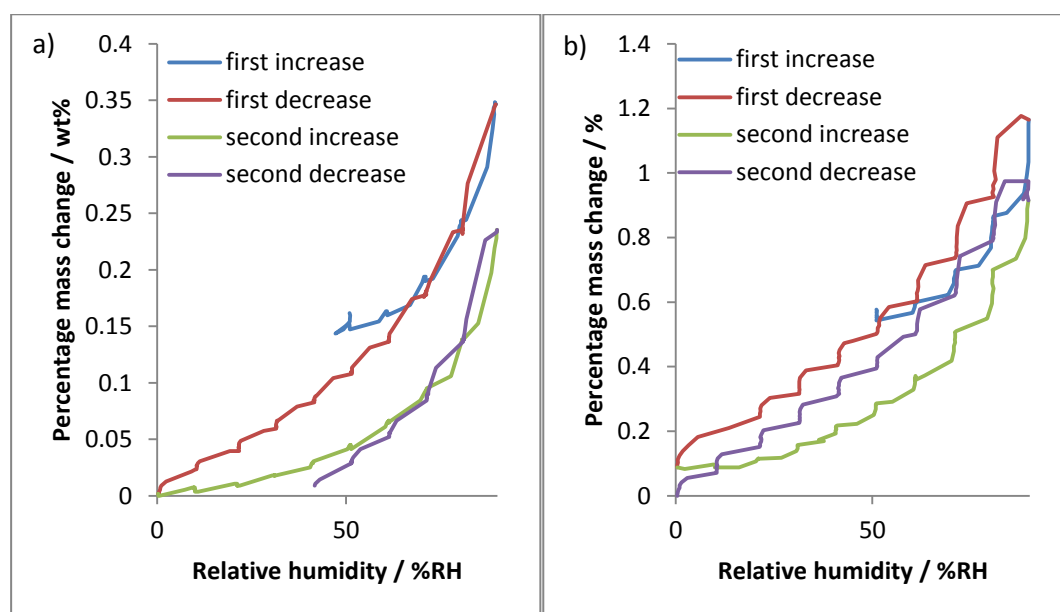

Figure 7.14 - DVS plot of a) crystalline bisVCap and b) amorphous bisVCap.

In conclusion, bisVCap has the capability to stabilise the amorphous form of a range of drugs. Carisoprodol in particular showed promise, with a low loading of bisVCap and a long shelf life. BisVCap is also much less likely to absorb water than PVP, which would prolong the shelf

life of any pills formulated with it. Future experiments would need to include more in-depth analysis of the lifetime of the amorphous forms, toxicity testing to see if bisVCap is safe for human consumption, experiments into the physical properties of the amorphous forms and which method of pill formation would work best, as well as the solubility of the amorphous forms.

7.8   Experimental

7.8.1   Differential scanning calorimetry

Differential scanning calorimetry scans were recorded on a TA Q2000 using standard aluminium pans containing 3 – 12 mg of sample. Standard mode was used. The heat/cool/heat cycles began with a heating cycle at a rate of 10 °C min^{-1}, then cooling cycle at 10 °C min^{-1} and finally a second heating cycle at 10 °C min^{-1}.

7.8.2   Dynamic vapour sorption

DVS was performed using an SMS DVS-1 with a 10 %RH step between humidity values with equilibrium achieved at 0.01% weight change before moving to the next step. Methods began at the humidity of the room at ambient which was measured by a Rotronic A/H hygrometer. The humidity was then increased to 90%RH before cycling to 0%RH, to 90%RH, to 0%RH. Samples weighing between 5-20mg were used.

7.8.3   Hot stage microscopy

A Linkam LTS420 heating stage attached to a Olympus XC50 microscope was used to heat the samples. Samples were placed on a glass microscope slide with a thin glass cover slide.

For the amorphous material screening compounds were ground together as detailed in Table 7.1 and heated at 30 °C min^{-1} until the all of the sample had melted. Samples were then removed from the hot stage and allowed to cool.

Model compound	Weight / g	Drug	Weight / g
bisVCap	0.08	benzocaine	0.05
	0.07	caffeine	0.05
	0.06	carbamazepine	0.05
	0.03	carbamazepine	0.05
	0.02	carbamazepine	0.05
	0.05	carisoprodol	0.05
	0.03	carisoprodol	0.05
	0.02	carisoprodol	0.05
	0.01	carisoprodol	0.05
	0.09	dopamine	0.05

	0.08	ethionamide	0.05
	0.07	ibuprofen	0.05
	0.10	isoniazid	0.05
	0.05	isoniazid	0.05
	0.03	isoniazid	0.05
	0.11	metformin	0.05
	0.08	mexiletine	0.05
	0.05	tolfenamic acid	0.05
	0.03	valsartan	0.05
	0.05	ROY	0.05
	0.03	ROY	0.05
	0.02	ROY	0.05
bisVP	0.07	benzocaine	0.05
	0.06	caffeine	0.05
	0.05	carbamazepine	0.05
	0.04	carisoprodol	0.05
	0.07	dopamine	0.05
	0.07	ethionamide	0.05
	0.05	ibuprofen	0.05
	0.08	isoniazid	0.05
	0.09	metformin	0.05
	0.06	mexiletine	0.05
	0.04	tolfenamic acid	0.05
	0.03	valsartan	0.05
	0.04	ROY	0.05

Table 7.1 – Compositions of model compound drug mixtures.

BisVCap was ground in 1:1 molar mixture, as detailed in Table 7.1 with carbamazepine, carisoprodol, isoniazid and ROY. The carbamazepine/bisVCap sample was heated from room temperature to 170 °C at a rate of 10 °C min^{-1}, cooled at °C min^{-1} to -40 °C, then heated at 10 °C min^{-1} to 165 °C min^{-1}. The carisoprodol/bisVCap sample was heated from room temperature to 150 °C at a rate of 10 °C min^{-1}, cooled at °C min^{-1} to -75°C, then heated at 10 °C min^{-1} to 145 °C min^{-1}. The isoniazid/bisVCap sample was heated from room temperature to 175 °C at a rate of 10 °C min^{-1}, cooled at °C min^{-1} to -100 °C, then heated at 10 °C min^{-1} to 125 °C min^{-1}. The ROY/bisVCap sample was heated from room temperature to 150 °C at a rate of 10 °C min^{-1}, cooled at °C min^{-1} to -90 °C, then heated at 10 °C min^{-1} to 155 °C min^{-1}.

7.8.4   Infrared spectroscopy

Experiments were performed on a Perkin Elmer FTIR spectrum 100 with an attenuated total reflectance (ATR) attachment. Data were recorded at a resolution of 2 cm^{-1} for 16 scans over the range 4000 – 600 cm^{-1}. Samples were run by placing on the ATR crystal and applying pressure using the side arm. Spectral analysis was performed using SpekWin32.[30]

Ground samples were prepared by grinding together in the desired ratio of the two components using a mortar and pestle for one minute. Melted samples were prepared by grinding together in the desired ratio of the two components using a mortar and pestle for one minute before placing the ground material into 5 mL glass vial with a plastic screw lid. After the lid was secured the sample was heated above the melting point of the highest melting component until everything had melted using a stirrer hotplate and appropriate heating block.

7.8.5 Crystallographic analysis

X-ray powder diffraction patterns were recorded on a PANalytical Empyrean diffractometer using Cu Kα radiation (λ = 1.54 Å), tube voltage of 40 kV and 40 mA current. Intensities were measured from 2° to 40° 2θ. Soller silts and an incident beam divergent slit of $\frac{1}{8}$°, anti-scatter slit of $\frac{1}{4}$° and diffracted beam anti-scatter slit of 7.5 mm.

7.9   References

(1)   Savjani, K. T.; Gajjar, A. K.; Savjani, J. K. *ISRN Pharm.* **2012**, *2012*, 195727.

(2)   Williams, H.; Trevaskis, N.; Charman, S.; Shanker, R.; Charman, W.; Pouton, C.; Porter, C. *Pharmacol. Rev.* **2013**, *65* (1), 315–499.

(3)   Babu, N. J.; Nangia, A. *Cryst. Growth Des.* **2011**, *11* (7), 2662–2679.

(4)   Aaltonen, J.; Allesø, M.; Mirza, S.; Koradia, V.; Gordon, K. C.; Rantanen, J. *Eur. J. Pharm. Biopharm.* **2009**, *71* (1), 23–37.

(5)   Najar, A. A.; Azim, Y. *J. Indian Inst. Sci.* **2014**, *94*, 45–67.

(6)   Jones, W.; Motherwell, W. D. S.; Trask, A. V. *MRS Bull.* **2006**, *31*, 875–879.

(7)   Dengale, S. J.; Grohganz, H.; Rades, T.; Löbmann, K. *Adv. Drug Deliv. Rev.* **2015**, *100*, 116–125.

(8)   Bailly, N.; Thomas, M.; Klumperman, B. *Biomacromol.* **2012**, *13* (12), 4109–4117.

(9)   Vihola, H.; Laukkanen, A.; Tenhu, H.; Hirvonen, J. *J. Pharm. Sci.* **2008**, *97* (11), 4783–4793.

(10)   Vihola, H.; Laukkanen, A.; Hirvonen, J.; Tenhu, H. *Eur. J. Pharm. Sci.* **2002**, *16* (1–2), 69–74.

(11)   Surikutchi, B.; Patil, S.; Shete, G. *J. Excipients Food Chem.* **2013**, *4* (3), 70–94.

(12)   Parikh, D. M. *Handbook of Pharmaceutical Granulation Technology*, Third Edit.; Parikh, D. M., Ed.; CRC Press: Boca Raton, 2005.

(13)   Serajuddin, A. T. M. *J. Pharm. Sci.* **1999**, *88* (10), 1058–1066.

(14)   Rumondor, A. C.; Taylor, L. S. *Mol. Pharm.* **2010**, *7* (2), 477–490.

(15)   Florence, A. T.; Attwood, D. *Physicochemical Principles of Pharmacy: In Manufacture, Formulation and Clinical Use*, Sixth Edit.; Pharmaceutical Press: London, 2015.

(16)   Corner, P. A.; Harburn, J. J.; Steed, J. W.; McCabe, J. F.; Berry, D. J. *Chem. Commun.* **2016**, *52*, 6537–6540.

(17)   Löbmann, K.; Laitinen, R.; Strachan, C.; Rades, T.; Grohganz, H. *Eur. J. Pharm. Biopharm.* **2013**, *85*, 882–888.

(18)   Löbmann, K.; Grohganz, H.; Laitinen, R.; Strachan, C.; Rades, T. *Eur. J. Pharm. Biopharm.* **2013**, *85*, 873–881.

(19)   Löbmann, K.; Laitinen, R.; Grohganz, H.; Strachan, C.; Rades, T.; Gordon, K. C. *Int. J. Pharm.* **2013**, *453*, 80–87.

(20)   Löbmann, K.; Laitinen, R.; Grohganz, H.; Gordon, K. C.; Strachan, C.; Rades, T. *Mol. Pharm.* **2011**, *8* (5), 1919–1928.

(21)   Löbmann, K.; Strachan, C.; Grohganz, H.; Rades, T.; Korhonen, O.; Laitinen, R. *Eur. J. Pharm. Biopharm.* **2012**, *81* (1), 159–169.

(22)   Chen, S.; Guzei, I. A.; Yu, L. *J. Am. Chem. Soc* **2005**, *127* (27), 9881–9885.

(23)   Yu, L. *Acc. Chem. Res.* **2010**, *43* (9), 1257–1266.

(24)   Chen, S.; Xi, H.; Yu, L. *J. Am. Chem. Soc.* **2005**, *127* (49), 17439–17444.

(25)   Jensen, L. H. *J. Am. Chem. Soc* **1954**, *76* (18), 4663–4667.

(26)   Davenport, J. R.; Musa, O. M.; Paterson, M. J.; Piepenbrock, M.-O. M.; Fucke, K.; Steed, J. W. *Chem. Commun.* **2011**, *47* (35), 9891–9893.

(27)   Macrae, C. F.; Bruno, I. J.; Chisholm, J. A.; Edgington, P. R.; McCabe, P.; Pidcock, E.; Rodrigues-Monge, L.; Taylor, R.; van de Streek, J.; Wood, P. A. *J. Appl. Cryst.* **2008**, *41*, 466–470.

(28)   Heinz, A.; Gordon, K. C.; McGoverin, C. M.; Rades, T.; Strachan, C. J. *Eur. J. Pharm. Biopharm.* **2009**, *71* (1), 100–108.

(29)   Strachan, C. J.; Howell, S. L.; Rades, T.; Gordon, K. C. *J. Pharm. Pharmacol.* **2004**, *35* (5), 401–408.

(30)   Menges, F. http://www.effemm2.de/spekwin: Berchetesgarden 2016.

Conclusion

The initial aim of the work was to study how low molecular weight models of polymeric kinetic hydrate inhibitors used in the oil industry interact with a range of materials to hopefully discover some insight into how KHIs prevent crystallisation. If a mechanism of hydrate inhibition can be proven then new, more effective inhibitors can be designed.

Small molecules containing lactam functionalities were synthesised to model PVP, PVCap and copolymers thereof. A wide range of compounds were used to try and cocrystallise the model compounds, with only a few successes, suggesting that the models are effective at inhibiting crystallisations, like the polymers they are designed to mimic which suggest that they are reasonable models to study the polymers.

The effects of sour gas on the KHIs was explored. There was no observable difference in sweet and sour systems of the KHIs and their models interactions with water. The increased clathrate hydrate in formation in sour pipelines is more likely due to an increase in clathrate formation than a decrease in KHI efficiency.

Cocrystals of boric acid and 1,4-phenyldiboronic acid with the model compounds were effective at gelling guar. Though no change in the kinetics or final products was observed with the pure boronic acid or cocrystals. There are no strong enough interactions between the components of the cocrystals in solution to change the gel onset time, meaning that there is no industrial advantage to using cocrystals to gel guar.

Neutron diffraction of PVCap and butoxyethanol in water was not completely successful. Systems which did not contain any polymer gave sensible results, giving smooth and plausible hydration sphere. The polymer containing system on the other hand, resulted in meaningless fluctuations in water density. Neither the technique nor the simulation program were designed to handle polymers and the system investigated was beyond capabilities of the technique so far.

BisVCap has shown potential as an amorphous stabiliser for a selection of drugs. The amorphous forms of carbamazepine, carisoprodol and ROY were all stabilised by bisVCap added in a stoichiometric ratio. Carbamazepine was particularly stable over time and showed good potential for drug formulation.

Future Work

Halogen bonding coformers have shown potential at cocrystallising with the KHI model compounds. Only a small number of commercially available halogen bonding components have been tested. There is potential that other strong halogen bond donors will also cocrystallise with the model compounds.

Synthesis of ether containing model compounds which are stable to Lewis acidic conditions may lead to a variety of new ligands for heavy metals. Adding a second carbon between the lactam ring and the oxygen, similar to HEP, should help the ether linkage be more stable in acidic conditions, as bisHEP is stable to metals when Et(OVCap)$_2$ and HEPVCap are not.

Further research into the potential of bisVCap as an amorphous stabiliser for drugs should also be undertaken. The shelf life of the amorphous mixture, the processability of the coamorphous materials and the toxicity of bisVCap would require investigation before a drug delivery system could be implemented.

The polymorphs of ROY which crystallise from melts with the model compounds are also of interest. Different polymorphs seem to form depending on which model compound was added. Also the polymorphs are not necessarily touching, which differ from the cross polymorph nucleation observed in the cooling of the melt of pure ROY.

Appendix

Synthesis of ethylcaprolactam

Ethylcaprolactam was produced by hydrogenating vinylcaprolactam using hydrogen balloon and 5 % Pd/C catalyst to give a yellow liquid.
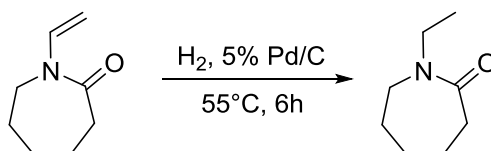

VCap (2.00 g, 14.4 mmol) was dissolved in ca. 50 mL of methanol. 0.05 g of 5 % active palladium on activated carbon was added. A hydrogen balloon and exit needle were used to purge the reaction for one minute before the exit needle was removed. The mixture was stirred at 55 °C for 6 hours. Every hour the exit needle was introduced to relieve pressure, once the exit needle was removed the reaction vessel was shaken to assure good accessibility of the hydrogen. After the 4 hours, the reaction was turned off and allowed to cool to room temperature. The solution was then filtered through Celite. The methanol evaporated under vacuum leaving a yellow liquid. This liquid was then thoroughly mixed with 40 cm^3 of ether which was the evaporated under vacuum. The addition of ether and evaporation was repeated 3 times. The resulting yellow liquid was left in a vacuum desiccator under vacuum overnight.

^1H NMR (400 MHz, CDCl$_3$) δ 3.42 (q, J = 8.0 Hz, 2H), 3.34-3.32 (m, 2H), 2.52-2.49 (m, 2H), 1.75-1.31 (m, 6H), 1.10 (t, J = 8.0 Hz, 3H)

^{13}C {^1H} NMR (101 MHz, CDCl$_3$) δ 175.52, 50.35, 49.12, 42.92, 37.19, 29.95, 28.74, 23.37, 13.16

Synthesis of 1,3,2-dioxathiepene-2-oxide

The method of creating vicinal diol cyclic sulfates by Gao et al.[1] was used to synthesise 1,3,2-dioxathiepene-2-oxide, compound **12**, Scheme 3.3. The product was prepared in a yield of 47 %. Compound **12** is a liquid at room temperature, the oxidised analogue 1,3,2-dioxathiepene-2,2-dioxide is a solid at room temperature as described by Gao et al.[1]. Crystallisations experiments were performed using compound **12** and can be found in section 3.2.4.4.
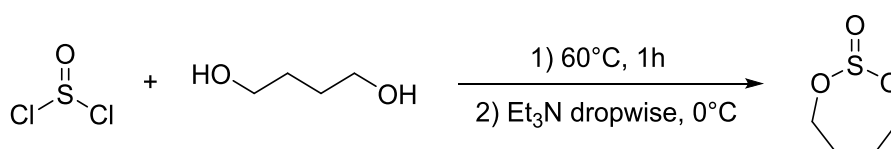
Butane-1,4-diol (2.04 cm^3, 34.0 mmol) was added to chloroform (20 cm^3) at room temperature. Thionyl chloride (2.5 cm^3, 34.4 mmol) in chloroform (20 cm^3) was added dropwise to the butane-1,4-diol solution over the course of 40 minutes. The reaction was heated to 60 °C for one hour. The reaction mixture was then cooled to 0 °C using an ice bath. Triethylamine was added dropwise until the fumes were no longer formed upon addition. The reaction mixture was added to a separating funnel and diluted with diethylether (80 cm^3). The organic layer was washed with distilled water (20 cm^3), saturated aqueous NaHCO$_3$ solution (2 x 20 cm^3) and finally brine (20 cm^3). Solvent was evaporated under vacuum to leave a pale yellow liquid.

Yield 2.2 g, 16.2 mmol, 47 %

*^{1}H NMR* (400 MHz, CDCl$_3$) δ 4.49-4.43 (m, 2H), 3.98-3.93 (m, 2H), 1.91-1.80 (m, 4H)

^{13}C {^{1}H} NMR (101 MHz, CDCl$_3$) δ 64.05, 28.36

m/z 137 (M+H$^+$, 100 %), 102 (16), 73 (30), 55 (34)

Synthesis of cucurbituril mixtures

A mixture of cucurbiturils with ring sizes 5, 6, 7 and 8 referred to as CB5, CB6 CB7 and CB8, was successfully synthesised by the method of Day *et al.*[2] The acid catalyst chosen was 5 M HCl, as this maximised the production of CB6 and CB7 according to the study of reaction conditions by Day *et al.*[2] To separate the cucurbiturils a series of fractional crystallisations are required. As the exact ring size requirement to host the model compounds and create inclusion complexes of the model compounds in macrocyclic rings is not known, it was decided to use crude mixtures as a thorough and complete fractional crystallisation is time consuming and the selectivity for a particular ring size should aid crystallisation. Whilst a full fractional crystallisation was not undertaken, the first step of the fraction crystallisation outlined by Senler[3] was performed. As much of the crude material as possible was dissolved in water. That which did not dissolved, fraction 1, was filtered off. The filtrate was evaporated to leave fraction 2. Carbon-13 NMR spectroscopy was used to identify which cucurbiturils are present in reaction mixtures as the chemical shift for the methine and methylene carbon atoms increases with ring size. Fraction 1 shows a single methylene peak and a single methine peak at 67.3 and 48.6 ppm respectively. The attempted recrystallisation of fraction 1 with bisVCap from dilute HCl resulted in crystals of CB6 with a chloride ion, hydronium ion and water and no bisVCap, confirmed by single crystal x-ray crystallography. The crystals are of too low quality to allow full placement of the solvent and cation which are very disordered. Positive identification of CB6 confirms that the peaks in at 67.3 and 48.6 ppm in the ^{13}C NMR spectrum correspond to CB6.

Fraction **2** gave two methine peaks at 49.9 and 47.3 ppm and two major methylene peaks at 68.4 and 66.3 ppm. As one set of peaks is at higher chemical shift than that for CB6 and one set of peaks is lower than that for CB6 and according to the scheme by Senler[3] this fraction should contain CB5 and CB7, the peaks at 68.4 and 49.9 ppm were assigned to CB7 and the peaks at 66.3 and 47.3 ppm assigned to CB5. The carbon-13 NMR spectrum of fraction **2** also has a weak peak at 67.3 ppm, suggesting that there is a small amount of CB6 present which is too small for the methine peak to be visible.
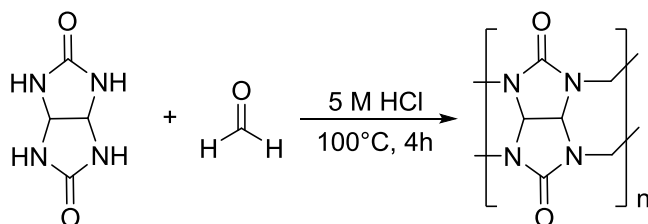
Glycouril (5.00 g, 35.2 mmol) was dissolved in 30 cm^3 of 5 M HCl. Paraformaldehyde (1.06 g, 35.2 mmol formaldehyde) was added slowly in 0.05 g portions at room temperature over 5 min. The reaction mixture was then heated to 100 °C for 4 hours. The reaction was then cooled and the solvent removed under vacuum resulting in a solid off white residue.

50 cm^3 of water was added to the off-white product and sonicated for 10 min. Any undissolved solid, fraction **1,** was filtered off and dried in a vacuum desiccator. The filtrate was evaporated by heating resulting in an off-white solid, fraction **2**, which was then thoroughly dried in a vacuum desiccator.

*Fraction **1***

^{1}H NMR (400 MHz, DCl) δ 2.17 (s, 1H), 2.05 (d, J = 16.0 Hz, 1H), 0.93 (d, J = 16.0 Hz, 1H)

^{13}C {^{1}H} NMR (101 MHz, DCl) δ 153.7, 67.3, 48.6

*Fraction **2***

^{1}H NMR (400 MHz, DCl) δ 2.31 (s, 1H), 2.22 (d, J = 17.0 Hz, 1H), 1.04 (d, J = 17.0 Hz, 1H)

^{13}C {^{1}H} NMR (101 MHz, DCl) δ 154.0, 68.4, 67.3, 66.3, 49.9, 47.3

References

(1)   Gao, Y.; Sharpless, K. B. *J. Am. Chem. Soc* **1988**, *110*, 7538–7539.

(2)   Day, A.; Arnold, A. P.; Blanch, R. J.; Snushall, B. *J. Org. Chem.* **2001**, *66*, 8094–8100.

(3)   Senler, S. Design and Synthesis of New Cucurbituril Systems and New Guests for Cucurbiturils, University of Miami, 2014.